BIOPHYSICAL STUDIES OF THE UNIVERSALLY CONSERVED NTPASES HFLX AND YCHF

HARLAND EDWARD BRANDON
Bachelor of Science, University of Lethbridge, 2014

A thesis submitted
in partial fulfillment of the requirements for the degree of

DOCTOR OF PHILOSOPHY

in

BIOMOLECULAR SCIENCE

Department of Chemistry and Biochemistry
University of Lethbridge
LETHBRIDGE, ALBERTA, CANADA

Biophysical Studies of the Universally Conserved NTPases HflX and YchF

Harland Edward Brandon

Date of Defence: March 5, 2021

Dr. H.-J. Wieden Thesis Supervisor	Professor	Ph.D.
Dr. T. Russell Thesis Examination Committee Member	Associate Professor	Ph.D.
Dr. T. Patel Thesis Examination Committee Member	Associate Professor	Ph.D.
Dr. U. Kothe Internal External Examiner Department of Chemistry and Biochemistry	Professor	Ph.D.
Dr. M.-N. Yap External Examiner Northwestern University Chicago, Illinois	Associate Professor	Ph.D.
Dr. M. Gerken Chair, Thesis Examination Committee	Professor	Ph.D.

Abstract

Antibiotic resistance is becoming an increasing global health concern. The bacterial protein synthesis machinery, including the ribosome and its associated factors, are the target of over half of the clinically relevant antibiotics currently in use, highlighting the importance of cellular protein production as antibiotic target. The ribosome associated factors HflX and YchF are members of the GTPase superfamily. Their cellular functions are only poorly understood. The overarching goal of this thesis was to determine the location where HflX and YchF bind on the bacterial ribosome. Data presented here confirm that YchF interacts with the ribosomal A-site, while HflX is unique within the GTPase family being able to bind to both the ribosomal A-site and E-site. From this data and subsequent biochemical and biophysical studies, a mechanism for both HflX and YchF function during protein synthesis, specifically under stress conditions, is proposed.

Acknowledgements

HJ: Thank you for taking me as a student a decade ago and believing that I had what it took to get to this point, when I wasn't sure I did. Your enthusiasm and dream of what science (specifically synthetic biology) could do for the world inspired me to more than you will ever know.

Mackenzie: You have there by my side since day 1 of this journey in grad school. It has been quite a journey for us both. Thank you for always being supportive of me, even when it took me far to long to finish up and move to Edmonton to be by your side. It was so hard every time an experiment failed, and I knew it meant I'd be apart from you even one more day. Nevertheless, we made it through those times apart and are stronger because of it. I cannot thank you enough for the love and support you have given me, and I strive everyday to be as supportive for you.

Mom and Dad: I can't thank you both enough for everything you have done for me, but more specifically everything you have done while I've been a poor university student. I know I took a bit longer to finish than we all hoped, but I think it will be worth it in the end. I will always appreciate everything you have done for me and all the support along the way.

My family: Doni, Katherine, Leon, Lane, Cathryn, Ted, Dorothy, and all my extended family.
No university degree can be done without the support of one's family. Even indirectly, you have all helped me get through this and stood by me as it ended up taking longer than I anticipated. I know you are all proud of me, and hopefully you will be even more proud once I have succeeded at completing this degree. I just want you all to know how thankful I am for your support.

Fan: Thank you for putting up with my crazy antics and the chaos I brought to our office over the years. It has been weird this past year having left that office in UHall moving the Science Commons where we no longer share an office, but I will always remember the good laughs from our gaming, the YouTube videos we watched, and just us teasing everyone else in the lab.

Jeff: You were heavily influential in my decision to pursue graduate studies, even though you had moved on to bigger and better things before I even considered enrolling in the master's program and eventually transferring to the Doctoral program. I hope I was able to carry the mantle of HflX group leader well. Thank you.

To the students I taught: In "relative" chronological order: Quinn S., Rachel, Chris I., Kieran, Ursula, Angela, Taylor L., Lena, Dora, Ronja, Valerie, Karin, Chris L., Jessica, Will, Amanda.
To each of you, I hope I was able to spread my joy of science, specifically the study of biochemistry and the ribosome! I want you all to know that I appreciate you taking the time to learn with me as I grew into being a better mentor and I hope you all the best in your futures.

To all other Wieden lab members: Luc, Dylan, Justin, Anthony, Dominic, Even, Evelina, Kirsten, Lindsay, Adam, Dustin, Tobi, Binod, Katherine, Jalyce, Raja, Andy, Graeme, Rhys, Senthil, Davinder, Taylor, Emily, Jumai, Preethi, Sydnee, Kristi, Fabian, and all the undergrads/HYRS students/iGEM students over the years.
Thank you for all the guidance, support, laughs, and good times. I will always look back on the memories of working alongside you all with fondness.

To my committee: Your support and guidance over this journey has not gone unnoticed or unappreciated. Thank you for helping me be a better scientist.

To Susan: Thank you for everything you have done to help me over the years. I think it goes without mentioning just how much you do for us all behind the scenes, but I want you to know I appreciate it.

To everyone else who has been apart of my graduate journey directly or indirectly: Thank you!

Table of Contents

List of Figures

List of Tables

List of Abbreviations

4-AzPB	4-Azidophenacyl bromide
aaRS	Aminoacyl-tRNA synthetase
ADP	Adenosine diphosphate
ADPNP	Adenosine [β, γ-imido] triphosphate
AMP	Adenosine monophosphate
AMV	Avian myeloblastosis virus
apo	Definition: In an inactive, unbound state
ATP	Adenosine triphosphate
ATPase	Adenosine triphosphatase
AZI	Azithromycin
AzP	4-Azidophenacyl
CCW	Counter-clockwise
CHL	Chloramphenicol
CLIND	Clindamycin
CP	Central Protuberance
Cryo-EM	Cryogenic electron microscopy
CW	Clockwise
DNA	Deoxyribonucleic acid
DTT	Dithiothreitol
E. coli	*Escherichia coli*
EF	Elongation factor
ERY	Erythromycin
FUS	Fusidic acid
GDP	Guanosine diphosphate
GDPCP	Guanosine
GDPNP	Guanosine [β, γ-imido] triphosphate
GTP	Guanosine triphosphate
GTPase	Guanosine triphosphatase
HAS-GTPase	Hydrophobic amino acid substituted guanosine triphosphatase
HPF	Hibernation Promoting Factor
HYGB	Hygromycin B
IC	Initiation complex
IF	Initiation factor
KAN	Kanamycin
KASUG	Kasugamycin
LINC	Lincomycin
lncRNA	long non-coding RNA or long non-coding ribonucleic acid
mRNA	messenger RNA or messenger ribonucleic acid
NTPase	Nucleotide triphosphatase
ORF	Open reading frame
PAGE	Polyacrylamide gel electrophoresis
PARO	Paromomycin
PEP	Phosphoenolpyruvate
PET	Peptide exit tunnel (sometimes referred to as nascent peptide exit tunnel or nPET)
P_i	Inorganic phosphate
PIC	Preinitiation complex
PK	Pyruvate kinase
PoTC	Post-termination complex
POST	Posttranslocation complex
(p)ppGpp	Guanosine tetraphosphate (pentaphosphate)
PRE	Pretranslocation complex
PTC	Peptidyl transferase center
QC	Quality control

Rb	Ribosome
RF	Release factor
RMF	Ribosome modulation factor
RNA	Ribonucleic acid
RRF	Ribosome recycling factor
rRNA	ribosomal RNA or ribosomal ribonucleic acid
SD	Shine-Dalgarno
SDS	Sodium dodecyl sulfate
SPC	Spectinomycin
STREP	Streptomycin
TET	Tetracycline
TOB	Tobramycin
tmRNA	transfer-messenger RNA or transfer-messenger ribonucleic acid
trGTPase	Translational guanosine triphosphatase
tRNA	transfer RNA or transfer ribonucleic acid
UV	Ultraviolet
VIO	Viomycin

CHAPTER 1: INTRODUCTION

1.1 – PREFACE

This chapter contains portions of two reviews published as a part of Harland E. Brandon's graduate work. The first review, "Cellular Roles of the human OBG-like ATPase 1 (hOLA1) and its YchF homologs" was a collaboration between the Thakor lab (Nirujah Balasingam, Joseph A. Ross, and Nehal Thakor) at the University of Lethbridge who study human OBG-like ATPase 1 (hOLA1) and the Wieden lab (Harland E. Brandon and Hans-Joachim Wieden) who are interested in the bacterial homolog of hOLA1 known as YchF. Sections pertaining to non-human homologs of YchF and "comparing and contrasting" YchF and hOLA1 were written by Harland E. Brandon, while sections pertaining to the functional roles of hOLA1 were written by Nirujah Balasingam and Joseph A. Ross of the Thakor Lab. This review was published in a special edition of Biochemistry and Cellular Biology journal (1). The second review, "To split or not to split, that is the question: The ribosome dissociation factor HflX (Tentative title)," was written by Harland E. Brandon and Hans-Joachim Wieden to summarize all HflX literature to date. The review was written for submission to Molecular and Cellular Biochemistry during the writing of the thesis. Together these reviews make up the final sections of this chapter providing the basis for the experimental work Harland E. Brandon performed during the thesis on both *Escherichia coli* YchF and HflX.

1.2 – OVERVIEW OF PROTEIN SYNTHESIS

Proteins perform many essential processes required for a cell to grow and divide, making their proper synthesis critical for life. As such, many antibiotics are inhibitors of bacterial protein synthesis leading to bacterial cell death and allowing the immune system to respond effectively. Protein synthesis, also referred to as translation, is the final step in the central dogma of biology following transcription of the deoxyribonucleic acid (DNA) code into messenger ribonucleic acid (messenger RNA or mRNA) (Figure 1.1). The DNA of every organism encodes not just the proteins it requires (in the form of mRNAs), but also non-coding RNA molecules that play a wide variety of

cellular roles, including the ribosomal RNA (rRNA) and transfer RNA (tRNA) which will be discussed in the following paragraphs.

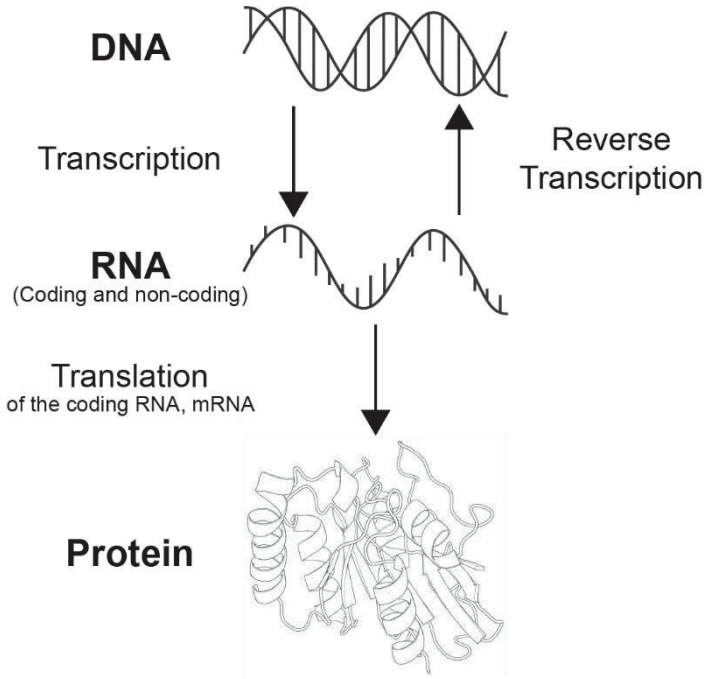

Figure 1.1 – The central dogma of biology. The genetic information stored in the DNA of all organisms is transcribed in RNA by RNA polymerases. RNA molecules are generally divided into two categories: coding and non-coding RNAs. Coding RNAs are messenger RNAs (mRNAs) as they contain the encoded "message" that the ribosome translates into a functional protein. Non-coding RNAs are those which perform cellular functions aside from encoding proteins, although this is not a strict rule. In this thesis, the main non-coding RNAs that will be discussed are transfer RNAs (tRNAs) and the ribosomal RNAs (rRNAs) that make up the ribosome. The protein depicted is the conserved G-domain found in all GTPases, specifically that of YihA (PDB 1SVI).

Protein synthesis is facilitated by the ribonucleoprotein complex called the ribosome that is made up of 3 rRNAs in *E. coli* and over 50 ribosomal proteins (r-Proteins). One *E. coli* cell contains ~36 000 – 45 000 ribosomes under optimal growth conditions (2, 3) and which are constantly being used to synthesize proteins in a cyclic process known as the ribosomal cycle (Figure 1.2). The ribosome consists of two subunits, a large 50S ribosomal subunit and a small 30S ribosomal subunit. The separation and joining of these subunits are important for protein synthesis. This thesis primarily focuses on the *E. coli* translation apparatus and all proteins and RNAs described are from *E. coli* unless otherwise noted.

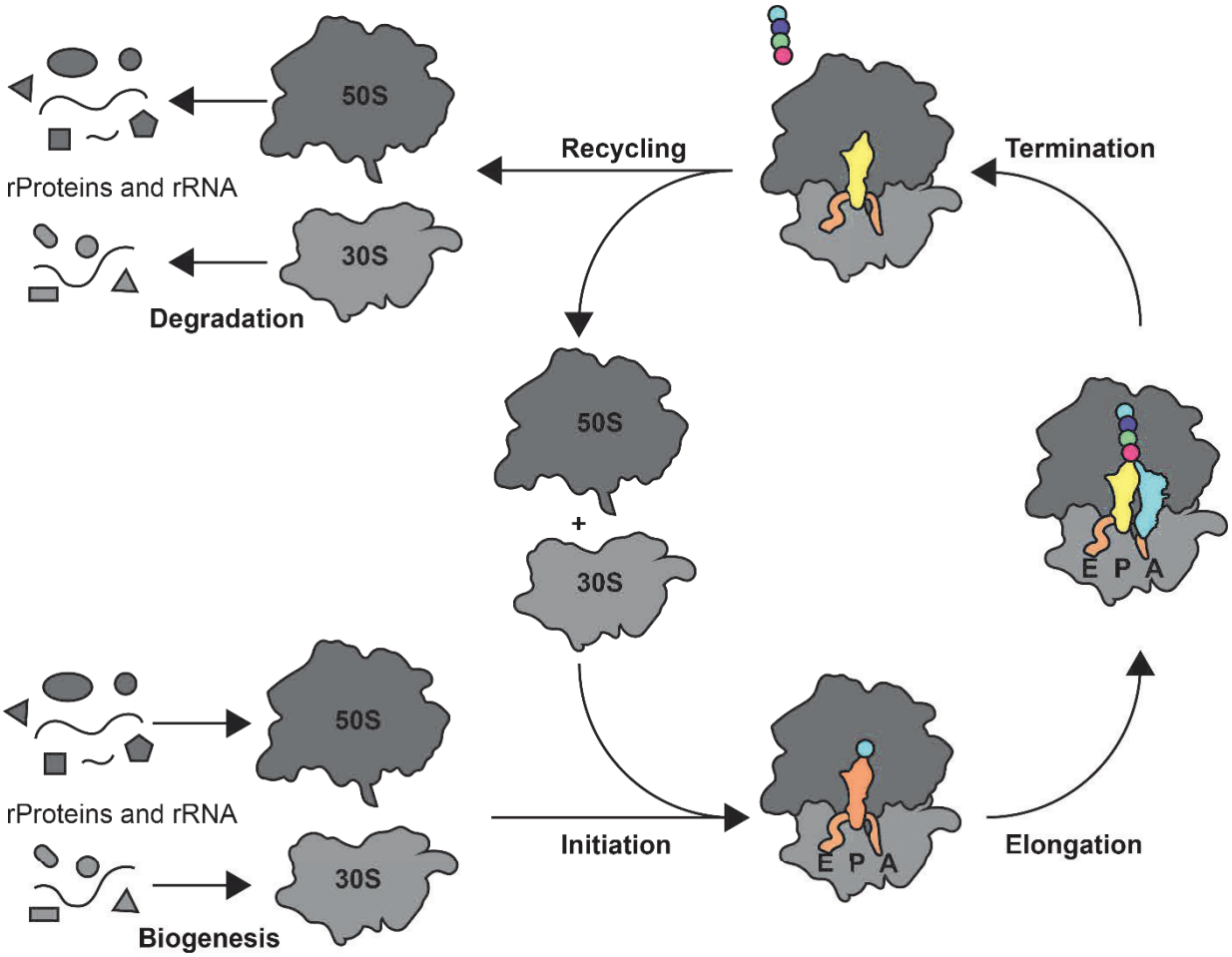

Figure 1.2 – The ribosomal cycle. The ribosome is the focal point for protein synthesis in the cell and its regulation occurs not only during the synthesis but also during biogenesis of new ribosomal subunits, recycling of the subunits following protein synthesis, as well as the degradation of damaged subunits. Assembly of new ribosomal subunits is a highly coordinated process that is constantly replenishing the pool of functional subunits as damaged subunits are degraded to prevent errors in translation. A pair of free 50S and 30S ribosomal subunits are brought together onto an mRNA during translation initiation, move along an mRNA during the elongation of the polypeptide, and upon reaching the stop codon of the mRNA, terminate translation through the release of the synthesized protein. Following termination, the ribosomal subunits remain joined on the mRNA and are separated from each other, or recycled, to allow each subunit to initiate another round of translation.

Like all biomolecules, each ribosome must be assembled before it can be used in protein synthesis and is eventually degraded and recycled by the cell (Figure 1.2). Each ribosomal subunit is assembled from the individual rRNAs and r-proteins in a process known as ribosome biogenesis. There is increasing evidence for the importance of ribosome biogenesis during the modulation of translation, errors in this process lead to downstream problems in protein synthesis. In humans,

errors in ribosome biogenesis or ribosomal proteins can lead to disorders commonly referred to as ribosomopathies (4-7).

Newly synthesized ribosomal subunits are added to the pool of active subunits which are constantly binding to mRNAs to start a new round of protein synthesis. The ribosome proceeds through four phases during the synthesis of a protein including initiation, elongation, termination, and recycling (Figure 1.2). The elongation phase is repeated for each amino acid added to the growing polypeptide chain. Regulation of these steps can influence which proteins are synthesized and how many copies of each protein are produced. Over 50% of antibiotics are known to disrupt one or more of these phases of translation, primarily translation initiation and elongation, which further emphasizes the importance of protein production in the cell (8).

The ribosome is the site of protein synthesis, yet it is the rRNA that catalyzes the formation of each peptide bond between amino acids. Peptide bond formation can be catalyzed by the ribosome alone, however, this process is to slow to support the elongation rates observed *in vivo* (9, 10). To achieve the rates and accuracy of protein synthesis that can sustain cell growth, additional ribosome-binding proteins and RNA factors are required, including an important class of enzymes, the guanosine triphosphatases (GTPases).

1.3 – GTPASES IN PROTEIN SYNTHESIS

P-loop nucleotide triphosphatases (NTPases) comprise the largest group of nucleotide binding proteins (10-18%) in most organisms (11). Although most of the P-loop NTPases utilize adenosine triphosphate (ATP) as an energy source, the superfamily of P-loop GTPases are an exception of this rule, utilizing guanosine triphosphate (GTP) as a substrate to regulate a variety of critical cellular processes (11). Based on structural features and conserved sequences, P-loop GTPases can be sorted into two main classes: the translation factor related class (TRAFAC) and the signal recognition particle, MinD, and BioD (SIMIBI) NTPases (11, 12). These GTPases have been grouped together based on the common core G-domain that contains five conserved G-motifs (11).

GTPases play important roles in the ribosomal cycle and regulate different cellular functions through a cyclic nucleotide-dependent process (Figure 1.3). The guanosine triphosphate-

bound (GTP-bound) state represents the “active” state. Interaction with its functional target leads to hydrolysis of the bond between the beta (β) and gamma (γ) phosphate of GTP. The subsequent release of the gamma phosphate leaves the GTPase in the guanosine diphosphate-bound (GDP-bound), “inactive” state. The bound GDP can be exchanged with another GTP molecule from the cellular pool (nucleotide exchange) to renew the “active” state. During nucleotide exchange the GTPase transiently exists in a no nucleotide is bound state, the *apo* state. Generally, the *apo* state is short-lived *in vivo* as the affinity for and cellular concentration of GTP and GDP would lead to a nucleotide bound state. The exact role nucleotide hydrolysis plays during the functional cycle of each GTPase is context dependent. Some GTPases utilize the energy released from nucleotide hydrolysis to power conformational changes within the GTPase and/or interaction partner (13-15) while some GTPases use hydrolysis as a molecular timer to disassociate from one or more interaction partners (16, 17).

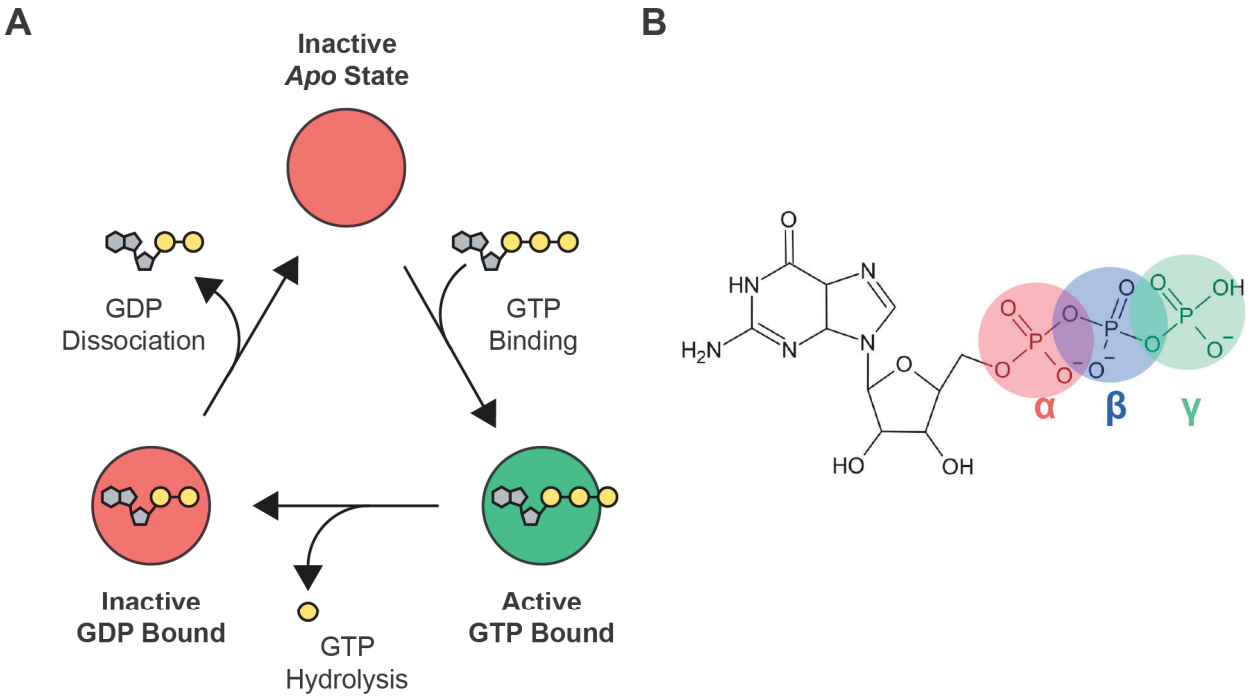

Figure 1.3 – The GTPase cycle and structure of guanosine triphosphate. A) The active state of a GTPase occurs when GTP is bound. The binding of a GTPase activating protein (GAP) activates the hydrolysis of the bound GTP to GDP and P_i. After P_i and GAP dissociation, GDP remains bound leaving the GTPase in the inactive state. The binding of a guanosine exchange factor (GEF) facilitates the dissociation of GDP to allow a new GTP molecule to bind the GTPase, switching the enzyme back to the active state. B) Chemical structure of guanosine triphosphate denoting the α, β, and γ phosphates.

The structures of many ribosome-associating GTPases have been determined by X-ray crystallography and cryo-electron microscopy (cryo-EM) over the past several decades (Figure 1.4; (18-24). One distinguishing feature is the conserved GTP-binding domain (G-domain) present in the majority of GTPases. The G-domain has a defined structure consisting of six-stranded β-sheets surrounded by α-helices (25). The nucleotide binding site within the G-domain is comprised of 4-5 conserved "G-motifs" designated G1-G5. The G1 motif (also referred to as the P-loop or Walker A motif) has the conserved sequence GxxxxGK(S/T) and binds to the α and β phosphates of the guanine nucleotide. The G2 motif (switch 1) has the conserved sequence x(T/S)x which coordinates the bound magnesium ion (Mg^{2+}) with the G3 motif (switch 2 or Walker B motif). G3 has the sequence DxxG and additionally contacts the γ-phosphate of the guanine nucleotide. The conformation of G2 and G3 differ depending on whether GTP or GDP is bound to the G-domain, giving rise to the molecular switch that GTPases are attributed to acting as. The G3 motif typically contains a key residue that is involved in coordination of the catalytic water molecule required for GTP hydrolysis. Some GTPases lack this residue (typically a glutamine or histidine) and in its place have a hydrophobic amino acid. These GTPases are termed hydrophobic amino acid substituted GTPases (HAS-GTPases) and will be described in more detail later (26, 27). The G4 motif (sequence (N/T)KxD) and G5 motif (sequence (T/G)(C/S)A) interact with the base of the nucleotide, thereby providing nucleotide specificity to the G-domain. Together these G-motifs are responsible for the binding of guanine nucleotides and any mutations to the key residues in these motifs can lower the affinity significantly, if not abolishing nucleotide binding entirely (28).

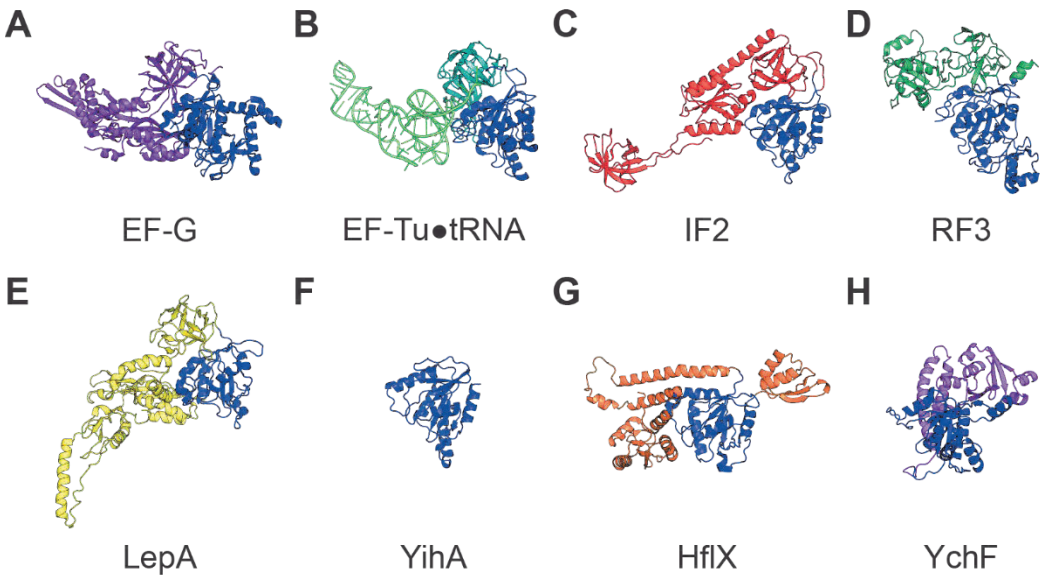

Figure 1.4 – Structures of ribosome associated GTPases in *E. coli*. The G-domain of each GTPase is shown in blue and other domains shown in a representative colour used throughout this text. A) Elongation factor G (EF-G; PDB 4V9L); B) Elongation factor Tu (EF-Tu) and bound tRNA (PDB 5WE4); C) Initiation factor 2 (IF2; PDB 3JCJ); D) Release factor 3 (RF3; PDB 6GXO); E) LepA (PDB 3JCE); F) YihA (PDB 1SVI); G) HflX (PDB 5ADY); H) YchF (PDB 1JAL). All structures are orientated relative to the positioning of G-domain in HflX (G).

Some GTPases have low intrinsic rates of nucleotide hydrolysis and require a GTPase activating protein (GAP) to facilitate hydrolysis at physiological relevant rates. For GTPases such as Ras, the GAP contributes a conserved arginine (arginine-finger) to the active site of Ras, providing a positively charged group to neutralize the local negative charge from the phosphates of the bound nucleotide thereby lowering the activation energy for catalysis (29). Other mechanisms for activating GTP hydrolysis in GTPases with low intrinsic rates of hydrolysis have also been discovered, including the GTPases that associate with the ribosome (30-33). One unique feature of some of these GTPases is that RNA plays a GAP-like role in activation of hydrolysis. For example, elongation factor G (EF-G) binds to the GTPase associated center (GAC) of the ribosome where the G-domain of EF-G interacts with several ribosomal proteins and the rRNA, including the Sarcin-Ricin Loop (SRL) (18). The SRL is name after the two toxins, α-sarcin and ricin, that are known to cleave and be involved in the depurination of a nucleotide (A2660) within the GAGA tetraloop itself (34-36). A2660 has been shown structurally and biochemically to form several interactions with the G-domain (32). These interactions lead to a conformational change in the G-

domain that allows the catalytic histidine following the G3 motif to activate a water molecule for nucleophilic attack on the γ-phosphate of the bound GTP, leading to nucleotide hydrolysis. Not all ribosome associated GTPases utilize this mechanism, however, as will be described later in this thesis.

Following nucleotide hydrolysis, the inorganic phosphate (P_i) dissociates from the GTPase leaving a bound GDP molecule. The affinity each GTPase has for either guanine nucleotide (GTP and GDP) will influence how the enzyme cycles back to its active state (Figure 1.3). If the affinity for GDP is low, following hydrolysis the bound GDP will dissociate, allowing another GTP molecule from the cellular pool to bind. Some GTPases however, have a higher affinity for GDP than GTP and consequently require a guanine exchange factor (GEF) to facilitate efficient GDP dissociation necessary for the GTPase cycle to continue *in vivo*. For example, EF thermo unstable (EF-Tu) has a higher affinity for GDP than GTP requiring the GEF, EF thermo stable (EF-Ts). EF-Ts binds to EF-Tu and inserts a conserved phenylalanine into the nucleotide binding pocket of EF-Tu, disrupting the Mg^{2+} binding site, leading to the dissociation of GDP (25).

In the following sections each step in the ribosomal cycle will be briefly discussed to highlight key similarities and differences, while discussing the protein and RNA factors utilized in each step, with emphasis on the GTPases involved. Many of the GTPases depicted in Figure 1.4 are involved in translation including IF2, EF-G, EF-Tu, RF3, as well as the specialized EF-Tu factor SelB that delivers the 21st amino acid, selenocysteine, to the translating ribosome (37, 38). Ffh and FtsY are involved in directing the newly synthesized protein into the cellular membrane (39, 40). The functional role of LepA, the third most highly conserved protein in bacteria, is still highly debated in the literature. LepA has proposed roles ranging from ribosome biogenesis over translation initiation to back-translocation, as detailed in Heller *et al*. and references therein (41). Several GTPases including BipA, YihA, Era, Der, and Obg have substantial evidence suggesting their functional roles in ribosome biogenesis (42-45). MnmE is a tRNA modification enzyme introducing either a 5-aminomethyluridine or 5-carboxymethylaminomethyluridine modification at the position of the wobble uridine in some tRNA isoacceptors (42, 46, 47). In this thesis, the functional roles of HflX and YchF are further characterized revealing that HflX is a stress response factor involved in

dissociating a stalled 70S ribosome or hibernating 100S ribosome dimer while YchF is involved in checking and maintaining ribosome quality during the steps of ribosome biogenesis and throughout the ribosome's life cycle.

1.4 – RIBOSOME BIOGENESIS IN BACTERIA

The process of synthesizing new ribosomal subunits is a highly regulated and coordinated effort facilitated by over 100 different proteins in *E. coli* (43, 48-50). Biogenesis starts with transcription of the pre-rRNA by RNA polymerase (RNAP). As the pre-rRNA is transcribed secondary structural elements begin to fold and ribosomal proteins (rProteins) bind, along with assembly factors that perform different functional roles in the maturation of the ribosomal subunit including cleavage of the pre-rRNA, post-transcriptional modifications, and folding of the rRNA (Figure 1.5). These assembly factors include helicases/chaperones, RNA modification enzymes, and GTPases (43, 49). Additionally, some of these factors act as sensors of checkpoints in the assembly process to coordinate assembly and proper folding of the precursor ribosomal subunits. An example of this is the dimethyltransferase KsgA that is involved in late-stage maturation of the 30S subunit (51). These checkpoints ensure that critical steps in the assembly of each subunit are reached before proceeding in subsequent assembly steps, yet these check points are specific for the assembly of the subunits individually and are unable to ensure intersubunit functionality. As the interaction between the large and small subunits plays important roles in different stages of protein synthesis, ensuring that newly synthesized subunits can make productive interactions with the opposite subunit is important for maintaining efficiency and accuracy of translation. Recently, two studies in *E. coli* have demonstrated that the initiator tRNA ($tRNA^{fMet}$) and the GTPase LepA are involved in the late stages of quality control during ribosome biogenesis (52, 53). Following biogenesis of either subunit, the newly formed subunit is speculated to be subject to "test initiation" to assess that intersubunit interactions are correct. The initiator tRNA binding to the "test initiation" complex triggers the final processing of the 16S rRNA-ends while LepA is hypothesized to provide a structural check of the ribosome, potentially through its interactions with the P-site tRNA near the CCA end of the tRNA (41). The "test initiation" of newly synthesized ribosomal subunits is a

relatively recent hypothesis and is still being evaluated in the literature but has been observed in eukaryotes as well (54, 55).

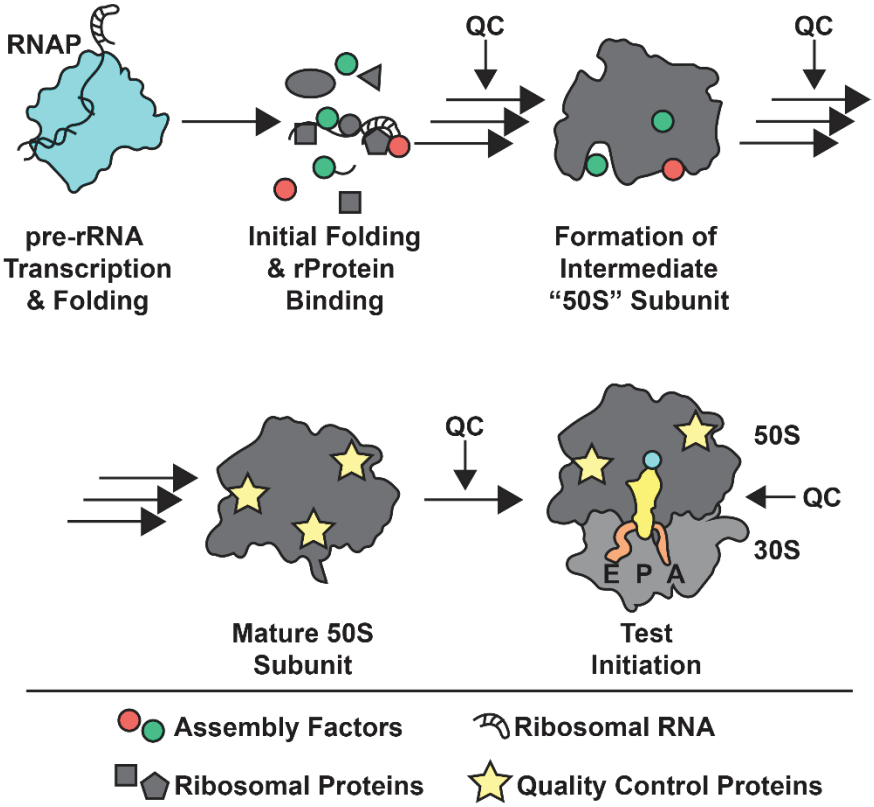

Figure 1.5 – Overview of events in ribosome biogenesis. Shown is a graphical representation of the assembly of a new 50S ribosomal subunit. While the pre-rRNA is being transcribed, secondary structure begins to fold aided by the binding of early stage ribosomal proteins. There is hierarchy of ribosomal proteins assembled into the immature ribosomal subunit precursor, coordinated by assembly factors that bind at specific times to perform their functional roles in biogenesis and act as quality control (QC) checks. Coordinated assembly leads to the formation of intermediate ribosomal subunits that can be isolated from strains lacking an assembly factor. Once mature, the 50S ribosomal subunit forms a 70S ribosome with a 30S ribosomal subunit to test intersubunit connections and signal relaying before proceeding into translation initiation. Multiple arrows denote multiple steps occurring.

The current hypothesis is that the GTPases involved in biogenesis also act as molecular timers coordinating the timing of each assembly step by dissociating only after GTP hydrolysis occurs, which occurs only once a certain stage of biogenesis has been reached. The exact functional roles of many of these ribosome biogenesis GTPases are a current focus of research. This group of GTPases includes, but is not limited to, RbgA, ObgE, YihA (YsxC), and YphC which are involved

in the biogenesis of the 50S ribosomal subunit and Era, RsgA, YqeH which are involved in the assembly the 30S ribosomal subunit (43).

While research in ribosome biogenesis dates back several decades, there are still many unanswered questions in ribosome biogenesis including the functional role of each assembly factor, the kinetic order of events leading to mature ribosomal subunits, and the structures of intermediates along the biogenesis pathway. Impairment of ribosome biogenesis is deleterious to cell growth, and thus further understanding of this process may provide a wealth of new antimicrobial drug targets.

1.5 – TRANSLATION INITIATION IN BACTERIA

Translation initiation is the rate-limiting step of protein synthesis and is highly regulated (15, 56-58). To start synthesis of a new protein, the mRNA encoding the respective protein binds to the 30S ribosomal subunit along with the initiator tRNA (fMet-tRNA^{fMet}) and initiation factors 1, 2, and 3 (IF1-IF3). The order of these factors binding to the 30S ribosomal subunit has been characterized previously and is summarized in Figure 1.6 (adapted from (56)).

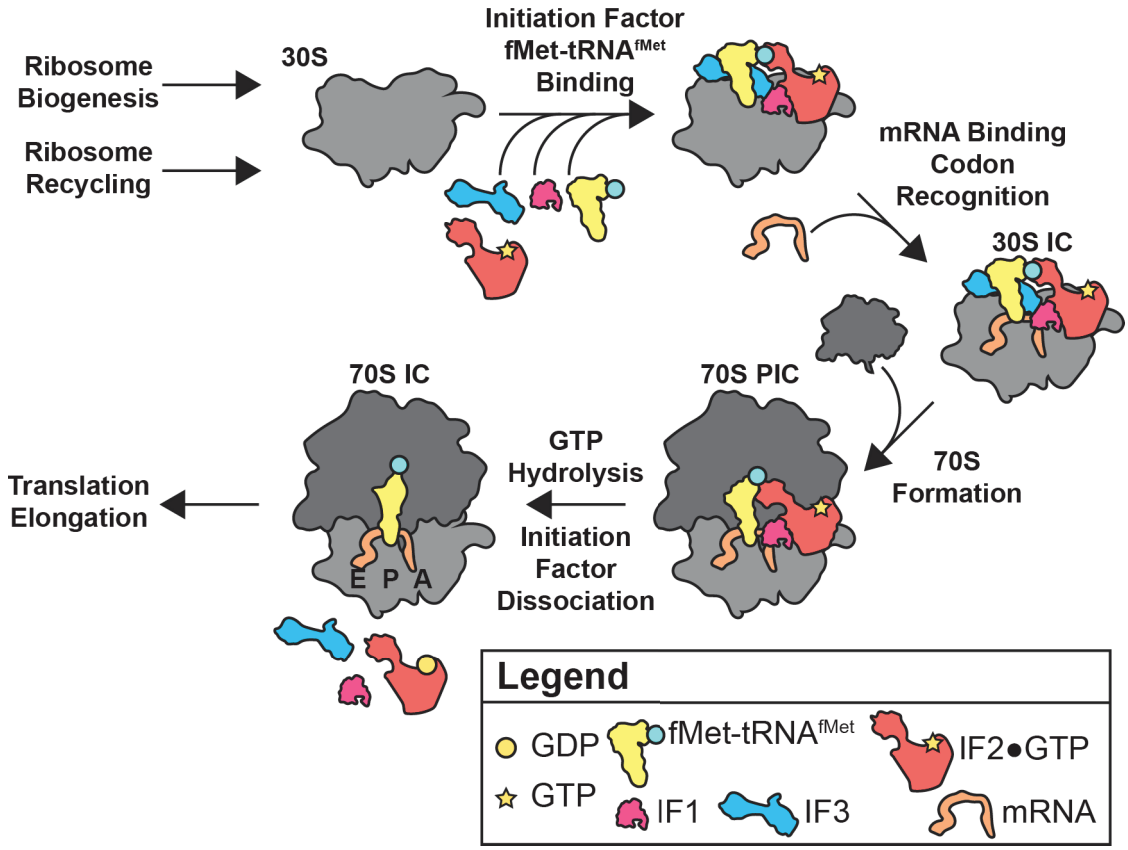

Figure 1.6 – Mechanism of canonical translation initiation. Graphical representation of the stages of translation initiation. Following ribosome biogenesis or recycling, the 30S ribosomal subunit binds to IF3 and IF2•GTP, followed by IF1, and the initiator tRNA fMet-tRNA^{fMet}. The mRNA binds forming the leading to codon recognition between the mRNA and initiator tRNA. Upon codon recognition, the 30S initiation complex is formed and can associate with the 50S ribosomal subunit. Formation of the 70S pre-initiation complex triggers GTP hydrolysis by IF2, and the subsequent dissociation of the initiation factors from the ribosome. Once the initiation factors have departed, the 70S IC ribosome contains an mRNA and initiator tRNA in the ribosomal P-site and is ready to enter the elongation phase of translation. Adapted from (56).

The 30S ribosomal subunit is initially bound by the GTPase IF2 and IF3 followed by the binding of IF1 (56). The initiator tRNA, fMet-tRNA^{fMet} binds to the complex interacting with IF2 and IF3 before the recruitment of the mRNA. The binding of the mRNA to the mRNA channel on the 30S ribosomal subunit prior to base pairing of the initiator tRNA to the start codon results in the formation of the 30S preinitiation complex (30S-PIC). In bacteria, mRNA generally have a Shine-Dalgarno (SD) sequence upstream of the start codon that binds a complementary sequence in the 16S rRNA known as the anti-Shine-Dalgarno (anti-SD) sequence to place the start codon in the ribosomal P-site (21, 57, 59). The start codon in the P-site base pairs with the initiator tRNA anti-

codon forming the 30S initiation complex (30S-IC) that subsequently associates with the 50S ribosomal subunit, forming a 70S ribosome (70S-IC) (56). The initiation factors dissociate leaving the initiator tRNA in the P-site and the A-site vacant to accept the first elongator tRNA.

Translation initiation can vary in several ways compared to the canonical process described above (60-62). Variations in the 5' untranslated region (UTR) of mRNA can alter how efficiently an mRNA is recruited during initiation, the number of initiation factors required, and regulation of translation from the mRNA. Leaderless mRNA lacks the 5' UTR while other mRNAs have highly structured 5' UTRs, some of which can initiate translation in the absence of initiation factors. How translation is initiated on these mRNA with non-canonical 5' UTRs is a major research focus in the field, especially how they can be appropriated for use in bioengineering and synthetic biology (62, 63).

1.6 – TRANSLATION ELONGATION IN BACTERIA

The second step of the ribosomal cycle is the successive addition of amino acids to the mRNA-encoded polypeptide, which is referred to as translation elongation (Figure 1.2). There are three stages of elongation that are repeated for each amino acid attached to the polypeptide starting with decoding, peptide bond formation, and translocation (Figure 1.7). Translation elongation is facilitated by two elongation factors (EF), EF-Tu and EF-G (14, 15, 64), that deliver aminoacylated tRNA (aa-tRNA) to the ribosomal A-site and move the ribosome along the mRNA after peptide bond formation has occurred, respectively. Each tRNA is specifically charged at the 3' acceptor stem with the cognate amino acid by aminoacyl tRNA synthetases (65). These enzymes ensure that the correct amino acid is attached to each tRNA so that the genetic code is upheld and properly decoded. The formed aminoacyl-tRNA bond is sensitive to hydrolysis under cellular conditions. EF-Tu binds to aa-tRNA to protect the aminoacyl-tRNA bond and deliver it to the ribosome (66). EF-Tu is the most abundant protein in the bacterial cell and is at a high enough concentration to saturate the aa-tRNA pool, ensuring that there are no free aa-tRNA *in vivo* (67, 68). The EF-Tu ternary complex contains EF-Tu bound to a GTP molecule and the aa-tRNA.

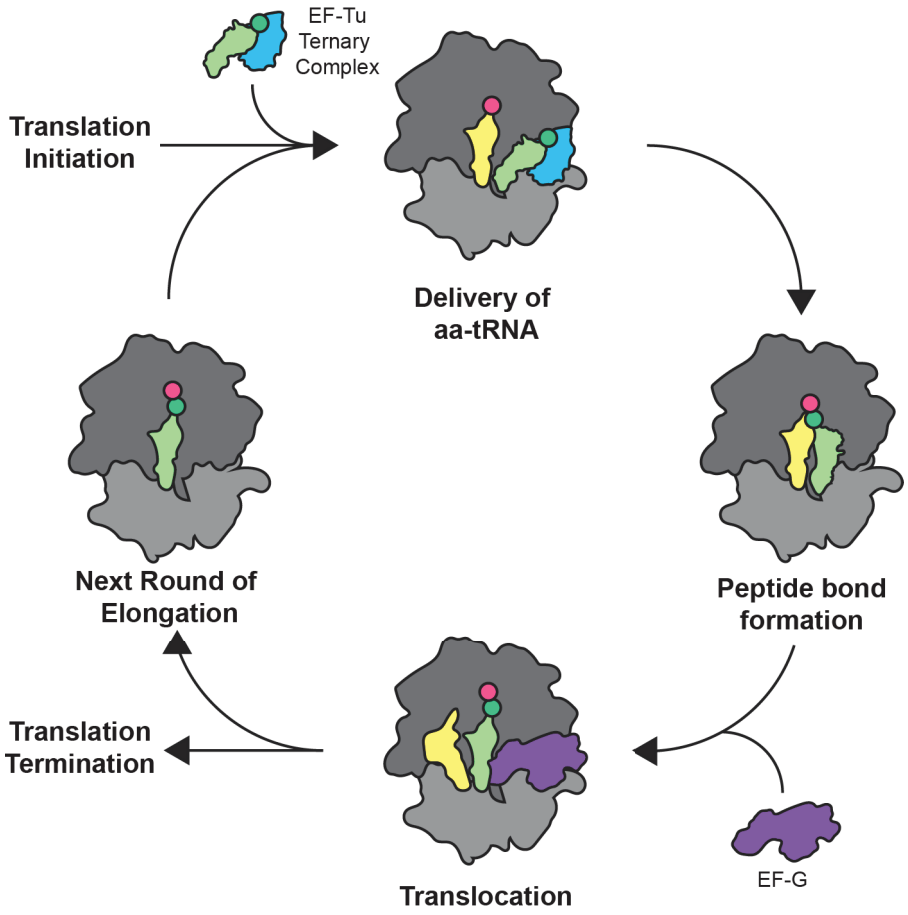

Figure 1.7 – The elongation cycle. The EF-Tu ternary complex delivers an aminoacylated tRNA to the A-site of an mRNA bound 70S ribosome. Correct codon-anticodon base pairing between the mRNA and tRNA respectively, triggers EF-Tu to release the tRNA and dissociate from the ribosome. The tRNA is accommodated into the A-site and peptide bond formation occurs by a nucleophilic attack by the amino group of aminoacyl-tRNA on the carbonyl carbon of the peptidyl-tRNA. This results in a deacylated tRNA in the P-site and a peptidyl-tRNA in the A-site. Elongation factor G (EF-G) binds to this post peptide bond formation complex and induces translocation along the mRNA, moving the peptidyl-tRNA from the A- to P-site, and the deacyl-tRNA into the E-site followed by its dissociation from the ribosome. Ultimately, this leaves the peptidyl-tRNA in the P-site with the next codon placed into the A-site to start this cycle anew, unless there is a STOP codon or no mRNA in the A-site. Should either of these be the case, translation termination or rescue mechanisms begin. (See later sections).

The ribosome recruits EF-Tu ternary complexes to the ribosomal A-site via ribosomal proteins L7/L12 which are located on the L10 stalk (69, 70). The decoding step occurs as the aa-tRNA anticodon stem loop base pairs with the corresponding mRNA codon (Figure 1.8). Correct base pairing results in conformational changes in the decoding center, specifically G530 of the 16S rRNA on the small ribosomal subunit acting as a latch, causing a larger scale domain closure in the 30S ribosomal subunit bringing the bound EF-Tu ternary complex in proximity of the SRL (71,

72). GTP hydrolysis of the EF-Tu ternary complex is triggered by the SRL, resulting in inorganic phosphate (P_i) release and a conformational change in EF-Tu (GDP-bound, inactive state) that releases the aa-tRNA and causes EF-Tu to dissociate from the ribosome (69). The aa-tRNA then accommodates into the A/A-site (anticodon stem loop in the A-site of the 30S subunit and acceptor stem in the A-site of the 50S subunit) from the A/T-site when bound to EF-Tu (71, 73). Following EF-Tu•GDP dissociation from the ribosome, the EF-Tu•GDP complex binds to EF-Ts, the GEF for EF-Tu, that triggers dissociation of GDP and association of GTP to regenerate the active complex that subsequently binds to a new aa-tRNA (15).

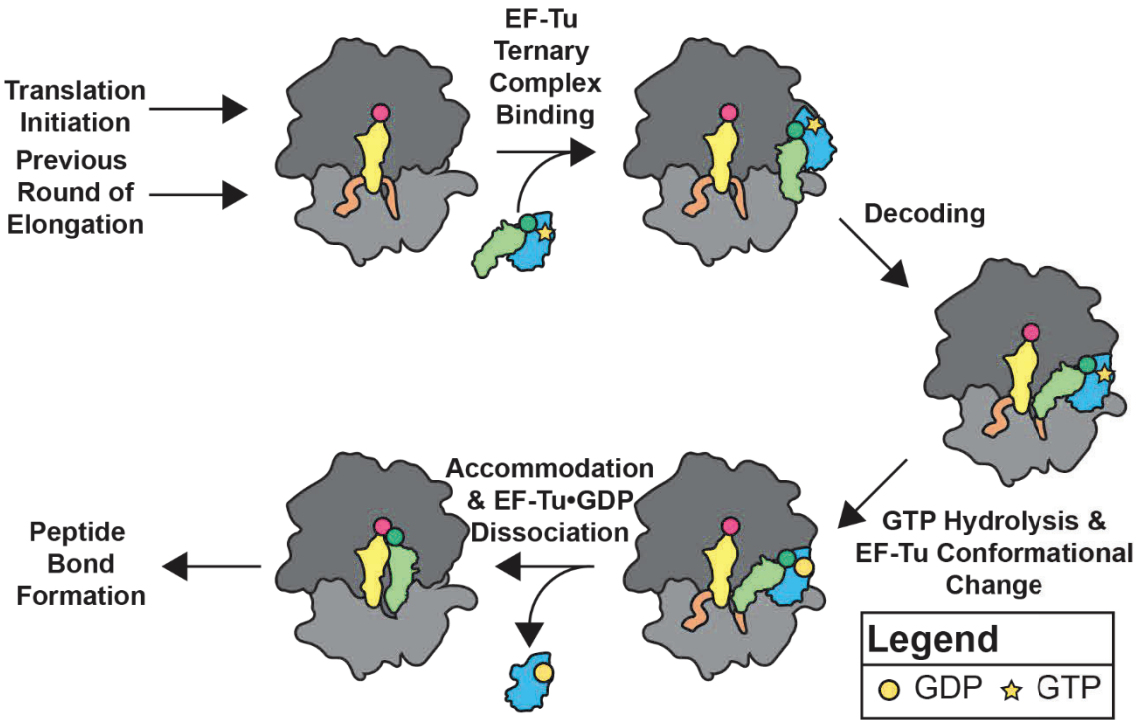

Figure 1.8 – Delivery of the aminoacylated tRNA to the ribosome. Following translation initiation or the previous round of elongation, the EF-Tu ternary complex delivers the next amino acid to the ribosome via an aminoacylated tRNA corresponding to the A-site codon. Upon formation of the codon-anticodon complex, EF-Tu is triggered to hydrolyze GTP resulting in a conformational change of EF-Tu and release of the aminoacylated tRNA into the ribosomal A-site. EF-Tu•GDP then dissociates from the complex allowing for peptide bond formation to occur.

After EF-Tu delivers the aa-tRNA to the ribosomal A-site, the acceptor stem of aa-tRNA moves into the A-site of the 50S subunit (15). The amino acid of the aa-tRNA is then in proximity to the polypeptide of the peptidyl-tRNA in the ribosomal P-site. The amine group of the amino acid attached the A-site tRNA acts as a nucleophile and attacks the carbonyl carbon of the ester bond between the P-site tRNA and polypeptide chain. A new peptide bond is formed, moving the polypeptide onto the A-site tRNA. The resulting complex contains a deacyl-tRNA in the P-site and a peptidyl-tRNA in the A-site, a complex referred to as the pre-translocation (PRE) complex.

Translocation of the tRNAs along with the mRNA is required following peptide bond formation to allow the next aa-tRNA to be delivered into the A site of the ribosome (Figure 1.9). Elongation factor G (EF-G) facilitates rapid translocation and ensures the forward movement of tRNAs by occupying the ribosomal A-site (15, 74, 75). The pre-translocation complex can fluctuate between a rotated (R) and non-rotated (N) state of the ribosomal subunits relative to each other. The rotated state involves the counter-clockwise (CCW) rotation of the 30S subunit relative to the 50S subunit. EF-G can bind to either of the two states, and consequently stabilizes the rotated state. The delivery of aminoacyl-tRNA by EF-Tu, peptide bond formation, and EF-G-mediated translocation along the mRNA are repeated for each amino acid added to the polypeptide until a stop codon is reached, followed by translation termination as detailed in the following section.

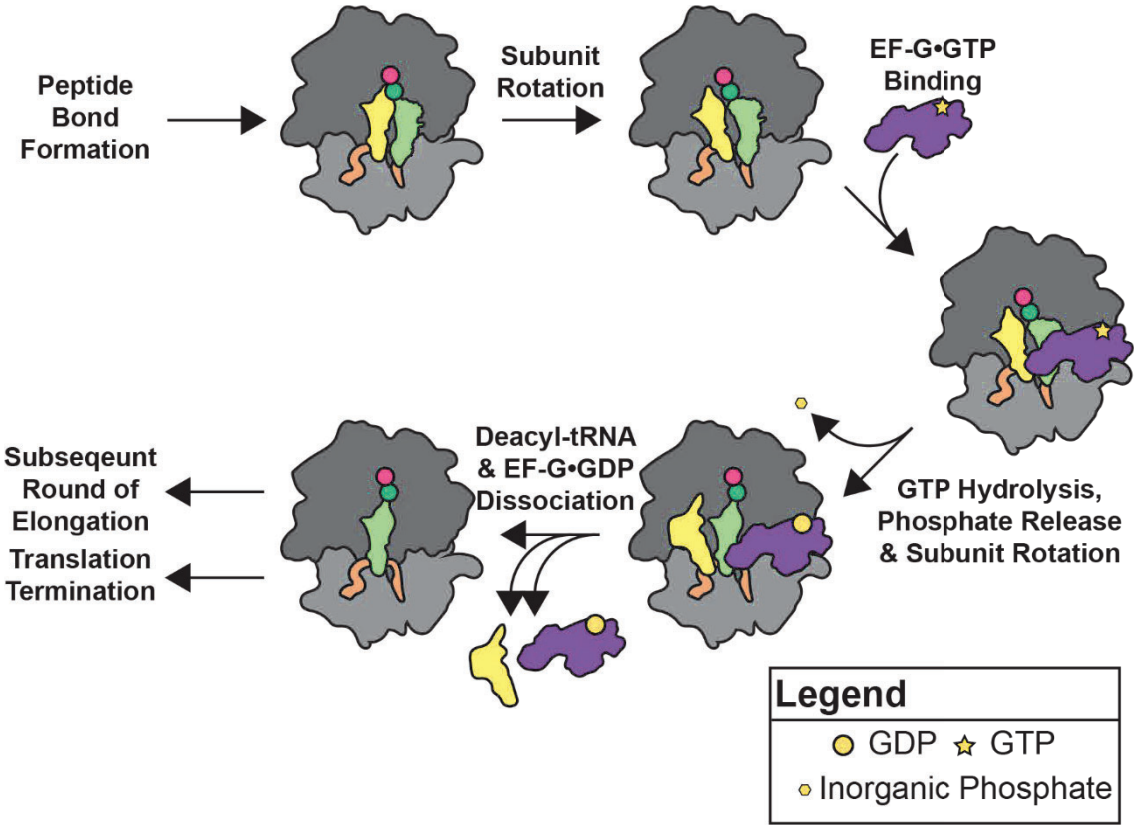

Figure 1.9 – Translocation of the ribosome along the mRNA. Following peptide bond formation, the ribosome samples two conformational states, the non-rotated (tRNAs in the A/A and P/P positions) and the rotated state (tRNAs in the A/P and P/E positions). EF-G•GTP binds preferentially to the rotated state of the 70S ribosome. Upon binding, EF-G hydrolyzes GTP to GDP and Pi release allows for the subunits to rotate back to the non-rotated state positioning the tRNAs in the P/P and E/E positions and moving the next codon into the A-site. EF-G•GDP and the deacyl-tRNA in the ribosomal E-site dissociate from the ribosome complex allowing for subsequent rounds of elongation or translation termination to occur.

1.7 – TRANSLATION TERMINATION IN BACTERIA

Termination of translation occurs when the ribosome encounters a STOP codon in the 70S ribosomal A-site, a complex referred to as the pre-hydrolysis complex (PreHC) (76, 77). The post-hydrolysis complex (PostHC) is a 70S ribosome complex with a P-site tRNA, mRNA and release factor(s) bound. Three STOP codons can signal the termination of protein synthesis, UGA, UAA, and UAG. The UAG codon is recognized by release factor 1 (RF1) while the UGA codon is recognized by RF2 and both recognize the UAA codon. Stop codon recognition is the first step of translation termination, followed by hydrolysis of the peptidyl-tRNA bond and subsequent

dissociation of the release factors (Figure 1.10). RF1/RF2 bind into the ribosomal A-site and interact directly with the stop codon through a conserved motif present in either protein, proline-glutamine-threonine (P-E-T) in RF1 and serine-proline-phenylalanine (S-P-F) in RF2. Recent structural data has shown that RF2 binds to the A-site in a compact form with the catalytic domain positioned away from the PTC (78). Successful positioning of the P-E-T / S-P-F motifs of RF1/RF2 allows the catalytic domain to reposition the glycine-glycine-glutamic acid (G-G-Q) motif into the PTC where it can promote the peptidyl-tRNA hydrolysis, thereby releasing the newly synthesized polypeptide.

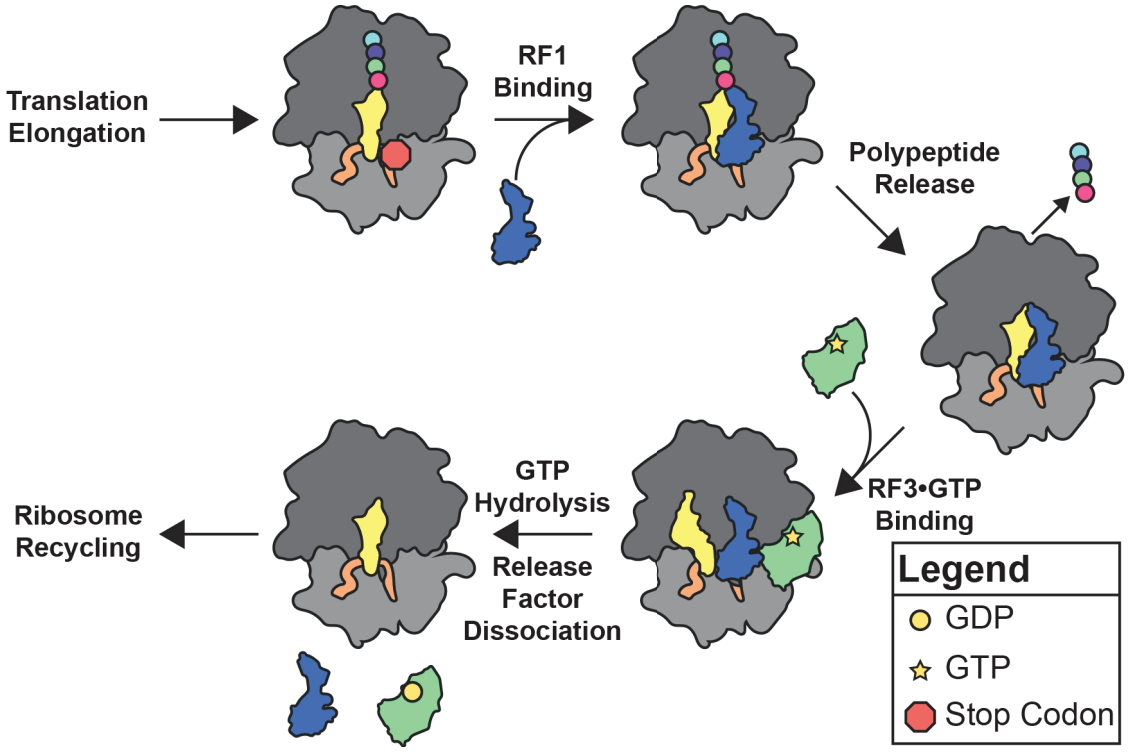

Figure 1.10 – Mechanism of translation termination. Upon reaching a STOP codon in the mRNA transcript, three steps of translation termination occur to result in the release of the newly synthesized polypeptide from the ribosome. 1) The pre-hydrolysis complex (70S with peptidyl-tRNA in the P-site and STOP codon in the A-site) is bound by either release factor 1 or 2 depending on the stop codon presented in the A-site in the first step, STOP codon recognition. 2) Following RF1/RF2 binding, domain 1 containing the conserved GGQ domain is positioned into the PTC and facilitates hydrolysis of the peptidyl-tRNA bond, resulting in the release of the polypeptide. 3) Post-hydrolysis, RF3-GDP binds to the complex, exchanges GDP for GTP, and in doing so changes conformation inducing the dissociation of RF1/RF2. GTP hydrolysis by RF3 promotes its dissociation from the complex, leaving a 70S-mRNA complex with a P-site deacyl-tRNA.

Release factor 3 (RF3) is a GTPase that binds following RF1/RF2 binding and increases the rate of RF1/RF2 dissociation from the ribosome following peptide release. RF3 is a non-essential protein in *E. coli* (79) as both RF1 and RF2 can dissociate from the PostHC without RF3, albeit RF1 has a faster dissociation rate in the presence of RF3 (76). RF3 has a higher affinity for GDP than for GTP, and as such, binds under cellular conditions to the 70S in its GDP-bound state (80). The presence of RF1 or RF2 bound to the 70S (independent of peptidyl-tRNA hydrolysis) triggers GDP dissociation and GTP association in RF3 (81) with the resulting conformational change to the GTP-bound active form that subsequently induces dissociation of RF1/RF2. Hydrolysis of GTP by RF3 promotes its own dissociation from the complex. The exact order of release factor dissociation in RF3-utilized termination has yet to be determined, yet both RF1 and RF2 can dissociate in the absence of RF3.

The ribosome dynamics during translation termination are important for dissociation of the release factors following hydrolysis. Initially, binding of RF1/RF2 stabilizes the non-rotated (N) state of the ribosome while binding of RF3 to the RF1/RF2-bound 70S complex stabilizes the rotated (R) state (76, 82). In the rotated state, the deacylated acceptor stem of the P-site tRNA moves out of the PTC (into a P/E-tRNA hybrid conformation) allowing the catalytic domain of RF2, and presumably RF1, to reposition, blocking the peptidyl transferase center (PET) biasing peptide diffusion out of the ribosome (78). This repositioning of the catalytic domain was observed in the absence of RF3. Full rotation of 30S subunit relative to the 50S, causes the catalytic domain of RF2 to collapse back onto the other domain away from the PTC, and along with rotation of the 30S head domain and helix 69 (H69) movement, induces RF2 dissociation. Presumably, the RF3 stabilized rotated state would promote RF1/RF2 dissociation by inducing 30S head rotation and H69 movement away from the decoding center, similar to what has been observed in the absence of RF3 using cryo-EM (78).

1.8 – RIBOSOME RECYCLING IN BACTERIA

Following the release of the polypeptide from the termination complex, the 70S ribosome remains bound to the mRNA with a tRNA in the P-site and the stop codon in the A-site, a complex referred to as the post-termination complex (PoTC). To allow the ribosome to partake in another round of protein synthesis, the subunits need to be recycled and removed from the bound mRNA and tRNA.

The factors involved in ribosome recycling are ribosome recycling factor (RRF) and EF-G. RRF binds to the empty ribosomal A-site followed by EF-G•GTP to initiate recycling (Figure 1.11) (83-86). The binding of RRF stabilizes the rotated state of the ribosome positioning the deacyl-tRNA in the P/E-site (anticodon stem loop in the P-site of the 30S subunit and the acceptor stem in the E-site of the 50S subunit;). Domain 1 of RRF is located in the ribosomal A-site and the P-site of the 50S subunit, while domain 2 initially is positioned on the 50S (87, 88). The movement of domain 2 toward inter-subunit bridge B2a (Helix 69 of the 23S rRNA and helix 44 of the 16S rRNA (89)) is hypothesized to be caused by EF-G binding, GTP-hydrolysis by EF-G, Pi release from EF-G, or a combination of these different events (87). Ultimately, EF-G's role in ribosome recycling is to push domain 2 of RRF against key inter-subunit bridges, thereby promoting subunit dissociation (83, 90). One study suggests that EF-G is also involved in the dissociation of mRNA during ribosome recycling (91), while other reports suggest that initiation factor 3 (IF3) is required in the late stage of ribosome recycling preventing subunit reassociation and potentially dissociation of the deacylated tRNA that remains bound post-subunit dissociation (85, 92-94). Regardless, EF-G and RRF dissociate the PoTC into 50S and 30S ribosomal subunits that subsequently can be used in further rounds of protein synthesis.

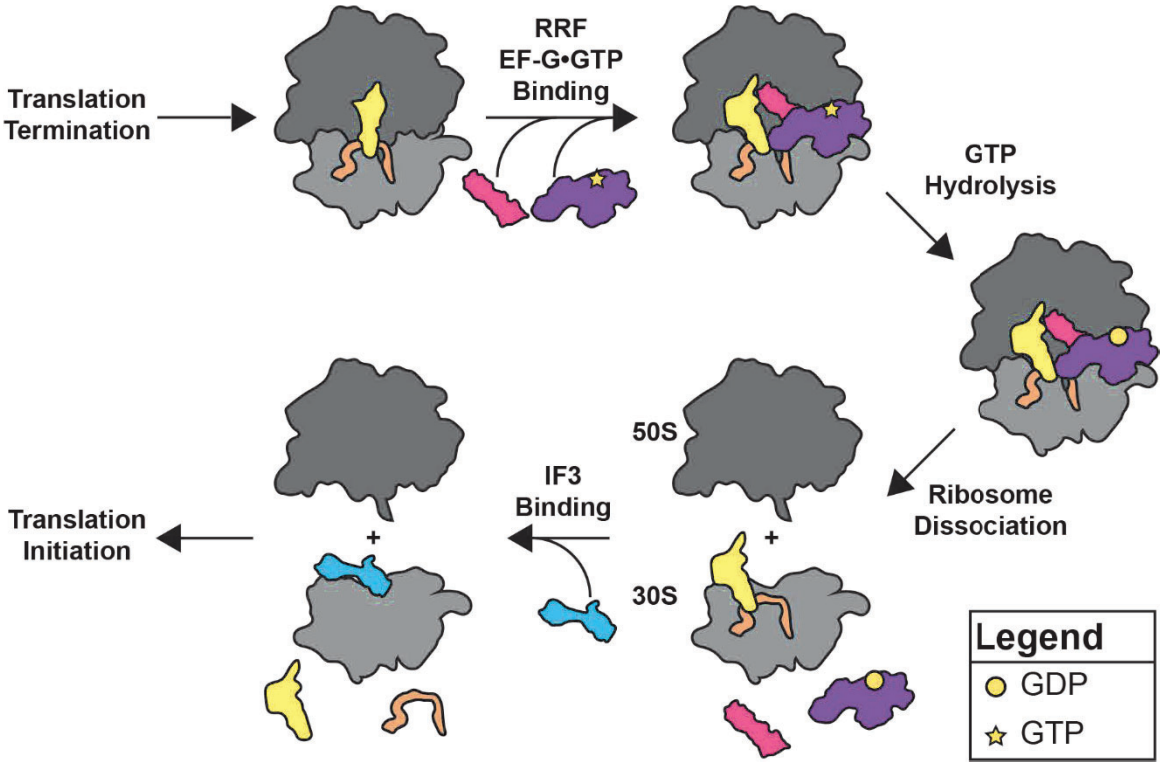

Figure 1.11 – Mechanism of ribosome recycling. Following termination and release of the polypeptide, the ribosome needs to be recycled to allow the subunits to be used in another round of translation. RRF initially binds to the PoTC stabilizing the rotated state with deacyl-tRNA in the P/E-site. Binding of, GTP hydrolysis by, and conformational change of EF-G induces RRF domain 2 to interact with and break inter-subunit bridge B2a, resulting in subunit dissociation. IF3 binds to the 30S-mRNA-deacyl-tRNA complex triggering tRNA dissociation and preventing subunit reassociation. The mRNA spontaneously dissociates allowing the ribosomal subunits to be used in another round of translation.

1.9 – RIBOSOME STALLING AND ALLEVIATION MECHANISMS

Errors in protein synthesis can occur at anytime and the cell needs mechanisms to rectify the situation, especially under conditions of cellular stress. The accumulation of stalled ribosomes in the cell depletes the cellular ribosome pool, thereby reducing the protein synthesis capacity and indirectly stalling any trailing ribosomes on the same mRNA. Cells have several quality control mechanisms to rescue stalled translation from non-stop and no-go translational events (95, 96). Non-stop translational events occur when the ribosome either reaches the end of an mRNA that is devoid of a stop codon due to truncation, or erroneously translated through the stop codon. In this case, canonical translation termination and ribosome recycling does not occur, leaving the newly

synthesized polypeptide connected to the ribosome and the ribosomal subunits unable to undergo another round of synthesis. To overcome non-stop translational events, the bacterial cell has one or more systems in place that can facilitate ribosome recycling including tmRNA/SmpB, ArfA, and ArfB (95-98).

When the ribosome reaches the end of an mRNA and there is no codon in the A-site to base pair with a tRNA, the trans-translation system is typically utilized in all bacteria. Trans-translation is carried out by a long non-coding RNA (lncRNA) known as transfer-messenger RNA (tmRNA) and the small basic protein SmpB. tmRNA (also known as 10S RNA or SsrA) is a highly structured RNA that mimics both a tRNA and mRNA (97, 98). The tRNA-like domain (TLD) is aminoacylated with an alanine and interacts with EF-Tu to form a ternary complex but does not contain an anticodon stem-loop (99, 100). The tmRNA, EF-Tu•GTP, SmpB quaternary complex binds to the empty ribosomal A-site where SmpB binds into the decoding center and the TLD of tmRNA is positioned into PTC to allow for peptide bond formation to occur (97, 98). The C-terminus of SmpB interacts with the mRNA channel ensuring that the quaternary complex only binds in the absence of mRNA (97, 101). GTP hydrolysis by EF-Tu releases tmRNA•SmpB into the ribosomal A-site as it does during canonical translation elongation (see *Section 1.6 – Translation elongation in bacteria*).

Once the tmRNA•SmpB has been delivered and the polypeptide has been transferred to the tmRNA, EF-G facilitates translocation of tmRNA•SmpB into the P-site and in doing so, positions the mRNA-like open reading frame (ORF) of the tmRNA into the ribosomal A-site (99, 102, 103). Translation elongation proceeds as normal along the tmRNA ORF until the stop codon is reached and translation termination occurs. The ORF on the tmRNA encodes a 10 amino acid peptide that along with the alanine residue on the tmRNA, tags the synthesized polypeptide for protease degradation. If an mRNA was truncated prematurely, the cell degrades the polypeptide to avoid the risk of toxic effects the truncated protein may have. If the trans-translation system is damaged or overwhelmed several alternative rescue mechanisms have been discovered including ArfA•RF2-mediated rescue, ArfB, ArfT, RqcH, and ResQ (104-110) can be utilized by the cell. Briefly, ArfA, or Alternative ribosome rescue factor A, binds to a ribosome with a peptidyl-tRNA in the P-site but

no mRNA in the A-site, similar to the trans-translation system (111-114). The C-terminus of ArfA binds into the empty mRNA channel positioning the N-terminus in the 30S A-site. Upon ArfA binding, RF2 binds and positions its GGQ motif into the PTC to hydrolyze the peptidyl-tRNA bond as it does during canonical translation termination (see *Section 1.7 – Translation termination in bacteria*). The release of the polypeptide and subsequent release of RF2 and ArfA allows the ribosome to be a target for the canonical ribosome recycling machinery (see *Section 1.8 – Ribosome recycling in bacteria*).

No-go translational events occur when the ribosome pauses before reaching the STOP codon. This typically occurs under nutrient deprivation conditions, where the cell is lacking nutrients required to maintain cellular growth. Under such conditions, the amount of aminoacylated tRNAs present in the cell is reduced, thereby lowering the cellular concentration of EF-Tu ternary complexes (115). Low levels of EF-Tu ternary complexes lead to slowing and can cause halting of translation if availability of a ternary complex required for decoding of a particular codon is limiting. Under such conditions, RelA otherwise known as (p)ppGpp Synthase I, binds to the unoccupied ribosomal A-site of ribosomes stalled mid-elongation (116-118). The binding of deacylated tRNA to the RelA•70S elongation complex induces RelA to bind ATP and either GTP or GDP. RelA can synthesize guanosine tetraphosphate (ppGpp) or guanosine pentaphosphate (pppGpp) by transferring to the β and γ-phosphates from ATP to GDP or GTP, respectively (119, 120). ppGpp and pppGpp are collectively referred to as (p)ppGpp or the alarmone nucleotides and are responsible for the stringent response adaption pathway in bacteria. Production of (p)ppGpp causes changes in the cellular transcriptome and metabolic pathways to allow the cell to adapt to the stress. Stringent response has been shown to be important for bacterial stress survival, antibiotic resistance, and virulence (121-123).

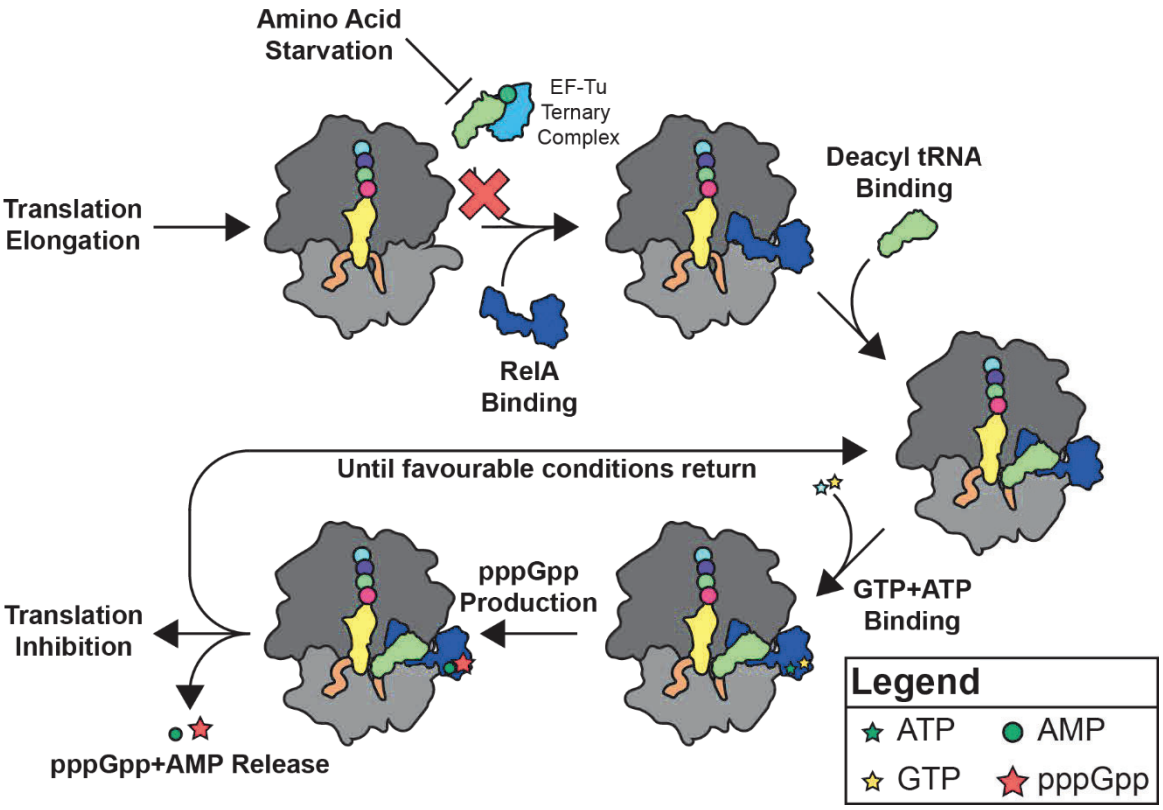

Figure 1.12 – Stringent response effect on translation. Under nutrient starvation conditions, such as amino acid starvation, a decrease in aminoacylation of tRNAs and the corresponding increase in deacyl-tRNAs leads to vacant A-sites of translating ribosomes. RelA binds to the vacant A-site followed by a deacylated tRNA triggering the binding of GTP and ATP to RelA. The binding of both nucleotides is followed by the transfer of the β and γ phosphates from ATP to the 3' hydroxyl group of the bound GTP molecule forming the alarmone pppGpp. pppGpp and AMP dissociate from the stalled 70S•RelA•tRNA complex and pppGpp inhibits the function of GTP binding proteins and induces the expression of stress response operons. Furthermore, the binding RelA•tRNA to the ribosome prevents any further rounds of peptide elongation should any of the corresponding aminoacylated tRNA be present.

1.10 – RIBOSOME HIBERNATION IN BACTERIA

Bacterial cells can persist through harsh conditions by going dormant or into a dormant-like state (124-126). Dormancy requires the cell to 1) conserve energy and 2) have the ability to quickly leave dormancy when conditions are favourable for growth. Protein synthesis and ribosome biogenesis are the most energy demanding processes in the cell utilizing approximately 90% of the cellular ATP reserves, and as such inactivation of translation coupled with prevention of ribosome degradation are critical for energy conservation and ultimately for dormancy (127-129). Recovery from dormancy occurs within minutes (130, 131). Ribosome degradation is one strategy of

preventing translation, however, it is energetically costly to produce new ribosomes following the return to favourable conditions. Furthermore, substantial assembly time is required preventing the cell from taking advantage of the emerging favourable conditions (132-135). In addition, degradation of too many ribosomes would be detrimental to the cell by limiting the cellular translational capacity required for cell growth. To withstand cellular stress, bacterial cells utilize a system of ribosomal inactivation that prevents ribosome degradation and that can easily be reversed to start protein synthesis immediately after favourable cellular conditions are present. This process is called ribosome hibernation (136).

Ribosome hibernation machinery in *E. coli* involves three different proteins; ribosome modulation factor (RMF), hibernation promoting factor (HPF), and YfiA (137, 138). RMF and HPF bind to a 70S ribosome causing dimerization with another RMF/HPF bound 70S ribosome forming a 100S ribosome dimer (Figure 1.13). The 100S ribosome dimer remains translationally inactive until cellular conditions improve and 100S dimers are released back into 70S ribosomes or into 50S/30S ribosomal subunits to allow protein synthesis to resume. It has been shown that EF-G and RRF are required for recycling 100S ribosomes in addition to their role in 70S ribosome recycling (139), however, a recent study has shown that the universally conserved GTPase HflX is also involved in facilitating 100S dissociation in *Staphylococcus aureus* (140). Currently, evidence suggests that in *S. aureus* the EF-G/RRF-mediated 100S disassembly is the general pathway, while *S. aureus* HflX (SaHflX) is upregulated under heat stress and likely involved in 100S disassembly under these conditions (139, 140). Currently the exact order of hibernation factor binding and ribosome dimerization along with the order of disassembly of the 100S dimer are poorly understood, Furthermore, it is unclear if HflX orthologs in other species can split the 100S ribosome. For further discussion to the involvement of HflX in dissociation of the 100S ribosome see *Section 1.12.4 – Role of in Ribosome Hibernation*.

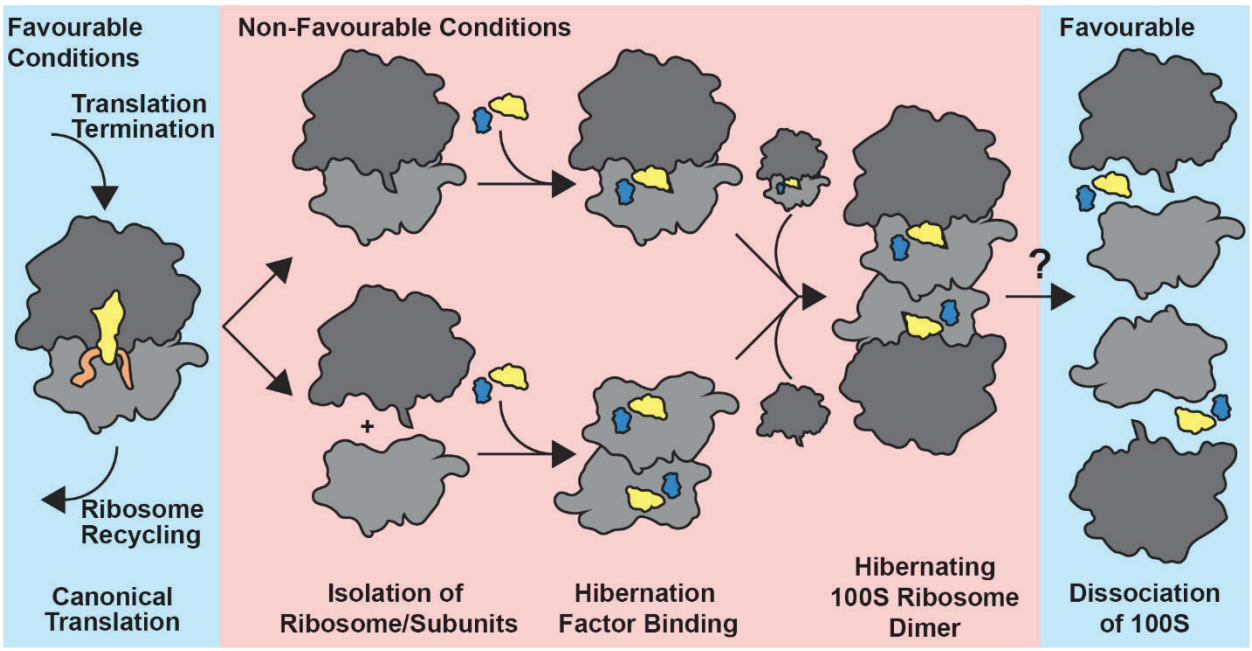

Figure 1.13 – Ribosome dimerization during translational dormancy in *E. coli*. Following translation termination under non-favourable growth conditions, the 70S ribosome is removed from the mRNA or split into 50S and 30S ribosomal subunits. Hibernation factors, RMF (Blue) and HPF (Yellow), bind to a vacant 70S ribosome or 50S/30S ribosomal subunits inducing dimerization of two 70S ribosomes into the 100S ribosome dimer. Upon the return of favourable growth conditions, the 100S ribosome dimer is split into 70S ribosomes or 50S/30S ribosomal subunits and the hibernation factors dissociate to allow for translation initiation to resume. This process of dissociating the 100S ribosome dimer is thought to be facilitated by the GTPase HflX.

The 100S ribosome dimer has several species-specific differences. Comparison of the 100S in the gram-positive bacterium *S. aureus* and the gram-negative bacterium *E. coli* highlights the differences in the factors involved in dimerization and the overall structure of the 100S dimer. *E. coli* 100S ribosomes require two hibernation factors, RMF and HPF (EcRMF and EcHPF) while in *S. aureus* no RMF homolog is present (129, 141, 142). The HPF homolog in *S. aureus* (SaHPF) is longer than *E. coli* HPF (EcHPF) and the N-terminal region of SaHPF shares high levels of similarity with EcHPF (Figure 1.14A) (143, 144). Structurally, the 100S ribosome dimer differs between the *S. aureus* and *E. coli* 100S dimers (Figure 1.14B). In *E. coli*, the 70S ribosomes that form the dimer are arranged such that the intersubunit bridge between either 30S subunit are facilitated by ribosomal proteins bS1 with uS4 and uS2 with uS3 (138, 145). In gram positive bacteria, dimerization requires the interaction between HPF bound to either 70S along with the 16S rRNA forming intersubunit bridges. The *S. aureus* 100S structure contains two 70S ribosomes

rotated 180° relative to each other (Figure 1.14B) (146). Additional intersubunit bridges between the 16S rRNA of one 70S and HPF and uS2 of the other 70S particles mediate dimerization. This is also observed in *Lactococcus lactis* 100S ribosomes, while in *B. subtilis* uS2 also form interactions with bS18 (147, 148). Although the intersubunit bridges are mediated by different proteins and rRNA in gram positive and negative 100S structures, they share an overlapping dimerization site. The functional importance of dimerization via the solvent exposed side of the 30S subunit is currently unknown but has been hypothesized to protect a vulnerable region of the rRNA and labile proteins, or potentially preventing RNAP from binding (129, 149, 150).

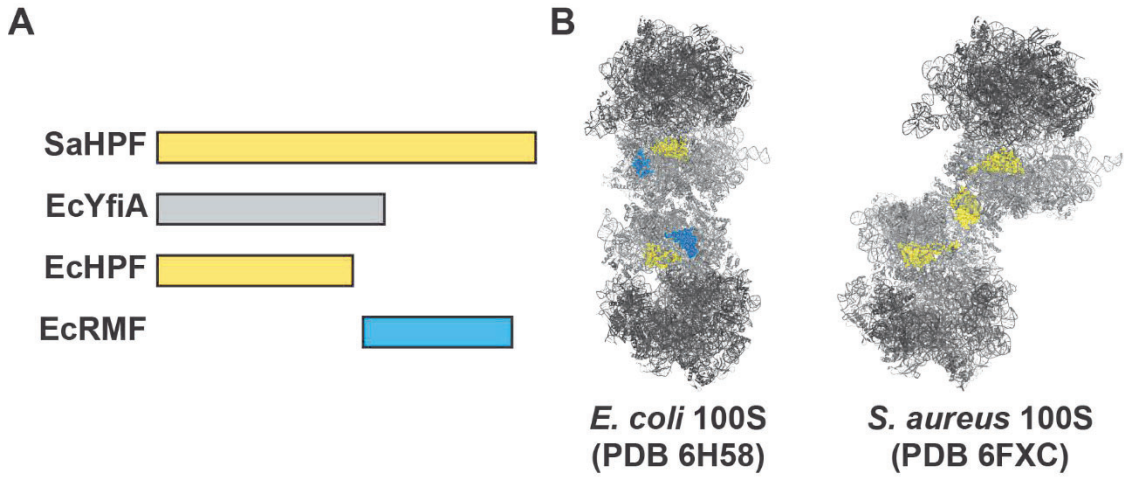

Figure 1.14 – Ribosomal hibernation factors and the 100S ribosome dimer. A) Graphical alignment of hibernation factor genes in *E. coli* and *S. aureus*. Hibernation factors are coloured as they appear in panel B, aside from EcYfiA that is not depicted in panel B. (Panel A adapted from Basu *et al*., NAR, 2016). EcRMF shows homology to the C-terminal portion of SaHPF. B) Structures of the Ec100S and Sa100S ribosome dimers. Large and small ribosomal subunits shown in dark and light grey, respectively. EcHPF and SaHPF shown in yellow and EcRMF shown in blue. PDB structures 6H58 and 6FXC.

In addition to the hibernation factors described previously, the protein YfiA is also involved in silencing translationally active ribosomes in *E. coli* (151, 152). YfiA, otherwise known as pY in some organisms, does not induce 100S formation except in *L. lactis* (153). Structural information of YfiA bound to the 70S ribosome suggests that it overlaps with the binding site of HPF in several organisms suggesting that YfiA and HPF compete for inactivation (138, 154). Why both systems for inactivation exist is not currently understood. However, the one likely acts as backup for the

other, much as the ArfA•RF2 and ArfB systems act as a backup to the trans-translation system (see *Section 1.9 – Ribosome stalling and alleviation mechanisms*).

Ribosome hibernation is connected to the stringent response mechanism described in section 1.9 as the alarmone (p)ppGpp plays several roles in modulating different hibernation factors. (p)ppGpp is, for example, required for the transcription of the *rmf* and *hpf* genes (155-157). Furthermore, (p)ppGpp has been shown to modulate the activity of both EF-G and HflX (139, 140). Overall, (p)ppGpp plays an integral role in facilitating bacterial persistence through different stresses including nutrient deprivation, antibiotic stress, host colonization, dark adaptation, and biofilm formation (128). The formation of the 100S ribosome dimer serves not only to inhibit further protein synthesis, but also to protect the ribosomes until favourable conditions are present again. Interestingly, 100S ribosomes can be found in eukaryotes as well, specifically the chloroplasts of plants and in nutrient-deprived cancer cells, opening many more questions from how 100S ribosome formation and disassembly is regulated and what factors are involved in each organism (144, 158).

1.11 – YCHF: THE CONSERVED ATPASE IN THE GTPASE FAMILY

(Adapted from Cellular Roles of the human OBG-like ATPase 1 (hOLA1) and its YchF homologs by Nirujah Balasingam, Harland E. Brandon, Joseph A. Ross, Hans-Joachim Wieden, and Nehal Thakor as described in 1.1 – PREFACE)

YchF is a unique member within the Obg family of TRAFAC class GTPases as it preferentially binds and hydrolyzes ATP over GTP (31, 159, 160). This makes it the only G-protein known to use another energy pool in the cell, an enzymatic feature whose functional implications have not been determined. YchF contains the same G-motifs found in other G-proteins except for a non-canonical G4 motif found in YchF homologs (NKxD in canonical GTPases; NVNE in *Escherichia coli*; NMSE in yeast; NLSE in humans) (159). The human homolog, human obg-like ATPase 1 (hOLA1) shares 45% sequence identity and 62% sequence similarity with the *E. coli* homolog (EcYchF) and utilizes ATP preferentially. There are some reported homologs of YchF,

notably rice (*Oryza sativa*), OsYchF1, is able to utilize both ATP and GTP (161). The functional role that ATP utilization of YchF is not known.

1.11.1 – SEQUENCE AND STRUCTURE OF YCHF

Structural information for YchF is available from crystal structures of *Homo sapiens* (hOLA1), *Haemophilus influenzae* (HiYchF), *Schizosaccharomyces pombe* (SpYchF), and two of *Thermus thermophilus* (TtYchF) (162). The G domain of YchF/hOLA1 is separated in the primary sequence by an inserted coiled-coil domain and followed by a TGS domain (Figure 1.15). Like other Obg family GTPases, YchF possess a C-terminal RNA-binding domain, the TGS (ThrRS, GTPase, SpoT) domain and an additional glycine-rich motif (GAxxGxGxGxxx(I/L/V)) following the switch II region (Walker B motif; except NogI) (11). The G-domain bridges the coiled-coil and TGS domains, forming a positively charged cleft that has been proposed to bind nucleic acids (159). The nucleotide (i.e. GTP/ATP) binding pocket is located opposite the cleft. Furthermore, YchF is a member of the HAS-GTPase family in which the canonical catalytic glutamine is substituted with a hydrophobic amino acid, such as Isoleucine or Leucine in the case of YchF and hOLA1, respectively (163). As such, HAS-GTPases utilize an alternative mode to catalyse GTP hydrolysis (26, 27). Recently, using molecular dynamics and biochemical analysis, Rosler and coworkers determined the catalytic residue of EcYchF to be histidine 114 (histidine 134 in hOLA1), located in a flexible loop of the G-domain not resolved in the crystal structure (163). This catalytic histidine is conserved across all homologs. Overall, based on the sequence identity and similarity, conservation of important residues (Appendix Figure 1.1), and similar structural fold, it is likely that YchF and hOLA1 have maintained corresponding functional roles in bacterial and human cells.

P-loop NTPases typically have different conformations based on whether the tri- or di-phosphate form of the nucleotide is bound (164). Structural data for YchF homologs in both tri- and di-phosphate forms have been reported previously. The TtYchF crystal structure was obtained in both the *apo*-state and the GDP-bound state, as YchF was initially annotated to be a GTPase based on sequence homology. Additionally, the structure of the rice homolog (OsYchF1) has been solved in the *apo*, GDPNP-, and ADPNP-bound states (161). Although the sequences are highly

conserved, the sequence differences that do exist between YchF homologs allow for some species-specific interactions, such as the interaction between OsYchF1 and the membrane associating GTPase activating protein 1, OsGAP1, in rice (161, 165). Interestingly, the serine residue in EcYchF (S16; *E. coli* numbering) involved in phosphorylation is conserved across species while the cysteine residue (C35; *E. coli* numbering) implicated in YchF dimerization is missing in some organisms but is present in both *E. coli* and humans (Appendix Figure 1.1).

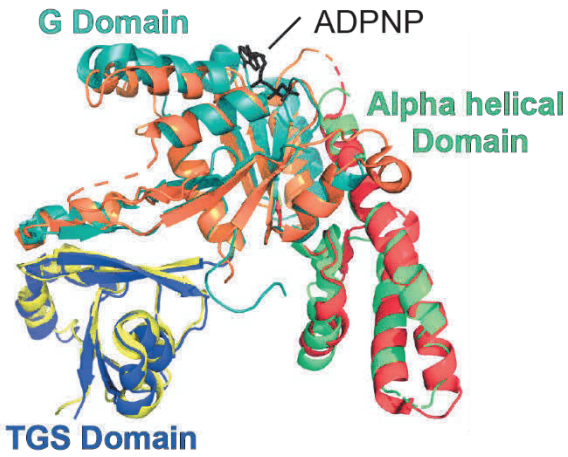

Figure 1.15 – Structural comparison of hOLA1 and *H. influenzae* HiYchF. Crystal structures of the hOLA1-AMPPCP (PDB 2OHF) and HiYchF (PDB 1JAL) were aligned using pymol. No nucleotide was present in the crystallization of HiYchF. Both structures can be superimposed with minimal deviation (RMSD = 1.520). The three domains that are found in all YchF homologs are highlighted as follows: the G-domain is orange in HiYchF and teal in hOLA1, the alpha-helical domain is red in HiYchF and green in hOLA1, and the TGS-domain is yellow in HiYchF and blue in hOLA1. Differences in nucleotide bound states have previously been shown to induce structural changes within the G-domain of YchF (163), and it is presumed that these nucleotide-dependent changes give rise to the slight deviations in the aligned structures. The bound AMPPCP from the hOLA1-AMPPCP crystal structure is shown as black sticks bound to the G-domain. Adapted from Figure 2 in Balasingam *et al*. (1).

Bacterial YchF has been implicated in a number of cellular processes, ranging from protein synthesis (162, 166) and ribosome biogenesis (162) to regulation of iron usage (161, 167) and oxidative stress response (168). Of these, oxidative stress response and the interaction with translation components are regulatory functions that YchF has in common with hOLA1 (169, 170).

1.11.2 – ROLE IN OXIDATIVE STRESS

In both *E. coli* and human cells (HeLa and BEAS-2B cell lines), overexpression of YchF or hOLA1 respectively confers a greater sensitivity of cells to oxidative stress (171, 172). It was recently shown in *E. coli* that cysteine-35 of EcYchF allows for dimerization under oxidative conditions, which reduces the ATPase activity of EcYchF (168). This cysteine is conserved in most other species, including hOLA1 (Appendix Figure 1.1), suggesting that dimerization of hOLA1 is also possible, but this has not yet been confirmed. Furthermore, *E. coli* expressing an ATPase-deficient variant of YchF do not display hypersensitivity to hydrogen peroxide, suggesting that ATP hydrolysis is required for the inhibition of oxidative stress response (171).

It has been shown that EcYchF interacts with antioxidant enzymes KatG, KatE, and AhpCF (Appendix Table 1.1) under non-stress conditions (171), potentially inhibiting their function until needed. Under oxidative stress, the dimerization of YchF presumably results in the release of bound antioxidant enzymes, allowing for these enzymes, such as catalase KatG, to detoxify the cell of hydrogen peroxide. This would suggest that YchF can regulate endogenous hydrogen peroxide concentrations through its control of these antioxidant enzymes. The inactivated YchF homodimer can then interact with thioredoxin 1 (TrxA) or other redox controlling enzymes (Appendix Table 1.1) which reduce the cysteines involved in dimerization, returning YchF to its monomeric state where it can once again inhibit oxidative stress response (168). Interestingly, the Koch lab proposes that YchF and homologs may have evolved to utilize ATP over GTP due to guanine being particularly sensitive to oxidation (168). Additionally, the cellular level of ATP rises upon oxidative stress, most-likely due to the inhibition of processes using ATP (173). This raises the question why in some organisms the YchF/hOLA1 homologs can utilize ATP and GTP. The rice homolog, OsYchF1, is one such homolog where ATP binding has been shown to be important for biotic stress response but not abiotic stress, while the opposite is true for GTP (161).

1.11.3 – INTERACTION BETWEEN YCHF AND THE RIBOSOME

The interaction between YchF and the bacterial ribosome is the most extensively characterized of its proposed functional roles *in vivo*. In *E. coli*, YchF has been shown to interact with the ribosome, suggesting a role in translation and/or ribosome biogenesis (174), while in *Arabidopsis thaliana* the YchF homolog (AtYchF) has been confirmed to be involved in ribosome biogenesis (175). Polysome profile analysis found that YchF co-fractionates with the 50S ribosomal subunit and the 70S ribosome in *E. coli* (176), and with the 60S/40S ribosomal subunits, the 80S ribosome, and polysomes in *T. cruzi* (160). This interaction suggests a functional role for YchF on the ribosome during protein synthesis or potentially during ribosome biogenesis. Furthermore, an unknown component of the 70S ribosome stimulates the ATPase activity of YchF, indicating that, in bacteria, the 70S ribosome acts as a GAP-like factor for YchF (174). However, it is unclear whether YchF binds to the canonical GTPase binding site near the ribosomal A-site or elsewhere

on the ribosome, or a precursor ribosomal particle. Details regarding the exact binding site of YchF on the bacterial ribosome and mechanistic insights into YchF's functional role on the ribosome are discussed in Chapter 2 of this thesis. Currently, it is not known at what stage of the ribosome cycle (Figure 1.2) YchF is involved or what its functional role when bound to the ribosome is. Further work is needed.

1.11.4 – INVOLVEMENT IN PROTEIN DEGRADATION

Previous studies in *T. cruzi* have also shown that TcYchF interacts with the proteasome and go on to speculate that YchF bridges the ribosome and proteasome, allowing for degradation of proteins damaged during synthesis (160). Furthermore, the yeast homolog of YchF (YBR025c) was also implicated in interacting with the 26 S proteasome via *in vivo* protein-protein cross-linking followed by mass spectroscopic analysis (177). The functional implications for YchF interacting with the proteasome have not been further characterized to date but would provide an interesting link between protein synthesis and degradation. One potential mechanism follows: during oxidative stress, damage could occur to the translation machinery or the protein being synthesized. YchF would bind to the damaged ribosome, or to the ribosome with the damaged-polypeptide, and recruit the proteasome to degrade the polypeptide before it can cause any negative downstream effects and/or allow repair of the ribosome.

1.11.5 – CELLULAR ROLES OF HOLA1

Koller-Eichhorn *et al*. identified the human homolog of bacterial YchF by phylogenetic analysis of Obg-related proteins (159). This uncharacterized protein was named human Obg-like ATPase 1 (hOLA1) (159, 178). The same study reported another uncharacterized protein that is only found in higher eukaryotes: the human GTP-binding protein (GTPBP10) (159, 178). However, the function of GTPBP10 has not yet been elucidated. hOLA1 is well conserved across all domains of life, sharing 45% sequence identity and 62% sequence similarity with EcYchF. This suggests functional conservation of YchF/hOLA1 across all domains of life, something normally characteristic of ribosomal proteins (179). Like EcYchF, hOLA1 preferentially utilizes ATP over GTP

(159). Accordingly, hOLA1 is a regulatory protein that likely changes conformation depending on whether ATP or ADP is bound, presumably while interacting with effector protein(s), to carry out its downstream function(s) (159). While the bacterial ribosome triggers ATP hydrolysis for EcYchF, it is not known if the effector protein that bind to hOLA1, or the human ribosome, are able to trigger ATP hydrolysis, resulting in the ATP to ADP conformational change.

Several studies have implicated hOLA1 in the regulation of numerous cellular processes during stress conditions, such as oxidative stress response, heat shock, protein synthesis, integrated stress response (ISR), cell cycle regulation, and cancer metastasis (159, 180-183). Sun *et al.* reported that hOLA1 is overexpressed in many different cancers, such as colon, rectum, stomach, lung, ovary and uterus (184). hOLA1 is also regulated by DNA damage, as the levels of hOLA1 are downregulated in cells treated with DNA damaging agents. However, ER stress-inducing agents do not affect the level of hOLA1 (184). Therefore, hOLA1 was initially dubbed DOC45 (DNA damage-regulated overexpressed in cancer 45) by Sun *et al*. However, the mechanism by which genotoxic compounds regulate the expression of hOLA1 is not yet clear (184). Additionally, Sun *et al.* (2010) reported that DOC45 is overexpressed in cells expressing oncogenic proteins, such as H-Ras and R-Ras2. These proteins are known to activate the phosphoinositide 3-kinase (PI3K) pathway, suggesting that expression of hOLA1 is linked to the PI3K pathway. Around the same time as the study of DOC45 by Sun *et al.* (2010), structural and functional aspects of hOLA1 were published by Koller-Eichhorn *et al*. (2007).

hOLA1 has been implicated in translation initiation in humans (170). In bacteria, however, translation initiation occurs by a mechanism that primarily entails the binding of the 30S ribosomal subunit to the three bacterial initiation factors (IF1-3) and the initiator tRNA fMet•tRNA^{fMet} (56). Following the 30S-initiation factor complex formation, the 30S subunit binds to the Shine-Dalgarno sequence in the 5’ untranslated region of the mRNA before selection of the start codon. This mechanism differs greatly from that employed by mammalian cells. Notably, the eIF2α-initiator tRNA complex—the formation of which hOLA1 represses in humans—differs significantly from its bacterial counterpart. Further studies are required to determine the binding site of hOLA1 on eIF2. Moreover, the mechanism by which hOLA1 might facilitate hydrolysis of eIF2-bound GTP is

unclear. It would be interesting to study whether hOLA1 directly hydrolyzes GTP bound to eIF2, stimulates eIF2s GTPase activity, or functions as an exchange factor removing the GTP from eIF2 and then allowing GDP to bind eIF2α. Alternatively, hOLA1 may prevent either nucleotide exchange (GDP to GTP on eIF2) or hydrolyze all the local GTP prior to GTP binding to eIF2. To date, there is no evidence suggesting that other YchF homologs interacts with IF2 or fMet•tRNA^{fMet} to regulate translation initiation. Furthermore, the observation that both YchF and hOLA1 interact with the 70S/80S ribosome and polysomes, respectively, supports the hypothesis that both factors are involved in a step(s) downstream of translation initiation. However, no exact functional role outside of translation initiation has been postulated yet. Currently, it is not known if the human cytosolic or mitochondrial ribosomes can act as a GAP for hOLA1.

Cells are often challenged by diverse stresses, such as hypoxia, oxidative stress, and nutrient deprivation. A failure of cells to respond to such stresses can lead to severe disease states, such as cancer. hOLA1 plays crucial roles in tumorigenesis, antioxidant suppression, inhibition of global protein synthesis, cell cycle regulation, cell migration, invasiveness, and cell adhesion (172, 180, 185-187). An important hallmark of cancer cells is persistent survival under various stress conditions. As hOLA1 is implicated in the cellular response to such conditions, hOLA1 may represent a novel therapeutic target for cancer treatment.

1.12 – HFLX: THE GTPASE THAT SPLITS THE RIBOSOME

1.12.1 – SEQUENCE AND STRUCTURE OF HFLX

HflX is one of eight universally conserved GTPases found in all domains of life (12, 164). While HflX is present in all domains of life, there are several notable examples of organisms that lack HflX including Methanobacterium, Mycoplasma, ε-proteobacteria, spirochaetes, and fungi (164). The most extensively studied bacterial ortholog is from *Escherichia coli* (EcHflX) which shares 28% identity and 46% similarity with the human ortholog (GTPBP6 or HsHflX in this thesis). A sequence alignment of HflX orthologs that have previously been studied reveals conservation of domain arrangement and key functional regions across all domains of life (Appendix Figure 1.2).

Conservation on the sequence and structural level (detailed below) suggests that the functional role of HflX may also be evolutionarily conserved, yet there exist organism-specific differences.

The first 3 dimensional structural information on HflX was obtained by x-ray crystallography of the archaeal ortholog in *Sulfolobus solfataricus* (SsoHflX) (188). SsoHflX contains three domains, with the C-terminal domain being a canonical P-loop containing G domain present in all GTPases (Figure 1.16). The two N-terminal domains were initially considered to be one domain collectively referred to as the "HflX domain" because of its uniqueness to HflX orthologs (188). In this thesis, only the first of these two domains will be referred to as the HflX domain, while the second domain comprised of two alpha helices will be referred to as the linker domain. Recent evidence suggests that the HflX domain and the linker domain harbour a second nucleotide binding site in addition to the conserved guanine nucleotide binding site found in the G domain (189, 190). Furthermore, the HflX and linker domains undergo a conformational change relative to each other in the presence of ADPNP (non-hydrolysable analog of ATP) (191) supporting that these are independent domains of HflX.

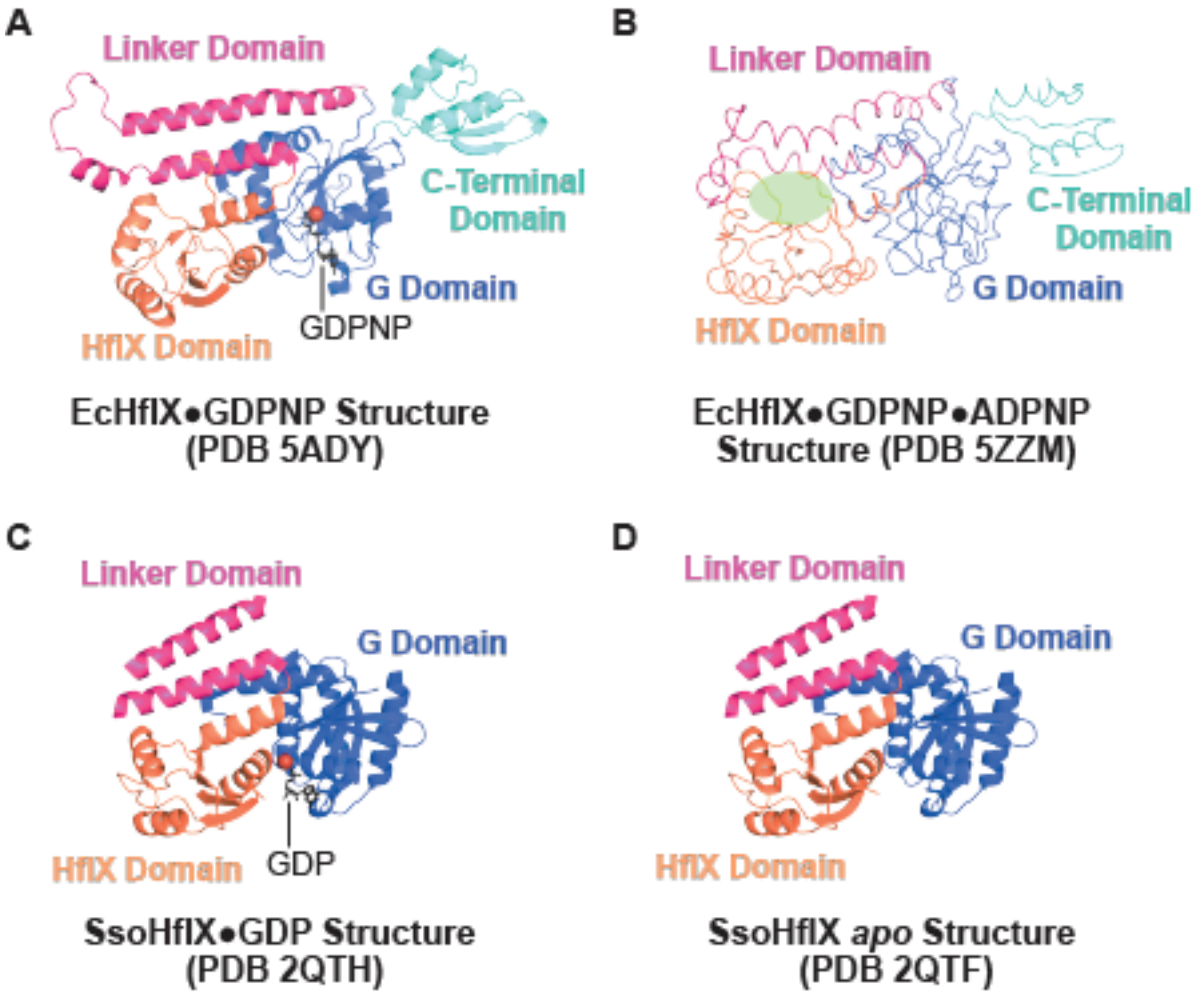

Figure 1.16 – Structural model of the archaeal and bacterial HflX orthologs. Structural model of (A) EcHflX•GDPNP from the 50S bound structure (PDB 4ADY) (19), (B) EcHflX•GDPNP•ADPNP from the 50S bound structure (PDB 5ZZM) (191), (C) SsoHflX•GDP (PDB 2QTH) (188), and (D) *Apo* SsoHflX (PDB 2QTF) (188). The four domains of HflX in sequential order are the HflX domain (Orange), Linker domain (Pink), G domain (Blue), and C-terminal domain (CTD; Teal). Archaeal HflX (SsoHflX) lacks the CTD found in the bacterial and eukaryotic orthologs. The bound nucleotide is shown as sticks (black) along with a coordinating magnesium (brown sphere). Predicted adenosine nucleotide binding site shown in (B) as a green oval as proposed by Sengupta and colleagues (192).

SsoHflX and other archaeal orthologs lack a fourth domain following the G domain found in bacterial and eukaryotic orthologs referred to as the C-terminal domain (CTD). It is currently unknown why archaeal orthologs lack the CTD. Interestingly, the CTD lacks overall sequence conservation amongst the orthologs that contain a CTD, suggesting that its functional role may be

species specific. The structure of SsoHflX was solved in both the *apo* and G domain GDP-bound states which revealed no significant structural changes between the two states (188, 193). Notably, the switch 1 region of the G-domain was disordered, indicating its flexibility while the switch 2 region forms interdomain contacts with the HflX and linker domains. These interdomain contacts are hypothesized to be important for the regulation of HflX activity, as the removal of the HflX and linker domain increases the rate of GTP hydrolysis by the G domain alone for both SsoHflX and EcHflX (188, 189, 193).

The first GTP-bound (bound to the non-hydrolysable GTP analog GDPNP) structural information of bacterial HflX was obtained from the cryo-EM structure of EcHflX bound to the 50S ribosome (Figure 1.16) (19). The 50S•EcHflX•GDPNP complex was found to be the most stable HflX-ribosome complex based on sucrose density gradient ultracentrifugation (SDGU) experiments. All four domains of EcHflX were resolved in the 4.5 Å resolution 50S•EcHflX•GDPNP structure with EcHflX bound to the ribosomal A-site (see Chapter 3 – *Ribosomal binding site of and ribosomal subunit dissociation by HflX* for further ribosome details). Switch 2 makes the same interactions with the HflX and linker domains as it does in SsoHflX. Additionally, the switch 1 region is resolved in this structure forming several interactions with the HflX domain, strongly supporting that the HflX domain regulates the G domain, and GTP hydrolysis.

To address the hypothesis of a second nucleotide binding site between the HflX and linker domains, 50S•EcHflX complexes in the presence of the non-hydrolysable analog of ATP, ADPNP, were solved using cryo-EM (191). A 50S•EcHflX•GDPNP•ADPNP complex and a 50S•EcHflX•ADPNP complex were solved to 8 Å and 10 Å resolution, respectively. At that resolution, no distinguishing electron density for the bound nucleotide(s) could be identified, leaving the exact binding site for ATP unknown. Interestingly, the ADPNP-bound structures reveal a distinct conformational change of the HflX and linker domains relative to the G domain (Figure 1.16B). This conformational change positions the linker domain 20 Å away from the HflX domain and further into the peptidyl transferase center (PTC). It is hypothesized that upon ATP hydrolysis, the linker

domain moves back into a position closer to the HflX domain as has been observed in the 50S•EcHflX•GDPNP complex.

The ribosomal binding site of HflX is one of the primary questions addressed in this thesis, with Chapter 3 discussing the binding site determined by covalent cross-linking. While the manuscript that makes up Chapter 3 was in submission, the first cryo-EM structure of a pre-ribosome dissociation complex of HflX bound to the 50S ribosomal subunit was published (19) that presented an alternative binding site for HflX on the ribosome. These binding sites are further discussed in Chapter 3 and Chapter 4 of this thesis.

1.12.2 – GENOMIC LOCATION AND EXPRESSION PROFILE OF HFLX

In *E. coli*, the *hflX* gene is a part of a superoperon with the genes *miaA*, *hfq*, *hflK*, and *hflC* (194). Based on its location upstream of *hflK* and *hflC*, it was hypothesized that *hflX* may also be involved in the lysis-lysogeny decision (see *Section 1.12.5 – Role in Lysis-Lysogeny decision*), a role that was refuted in 2009 (195) but may still be valid as will be discussed later. The *hflX* gene is located downstream of the *hfq* gene suggesting a possible role for HflX in general stress response, however, this operon of *hfq* and *hflX* is only found in other enterobacterial and α-proteobacterial species (196). Based on its genomic location variability, the functional role of the *hflX* gene does not appear to be tied to any process other than the general stress response in organisms where it is transcribed with *hfq*.

As a part of the superoperon in *E. coli*, the *hflX* gene is controlled by several promoters including σ32 heat shock promoters and “housekeeping” σ70 promoters (197-199). The σ70 promoters within the superoperon suggest that *hflX* is constitutively expressed under normal growth conditions. Furthermore, the human ortholog is also constitutively expressed. Heat stress activation of *hflX* expression by σ32 heat shock promoters has been reported on both, the transcriptional and translational level (19, 197). Additionally, *hflX* is upregulated under sub-inhibitory concentrations of silver nanoparticles in *E. coli* (200). These studies suggest that HflX, in organisms across all

domains, functions under normal cellular growth conditions, but provide a strong cellular fitness advantage under stress.

In several bacterial species, including *L. monocytogenes*, the *hflX* gene has been duplicated or a second copy has been acquired through horizontal gene transfer (201). One copy of the *hflX* gene was shown to confer resistance to several ribosome targeting antibiotics, while the other is unable to confer such resistance raising the question what the difference is with respect to function and mechanism (see *Section 1.12.7 - Role in antibiotic resistance*).

1.12.3 – PURINE NUCLEOTIDE PREFERENCE AND NUCLEOTIDE BINDING PROPERTIES

The canonical G domain of HflX binds and hydrolyzes GTP *in vitro*, yet HflX also shows activity toward ATP (202). Furthermore, the rate of GTP and ATP hydrolysis are increased in the presence of the 70S ribosome and 50S ribosomal subunit, with GTP hydrolysis stimulated to a ten-fold higher rate than ATP hydrolysis (30, 202). Based on the affinities for each purine nucleotide (30, 203), HflX is primarily bound to GDP *in vivo* when not associated with the ribosome. The preferential utilization of GTP over ATP was regarded as normal until it was hypothesized that the HflX and linker domains, unique to HflX orthologs, may specifically bind to and hydrolyze ATP (189) (see *Section 1.12.4 – Second nucleotide binding site*). The exact ATP binding site is unknown but has been computationally predicted to be between the HflX and linker domains (Figure 2B) (192), while several studies of truncated HflX variants show that the HflX and linker domains together specifically bind/hydrolyzes ATP (189, 191). Overall, this suggests that HflX may utilize energy from different purine nucleotide pools to perform the different functional role(s) it is proposed to have in the cell. Why HflX utilizes both nucleotides instead of binding to identical purine nucleotides like other GTPases and ATPases remains unknown (EttA, VlmR, EngA, and ABCE1 (204-208)). The K_Ds for HflX to each guanine and adenine nucleotide were determined under the assumption that HflX contained only one nucleotide binding domain, the G domain, and as such, these K_Ds will need to be reassessed once the exact nucleotide binding site in the HflX and linker domains is elucidated.

Recently, HflX was identified in a screen for proteins that bind the stringent response molecule, or alarmone, (p)ppGpp in *E. coli* and *S. aureus* (140, 209, 210). Furthermore, it was confirmed that the *B. subtilis*, and *E. faecalis* orthologs of HflX (BsHflX and EfHflX) also bind (p)ppGpp (209). Guanosine tetra- or penta-phosphate (p)ppGpp is upregulated under several stress conditions including amino acid starvation, iron limitation, and osmotic shock, where it regulates global transcriptional changes to allow cells to adapt to the changing cellular environment (211, 212). Notably, many virulence factors in bacteria are upregulated by (p)ppGpp thereby coupling pathogenesis to metabolic regulation (122, 123). Whether HflX plays a role in virulence or not has yet to be determined (see *Section 1.12.8 – Role in Virulence*) but binding to (p)ppGpp has been shown to influence the selectivity of ribosome dissociation activity by HflX, with (p)ppGpp inhibiting dissociation of 100S ribosome dimers but not 70S monomers (140) (see *Section 1.12.6 – Role in Ribosome Hibernation*). Under these conditions, (p)ppGpp binding facilitates cell survivability by preventing 100S dissociation until conditions are favourable and the cellular concentration of (p)ppGpp decreases. Is the modulation of ribosome dissociation activity for different ribosomal targets the extent of (p)ppGpp influence on HflX? If not, how does (p)ppGpp binding alter other functions of HflX? The level of (p)ppGpp in the cell fluctuates in relation to several external stimuli, but at what concentration does that alter HflX's activity? Further studies are required to understand the importance of (p)ppGpp binding to HflX function and structural dynamics.

1.12.4 – SECOND NUCLEOTIDE BINDING SITE

Early studies of HflX's biochemical properties showed that HflX could hydrolyze both GTP and ATP (30, 188, 195, 202). Several studies looking at truncated forms of HflX noticed that the two N-terminal domains (the HflX and linker domains) showed nucleotide hydrolysis activity in the absence of the G domain (189, 190). These results provided the first evidence for the hypothesis of a second nucleotide binding site between the HflX and linker domains that preferentially binds ATP.

Currently, the exact ATP binding site in the N-terminal domains remains unknown, although it has been computationally predicted to lie at the interface between the HflX and linker domains (192). Structural studies of HflX bound to the 50S subunit in the presence of the non-hydrolysable ATP analog, ADPNP, showed a distinct conformational change in the N-terminal domains of HflX (191) (Figure 2B). However, the resolution of the ADPNP-bound structure precluded the identification of the adenine nucleotide binding site. Determining the nucleotide binding site in the HflX and/or linker domains will provide valuable information for future studies to elucidate the functional purpose two nucleotide binding domains in HflX serves.

Two nucleotide binding domains is not a novel feature exclusive to HflX but is a common structural and functional feature of many other ribosome-associated factors including EttA, VlmR, EngA, and ABCE1 (204-208). Interestingly, all these multi-nucleotide binding domain proteins bind to either two ATP or two GTP molecules, while HflX binds both GTP and an ATP molecule. Binding of GTP has been tied to HflX's ability to dissociate the 70S ribosome (and 100S ribosome dimer) into subunits (see *Section 1.12.6 – Role in Ribosome Hibernation* (19, 213)), while ATP binding to the HflX and/or linker domains has been associated with HflX's RNA helicase activity (191). Why HflX utilizes nucleotides from either energy pool remains to be determined. Potentially, if one energy pool is depleted HflX may still be able to perform its functional role with the opposite energy pool. For example, if the cellular ATP concentration drops, HflX may not utilize its RNA helicase activity but remains able to dissociate the 70S ribosome into its subunits via GTP, or vice versa. Furthermore, the HflX and linker domains have been shown to influence GTP hydrolysis of the G domain (189), yet there may be further regulatory influence by the HflX and linker domain when ATP/ADP is bound. Regulation may not just be imparted by the HflX and linker domains either, as the G domain could possibly have influence over the HflX and linker domains and their helicase activity as well. Understanding how these two nucleotide binding domains influence each other and the other domains in HflX in order to modulate HflX function in the cell is important for future inhibitor development against the processes HflX is involved in.

1.12.5 – ROLE IN THE LYSIS-LYSOGENY DECISION

Lysogeny is one of the two viral cycles whereby the viral nucleic acid is either integrated into the host bacterium's genome or forms a circular replicon and is replicated as new daughter cells are produced. These viral nucleic acids can remain dormant until conditions are favourable, at which point they enter the lytic cycle producing many viral particles until the cell lyses. Cellular fate upon viral infection is determined by proteins in the *hfl* gene family, which includes HflX. High frequency of lysogeny factor X, or HflX, was initially proposed to be involved in the lysis-lysogeny decision in *E. coli* infected by bacteriophages due to its genomic location downstream of the *hflC* and *hflK* genes together known as *hflA* (194, 214). HflC and HflK are membrane bound proteins that interact with HflB (FtsH), an ATP-dependent protease (215, 216). Together the complex of HflB, HflC, and HflK have protease activity toward cII, a key determinant in the lysis-lysogeny decision where degradation of cII induces the lytic cycle (217). Together with another membrane protein, HflD, which binds cII and keeps it localized near the membrane, HflB degrades cII (218, 219). cII is a transcriptional regulator that upregulates genes involved in lysogeny. Therefore, mutations to any of the *hfl* genes resulted in a decrease in cII proteolysis and a corresponding high frequency of lysogeny.

The *hflX* gene was proposed to be involved in regulating HflK/C because of its classification as a GTPase (194), yet this role went unexamined for several years. A direct role of HflX in the lysis-lysogeny decision was disproven in 2009 when Parrack and colleagues reported that not only did an in-frame deletion of the *hflX* gene in *E. coli* not affect the lysis-lysogeny decision of cells, but HflX also did not interact with HflK/C as previously predicted (195). An indirect role in the lysogeny decision was discovered in relation to *E. coli* lacking *hflX* (Δ*hflX*), which are unable to regulate the influx of manganese which subsequently alters the cellular levels of other metal ions including zinc and iron (220). *E. coli* Δ*hflX* stressed with increased manganese in the media have higher cellular zinc concentrations, which enables increased HflB proteolysis of cII and thereby a decrease in the frequency of lysogenation by bacteriophage λ. This indirect control of the frequency of lysogenation by HflX via maintaining manganese (and thereby zinc) homeostasis is the first evidence that HflX may indeed be involved in the lysis and lysogeny decision for which it was originally named. There

are still many unanswered questions regarding HflX and manganese homeostasis (see *Section 1.12.9 - Role in Manganese Homeostasis*) specifically, how HflX regulates manganese homeostasis and what cellular signals trigger alterations in HflX-mediated manganese homeostasis activity such that zinc levels can decrease the frequency of lysogeny.

1.12.6 – ROLE IN RIBOSOME HIBERNATION

While evidence suggests that HflX may target stalled translating ribosomes, a recent study has found that *S. aureus* HflX (SaHflX) dissociates the hibernating 100S ribosome dimer allowing the subunits to enter the active ribosome pool again (140). These hibernating ribosomes are a hallmark of bacterial persister cells as they are translationally inactive, to conserve cellular resources, and are protected from degradation, so they may be used again immediately upon favourable growth conditions (129, 221). 100S ribosome dimers are formed from two empty 70S ribosomes joined end-to-end by the 30S ribosomal subunits by one or more stationary-phase proteins (138, 146, 222, 223).

In most bacteria, including *S. aureus*, 100S formation is directed by the binding of hibernation promoting factor (HPF) to each 70S ribosome (142, 221, 224). *S. aureus* HflX (SaHflX) can split the 100S in a GTP-dependent manner but is inhibited by (p)ppGpp (140). Under stress conditions, cellular levels of (p)ppGpp are increased thereby preventing HflX from dissociating any 100S dimers prematurely. Upon returning to favourable growth conditions, (p)ppGpp levels decrease and HflX•GTP splits the 100S ribosome dimer into subunits that can resume translation (Figure 1.17). Interestingly, SaHflX•GDPNP is unable to dissociate the 100S ribosome dimer confirming that GTP hydrolysis is required for 100S dissociation (140). What role nucleotide hydrolysis serves in 100S dissociation has yet to be determined.

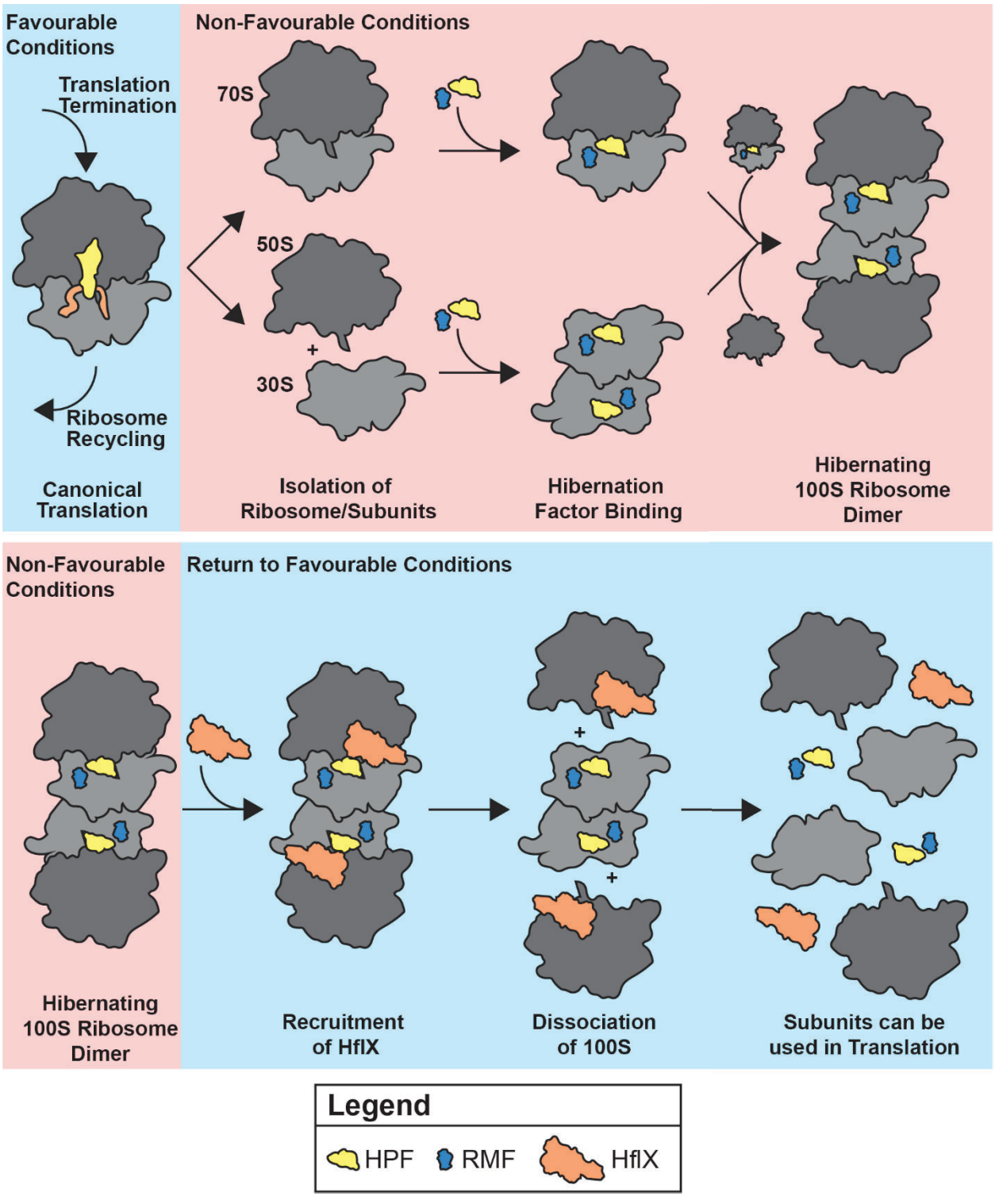

Figure 1.17 – The role of HflX in resumption of translation post-hibernation in γ-proteobacteria *E. coli*. Following translation termination under non-favourable growth conditions, the 70S ribosome is removed from the mRNA or split into 50S and 30S ribosomal subunit. RMF and HPF bind to a vacant 70S ribosome or 50S/30S ribosomal following translation termination and ribosome recycling. Binding of RMF and HPF induces dimerization of two 70S ribosomes into the

100S ribosome dimer. Upon the return of favourable growth conditions, the GTPase HflX binds to the 100S ribosome dimer and splits into 70S ribosomes or 50S/30S ribosomal subunits to allow for translation initiation to resume.

The 100S ribosome structure differs slightly between bacterial species, with γ-proteobacteria *E. coli* requiring two stationary-phase proteins to form a 100S dimer that position each 70S ribosome in the dimer in a rotated conformation relative to the *S. aureus* 100S dimer (129). These two proteins are a truncated HPF homolog and ribosome modulation factor (RMF). RMF binds to the 30S subunit in the same position as the mRNA Shine-Dalgarno sequence, thereby preventing mRNA binding and translation from occurring whereas HPF binds into the A- and P-sites of the 30S subunit blocking the mRNA and initiation factors from entering in both *E. coli* and *S. aureus* (138, 151). In addition to RMF and HPF, *E. coli* has a third stationary-phase protein that is a homolog of HPF, YfiA (151). YfiA binds in the identical position as HPF and its C-terminal extension binds into the mRNA channel blocking RMF (138). YfiA-bound ribosomes do not form 100S dimers in *E. coli* but is considered translationally inactive. Why both a HPF-mediated and a YfiA-mediated ribosome inactivation pathway exist is currently unknown. For further information on the hibernating ribosome literature see reviews from the Wada and Yap labs (129, 221). Furthermore, HflX bound to the A-site (19) does not overlap with HPF bound into the A-site (138) suggesting that HflX could split from either the A-site or the E-site of the 100S ribosome dimer.

Work from the Yap lab clearly shows that HflX can dissociate the 100S ribosome dimer in *S. aureus* to allow protein synthesis to restart following hibernation, yet it may only do so under stress conditions as EF-G/RRF have also been shown to dissociate the 100S ribosome dimer. Several questions remain on how HflX facilitates disassembling the 100S ribosome including: What conditions determine when HflX dissociates the 100S ribosome dimer, if at all *in vivo*? Does HflX split the 100S dimer into two 70S ribosomes and subsequently into the corresponding subunits, or does it split the individual 70S ribosomes into 50S and 30S subunits in the dimer? Does HflX stimulate dissociation of HPF and/or RMF (depending on the bacterial species) or break intersubunit bridges leading to dissociation of HPF and/or RMF? Is HflX able to split YfiA-bound hibernating 70S ribosomes as well? What is the functional relevance of having both the RMF/HPF-

bound 100S and YfiA-bound 70S hibernating ribosomes in *E. coli* and other bacterial species? These questions are important for understanding how bacteria can use translational dormancy to survive through antibiotic treatments and provide the basis for targeting HflX's function for future antibiotic design to inhibit ending hibernation.

1.12.7 – ROLE IN ANTIBIOTIC RESISTANCE

Recent studies looking for antibiotic resistance genes (ARGs) in regions with high antibiotic use or run-off from production facilities found that the *hflX* gene can provide resistance to macrolide antibiotics that target the PET (225, 226). The *hflX* genes identified were from the bacterial species *Simkania negevensis* (related to Chlamydia) and *Emergencia timonensis*, which are gram-negative and -positive respectively. *E. timonensis* is in the same phylum as *Listeria monocytogenes*, a bacterial species that has two *hflX* genes, one of which is upregulated in the presence of sub-inhibitory concentrations of lincosamides antibiotics which target the PTC near the PET, specifically lincomycin (LINC) (201, 227). Upregulation of HflX in the presence of sub-inhibitory concentration of LINC has also been reported in *Streptomyces coelicolor* A3(2), *Mycobacterium abscessus,* and *Mycobacterium smegmatis* (228-230).

In the *L. monocytogenes* study, the upregulated *hflX* gene is downstream of an ORF (*rli80*) that contains a macrolide resistance motif in its coding region (201). In the presence of the macrolide erythromycin (ERY) or LINC, the ribosome stalls on the resistance motif in the *rli80* cistron causing a stem-loop in the mRNA to unfold and allowing the downstream *hflX* gene to be translated. HflX produced from this gene can confer resistance to both ERY and LINC which prompted the authors to rename this *hflX* gene *hflXr* (*hflX* resistance). No other genes are transcribed along with *rli80* and *hflXr*. Interestingly, the second *L. monocytogenes hflX* gene was unable to confer resistance even under the attenuated control of the *rli80* gene. The sequence differences between *L. monocytogenes* HflX (LmHflX) and HflXr (LmHflXr) provide no obvious clue as to how LmHflXr evolved to provide antibiotic resistance. Whether LmHflXr is enough to

compensate in the absence of LmHflX, or whether the specialized function of LmHflXr impedes on the primary role that LmHflX evolved to fill is unknown.

Recently, Pallavi Ghosh and co-workers have shown that the HflX orthologs in the *Mycobacterium* species *M. abscessus* and *M. smegmatis* (MabHflX and MsHflX, respectively) confer resistance to lincosamide and macrolide antibiotics in the absence of the primary resistance gene *erm41* suggesting that HflX can confer the same level of resistance (231). How *L. monocytogenes* HflXr (LmHflXr), MabHflX, and MsHflX confer resistance to lincosamide and macrolide antibiotics that bind to the PTC and PET is hypothesized to be tied to the ribosome dissociation activity shown by the *E. coli* and *S. aureus* HflX homologs (EcHflX and SaHflX) (19, 140, 213). Ribosomes stalled by either ERY or LINC would be the target for HflX that would induce in presence of the bound antibiotic ribosome dissociation (213) as neither ERY nor LINC inhibit ribosome dissociation (Chapter 4). MsHflX can dissociate the 70S ribosome into ribosomal subunits *in vitro* in the absence of antibiotic and binds tightly to 50S subunits in *M. smegmatis* cells treated with CLIND or ERY (231). Interestingly, the binding of MsHflX does not occlude ERY binding or remove bound ERY. Taken together, these results suggest that the HflX can act as an antibiotic resistance protein in some bacterial species through a mechanism that requires 70S ribosome dissociation into subunits. This mechanism is further supported by MsHflX variants unable to dissociate the ribosome do not confer resistance to ERY (231).

Following 70S ribosome dissociation into 50S and 30S ribosomal subunits, HflX likely remains bound to the antibiotic-bound 50S ribosomal subunit. In several bacterial species HflX has been found to be associated with the 50S ribosomal subunits upon separation of the ribosomal particles on SDGU, suggesting that HflX remains bound following 70S dissociation (140, 202, 231-233). As MsHflX is unable to dissociate 70S ribosomes bound ERY (231), it is likely that the primary role of HflX in antibiotic resistance is to split ribosomes stalled by PTC/PET binding antibiotics (Figure 1.18). At this point, the HflX•50S•antibiotic complex is either sequestered from translation by the bound HflX or acts as a substrate for an accessory protein involved in the dissociation of the bound antibiotic. In *M. abscessus*, two ABC-F proteins speculated to be involved in antibiotic

displacement from the ribosome, MAB_1846 and MAB_2355, are upregulated in the presence of macrolides and lincosamides (230). In *L. monocytogenes*, the lmo0919 gene is proposed to encode an antibiotic displacement factor as well (201). Whether other antibiotic dissociation proteins are found in organisms where HflX confers resistance to macrolides or lincosamides is unknown. Interestingly, HflX is upregulated in the presence of non-PTC/PET binding antibiotic tetracycline (TET) in *S. coelicolor* where the *hflX* gene is under the transcriptional control of WblC that is required for regulating intrinsic antibiotic resistance (229). It is not known if *S. coelicolor* HflX (ScHflX) can dissociate a stalled 70S ribosome, but if it can, this suggests that HflX-mediated antibiotic resistance may not be limited to just macrolide/lincosamide antibiotics that bind to the PTC/PET. Taken together, HflX works in conjunction with other enzymes to allow protein synthesis to continue, otherwise the antibiotic would rebind and continually inhibit translation.

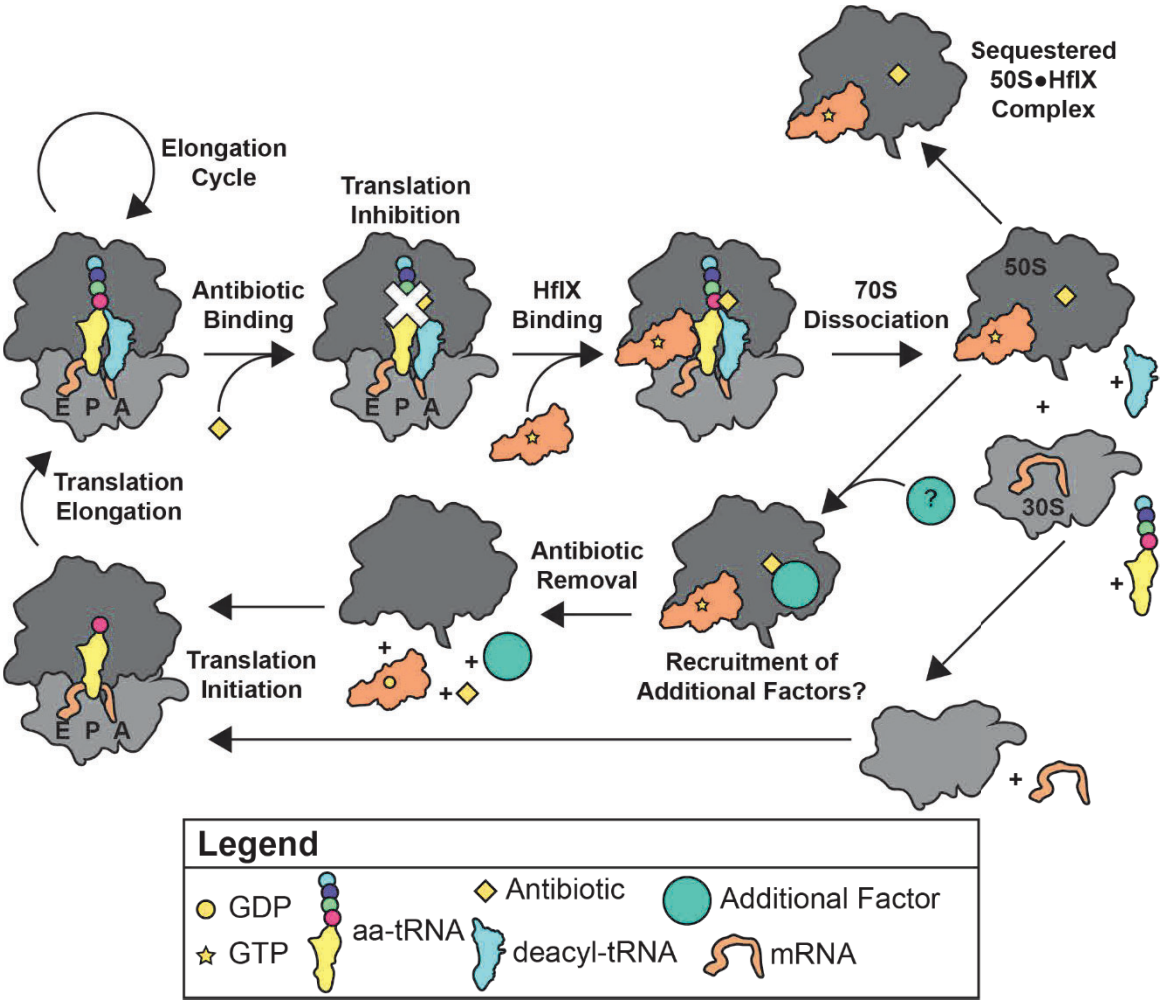

Figure 1.18 – Role of HflX in antibiotic resistance. HflX has been shown to provide resistance to clinically relevant antibiotics that bind to the PTC/PET of the ribosome including erythromycin, clindamycin, and lincomycin among others. These antibiotics block peptide bond formation and/or the growing polypeptide chain from exiting the ribosome, thereby stalling the ribosome mid-translation. HflX is hypothesized to bind to these antibiotic stalled ribosome complexes and dissociate the complex. This results in a HflX-50S-antibiotic complex that is either sequestered or recruits another factor(s) that dissociates the antibiotic from the 50S subunit, allowing the 50S and 30S ribosomal subunits to be used in further rounds of translation.

1.12.8 – ROLE IN VIRULENCE

HflX has been proposed to be important for virulence in several organisms including *Chlamydia pneumoniae*, *Escherichia coli* O157:H7, *Actinobacillus pleuropneumoniae*, and *Vibrio anguillarum* (234-238). The exact role HflX plays in virulence has not been determined but is most likely tied to its function in translation under stress and resumption of translation following

hibernation of dormant cells. Upon bacterial infection, the pathogen begins to rapidly grow and divide, a process that requires translation occurring at a high rate. Recent evidence suggests that the *hflX* gene is upregulated upon infection of a host organism by the bacterial pathogens including *E. coli* (235) and *A. pleuropneumoniae* (236, 237). Other studies have found ribosome associated GTPases Era and BipA upregulated upon host infection by pathogenic species *Borrelia burgdorferi* and *Streptococcus equi* ssp. *zooepidemicus,* respectively (239, 240). These results suggest that upregulation of ribosome biogenesis and modulation of translation are important for virulence.

Bacterial infection triggers host immune responses that can be aided by antibiotic treatment, leading to unfavourable growth conditions for the pathogen. These unfavourable conditions lead to the formation of bacterial persister cells that remain in the host until favourable conditions return and the pathogen can divide and infect the host again. One of the key facets of persister cells is their ability to rapidly initiate translation again once conditions improve, done so by the storage of empty 70S ribosomes as stable 100S ribosome dimers during unfavourable growth conditions (see *Section 1.12.6 - Role in Ribosome Hibernation*). HflX can dissociate these 100S ribosome dimers into ribosomal subunits immediately capable of facilitating translation. The return of favourable growth conditions is correlated with a decrease in (p)ppGpp thereby allowing HflX to bind GTP, thus releasing the stored ribosomal particles to partake in translation once again, starting up the rapid growth and division required for virulence. In this way, HflX is important for the prolonged virulence of a pathogen.

Intriguingly, the *hflX* gene has been used as a marker gene for molecular typing of different Chlamydial strains using multilocus sequence typing (MLST) (241-245). The *hflX* gene was initially chosen as a target, along with six other genes, because it fit three specific criteria: 1) not located near genes with high diversifying selection in the genome (such as outer membrane or secreted protein genes); 2) distant from other chosen target genes on the genome; and 3) has a similar extent of nucleotide substitutions as the other target genes (244). Differences in the sequence of just one gene is enough to designate a different Chlamydial sequence type which allows for the understanding and tracking of pathogen diversity within a population.

As HflX is upregulated in pathogens upon infection, sequencing it to characterize different Chlamydial samples provides additional information than just which sequence type caused the infection, but also what mutations in the *hflX* gene (and the other genes) caused that chlamydial sequence type to be more or less infectious than others. In some studies, the difference between tested sequence types is in the *hflX* gene giving rise to different Chlamydial sequence types (242, 243), while other studies either do not report differences or have not observed differences in the *hflX* gene (241).

HflX has another proposed role in manganese (Mn^{2+}) homeostasis that could have implications in virulence as well (see *Section 1.12.9 - Role in manganese homeostasis*). Acquisition of manganese and other metal cofactors from a host is critical for virulence of bacterial pathogens including *S. aureus, B. subtilis,* and *E. coli* (246-250). Pathogenic species of *E. coli* are reported to have additional manganese importer genes aside from the canonical manganese-influx system (246). While HflX has not been shown to transport manganese directly or regulate manganese importer proteins, its involvement in metal cation homeostasis and proposed roles in virulence may not be mutually exclusive. Further studies into how HflX modulates manganese homeostasis, and thereby the homeostasis of other metal cations, will be important for assessing its role in virulence via metal acquisition from host cells upon infection.

The exact functional role HflX plays in virulence has yet to be determined but having a role in virulence itself signifies that HflX is an interesting target for medical therapeutics. The use of HflX as a vaccine in mice to ward off *A. pleuropneumoniae* infection has already shown some promising results, with the injection of ApHflX into mice increasing survivability by 62.5% after infection 20 days following (236). Whether developing antibiotics against HflX to inhibit its functional role or using HflX in vaccines to prevent infection by specific pathogens, understanding how HflX is contributing to virulence will increase our overall understanding of infection.

1.12.9 – ROLE IN MANGANESE HOMEOSTASIS

Metalloproteins utilize different metal cofactors to facilitate their molecular function such as iron (Fe^{2+}) in oxygenases and hydrogenases, and magnesium (Mg^{2+}) in nucleotide binding proteins, such as the trGTPases. Manganese (Mn^{2+}) is another metal cofactor used by several proteins that can replace other metal cofactors to allow cells to survive through oxidative stress. Manganese is "nonoxidizable" thereby restoring functionality to oxidizable Fe^{2+} bound enzymes while being involved in reducing superoxide radicals bound to SodA (251, 252). High concentrations of manganese can be detrimental as manganese can replace iron, magnesium, and other metal cofactors effectively inactivating some enzymes that require these other metal ions (253, 254). Manganese does have implications in several biological processes including glycolysis, stringent response, pathogenesis, signal transduction, and sporulation making its regulation very important to cellular fitness (255). *E. coli* has a manganese regulation system including the manganese-dependent transcription factor MntR that regulates the production of the manganese efflux pump MntP and manganese importer MntH (253, 256). Furthermore, HflX has been implicated in a MntR-independent mechanism of manganese homeostasis in *E. coli* (220).

Initially, the phenotypic response to manganese in *E. coli* Δ*hflX* was tested because it had an unanticipated effect on the autophosphorylation of HflX by GTP (220). In the presence of manganese, autophosphorylation was more efficiently facilitated than the presence of magnesium. Whether autophosphorylation of HflX under high manganese concentrations signals HflX to perform an alternative cellular function is still unknown but the absence of HflX leads to an accumulation of manganese to toxic levels in *E. coli*. Alterations in the cellular manganese concentration, such as excess manganese activates the MntR transcription factor altering the transcriptome and leads to imbalances in other metal cofactor concentrations (increased zinc and decreased iron concentration) suggesting a connected homeostasis network among the metal ions. Furthermore, alterations in zinc and iron levels alter transcriptional patterns from the zinc-dependent Zur and ZntR, and the iron-dependent Fur transcription factors (249). As HflX can mediate manganese-homeostasis, indirectly it can also adjust other metal ion concentrations and therefore alter transcriptional patterns. How HflX regulates manganese concentrations may be

through alternative manganese importer proteins including the zinc importer ZnuABC (220) but the mechanism by which HflX does so has yet to be elucidated.

In the absence of HflX, *E. coli* exhibits severe reductions in growth rate at increasing manganese concentrations (up to 1 mM) and the morphology of these cells were elongated and filamentous suggesting an inhibition of cell division (220, 257). Within the elongated cells several segregated nucleoids can be observed after DAPI staining suggesting that it is not DNA replication that is inhibited, but cell division (257). This is consistent with the appearance of dark bands along the elongated cells marking probable sites of cell division formed by FtsZ rings that did not constrict (258). Furthermore, the only antibiotics that had significant inhibitory effect on the Δ*hflX* strain were B-lactam antibiotics that inhibit cell division and septation (257). Specifically, cephalothin, ampicillin, and cephalexin, all of which bind to and inhibit penicillin binding protein 3 (PBP3 also known as FtsI). PBP3 (FtsI) is a transpeptidase that is recruited to the FtsZ ring prior to cell division where it introduces cross-links in the peptidoglycan wall (259). Taken together, these data suggest that HflX is involved in progression of the cell cycle through cell division under manganese stress. Other studies have previously labeled HflX as a cell division protein due to its decrease regulation by the transcription factor SdiA, a homolog of the luxR quorum sensing system that is a known regulator of cell division proteins (260). Currently, there is no evidence that HflX is directly involved in cell division. *E. coli* lacking HflX show hallmarks of a cell division deficiency, but future studies will have to determine whether HflX interacts with any of the cell division proteins directly to modulate cell division, or if impairments in cell division are due to the absence of HflX performing an upstream functional role.

1.12.10 – HUMAN ORTHOLOG OF HFLX: GTPBP6 (PGPL)

In humans, the HflX ortholog is identified as GTP Binding Protein 6 (GTPBP6) or pseudoautosomal GTP-binding protein-like (PGPL) and is found at the pseudoautosomal region 1 (PAR1) of the sex chromosomes (261). The pseudoautosomal regions are short regions of homology between the two sex chromosomes that recombine during meiosis. Genes in this region

are inherited in an autosomal fashion rather than being sex-linked (262). PAR1 is the longer of the two pseudoautosomal regions and is more conserved evolutionarily compared to PAR2 which is specific to humans (263). These pseudoautosomal regions are at the termini of the chromosome near the telomere and GTPBP6 is the gene closest to the telomere in PAR1 (261). Initially, GTPBP6 was discovered because it escapes inactivation on the second X-chromosome in females thus allowing both copies of the gene to be expressed in both males and females (263). Being a pseudoautosomal protein, individuals that have X chromosome aneuploidies (the gain or loss of entire chromosomes) such as those with Klinefelter's Syndrome (XXY) would have a higher expression level of GTPBP6 along with other pseudoautosomal genes (264-266). Individuals with Klinefelter's Syndrome (XXY) or XXX Syndrome (XXX) have reduced language skills associated with reductions in the temporal and frontal lobes of the brain and higher rates of schizophrenia and schizotypy (267). Turner Syndrome (X) is the result of a missing or partially missing X chromosome and affects females. Individuals with Turner Syndrome lack the expression of genes that escape X-inactivation on the second chromosome resulting in varied symptoms including shorter height, failure in ovary development, reduced visual-spatial development due to a reduced parietal lobe and increased amygdala, and high levels of autism spectrum conditions (267). In a study of X-linked mental retardation (XLMR), one of the recurrent mutations resulting in a truncated gene product was in the GTPBP6 gene with a C118T mutation leading to a stop codon at position 40 in the protein (268). Furthermore, deletions and translocations of PAR1 and PAR2 have been correlated with male infertility (269-272). As such, increased or decreased levels of GTPBP6 from the addition or removal of X chromosomes may have implications in brain and reproductive organ development, which is likely due to alterations in mitochondrial function as will be described later in this section. The relevance of the GTPBP6 gene located in the pseudoautosomal region of the sex chromosomes in humans remains to be determined. At this position, GTPBP6 escapes X-inactivation indicating that both males and females could have the same levels of GTPBP6 present at basal levels, and the addition or removal of an X chromosome increases or decreases GTPBP6 levels in the cell leading to the developmental defects described. These studies raise the question of exactly how dysregulation of the functional role of GTPBP6 in humans leads to these defects.

GTPBP6 is ubiquitously expressed throughout the human body, not only in the brain and reproductive organs (261, 273-275). Nevertheless, high-throughput RNA-seq studies suggest that there is higher expression of the GTPBP6 mRNA in female reproductive tissues (273-275). Similar studies have shown that GTPBP6 mRNA is present in all tested cancer cell-lines and that the protein is expressed in these. Patient samples from individuals with prostate or lung cancer show increased levels of the GTPBP6 mRNA (276, 277) and in the androgen-sensitive human prostate adenocarcinoma cell line LNCaP in response to an androgen hormone analog, R1881 (276). This is the first indication that GTPBP6 may have functional implications in some types of cancer. From genome sequencing studies of different cancers, only a few have had mutations in the *GTPBP6* gene mainly being synonymous mutations, there were many reported missense mutations with none being overly prevalent. Many of these mutations cluster into the core domains that GTPBP6 shares with the bacterial orthologs, suggesting a conserved mechanism and that these mutations could be studied further in their bacterial counterparts. The increased levels of GTPBP6 in cancer, specifically reproductive tissues, may have some functional importance given the fact that additional X chromosome individuals have reproductive organ developmental issues. Further studies of different reproductive tissue cancers and non-reproductive tissue cancers are required to validate if altered levels of GTPBP6 influence the development of cancer or contribute to its pathogenicity.

GTPBP6 is localized to the mitochondria (274, 275, 278) via an N-terminal signal sequence (279). Mitochondrial localization is consistent with phylogenetic information suggesting that the human *hflX* gene (GTPBP6) was likely acquired via mitochondrial endosymbiosis (164). A recent study from the Richter-Dennerlein lab showed that GTPBP6 is peripherally associated with the inner mitochondrial membrane in HEK293T cells (278). Mitochondria have their own specialized ribosomes, commonly referred to as mitoribosomes, that synthesize components of the oxidative phosphorylation system and mitochondrial ribosome proteins (280, 281). Several human protein interactome studies have revealed that GTPBP6 interacts with mitochondrial ribosomal proteins including L4, L12, L23, and L35 (282-288). GTPBP6 was confirmed to bind to the mitochondrial ribosome (55S) in addition to the mitochondrial large ribosomal subunit (39S) and small ribosomal

subunit (28S) by FLAG-immunoprecipitation of FLAG-tagged GTPBP6 (278). Interaction of GTPBP6 with the mitochondrial ribosome mirrors that of the bacterial orthologs and the bacterial ribosome which, as discussed later, is not the only conserved functional role that GTPBP6 has in common with its bacterial counterparts.

In a HEK293T GTPBP6$^{-/-}$ knockout cell line, there is a decrease in mitochondrial translation in the absence of GTPBP6 (278). It was found that this decrease was due to the build-up of large and small mitochondrial ribosomal subunits and not a decrease in mitochondrial mRNAs or rRNAs. Separation of ribosomal particles from the HEK293T GTPBP6$^{-/-}$ cell line using sucrose density gradient ultracentrifugation showed that several mitochondrial ribosome biogenesis factors co-migrated with the 39S ribosomal subunit, suggesting the accumulation of a late stage 39S precursor subunit. This is the first experimental evidence that GTPBP6 is involved in ribosome biogenesis. Interestingly, one of the other proteins that GTPBP6 was found to interact with in the interactome studies was ribosome biogenesis factor YBEY (metalloendoribonuclease) further confirming the role of GTPBP6 in ribosome biogenesis (282-288). The exact role GTPBP6 plays in ribosome biogenesis has yet to be determined, but it is likely to be in the late stages of rRNA folding or rearrangements of the ribosomal proteins or rRNA as all ribosomal proteins are present in the 39S precursor subunits.

Interestingly, overexpression of GTPBP6 in HEK293T cells also led to a decrease in protein synthesis and the build-up of 39S and 28S mitochondrial ribosomes (278). The 39S ribosomal subunits did not co-migrate with ribosome biogenesis factors when GTPBP6 was overexpressed suggesting that ribosome biogenesis is not impaired. Alternatively, it was shown that GTPBP6 can dissociate the mitochondrial ribosome like the bacterial orthologs dissociate the 70S bacterial ribosome (see Chapters 3 and 4). It is currently not known whether GTPBP6 has retained the ability to dissociate the ribosome to alleviate translational stalling of the mitochondrial ribosome during mitochondrial stress. Mitochondrial stress can take several forms, ranging from the overproduction of reactive oxygen species (ROS) inherent in cellular respiration to unfolded protein response (289, 290). Translational stalling is known to occur within the mitochondria (291, 292) suggesting that GTPBP6 may be involved in dissociating stalled mitochondrial ribosomes like the bacterial

orthologs Specifically, GTPBP6-mediated dissociation of stalled ribosomes may occur following peptide release by peptidyl-tRNA hydrolases C12OFR65 and ICT1 that have been proposed to involved in ribosome rescue (278, 291, 293, 294) . In bacteria, the GTPBP6 ortholog (HflX) can dissociate not just the 70S bacterial ribosome, but also the 100S ribosome dimer (see *Section 1.12.6 – Role in Ribosome Hibernation*) thereby serving a role in resuscitation of protein synthesis in bacterial persister cells. However, there is no evidence for mitochondrial ribosome dimerization like the bacterial 100S ribosome dimer which is supported by the lack of RMF and/or HPF orthologs in humans but does not rule out different ribosome dimerization factors that may allow for ribosome dimerization.

Another cell line where GTPBP6 was found to be upregulated is in human umbilical vascular endothelial cells (HUVEC) after Ouabain treatment (295). Ouabain is the primary active component in Masai poison arrows and works by inhibiting sodium pumps and Na^+/K^+ ATPases resulting in cell depolarization including increased intracellular Ca^{2+} levels. Several Ouabain-like isomers are found naturally occurring in the human body and act as modulators of intracellular Na^+ and Ca^{2+} levels (296). Maintaining mitochondrial membrane potential is important to drive ATP production via the oxidative phosphorylation system (297). It is unclear if the upregulation of GTPBP6 has any functional implications during cellular depolarization but a similar upregulation of the *hflX* gene in *E. coli* because of changes in cellular ion levels such as sub-inhibitory concentrations of silver nanoparticles on the (200). Additionally, EcHflX has been shown to regulate cellular manganese levels in turn altering the cellular levels of other metal ions (see *Section 1.12.9 – Role in Manganese homeostasis*), therefore, as GTPBP6 shares several other functional attributes with bacterial orthologs it may also have some role in maintaining ion levels in the mitochondria. Overall, dysregulation of GTPBP6 levels in the cell leads to a decrease in mitochondrial protein synthesis and thus mitochondrial dysfunction. Issues with mitochondrial ribosome biogenesis have previously been connected to telomere dysfunction, given the GTPBP6 gene being located near the telomere, therefore, it is likely that the ribosome biogenesis issues were due to a decrease in GTPBP6 levels (298).

In addition to interacting with the mitochondrial ribosome, GTPBP6 was found to interact with SDF4 (Stromal cell derived factor 4), IP6K2 (Inositol hexakisphosphate kinase 2), THTPA (Thiamine triphosphatase), and ESR1 and ESR2 (estrogen receptors 1 and 2) (282-288). These potential interaction partners need to be independently verified. Protein interactome studies also revealed that GTPBP6 may interact with two estrogen receptors (ESR1 and ESR2). These two receptors are found in all tissues yet enhanced in reproductive tissues of both males and females (274, 275). Like other potential interaction partners, interaction between these receptors and GTPBP6 needs to be validated especially due to their differential localization *in vivo* (GTPBP6 to the mitochondria and ESR1/ESR2 to the nucleoplasm and vesicles). It is tempting to speculate that an interaction between GTPBP6 and ESR1/ESR2 may provide the link between individuals with altered levels of GTPBP6 due to X chromosome aneuploidies and the defects in reproductive organ development that these individuals have. There are many questions that remain to be answered about GTPBP6 biochemically and functionally, but evidence from orthologs in other organisms may provide insight into the role GTPBP6 plays in X chromosome aneuploidies and cancer.

CHAPTER 2: YCHF IS A HELICASE INVOLVED IN RIBOSOME QUALITY CONTROL THROUGH REMODELING OF THE RIBOSOMAL A-SITE

2.1 – PREFACE

Chapter two includes a manuscript written initially for submission to the journal Proceedings of the National Academy of Sciences of the United States of America (PNAS), describing the recent biochemical information on the function and ribosomal binding site of *Escherichia coli* YchF by members of the Wieden lab. Dr. Hans-Joachim Wieden and I wrote this version of the paper with input from other lab members (Dora Capatos, Dr. Binod Pageni, Dr. Senthilkumar Kailasam, and Fan Mo). Experiments were planned by Dr. Hans-Joachim Wieden, Dr. Senthilkumar Kailasam, and I. Dr. Senthilkumar Kailasam carried out the computational docking and modelling along with the analysis of the deep sequencing dataset. Fan Mo carried out the *in vivo* competition assay, expression analysis, and cold stress assay. Dr. Binod Pageni carried out the nitrocellulose filter binding, YchF/EF-G binding competition, nucleotide hydrolysis, and RNA unwinding assays. Dora Capatos carried out the purification and radiolabeling of tRNA along with performing the primer extension assays under the supervision of myself. Data analysis and figure preparation were carried out by Dr. Kailasam and I.

2.2 – INTRODUCTION

Protein synthesis is a highly regulated process essential to all living organisms carried out by the ribonucleoprotein complex known as the ribosome. The ribosome consists of two subunits that are assembled independently and brought together during translation initiation (see *Section 1.5 – Translation Initiation in Bacteria*) to begin the synthesis of the encoded mRNA message. Upon completion of the polypeptide, the ribosomal subunits are recycled and used in subsequent rounds of translation.

Occasionally, ribosomes stall during translation for several reasons including truncated mRNAs, cleavage to the ribosomal RNA (rRNA), missing ribosomal protein and improperly folded rRNA (299, 300). These events are more prevalent under conditions such as cold stress when

rRNA gets kinetically trapped during folding in higher order structures that prevent downstream subunit assembly or oxidative stress when rRNA can be damaged by free radicals (301, 302). When such assembly errors occur, the cell has several choices: (i) to repair the error to ensure proper translation, (ii) ignore the error accepting any downstream errors in protein synthesis, or (iii) degrade the ribosome to prevent downstream errors in protein synthesis. The choice the cell makes may depend on the severity of the error or damage to the ribosome, but under environmental pressures the latter two choices (ii and iii) would put the cell at a selective disadvantage. Of these two choices, ignoring the assembly issue could be more detrimental to the cell as faulty ribosomes are prone to erroneous translation resulting in potentially toxic translation products. Degradation of the faulty ribosomes is an energy loss to the cell, but the build-up of toxic products can be lethal. In eukaryotes, several pathways have been discovered to remove non-functional ribosomes (300, 303) while less is known about ribosome repair pathways, aside from the exchange of damaged ribosomal proteins with functional copies (304, 305). Ribosomes require a large energy expenditure to be produced, and as such repairing non-functional ribosomes would be advantageous to the cell.

During ribosome biogenesis, there are multiple stages in which the newly assembled subunits are checked for quality and activity (54, 133). Particularly, quality of the individual ribosomal subunits is checked before they enter translation (52, 53, 55). Recently, two studies in *E. coli* have shown that the initiator tRNA ($tRNA^{fMet}$) and the GTPase EF4 (LepA) are involved in the late stages of ribosome biogenesis. Together, they assess the 70S ribosome formed from a newly synthesized 30S subunit and indirectly recruit RNases (RNase II, RNase R, and RNase PH) to process the 3'-end of the 16S rRNA and allow the 3' domain of the 16S rRNA to refold into the correct conformation, respectively (52, 53). This is analogous to eukaryotic small ribosomal subunit biogenesis whereby the newly assembled 40S ribosomal subunit is assembled into the 80S ribosome by eIF5B as a functional translation-like check before the subunits are dissociated and used in protein synthesis (55). Interestingly, there have been no reports whether the large ribosomal subunit is checked for quality following assembly of the subunits into the 70S ribosome and before entering the translational pool. While a quality control step for the large subunit in a 70S ribosome may not be required, it seems likely that such a step occurs given that the large subunit

performs several important functions (peptide bond formation, recruitment and stimulation of translational GTPases) and that such mechanisms exist for assessing the small subunit. Potentially, proteins that are involved in quality control after biogenesis could also serve as ongoing quality control enzymes that maintain correct ribosomal structure after successive rounds of translation particularly upon instances in which damage to the ribosome may have occurred. Factors that bind to a common shared binding site on the ribosome and attempt to refold rRNA may provide a checkpoint at which the decision to either repair or to target the respective ribosome for degradation can occur. The A-site of the ribosome is a important binding site on the ribosome that is targeted not only by translational GTPases (trGTPases) but also by ribosome quality control factors (52, 53).

YchF is a known 70S ribosome binding NTPase whose ATP hydrolysis is stimulated by the 70S ribosome and not by its subunits (see *Section 1.11 – YchF: The conserved ATPase in the GTPase family*) (1, 174). Here we show that the universally conserved NTPase YchF binds to the ribosomal A-site, has RNA chaperone activity, and provides a fitness advantage to bacteria under optimal growth conditions. From this experimental evidence, we propose that YchF fills the role of a quality control factor for the large ribosomal subunit late in ribosome biogenesis, and throughout the life cycle of the ribosome. Through a YchF•tRNA complex that mimics canonical translation factors binding to the ribosomal A-site, YchF acts as a sensor of the structure of the 23S rRNA ensuring it is properly folded to allow for correct interactions with the canonical translation factors, thereby resulting in efficient protein synthesis.

2.3 – METHODS

2.3.1 – REAGENTS, PLASMIDS, & CELL STRAINS

All chemicals were purchased from BioBasic unless otherwise specified. *E. coli ychF* was previously cloned into the plasmid pET28a (174) and *E. coli stpA* was cloned by synthesis in the plasmid pET28a (GeneWiz). *E. coli fusA* was cloned into the plasmid pET28a. The *E. coli* $tRNA^{Phe}$ gene was previously cloned into the plasmid pCFO (306). The *E. coli rrnB* operon was previously

cloned into the plasmid pKK3535 (307). Keio wild type strain and the Keio knockout strain Δ*ychF* were obtained from the Keio collection (308).

2.3.2 – GROWTH CURVE ANALYSIS

E. coli MG1655 cells were grown overnight and used to inoculate the starting culture to 0.02 OD_{600}. Equal OD_{600} samples were taken at various timepoints and the total protein extracted using trichloroacetic acid (TCA). Resulting protein pellets were resuspended in 8 M urea and were analyzed on a 12% SDS-PAGE followed by Western blotting analysis with an anti-FLAG antibody (Sigma Aldrich). Western blot was imaged using an AI600 Chemiluminescent Imager (GE Healthcare).

2.3.3 – TEMPERATURE SENSITIVITY GROWTH ASSAY

E. coli BW25113 strains (wild type, Δ*ychF,* Δ*hflX*, and Δ*bipA)* were grown overnight and diluted to 1.0 OD_{600} before performing a serial dilution. Serial dilutions were spotted onto LB agar plates and grown at the indicated temperatures and durations.

2.3.4 – FITNESS COMPETITION ASSAY

E. coli BW25113 strains (wild type and Δ*ychF*) were cultured individually overnight in LB media. The overnight cultures were used to start fresh cultures grown to 1 OD_{600}. An equal number of cells from each culture were mixed to start the competition assay. The cell mixture was diluted 1:200 with LB media before incubation for 24 hours at 37°C. Samples of the culture were diluted to 1:200 twice before plating on selective (Kanamycin containing; 5 µg/mL) and non-selective (No antibiotic) LB agar plates. Colony forming units (CFU) were counted for both plates to determine the ratio of knockout cells (Kanamycin resistance containing; Δ*ychF*) to wild type. The culture for the subsequent day of growth was started from the previous days culture diluting 1:200 into fresh LB media. The ratio between the two strains was measured each day until one strain was completely absent in the culture.

2.3.5 – STRUCTURAL PREDICTIONS USING *IN SILICO* METHODS

The structure of ATP-bound *E. coli* YchF was prepared by as described in Rosler *et al*. by averaging a 30 ns molecular dynamics (MD) simulation of the previously modelled structure of *E. coli* YchF (309). This structure was utilized for all *in silico* work. The TGS-domain in the cryo-EM structure of RelA bound to the *E. coli* 70S ribosome and tRNA (PDB 5IQR) was used as the template for docking. YchF and RelA share a structurally similar TGS-domain that was used to position YchF onto the 70S ribosome (Appendix Figure 2.3). The model was refined by carrying out a short 1 ns molecular dynamics (MD) simulation in order to relieve steric clashes. This tRNA-bound conformation of YchF was used in all further analysis in the context of ribosome. To check for molecular mimicry, the ribosome-bound EF-G structure (PDB 4V9J) and ribosome bound EF-Tu (PDB 5AFI) were superposed on the YchF-bound ribosome structure. The electrostatic surface potential of YchF was calculated using the program APBS (310, 311). The conservation of residues was mapped onto the structure using ConSurf (312). The normal mode analysis for the internal coordinates of the model was calculated using iMODs (313).

2.3.6 – PREPARATION OF PURIFIED PROTEINS

All *E. coli* YchF variants were overexpressed and purified as described previously (174). *E. coli* Ribosomal protein S1 was purified as described previously (314). Both *E. coli* StpA and EF-G proteins were overexpressed in *E. coli* BL21 DE3 cells and purified using nickel sepharose chromatography followed by size exclusion chromatography to high purity. BSA was purchased from BioBasic. The ΔTGS-YchF variant was expressed from pET28b::*ychf* following Quikchange™ mutagenesis. The mutagenesis reaction was performed using the forward primer 5′-/5phos/TTA AGC TTG CGG CCG CAC TC- 3′ and the reverse primer 5′-/5phos/GTT CAG CAG TTT ATA ACC GGC ACG G- 3′ and the pET28b::*ychf* plasmid as template. *E. coli* DH5α chemically competent cells (NEB) were transformed with the mutagenesis product and the cells were grown overnight at

37°C. The variant was sequence confirmed, transformed into *E. coli* BL21 DE3 cells, and purified as described above.

2.3.7 – PREPARATION OF $tRNA^{Phe}$ AND ΔCCA $tRNA^{Phe}$

The *E. coli* $tRNA^{Phe}$ gene was amplified from the pCFO plasmid (Kind gift from U. Kothe (315)) by the polymerase chain reaction (PCR) with the forward primer 5´-TAATACGACTCACTATAGGG- 3´ and reverse primer 5′- mUmGGTGCCCGGACTCG - 3′. A PCR product encoding the truncated form of the gene lacking the 3 nucleotides CCA at the 3'most end of the tRNA (ΔCCA $tRNA^{Phe}$) was prepared using the same forward primer and the reverse primer 5'- mUmGCCCGGACTCGGAATC – 3'. Both the wild type and truncated $tRNA^{Phe}$ transcripts were made by *in vitro* transcription and purified using the same methods. An *in vitro* transcription reaction was prepared containing at a final concentration 40 mM Tris-HCl (pH 7.5), 10 mM DTT, 15 mM $MgCl_2$, 2 mM spermidine, 10 mM NaCl, 3 mM nucleotide triphosphates (NTPs), 0.36 μM of bacteriophage T7 RNA Polymerase, 10 mM guanosine monophosphate (GMP), 0.01 units/μL of inorganic pyrophosphatase, 0.15 units/μL of Ribolock RNase inhibitor (Thermo Scientific) and 10% v/v of template DNA. The *in vitro* transcription reaction was incubated at 37°C for 17 hours followed by digestion with one unit of DNase I for 1 hour. The *in vitro* transcribed RNA was purified by several steps starting with a phenol-chloroform extraction and subsequent ethanol precipitation using 95% ethanol and 0.3 M sodium acetate (pH 5.0) overnight at -20°C. Precipitated nucleic acid was recovered by centrifugation, dissolved in water, and loaded onto a Superdex-75 10/300 GL column (GE Lifesciences) for isolation of $tRNA^{Phe}$ from other reaction components. The fractions containing $tRNA^{Phe}$ were pooled and rebuffered into water using a microfiltration device (3 kDa MWCO, GE Lifesciences). Purified $tRNA^{Phe}$ was aliquoted, flash frozen, and stored at -80°C for future use.

2.3.8 – RADIOLABELING OF $tRNA^{Phe}$

$tRNA^{Phe}$ was dephosphorylated by incubation with shrimp alkaline phosphatase (Fermentas) for 1 hour at 37°C in a reaction containing 450 pmol of $tRNA^{Phe}$, 0.07 units/μL of shrimp alkaline phosphatase, 70 mM Tris-HCl (pH 7.6), 10 mM $MgCl_2$ and 10 mM DTT. The shrimp

alkaline phosphatase was inactivated by heating for 15 min at 65°C and the dephosphorylated tRNA was purified on an 8 M urea and 10% acrylamide gel. The dephosphorylated and purified $tRNA^{Phe}$ was 5'-end labelled with γ^{32}P-ATP by incubation in a reaction containing 10 µCi/µL of γ^{32}P-ATP, 450 pmol of $tRNA^{Phe}$, 0.3 units/µL of T4 polynucleotide kinase (NEB), 70 mM Tris-HCl pH 7.6, 10 mM $MgCl_2$ and 10 mM DTT for 1 hour at 37°C. The labelling reaction was purified by precipitation in 0.3 M sodium acetate (pH 5.0) and 95% ethanol overnight at -20°C. The radiolabelled $tRNA^{Phe}$ ([^{32}P]-$tRNA^{Phe}$) was resuspended in water, quantified by measuring the absorbance at 260 nm, aliquoted, flash frozen, and stored at -20°C for future use.

2.3.9 – NITROCELLULOSE FILTER BINDING ASSAY

[^{32}P]-$tRNA^{Phe}$ (100 nM) was unfolded and folded in $TAKM_7$ buffer by heating to 65°C for 5 min and slow cooling to 37°C prior to the experiment. 50 nM tRNA was incubated with increasing concentrations of either YchF, ΔTGS-YchF, or *E. coli* TruB (0-50 µM) in the presence or absence of 2 mM nucleotide for 15 minutes at 37°C in $TAKM_7$ buffer before filtering solution through a nitrocellulose membrane. Membranes were washed with ice cold buffer after applying the tRNA:protein solution to remove any loosely bound tRNA. The nitrocellulose membranes were dissolved for 30 min in EcoLite scintillation cocktail [EcoLite (+), MP Biomedical] before quantifying the amount of ^{32}P tRNA bound via scintillation counting (Perkin-Elmer Tri-Carb 2800TR liquid scintillation analyzer). The fraction of tRNA bound to YchF, ΔTGS-YchF or TruB retained on the membrane was determined by comparing the pmol of tRNA retained to the total amount of protein. To obtain the dissociation constant (K_D), the fraction bound as a function of the protein concentration was plotted and analyzed by fitting to a hyperbolic equation (Equation 1) where FB is fraction bound, FB_{max} is the maximum fraction bound, and [Protein] is the concentration of protein used.

$$FB = (FB_{max} \times [Protein]) / (K_D + [Protein]) \quad (1)$$

2.3.10 – BINDING COMPETITION OF YCHF AND EF-G

EF-G•70S ribosome complexes were formed by incubating 30 pmol of 70S ribosomes with increasing concentrations of EF-G (3-180 pmol) in the presence of 2 mM GTP and 1 mM fusidic acid (FUS; Sigma Aldrich) in $TAKM_7$ buffer for 15 min at 37°C. Reaction samples were centrifuged at 10,000 x g for 5 minutes using GE Healthcare vivaspin 500 (100 kDa MWCO) microfiltration devices following the protocol from the manufacturer to remove free EF-G. The complexes were washed with buffer and the concentration of EF-G•70S complexes was determined by absorbance measurements at 260 nm. Equivalent number of pmol of complexes were analyzed on a 12% SDS-PAGE and visualized by silver staining. EF-G•70S complexes (30 pmol) were incubated with YchF (150 pmol) in the presence of 2 mM GTP, 2 mM ATP, and 1 mM fusidic acid in $TAKM_7$ buffer for 15 min at 37°C. Ribosomal complexes were pelleted through a 10% sucrose cushion at 100 000 rpm for 4 hours (S140-AT; Thermo Scientific Sorvall). The resulting pellets were resuspended in $TAKM_7$ buffer, ribosomes quantified using the absorbance at 260 nm, and equivalent amounts of ribosomes were loaded on a 12% SDS-PAGE. Gels were silver stained and the amount of EF-G, YchF, and ribosomal protein L2 were quantified using ImageJ software (316). The fraction bound of YchF and EF-G was calculated with reference to ribosomal protein L2. Complex formation was repeated in triplicate.

2.3.11 – ATP HYDROLYSIS ASSAY

The ATP hydrolysis assay was performed using multiple turnover conditions as described previously (309).

2.3.12 – RNA UNWINDING ASSAY

Two RNAs covalently modified with fluorophores (Cy5–5'-AUGUGGAAAAUCUCUAGCAGU-3', Cy3–5'-ACUGCUAGAGAUUUUCCACAU-3') and competitor unlabeled RNA (5'-ACUGCUAGAGAUUUUCCACAU-3') were synthesized (Integrated DNA Technologies) as described by Rajkowitsch and Schroeder (317). The two-fluorophore tagged RNAs were annealed by heating at 95°C and then slowly cooled to room temperature. 10 nM of annealed RNAs in 200 µL of RNA chaperone buffer (50 mM Tris-HCl pH 7.5, 3 mM $MgCl_2$, and 1

mM DTT), 0.5 μM of target protein at 37°C for 15 minute and 20-fold of competitor RNA helicase was added and reaction was carried out for 180 seconds at 37°C in a Quanta Master Fluorescence spectrophotometer (Photon Technology International) after equilibrating the samples for 2 seconds. Excitation slit widths were set at 5 nm and emission at 10 nm. The Cy3 donor fluorophore was excited at 535 nm once every second and readings were taken at the two emission wavelengths 560 and 660 nm. The fluorescence resonance energy transfer (FRET) index was calculated as the ratio of acceptor to donor dye fluorescence, and values were normalized to 1 at t_0. The FRET index at 180 seconds was averaged and plotted.

2.3.13 – NEXT GENERATION SEQUENCING OF RNAs THAT CO-PURIFY WITH YCHF

Wild type *E. coli* YchF was overexpressed and purified as described in Becker *et al*. (174) with the indicated changes. During cell opening, sonication was not used to lyse the cells or sheer the nucleic acid. The YchF-containing fractions eluted from the nickel sepharose affinity chromatography resin were pooled and further purified on a HiPrep Sephacryl S400 HR size exclusion column (GE Healthcare). Fractions containing YchF were pooled, concentrated, and any RNA was extracted using a phenol-chloroform extraction. The RNA as described above. A cDNA library was prepared using the NEBNext Multiplex Small RNA Sample Prep Set for Illumina kit (New England BioLabs). Briefly, the adaptors were ligated to the 5'- and 3'-ends of the RNAs. cDNAs were prepared by first strand synthesis followed by 13 or 15 cycles of PCR for enrichment. The size of the PCR products was checked by radiolabeling the products with γ^{32}P-ATP and resolving the radiolabeled PCR products on a 6% polyacrylamide-TBE native gel. Purification of the PCR products was performed by pooling the PCR products from both the 13-cycle and 15-cycle reactions and purifying the pooled reaction using the Qiagen PCR Purification kit (Qiagen). The concentration of the purified PCR products was determined using a BioDrop spectrophotometer and built in software.

The cDNA library was sequenced by Illumina Hi-Seq 2500 using paired-end 150 nt reads (GeneWiz). The sequencing reads thus obtained were pre-filtered for quality and length using the Trimgalore program (Krueger F. Trim Galore!) with the following criteria: 1) the adapter sequence

was removed if detected with or without a maximum of one mismatch; 2) the sequences were truncated if Phred quality of base < 20; and 3) the length of the read should be greater than or equal to 25. Reads were mapped to the reference genome (NC_012971.2) using the READemption pipeline (318). Control total RNA seq reads for *E. coli* were obtained from the NCBI Sequence Read Archive (SRA) database (319).

2.3.14 – DMS MODIFICATION AND PRIMER EXTENSION

Complexes of *E. coli* 70S ribosomes (1 µM) and the indicated purified *E. coli* protein (YchF or EF-G; 10 µM) were incubated at 37°C in a water bath for 15 minutes. Nucleotide (GTP/ATP/ADP; 250 µM) or fusidic acid (1 mM) were added in the noted reactions. Dimethyl sulfate (DMS) diluted 1:8 in 95% ethanol to a final concentration of 42 mM was added to each complex for 10 minutes while incubating at 37°C. As a control, ethanol alone was added to 70S ribosomes as an unmodified control. Reactions were stopped by the addition of Stop solution (1 M Tris-HCl pH 7.5, 1 M β-mercaptoethanol, and 0.1 M EDTA). rRNA was isolated from complexes using phenol/chloroform extraction and ethanol precipitation as described above. rRNA was pelleted at 13 000 rpm for 10 minutes and the supernatant removed. The resulting pellet was washed with 75% ethanol, dissolved in water, and quantified by spectrophotometry to determine the amount and purity.

Reverse transcription of the isolated rRNA was carried out using ^{32}P-labeled primers specific for Sarcin-Ricin Loop and GTPase activating center (Details on primer design are given in Supplemental Section 1). Primers were labeled using the same strategy described above for tRNA. Isolated rRNA (1 pmol) was incubated with 50 pmol of ^{32}P-labelled primer at 65°C for 5 minutes followed by 47°C for 10 minutes to anneal the primer to the rRNA. Nucleotides (416 µM), DTT (25 mM), and buffer (50 mM Tris-HCl pH 8.3, 75 mM KCl and 3 mM $MgCl_2$) was added to each reaction and incubated at 47°C for an additional 5 minutes before adding 12.5 units of avian myeloblastosis virus (AMV) reverse transcriptase (New England BioLabs) to each. The extension reaction was carried out for 45 minutes at 47°C followed by 15 minutes at 70°C to inactivate the reverse transcriptase. Each reaction was ethanol precipitated as described above and pelleted at 13 000 rpm for 10 minutes. The resulting pellet was washed with 75% ethanol and resuspended in

formamide containing 20 mM EDTA. Equal amounts of cDNA were loaded onto a 0.4 mm 8% acrylamide 8 M urea PAGE gel (Dual Dedicated Height 20 cm x 60 cm Sequencer from CBS Scientific). Sequencing lanes were generated using PCR amplified fragments of the 23S rRNA gene and the same ^{32}P-labeled primer used in the reverse transcription reaction. The labeled cDNA product was generated using Sequenase DNA polymerase 2.0 according to the manufacturer's directions (Thermo Fisher Scientific). The gel was run at 50 W for 2.5 hours and subsequently dried onto Whatman filter paper at 70°C for 1 hour (Savant slab gel drier 2000). The dried gel was exposed to a phosphoimaging screen that was then scanned using a Typhoon Scanner (GE Healthcare).

The extent of modification was quantified in Image J (316). The relative modification intensity (RMI) value for each nucleotide position were calculated using equation 2 where the DMS control intensity is the intensity of the band in the 70S alone control and the Sample intensity is the intensity of the corresponding band in each 70S•protein complex lane.

$$\text{RMI} = \log(\text{DMS control intensity}/\text{Sample Intensity}) \quad (2)$$

Nucleotides protected (compared to the 70S ribosome control) from modification have negative RMI value while nucleotides that are less protected (compared to the 70S ribosome control) from modification have a positive RMI value. Each experiment was carried out in triplicate and nucleotides that showed an average RMI value greater than ±0.2 were considered to have undergone structural repositioning in the 70S•protein complexes compared to the 70S alone.

2.4 – RESULTS

2.4.1 – YCHF IS EXPRESSED THROUGHOUT THE BACTERIAL GROWTH CYCLE BUT UPREGULATED EARLY IN EXPONENTIAL PHASE

To determine whether YchF was constitutively expressed or upregulated at times during bacterial growth we measured the expression of endogenous YchF in *E. coli*. Cells were harvested at various points during the bacterial growth curve (Figure 2.1*A*) and the level of expression of YchF

was determined by western blotting (Figure 2.1*B*). YchF expression is markedly increased early in the exponential phase and remains steady throughout the entire growth curve. Expression throughout the *E. coli* life cycle suggests that the functional role of YchF is always required *in vivo*, but in particular as cells begin to rapidly grow and divide.

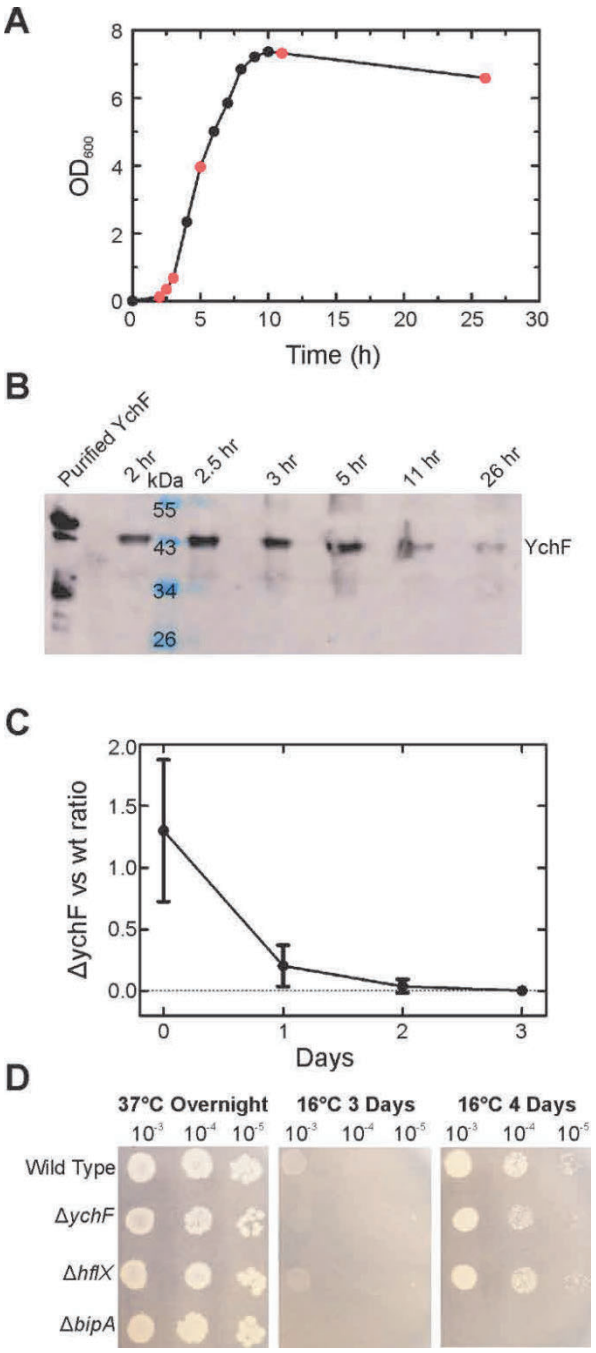

Figure 2.1 – YchF is upregulated during exponential growth phase and provides a fitness advantage to the cell. (A) *E. coli* DH5α cells were grown and harvested at various time points throughout the growth curve. Samples at each stage of growth were used to detect the relative level of YchF at each given time point (Red circles). (B) An equal amount of cells were lysed, analysed on an SDS-PAGE and western blot to detect YchF using an antibody produced against purified YchF. (C) Wild type and YchF knockout cells were grown in co-culture to determine the fitness advantage provided by the presence of YchF. Each day a sample was collected and used to determine the ratio of wild type to YchF knockout cells. (D) When grown at low (16°C) but not at optimal (37°C) temperatures, the Δ*ychF* strain showed reduced viability compared to the wild type or Δ*hflX* strains, yet not to the same extent as the known cold-sensitive Δ*bipA* strain. Experiments performed by Fan Mo.

2.4.2 – YCHF EXPRESSION PROVIDES A FITNESS ADVANTAGE UNDER OPTIMAL AND COLD STRESS CONDITIONS

We grew wild type and the Δ*ychF* strains in co-culture to determine if *E, coli* expressing YchF could outcompete YchF knockout *E.coli* strains (Figure 2.1*C*). Each day a sample was plated on solid LB-media with and without kanamycin to select for the Δ*ychF* strain or both strains, respectively. The number of colony forming units (CFU) on each plate was used to determine the ratio of wild type to Δ*ychF* cells on each sampling day. After three days of growth, wild type cells had completely outcompeted the Δ*ychF* strain in three separate trials (Figure 2.1*C*). The same experiment was also carried out with the Δ*hflX* strain resulting in the knockout strain being outcompeted after a week supporting the importance of YchF for cellular fitness. Furthermore, we wanted to see if there were any non-optimal growth conditions under which the absence of YchF would be detrimental to cell survival (Figure 2.1*D*). To do so, we performed serial dilutions of the Keio knockout strain of YchF (Δ*ychF*) (308) plated on solid LB-media and grown at different temperatures. Under normal *E. coli* growth conditions of 37°C, Δ*ychF* grew like wild type cells and two other knockout strains (Δ*bipA* and Δ*hflX*). When these strains were grown at 16°C, colonies took more than three days to appear, and the effect became more apparent after four days growth. As expected, the known cold sensitive strain Δ*bipA* did not grow at 16°C (320) while the Δ*ychF* strain demonstrated a reduced growth rate compared to the wild type and the Δ*hflX* strain. These results suggest that YchF plays an important role under cold stress in addition to providing a fitness advantage to cells grown under optimal growth conditions.

2.4.3 – YCHF IS AN RNA CHAPERONE

Cold stress leads to issues in both protein and RNA folding whereby either biomolecule can get kinetically trapped as intermediates during folding making them non-functional and potentially toxic to the cell (317, 321, 322). To overcome cold stress, cells have numerous chaperones and helicases that destabilize intermediates in the folding pathway and promote a path to the proper fold. Impairment or removal of chaperones/helicases tends to lead to cold sensitive phenotypes in bacterial cells (323, 324). As such we tested YchF for RNA strand displacement

activity indicative of helicases. Two complementary RNA oligonucleotides labeled with either Cy3 or Cy5 were annealed resulting in FRET between the dye pair upon excitation of the Cy3 dye (Appendix Figure 2.1*A*). Enzyme-mediated displacement of the two labeled RNAs from each other resulted in a decrease in FRET that was monitored overtime. The addition of an unlabeled competitor RNA oligonucleotide complementary to the Cy3 labeled RNA prevented re-association of the two labeled oligonucleotides. YchF addition to the labeled RNA duplex resulted in a decrease in FRET like that observed for known helicases StpA and S1 (Figure 2.2 and Appendix Figure 2.1*BC*). Ribosomal protein S1 is a helicase that is a part of the 30S ribosomal subunit and facilitates the binding of highly structured mRNAs to the ribosome for translation (325) and StpA is a helicase that associates with the double stranded DNA of the nucleoid in *E. coli* (326). The addition of elongation factor thermo stable (EF-Ts) and Bovine Serum Albumin (BSA), along with the addition of competitor oligonucleotide only resulted in an increase in FRET most likely due to further annealing of labeled oligonucleotides over the course of the experiment. EF-Ts was used as it is a non-ribosome binding translation factor and is only known to indirectly interact with tRNA through its interaction with elongation factor thermo unstable (EF-Tu), while BSA was included as a negative control for non-specific binding of RNAs by proteins (327). BSA also plays no role in translation and does not bind to ribosomal particles or to nucleic acids. Helicases are generally classified by utilizing the hydrolysis of ATP to provide energy to unwind nucleic acids (328). Surprisingly, there was no added effect on strand displacement in the presence of ATP by YchF (Figure 2.2*B* and Appendix Figure 2.1*C*) despite YchF's well-characterized ATP hydrolysis activity (174). Taken together, these results demonstrate that YchF is a nucleotide-independent RNA chaperone.

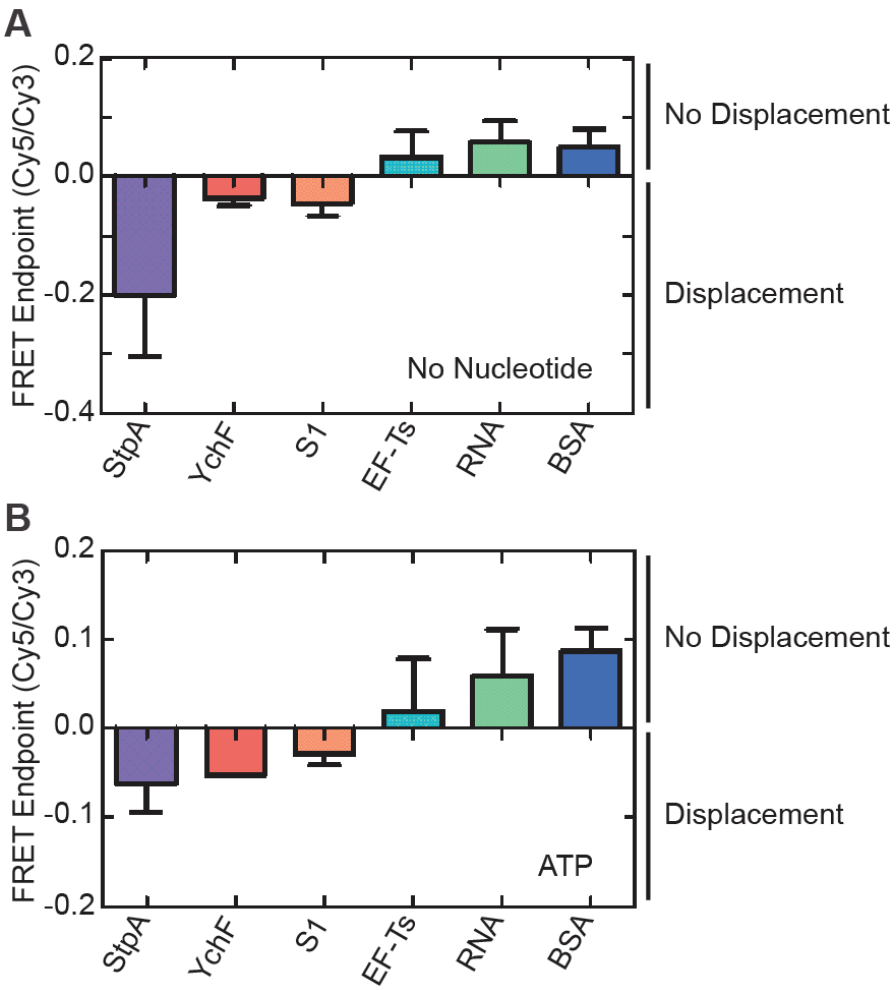

Figure 2.2 – YchF acts as a nucleotide-independent RNA chaperone. Cy5 and Cy3 labeled RNA oligonucleotides were annealed before adding an unlabeled competitor RNA and protein factor. Displacement of the two labeled RNA oligonucleotides was observed by a decrease in FRET over time. The reactions were carried out (A) in the absence of nucleotide and (B) in the presence of adenosine triphosphate (ATP). YchF (Red), StpA (Purple), and S1 (Orange) show a decrease in FRET over time while EF-Ts (Teal), BSA (Blue), and Buffer (Green) do not. Experiment performed by Dr Binod Pagani.

2.4.4 – YCHF BINDS TO tRNA *IN VIVO* AND *IN VITRO*

To determine what RNA molecules YchF could interact with *in vivo*, we performed a pull-down of polyhistidine tagged YchF followed by gel filtration. Previously, we used this technique to confirm that YchF co-purifies with the 70S ribosome (174). Gel filtration yielded two peaks of which the earlier fractions contained YchF and the 70S ribosome, and the later eluting peak containing YchF. Here we show that the later-eluting peak containing YchF also contained a small nucleic acid below 100 nucleotides in size (Figure 2.3*A*). RNA from this peak was phenol/chloroform extracted and a cDNA library of small non-coding RNAs was prepared for next generation sequencing using a NEBNext Multiplex Small RNA Sample Prep Set for Illumina kit. Paired-end 150 nucleotide reads from an Illumina Hi-seq 2500 were processed as outlined in the methods. The log fold change of enriched RNA molecules was normalized to take into account differences in cellular abundance is shown in Figure 2.3*B*. tRNAs are highly enriched in the pull-down with a four- to twenty-three-fold log enrichment over other small non-coding RNAs (Figure 2.3*B*), along with a modest two-fold enrichment of the 5S rRNA (Figure 2.3*B* inset). The most highly enriched tRNAs were two isoacceptors of $tRNA^{Phe}$, both having over 20-fold enrichment compared to other small non-coding RNAs. It should be noted that all tRNA are enriched in the pull-down though and the most enriched tRNAs are enriched by no more than four-fold over the least enriched tRNA species suggesting that YchF binds tRNA indiscriminately (Figure 2.3*B*).

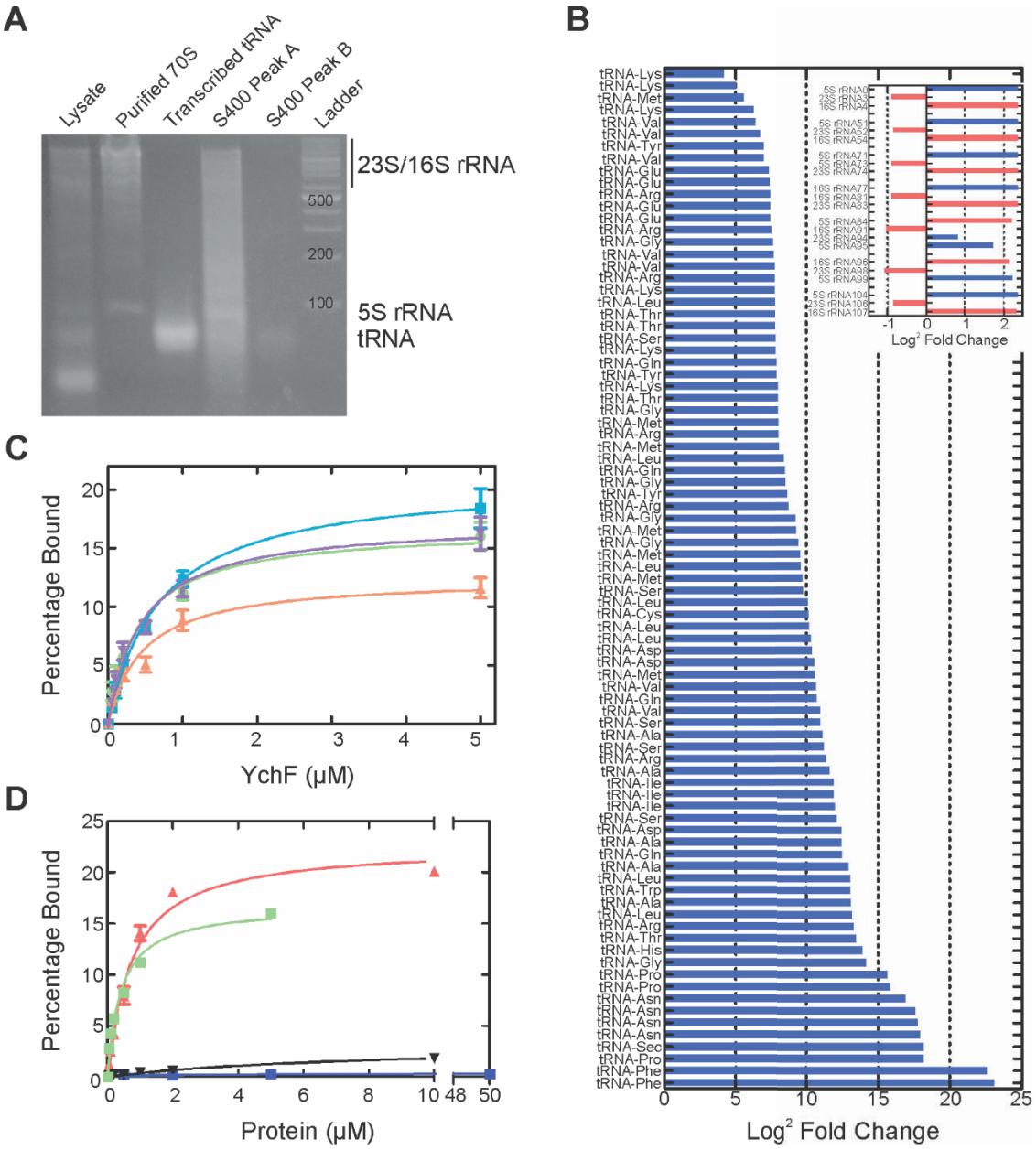

Figure 2.3 – YchF binds to tRNA *in vivo* and *in vitro*. Polyhistidine tagged YchF was purified initially by Ni^{2+}-Sepharose affinity chromatography followed by gel filtration using a Sephacryl S400 column. (A) RNA from the two peaks observed in the chromatogram was isolated and compared to RNA from the cell lysate, along with purified rRNA and tRNA. (B) RNA isolated from peak B was sequenced using a MiSeq and the log-fold enrichment of RNA molecules was plotted. Enrichment of the rRNA genes is plotted in the inset. (C) Binding curves from plotting fraction of $tRNA^{Phe}$ bound to YchF versus the concentration of YchF in the presence of ATP (Teal), ADPNP (Purple), ADP (Orange), or in the *apo*-form (Green). (D) Resulting YchF●tRNA binding curves using truncated $tRNA^{Phe}$ lacking the CCA-end (ΔCCA $tRNA^{Phe}$) to YchF (Black) or TruB (Red) in addition to using a truncated YchF lacking the TGS-domain (ΔTGS YchF) to full length $tRNA^{Phe}$ (Blue). Full length YchF (*apo*-form) and $tRNA^{Phe}$ same as in panel B (Green). Experiments performed by Dr Binod Pagani and deep sequencing analysis by Dr Senthilkumar Kailasam.

As YchF also purifies with the 70S ribosome, the finding that tRNA co-purifies with YchF could be an artifact resulting from tRNAs bound to the 70S ribosome in vivo. So, we performed nitrocellulose filter binding experiments to determine if YchF could bind tRNA in the absence of the ribosome. Using $tRNA^{Phe}$ transcribed with ^{3}H-UTP, we were able to determine the affinity of $tRNA^{Phe}$ to YchF to be 0.69 ± 0.09 μM in the presence of ATP (Figure 2.3*C* and Appendix Table 2.1). We created a truncated variant of YchF lacking the C-terminal TGS-domain (ΔTGS-YchF) that was unable to bind $tRNA^{Phe}$ in our nitrocellulose filter binding experiment. Another tRNA binding protein, RelA, contains a similar TGS-domain that is responsible for interacting with the 3' CCA end of tRNA (329). The ΔTGS-YchF variant showed an overall similar structure to the full length YchF using CD spectroscopy with a notable difference consistent with the removal of 25% of the β-sheet content found in the TGS-domain (Appendix Figure 2.2 and Appendix Table 2.1). Furthermore, ΔTGS-YchF was able to retain its ability to bind to adenine and guanine nucleotides (Appendix Table 2.2), evidence supporting that the remainder of the protein folded properly. The interaction between the TGS-domain of YchF and CCA end of tRNA was further demonstrated using an *in vitro* transcribed tRNA lacking the CCA end. This truncated tRNA is unable to bind the full length YchF but retained its binding to the tRNA modification enzyme TruB that binds to the elbow region of tRNA (Figure 2.3*D*) (330). These results confirm that YchF interacts with the 3'-CCA end of tRNA through its TGS-domain.

2.4.5 – COMPARISON OF THE TGS-DOMAIN CONTAINING PROTEINS YCHF AND RELA

While we were preparing this manuscript, the Wilson and Ramakrishnan labs published a cryo-EM structural model of the stringent response factor RelA bound to the 70S ribosome with A- and P-site tRNAs, and mRNA (116, 329). In this structure RelA was bound to the ribosomal A-site and contacted the A-site tRNA through its TGS-domain. The TGS-domain in RelA and YchF have enzyme specific extensions but have an overall conserved amino acid sequence and three-dimensional structure (Appendix Figure 2.3). Using the RelA•70S ribosome model, *E. coli* YchF was docked on the ribosome by aligning its TGS-domain with that of RelA (Figure 2.4*A*). The resulting structural model shows YchF bound to the A-site tRNA (Figure 2.4*B*) and the 70S

ribosome with YchF positioned to interact with the SRL and ribosomal proteins L11 and S12 (Figure 2.4*C*). The A-site tRNA is in an A/T position, like the EF-Tu ternary complex that delivers an aminoacyl-tRNA into the A-site during elongation. Whether YchF binding causes the A-site bound tRNA to adopt the A/T position, or whether YchF brings a tRNA into the ribosomal A-site has yet to be determined. Nevertheless, the tRNA is positioned so that the elbow region and anticodon stem-loop rest long the alpha helical domain of YchF, while the CCA end of the tRNA inserts right into the TGS-domain of YchF (Figure 2.4*BC*). Moreover, the CCA end of the tRNA is positioned such that the tRNA could only be charged with a small amino acid like glycine without steric interference (Figure 2.4*D*). Furthermore, the electrostatic surface potential of YchF perfectly matches with the positioning of the tRNA in the model (Appendix Figure 2.4).

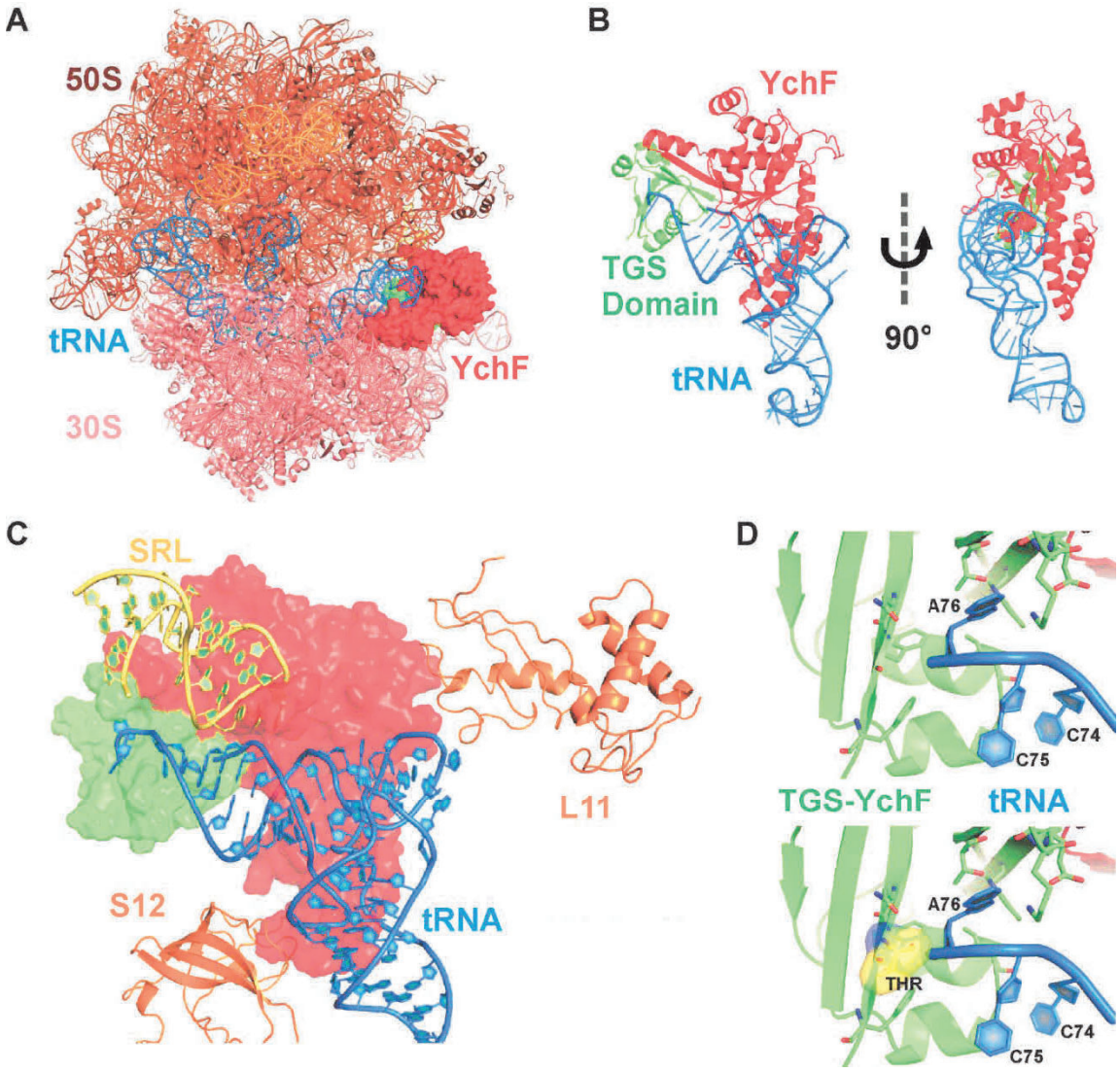

Figure 2.4 – Structural model of YchF bound to the ribosomal A-site. Using the published 70S-RelA-tRNA structure (PDB 5IQR), YchF was docked onto the ribosome by aligning the TGS-domains of both YchF and RelA. (A) 70S-bound YchF interacts with the A-site of the ribosome after aligning its TGS-domain with that of RelA with no apparent steric clashes. (B) The A-site bound tRNA in the RelA structure in the T/A-position interacts across the surface of the modeled YchF. (C) Like other trGTPases, the SRL interacts with the G-domain of YchF. (D) Interestingly, the 3' CCA end of the tRNA binds to the TGS-domain of YchF, but the presence of an amino acid would result in steric hinderance suggesting that YchF may only bind deacylated tRNA. Docking analysis done by Dr Senthilkumar Kailasam.

The overall structure of ATP-bound YchF and the conformation of the A-site tRNA in our docked model also mimics the structure of EF-G bound to the ribosome (Figure 2.5), where the tRNA bound to YchF mimics domain IV of EF-G. Overlaying the structure of the YchF•tRNA complex on space filling models of EF-G (Figure 2.5*B*) or the EF-Tu ternary complex (Figure 2.5*C*) revealed that YchF•tRNA has a near-identical three-dimensional structure as those two translational GTPases. The major difference between YchF•tRNA and either the EF-G or the EF-Tu ternary complex is the α-helical domain that extends down the tRNA toward the anticodon stem-loop. The functional implication of this molecular mimicry is discussed below.

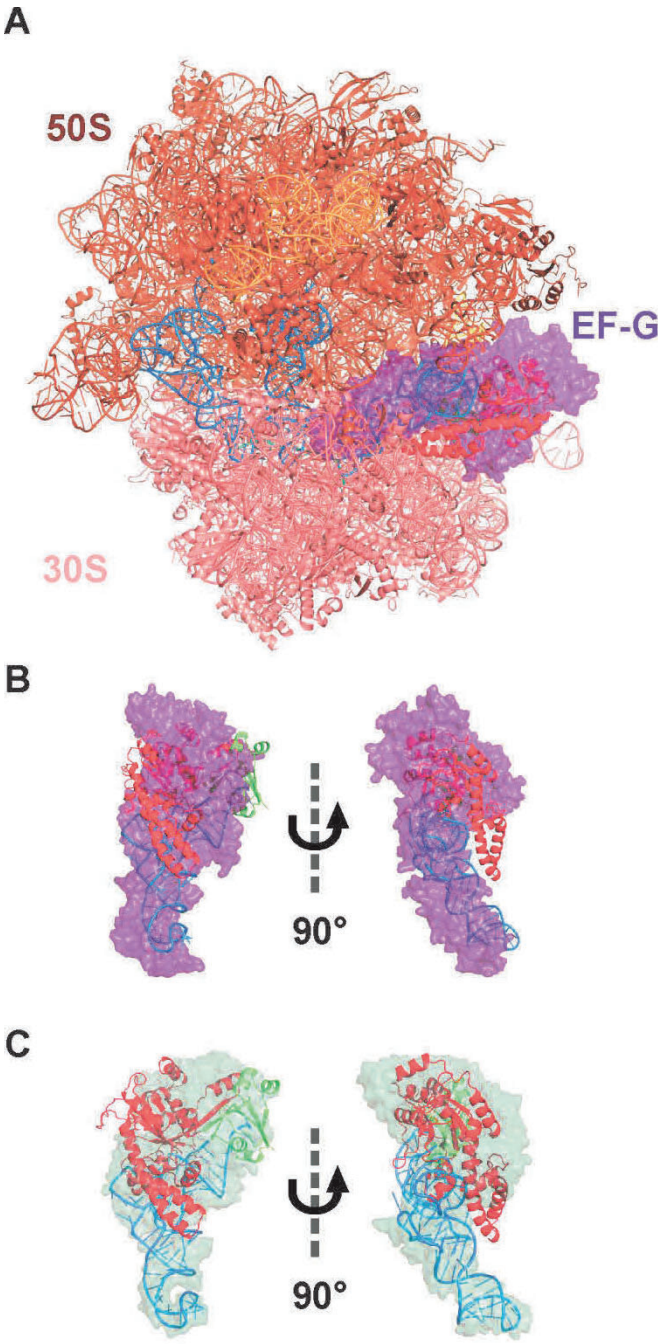

Figure 2.5 – YchF shows molecular mimicry to other trGTPases. (A) EF-G (Purple space filling model) bound 70S ribosome with YchF-tRNA model docked onto the A-site. Superimposition of the YchF-tRNA (Red-Green-Blue cartoon model) with (B) EF-G (Purple) and (C) EF-Tu (Teal) showing the overall structural similarity between each factor.

2.4.6 – YCHF BINDS TO THE A-SITE OF THE BACTERIAL RIBOSOME

To confirm that YchF binds to the A-site of the ribosome we performed several biochemical experiments (Figure 2.6). Initially, we used dimethyl sulfate (DMS) modification analyzed by primer extension to map regions of the rRNA that showed protection upon YchF or EF-G binding. EF-G protection of the SRL had previously been published (331) and if YchF does mimic the structure of EF-G and its interactions with the ribosome, we hypothesized that YchF would have a similar protection pattern to that of EF-G. We prepared complexes of EF-G•GTP in the presence or absence of fusidic acid (FUS), or YchF and ATP/ADP that were incubated with 70S ribosomes to form a factor-bound ribosome complex before DMS modification. Fusidic acid is an antibiotic known to lock EF-G onto the ribosome post GTP-hydrolysis and phosphate release, thereby preventing its dissociation from the ribosome (332). Complexes were prepared in both low (7 mM) and high (30 mM) magnesium containing buffer to maintain ribosome stability, respectively. Isolated rRNA from each complex was used in a reverse transcription reaction with ^{32}P-radiolabeled primers specific for the region surrounding the SRL or the L10 stalk, respectively. Following primer extension, the relative modification intensity for each nucleotide was plotted for each complex and region of the rRNA (Figure 2.6*AB* and Appendix Figures 2.5-2.8). Under both buffer conditions, we observed evidence of protections of the SRL by both EF-G•GTP•FUS and YchF•ATP as well as the protection of the SRL at A2660 by EF-G (Figure 2.6*A* and Appendix Figures 2.5-2.6) as has been observed previously for EF-G•GTP•FUS (331). From the histograms we can see regions of DMS-protection and deprotection caused by YchF or EF-G binding to the 70S ribosome (Appendix Figures 2.5-2.8) suggesting that they make some of the same interactions with the 23S rRNA. In the YchF•ATP bound complex, protection of nucleobases all along the SRL are observed indicating that YchF does interact with the SRL (Figure 2.6*B*). Of the protected bases observed, A2662 stands out because of its interaction with YchF in the docked model (Figure 2.4*C*) and because A2662 is known to interact directly with other trGTPases to stimulate GTP hydrolysis (333). Additionally, some of the protected and deprotected bases along both the SRL and L10 stalk differ based on the nucleotide bound to YchF (Appendix Figures 2.5-2.8), suggesting that conformational changes dependent on nucleotide and hydrolysis may alter the conformation of the rRNA.

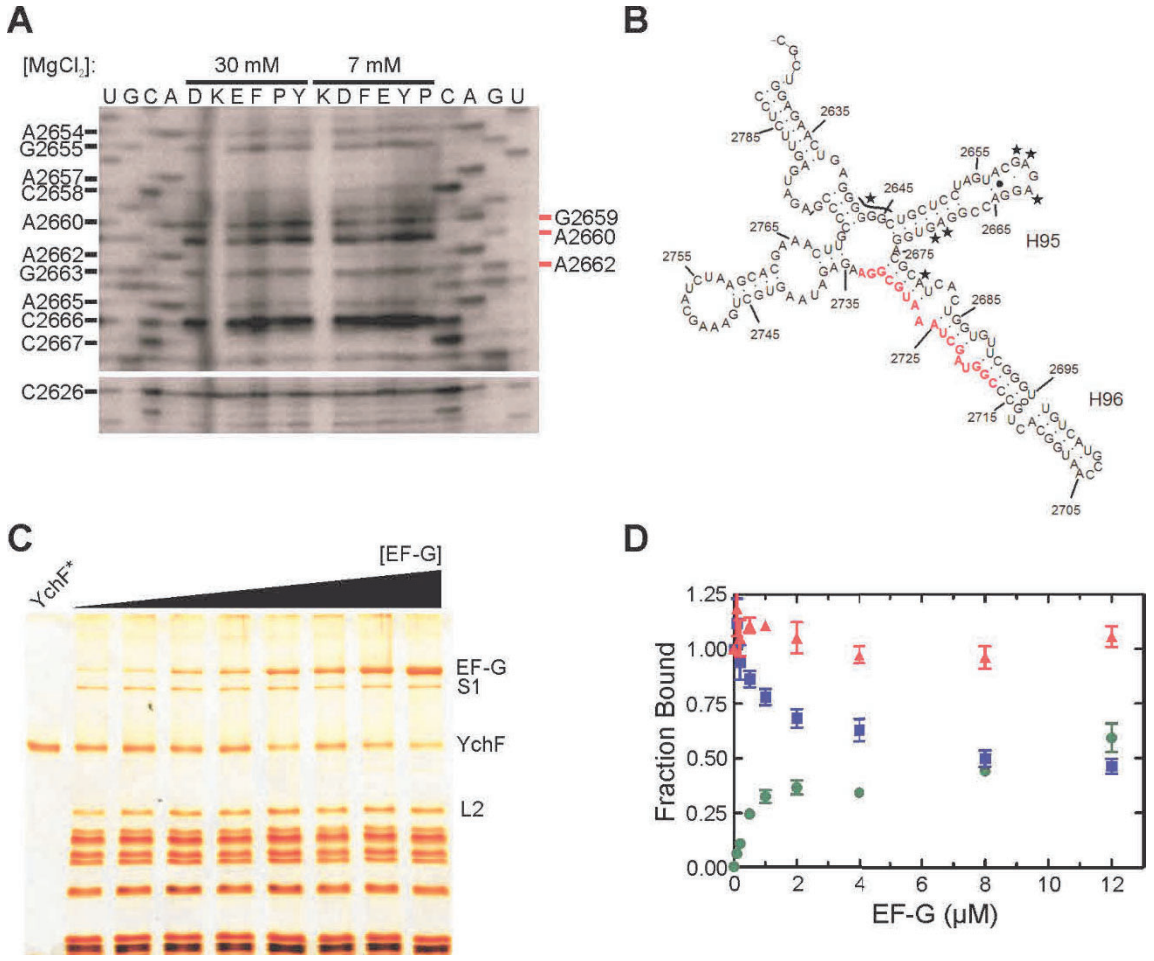

Figure 2.6 – YchF binds to the A-site of the bacterial ribosome like other trGTPases. (A) DMS modification pattern at the SRL of the 70S ribosome alone [D], with YchF●ATP [P], YchF●ADP [Y], EF-G●GTP [E], or EF-G●GTP●Fus [F] bound to the 70S ribosome. Unmodified 70S ribosomes are indicated as [K]. Sequencing lanes are shown on both ends of the gel and labelled according to sequencing on the left side. Nucleotide positions that show protection from DMS modification are indicated with red arrows and numbered on the right side of the gel according to the modified position which is the 5'-adjacent nucleotide from the sequencing position. These protected positions are G2659, A2660, and A2662 and are observed upon binding to the ribosome of YchF●ATP with both $MgCl_2$ concentrations or of EF-G●GTP●Fus with 7 mM $MgCl_2$. The secondary structure stop at C2626 is included to show equal loading of the gel lanes. (B) Positions at the SRL that show protection from DMS modification upon YchF●ATP binding are indicated with stars on the secondary structure of the rRNA. The sequence of the primer extension primer is highlighted in red. (C) Competition binding assay of EF-G and YchF to the 70S ribosome. (D) Fraction bound of EF-G (Green), YchF (Blue), and the sum-total of factor bound (Red) remaining constant at increasing concentrations of EF-G. Experimental data collected by Dora Capatos (Panel A and B) and Dr Binod Pagani (Panel C and D).

Independent of the DMS protection, we performed competition binding experiments between YchF and EF-G to investigate that they have overlapping ribosomal binding site. EF-

G•GDP•FUS•70S ribosome complexes with increasing concentrations of EF-G were formed before incubation with YchF•ATP. Complexes were pelleted through a sucrose cushion to remove any unbound factor before the resuspended pellet was analyzed by SDS-PAGE (Figure 2.6*C*). The amount of EF-G and YchF relative to ribosomal proteins was quantified and shown as fraction bound of each factor (Figure 2.6*D*). At all concentrations of EF-G, the total factor fraction bound was ~1 factor per ribosome, confirming that YchF and EF-G indeed share a binding site on the ribosome. Taken altogether, our data demonstrates that YchF is an RNA chaperone that binds to the A-site of the ribosome.

2.5 – DISCUSSION

The constant expression of YchF during growth, the marked increase during rapid growth, and the fitness advantage YchF expression confers (Figure 2.1) although it is not an essential protein (308) raise interesting questions about the role of YchF *in vivo*. The increase in YchF expression at the start of the exponential growth phase suggests that YchF functions in a process important to rapid growth. Rapidly dividing bacterial cells require high rates of protein synthesis, and thus high levels of ribosome synthesis. YchF is a ribosome binding ATPase whose ATP hydrolysis is stimulated by the 70S ribosome (174). As such, it is likely that YchF is involved in ribosome biogenesis or protein synthesis in particular during the early exponential phase when both ribosome biogenesis and protein synthesis are up regulated.

Previous studies have demonstrated that YchF is non-essential under optimal growth conditions (308, 334), so we asked whether YchF confers any growth advantage to cells that possess it. To test this, we grew wild type and Δ*ychF* cells in co-culture. If YchF did provide a fitness advantage, cells lacking YchF (Δ*ychF*) would be outcompeted. We observed that YchF does indeed confer a fitness advantage, because within three days the wild type cells had outcompeted the strain lacking YchF (Figure 2.1*C*). The fact that YchF's expression level is upregulated in the early exponential growth phase and the observation that YchF increases fitness of bacteria under optimal growth conditions confirm that the functional role of YchF *in vivo* involves likely more than simply acting as a stress response protein.

In seeking to understand the phenotype for a knockout of YchF, we grew the Δ*ychF* strain at 16°C to induce cold shock (Figure 2.1*B*). A serial dilution of wild type cells and the Δ*ychF* strain showed that at 16°C, a Δ*ychF* strain had impaired growth as apparent by a reduced number and size of colonies after growth for four days. In comparison, a Δ*hflX* strain showed growth like *E. coli* wild type cells, while the known cold sensitive Δ*bipA* strain did not grow under the same conditions. All cells grew at optimal *E. coli* growth conditions of 37°C. Several ribosome binding proteins known to be involved in ribosome biogenesis have decreased growth phenotypes when the respective knockout strains are grown at lower temperatures. This suggests that YchF is a ribosome biogenesis factor, which is further supported by its upregulation when cells are rapidly growing and producing new ribosomes to maintain a high growth rate. However, if YchF were a ribosome biogenesis factor, we would expect that it would co-purify with a premature or mature ribosomal subunit rather than the 70S ribosome as we have previously reported (174). Furthermore, the Δ*ychF* strain does not accumulate any precursor subunits (Data not shown) as is characteristic of other ribosome biogenesis factors (45, 335, 336). Additionally, the 70S ribosome but neither the 50S nor 30S ribosomal subunit stimulates the ATP hydrolysis activity of YchF (174). To reconcile these apparent discrepancies, we propose a hybrid model, in which YchF acts as a ribosome quality control enzyme ensuring that newly synthesized ribosomal subunits form active 70S ribosome. Furthermore, YchF monitors 70S ribosomes that have been through multiple rounds of protein synthesis for any defects that may have accumulated during their use (Figure 2.7).

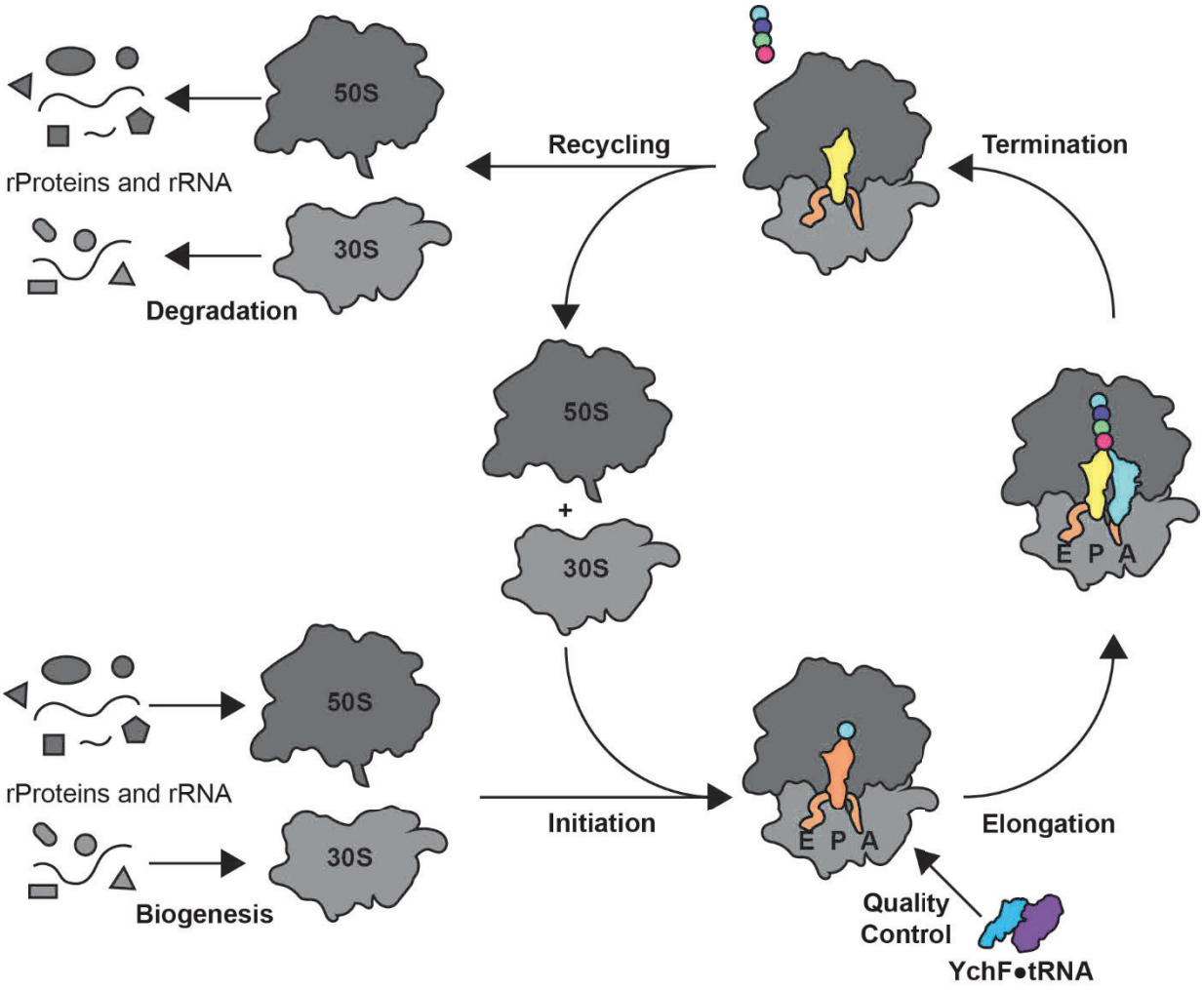

Figure 2.7 – YchF acts as a ribosome quality control enzyme to ensure 70S ribosome fidelity following biogenesis and after successive rounds of translation. Ribosomal subunits are produced after several hierarchical assembly steps whereby the ribosomal proteins (rProteins) are positioned onto the ribosomal RNA (rRNA), the rRNA is post-transcriptionally modified and processed, and the subunits are checked for proper assembly before entering initiation. Translation initiation results in the formation of a 70S initiation complex (70S IC) with a P-site bound fMet-tRNA^{fMet}. This 70S IC either enters translation elongation normally or we hypothesize it is unable to bind the EF-Tu ternary complex due to an improper rRNA fold or positioning allowing the YchF•tRNA complex to bind and correct the rRNA fold. Upon reaching the correct fold, the 70S IC can continue into elongation followed by translation termination and ribosome recycling before entering another round of translation. As the YchF•tRNA complex mediated quality control step proceeds initiation, it is likely that the YchF•tRNA complex can correct ribosomes that have been through several rounds of translation already instead of the ribosome sitting idle on an mRNA or being degraded.

A cold sensitive phenotype is a characteristic feature of RNA chaperone knockout strains (323, 324). As such, we tested YchF for RNA strand displacement activity (Figure 2.2). Using a FRET based measurement, we monitored the displacement of a Cy5 labeled RNA oligonucleotide

from one labeled with Cy3 by YchF or other proteins known to be helicases. YchF, along with ribosomal protein S1 and StpA, showed strand displacement activity in the presence and absence of ATP. This clearly indicates that YchF is a nucleotide independent RNA helicase. Nucleotide independent RNA unwinding supports our quality control hypothesis that if YchF were to bind a 70S ribosome that has a misfolded helix, it could unwind the helix and allow it to refold properly thus returning the 70S ribosome back into the pool of actively translating ribosomes. Not requiring energy for the unwinding activity may allow ATP hydrolysis to regulate when YchF dissociates from the ribosome, as YchF may need to remain bound until the correct conformation of the rRNA and a properly folded 70S ribosome is achieved. Strand displacement of the ribosomal RNA (rRNA) by YchF has yet to be confirmed.

YchF is a known ribosome binding protein (174) suggesting that it is the rRNA that YchF may act upon as a chaperone. We found that YchF co-purified with a small RNA after removal of the 70S ribosome through gel filtration (Figure 2.3*A*). From the next generation sequencing of small non-coding RNAs that bind to YchF *in vivo*, we found tRNA to be highly enriched (Figure 2.3*B*). It could be argued that the tRNA found enriched with YchF may be due to contamination of 70S ribosomes with bound tRNA. To confirm that YchF interacts with tRNA in the absence of the ribosome, we performed an *in vitro* binding experiment with highly purified components and found that YchF indeed interacts with tRNA at a nanomolar affinity (Figure 2.3*C*). Based on the distinctive surface charge distribution of YchF in which a cleft containing several positively charged residues is highly visible (Appendix Figure 2.4), we predicted that tRNA could bind across this cleft. Interestingly, the stringent response factor RelA also has a TGS-domain and binds to both tRNA and the ribosome (116, 329). In the 70S•RelA•tRNA structure, the TGS-domain interacts with the CCA end of the tRNA suggesting that similar interactions may be observed between YchF and tRNA. Using a truncated YchF lacking the TGS-domain along with an *in vitro* transcribed tRNA lacking the 3' CCA end, we were able to show that the interaction between YchF and tRNA likely mirrors that of RelA and tRNA, whereby the CCA end of the tRNA binds to the TGS domain of YchF (Figure 2.3*D*). These data suggest that the target for YchF's strand displacement activity could also be tRNA. While this is possible, we hypothesize that YchF forms a complex with a tRNA before

interacting with the ribosome, and the ribosome is the true target of YchF's RNA unwinding activity. Moreover, for the first time we show that YchF interacts with tRNA both *in vivo* and *in vitro* in the absence of the ribosome.

Using the recently published structure of RelA bound to the 70S ribosome and tRNA (329), we docked YchF onto the ribosome based on TGS-domain present in both YchF and RelA. In this model the A-site bound tRNA is positioned with the anticodon in the decoding center of the 30S subunit while the CCA end points out of the A-site to interact with the TGS-domain of RelA (329). The TGS domain of YchF makes similar interactions with the tRNA and has no steric clashes with the tRNA. Initially, we looked at the conservation of the TGS-domain both in amino acid sequence and three-dimensional structure (Appendix Figure 2.3). While there are differences between the TGS-domain in both proteins, the overall structure was maintained such that we could confidently dock YchF onto the ribosome (Figure 2.4*A*). The resulting docked YchF structure on the ribosome highlighted two key interactions. First, the position of the A-site tRNA relative to YchF has the acceptor arm and elbow of the tRNA placed along the positively charged cleft of YchF in an electrostatically favourable position suggesting that the role of this conserved cleft (20) is to bind tRNA (Figure 2.4*B* and Appendix Figure 2.4). Furthermore, the overall structure of the YchF•tRNA model is surprisingly similar to that of EF-G and the EF-Tu ternary complex (Figure 2.5) consistent with a similar binding site.

The second interaction that our model revealed was the orientation of YchF in the A-site such that the SRL contacts YchF's G-domain (Figure 2.4*C*). This A-site binding site is supported by cryo-EM structural information of the *P. falciparum* YchF (PfYchF) ortholog bound to the A-site of the 80S ribosome (Personal communication from Drs. Alexei Amunts and Yuzuru Itoh). The SRL is important for triggering GTP hydrolysis in other trGTPases by correctly positioning the catalytic histidine (H84 in EF-Tu) to position a water molecule for nucleophilic attack on the γ-phosphate (333). Previously, we have shown that YchF lacks the conserved histidine in switch II that other trGTPases have, but instead has a conserved histidine (H114) in a flexible loop that is close to the SRL in our model (309). We confirmed biochemically that YchF interacts with the A-site, specifically at the SRL and L10 stalk regions using DMS modification analyzed by primer extension (Figure

2.6A and Appendix Figures 2.5-2.8). A crystal structure of EF-Tu ternary complex bound to the 70S ribosome showed that H84 of EF-Tu interacts with A2662 of the 23S rRNA (337), which based on our data is protected from DMS modification in the presence of ATP-bound YchF (Figure 2.6*B*). The exact interaction A2662 makes with YchF is not known. Interestingly, YchF shows less protection of the SRL when bound to ADP (Appendix Figures 2.5-2.8) supporting the idea that YchF undergoes a conformational change upon ATP hydrolysis positioning it further away from SRL. Structural information of the *P. falciparum* 80S ribosome with PfYchF bound suggests that YchF has at least two different conformations when bound to the ribosome (Personal communication from Drs. Alexei Amunts and Yuzuru Itoh). In these structures, PfYchF is bound to ADP suggesting they are post-hydrolysis complexes whereby the rRNA has already been refolded by YchFs chaperone activity. The difference between these two structures is the distinct movement away from the SRL, suggesting that post hydrolysis a conformational change occurs in YchF before the YchF ternary complex dissociates from the ribosome. In the structure where YchF is closest to the SRL, YchF does not make any direct connections with the SRL, supporting the primer extension data for EcYchF (Appendix Figures 2.5-2.8). It is unclear if the further conformational change of YchF away from the SRL occurs in *E. coli* and other bacteria, or if it is specific to the eukaryotic orthologs, and what the functional importance of this conformational change is. Overall, this is the first evidence that YchF is a ribosomal A-site binding protein.

One of the most interesting outcomes of docking YchF onto the structure of RelA bound to tRNA and the 70S ribosome, was the similarity between YchF•tRNA and EF-G bound to the ribosome (Figure 2.5). Superimposing the YchF•tRNA structure on EF-G or the EF-Tu ternary complex (Figure 2.5*BC*), showed that YchF•tRNA has the same overall structure as either trGTPase. This would suggest a type of molecular mimicry whereby YchF is able to interact with the 70S ribosome similarly to EF-G and/or the EF-Tu ternary complex. The implications of this are quite intriguing, for EF-G and EF-Tu are essential proteins with key roles in translation. Molecular mimicry of EF-G and EF-Tu is not unique to YchF, for several homologs of EF-G exist in *E. coli* including EF4 (LepA), BipA, and TetO/TetM (41, 44, 338, 339). The interesting question with these molecular mimics is, when does each bind to the ribosome? This is because their cellular

concentrations relative to the ribosome binding affinities of EF-G and EF-Tu enable EF-G and the EF-Tu ternary complex to outcompete all other proteins for binding to the ribosome during translation elongation. For example, TetM/TetO bind to the ribosome after inhibition by the ribosome binding antibiotic tetracycline that prevents aminoacyl-tRNA accommodation (338-341). Upon binding, TetM/TetO removes bound tetracycline from the A-site of the small ribosomal subunit to allow translation to commence (338, 339). As such, factors like EF4 (LepA) and YchF would have to interact with the ribosome either during ribosome biogenesis, or under stress conditions whereby translation has stalled.

One question that arises from this work is whether a YchF•ATP•deacyl-tRNA complex (herein referred to as the YchF ternary complex) can form *in vivo*. YchF would have to compete with the aminoacyl-tRNA synthetases (aaRS) for binding to deacylated-tRNAs. The aaRSs charge deacyl-tRNA with their corresponding amino acid resulting in an aminoacyl-tRNA that is bound by EF-Tu. The aaRSs have a K_D for deacyl-tRNA (Histidyl-tRNA synthetase (HisRS) $K_{D,\ HisRS}$ = 246 nM; $K_{D,\ HisRS•Histidine}$ = 91 nM (342)) similar to that of YchF for deacyl-tRNA ($K_{D,\ YchF•ATP}$ = 690 nM). Additionally, the cellular concentration of each aaRS is within the same range as YchF under a range of growth conditions (343). The cellular concentration of deacyl-tRNA varies depending on the isoacceptor but on average 60% of tRNAs are aminoacylated in ideal growth conditions (344). Given the cellular concentration of total tRNA in *E. coli* is 1-30 μM depending on the isoacceptor species (345), of which 40% are deacylated, and that the K_D of YchF for tRNA is in the nanomolar range, we can expect that the majority of YchF would be bound to tRNA in the cell and thus a YchF ternary complex would interact with the ribosome *in vivo*.

Based on our findings presented here and previous biochemical data, we propose that the YchF ternary complex interacts with the 70S ribosome if translation elongation is stalled due to a misfolded rRNA segment (Figure 2.7). An improperly folded segment of the rRNA, such as the SRL which our data would suggest (Appendix Figures 2.5-2.6), would prevent binding or stimulation of GTP hydrolysis by either EF-G or the EF-Tu ternary complex during translation, thereby preventing protein synthesis by that ribosome, and every trailing ribosome on the same mRNA. The YchF ternary complex would bind the stalled ribosome, detect misfolding based on specific molecular

interactions between YchF and the ribosome that are formed or not formed upon binding, and unwind the misfolded region (Figure 2.8). If the proper fold is not achieved after unwinding, YchF would continue to unwind the refolded rRNA until the proper fold is achieved. Once the correct molecular interactions between YchF and the A-site of the ribosome are established by allowing the rRNA to refold properly, YchF is triggered to hydrolyze its bound ATP. We predict the interaction between YchF and the properly folded rRNA and ribosomal proteins are the same as those made between the ribosome and both EF-G and the EF-Tu ternary complex. Forming molecular contacts with the SRL has been demonstrated to be important for activating the GTP hydrolysis activity of many other trGTPases (337, 346). This supports the idea that the YchF ternary complex acts and molecular mimic to these elongation factors. Furthermore, these correct interactions between the YchF ternary complex and the properly folded rRNA act as the final check in quality control following ribosome biogenesis, or in maintaining a functional pool of active ribosomal subunits.

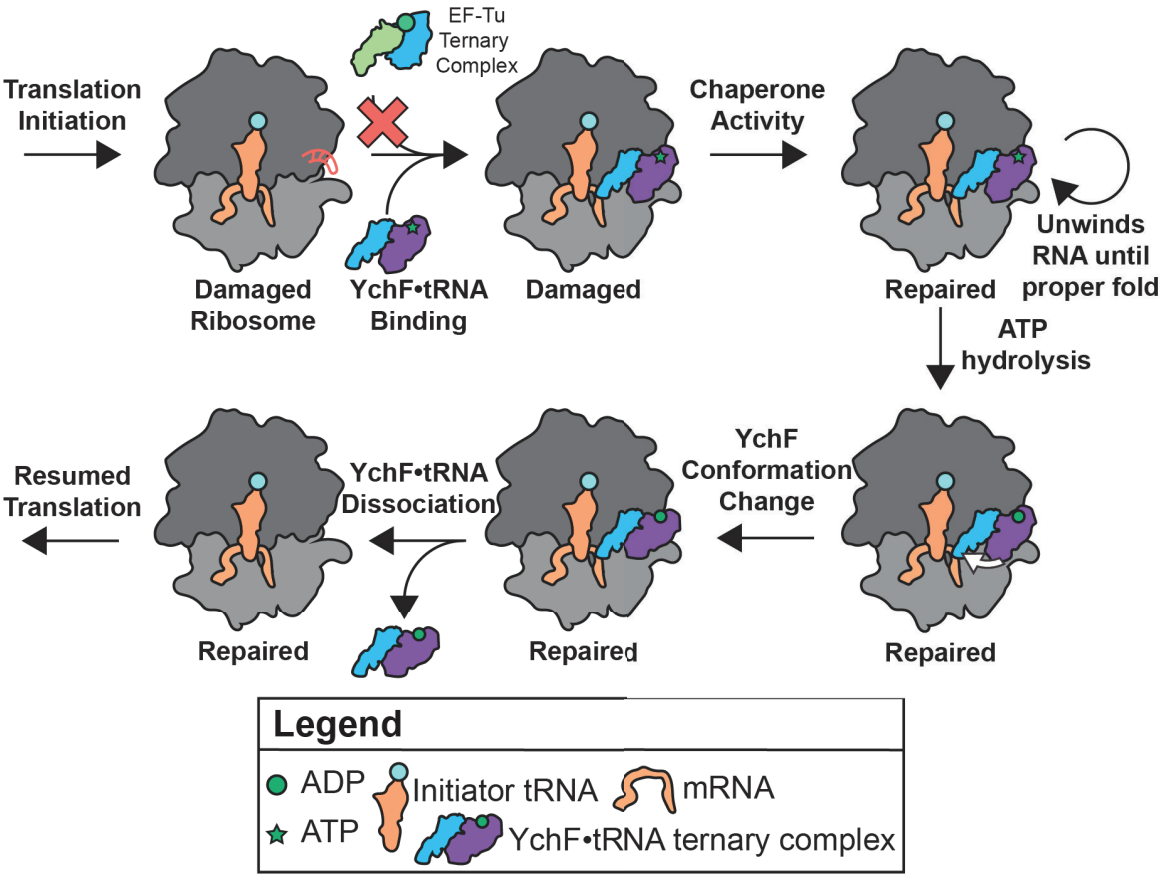

Figure 2.8 – Proposed model of YchF•tRNA mediated ribosome quality control. Following maturation of the individual ribosomal subunits, or following a previous round of translation, the ribosomal subunits are brought together during translation initiation. Throughout ribosome biogenesis different checkpoints are assessed to ensure the subunits will function properly, but the newly synthesized subunits are not assessed for intersubunit connections and signal relays until they are brought together for the first time in translation initiation. Any defects in the large subunit that prevent intersubunit connects would be detrimental to translation, in particular for the EF-Tu ternary complex that relies on signal transfer from the 30S subunit to the SRL of 50S subunit following codon recognition to trigger GTP hydrolysis and accommodation of the tRNA (see *Section 1.6 – Translation Elongation*). Such a defect would prevent EF-Tu ternary complex association resulting in a stalled, or "damaged" 70S ribosomal complex. This "damaged" ribosome complex would be the target for the YchF ternary complex (YchF•ATP•tRNA). Here, the YchF ternary complex would use its chaperone activity to unwind the rRNA and allow it to refold. Once the proper fold is achieved, YchF would be stimulated to hydrolyze ATP, resulting in a conformational change in YchF, and subsequent dissociation of the YchF ternary complex. The YchF conformational change is observed in structural information of *P. falciparum* YchF bound to the 80S ribosome (data not shown). As the YchF ternary complex structurally mimics other trGTPases, stimulation of its ATP hydrolysis activity would signal that the large ribosomal subunit is repaired and capable of interacting with the canonical translation factors and carrying out translation.

Misfolding of the rRNA in ribosomal subunits likely occurs throughout the life cycle of each subunit due to the dynamic nature of RNA secondary structure, however, there is higher chance that the rRNA is misfolded under conditions such as cold stress where the improper fold is a kinetic minimum. The same phenomenon could be applied to folding during ribosome biogenesis and general unwinding and refolding of the rRNA throughout its life cycle. Under optimal growth conditions, there is a higher propensity that rRNA can escape the kinetic minimum and refold into the correct structure. If the rRNA gets trapped in the improper fold it requires YchF to aid in unwinding the region of misfolded rRNA to allow the proper refolding to occur, otherwise build up of non-productive ribosomes could take place. As such, low level expression of YchF throughout growth could correct misfolded ribosomal subunits before they accumulate and cause downstream issues. As ribosome biogenesis is upregulated under exponential growth conditions, an upregulation of YchF would be beneficial to combat an increase in misfolded, non-productive ribosomes as well.

2.6 – CONCLUSION

YchF is unique among the GTPase family as it preferentially utilizes ATP over GTP in *E. coli* and humans (1). The human ortholog, hOLA1, has been implicated in several types of cancer including breast cancer (see *Section 1.11.5 – Cellular roles of hOLA1*). Here we show that EcYchF provides a fitness advantage to cells, which is amplified under cold stress conditions (Figure 2.1). Additionally, YchF binds to the ribosomal A-site and has RNA chaperone activity (Figures 2.2 and 2.6) in addition to binding to deacyl-tRNA *in vivo* (Figure 2.3). Taken together, these experimental results suggest a functional role for YchF in ribosome quality control and repair. Based on the sequence conservation, it is likely that this functional role spans across all domains of life. However, many questions remain regarding this proposed function that will be the basis for future studies of this enzyme. These include 1) what are the structural interactions the YchF ternary complex makes before nucleotide hydrolysis with the ribosome; 2) what region of the rRNA does YchF's chaperone activity unwind; 3) is the misfolded or "damaged" 70S ribosome the true target of the YchF ternary complex; and 4) how does YchF's role in oxidative stress influence its ribosome-associated

functional role? Further research into the mechanistic properties of EcYchF, and other orthologs, will be vital for understanding the ribosome quality control and repair, and the other proposed processes that YchF has been described to be involved in (see *Section 1.11 - YchF: The conserved ATPase in the GTPase family*). From this information we can elucidate if these processes are good targets for the rational design of new antimicrobial and anticancer agents.

CHAPTER 3: RIBOSOMAL BINDING SITE AND RIBOSOMAL SUBUNIT DISSOCIATION ACTIVITY OF HFLX

3.1 – PREFACE

This chapter contains most of a paper published in the journal Nucleic Acids Research (NAR) in 2016, describing the ribosomal binding site of *Escherichia coli* HflX (213). Sections of the paper were edited to fit into this thesis without being redundant. The project was planned by all the authors and was written by Dr. Hans-Joachim Wieden, Dr. Jeffrey Fischer, Mackenzie Coatham, and me. I carried out the primer extension experiments (Figure 3.2), and replicates/additional cross-linking, light scattering, and microfiltration experiments. Mackenzie Coatham carried out the mutagenesis, GTP hydrolysis (Figure 3.4), and microfiltration experiments (Figure 3.5). Dr. Jeffery Fischer carried out protein cross-linking experiments and analysis, and light scattering stopped flow experiments (Figure 3.6). Dr. Tobias Schummer carried out light scattering experiments under high magnesium concentrations.

3.2 – INTRODUCTION

Since the publication of the first structures of the ribosome in 2000 the number of ribosome structures deposited into the structural databanks has increased dramatically (66, 347-350). These structures revealed a range of different functional states of the ribosome bound to different protein, RNA, and small molecules such as antibiotics, that have help increase our understanding of how the ribosome as a molecular machine works. From this structural information there has been a large advancement in our understanding of protein synthesis in bacteria and eukaryotes (66, 351, 352). Specifically, how different protein factors, including the translational GTPases (trGTPases), facilitate the accurate and efficient protein synthesis observed *in vivo*. The 3 dimensional structures of these trGTPases share common structural features mimicking, to various degrees, the structure of tRNA (353-355). For example, the structure of EF-G•GDP shares a common shape with the ternary complex of EF-Tu•GTP•aminoacyl-tRNA (aa-tRNA) (356, 357). Furthermore, cryo-electron microscopy (cryo-EM) reconstructions of ribosome-bound EF-Tu•GTP•aa-tRNA (358), EF-G (359,

360), LepA (361, 362), BipA (363) and Tet(O)/TetM (364, 365), indicate a common binding site for the trGTPases in the ribosomal A-site. The crystal structure of EF-Tu•GTP•aa-tRNA bound to the 70S ribosome revealed that GTPase activation likely occurs through the correct positioning of the catalytic histidine residue at the end of switch II (DxxGH) by A2662 of the SRL, allowing a nucleophilic attack by a water molecule on the γ-phosphate of bound GTP (337). This mechanism has been proposed to be shared amongst trGTPases (337).

The universally conserved protein HflX (30, 202, 233), whose GTPase activity is also enhanced significantly by 50S and 70S ribosomal particles (30), provides an exception to the above common features of trGTPases. The X-ray crystal structure of HflX from *S. solfataricus* reveals that the N-terminus of the factor is unique, with no identifiable structural homolog (188). The *E. coli* homolog of HflX is a four-domain protein consisting of the unique N-terminal HflX-domain, an alpha helical linker domain, a central G-domain, and a C-terminal domain not found in the archaeal *S. solfataricus* homolog (Figure 1.16 and 3.1A). Additionally, *E. coli* HflX has a 22 amino acid N-terminal extension (Figure 1.16 and 3.1B). These extensions at the termini of HflX are not unique to the *E. coli* protein but are found in most bacteria and eukaryotes at varying lengths (Figure 1.16). Several studies have investigated truncations of these domains and found reduced binding to the ribosome and differences in nucleotide preference (189). Furthermore, knockout strains of *hflX* are viable, yet are more susceptible to high intercellular levels of manganese (220). In *E. coli,* the *hflX* gene is found downstream of the *hfq* locus, the universal stress response protein in bacteria. Both are under the control of a heat sensitive promoter (194, 199).

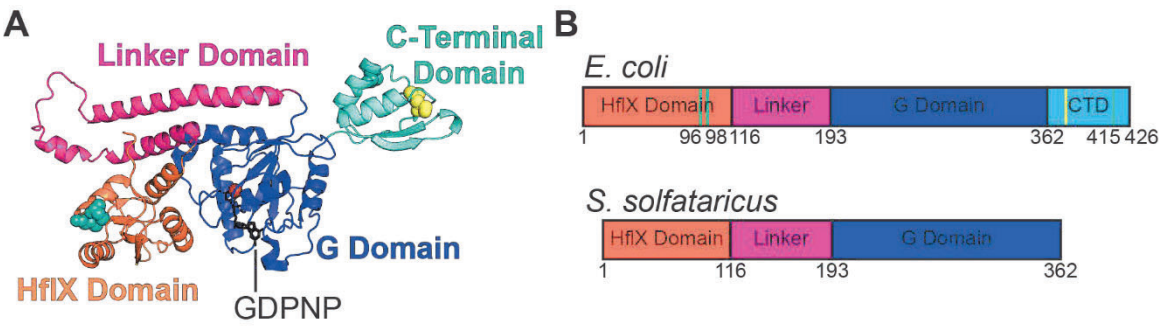

Figure 3.1 – Structural comparison of *Escherichia coli* and *Sulfolobus solfataricus* HflX structures. (**A**) Structural model of *E. coli* HflX from the 50S•HflX cryo EM structural (PDB 5ADY). HflX Is comprised of four domains, an N-terminal HflX-domain unique to HflX (orange), an alpha helical linker domain (pink), an internal G domain found in all GTPases (blue), and a C-terminal domain (CTD; Teal) not found in the *S. solfataricus* homolog. The cysteine residues (cyan spheres) are located within the HflX domain in proximity, while the third cysteine is in the C-terminal extension. (**B**) Graphical representation of *E. coli* HflX based on *S. solfataricus* domain layout and length comparison. The C-terminal domain conserved among bacteria but not found in the archaeal species *S. solfataricus,* is shown in teal. Truncation variant of HflX at position 372 indicated by yellow line in *E. coli* layout. The position of cysteines 96, 98 and 415 are indicated by cyan lines.

To elucidate the binding site of HflX on the ribosome, we conjugated the factor with the cysteine-specific UV-inducible crosslinking reagent 4-Azidophenacyl bromide (4-AzPB), like experiments performed with EF-G (366). Mass spectrometric analysis of crosslinks formed between HflX and ribosomal particles upon exposure to UV light revealed the presence of peptides mapped to ribosomal proteins L2, L5 and S18 near the ribosomal E-site. These data suggest that GTPase activation of HflX by the 50S ribosomal subunit could occur via a different mechanism compared to the canonical translational GTPases. To investigate this further, we examined the effect of numerous 50S- and 30S-specific antibiotics on the ribosome-stimulated GTPase activity of HflX: chloramphenicol, a peptidyl transferase centre (PTC) antibiotic, has previously been shown to inhibit this activity (30). Interestingly, additional antibiotics (PTC antibiotics clindamycin (CLIND), and lincomycin (LINC) and PET antibiotics azithromycin (AZI) and erythromycin (ERY)) also inhibit the ribosome stimulated GTPase activity of HflX without affecting ribosome binding. Inhibitors of EF-G (FUS (332)) and EF-Tu (TET (367)) and Streptomycin (STREP) (368)) had no effect on the ribosome-stimulated GTPase activation of HflX. Finally, while attempting to determine a 3D structure of HflX bound to the ribosome we discovered that HflX was able to split the 70S ribosome. Using light scattering in conjunction with stopped-flow rapid kinetics, we show that HflX can split

the ribosome in a nucleotide-dependent manner, like that of EF-G and RRF during ribosome recycling (369). The inclusion of HflX in a heat stress response operon downstream of the universal bacterial stress response protein Hfq (194, 199), suggests that this function of HflX may also be critical to the cell's response to stress.

3.3 – METHODS

3.3.1 - PLASMIDS

The pET28a plasmid encoding HflX from *E. coli* genomic DNA was previously constructed (30) for purification of wild type HflX via an N-terminal His6-tag. Plasmids containing the HflX C415L and HflX ΔL372 mutants were created using the QuikChange II site-directed mutagenesis protocol (Agilent Technologies) and primers that replaced the codon of Cys415 with a leucine and Leu372 with an amber stop codon. The resulting plasmids were sequence verified and called pET*hflX*-C415L and pET*hflX*-ΔL372.

3.3.2 – PURIFICATION OF HFLX AND RIBOSOMES

Vacant ribosomes were purified from *E. coli* MRE600 cells as described in Rodnina *et al. (370)*. Wild type HflX, HflX C415L and HflX ΔL372 were all purified as described in Shields *et al. (30)*.

3.3.3 – COVALENT CROSSLINKING

HflX was covalently linked to the cysteine-specific cross linker 4-Azidophenacyl bromide (4-AzPB). A total of 100 µM HflX was incubated with 300 µM 4-AzPB at 4°C for 24 h. The sample was then dialyzed against $TAKM_7$ high salt buffer (50 mM Tris-Cl pH 7.5 at 4°C, 70 mM NH_4Cl, 600 mM KCl, 7 mM $MgCl_2$) overnight to remove unreacted 4-AzPB. Small aliquots were flash frozen and stored at −80°C prior to use. 4-AzP covalently linked to HflX is referred to as AzP-HflX from hereon in. Complexes were formed in 20 µL volumes (100 pmol AzP-HflX, 20 pmol ribosomes, with or without 10 000 pmol guanine nucleotide) for 15 min at 37°C for 15 min in $TAKM_7$ buffer. Samples were then briefly placed on ice for 5 min and diluted to 500 µL with $TAKM_7$ before being subjected

to microfiltration (see *Microfiltration* below) until 20 µL remained. A total of 10 µL samples were placed in 96 well microtiter plates and exposed to 365 nm UV light (Spectroline model ENF-280C UV light) placed 1 cm above the sample for 15 min at 4°C. Crosslinking reactions were analyzed on 12% SDS-PAGE gels. For the additional bands observed in the presence of UV light after resolving the samples by SDS-PAGE, the gel corresponding to the different protein species were excised, individually de-stained in 100 mM NH_4HCO_3/acetonitrile (50:50) and subsequently digested at 37°C for 16 h. Tryptic peptides were first extracted from the gel and partially dried under vacuum to remove acetonitrile and then suspended in 5% acetonitrile and 1% formic acid. Peptide samples were analyzed using an Agilent 1200 nano-HPLC coupled to a LCQ Deca ion trap mass spectrometer (Thermo Scientific). Nanoflow chromatography and electrospray ionization were accomplished by using a PicoFrit fused silica capillary column (ProteoPepII, C18) with 100 µm inner diameter (300 Å , 5 µm, New Objective) and run at 500 nl/min using a 0–45% 45 min linear acetonitrile (with 0.2% formic acid) gradient. Data dependent analysis was performed on the LCQ Deca at a *m/z* range of 400–2000. The three most intense multiply charged ions were sequentially fragmented by using collision induced dissociation. After two fragmentations all precursors selected for dissociation were dynamically excluded for 60 s. The resultant data were analyzed using an in-house MASCOT server. Protein mass spectrometry was performed at the Institute for Biomolecular Design at the University of Alberta.

3.3.4 – PRIMER EXTENSION

rRNA was isolated from HflX-AzP complexes with 70S ribosomes that had been exposed to UV light, as described above. The rRNA was isolated by phenol-chloroform extraction of complexes after 15 min of UV light exposure. Initially 1 pM [^{32}P] 5'-end-labeled oligonucleotide primer and 10 µg isolated RNA were incubated at 65°C for 5 min and cooled to 47°C for 10 min to allow for denaturation and primer annealing. To the reaction 0.4 µM dNTPs, 10 mM DTT and 5U AMV Reverse Transcriptase (NEB) were added and extension was carried out at 47°C for 45 min followed by 15 min at 70°C to denature the reverse transcriptase. Samples were ethanol precipitated and analyzed on an 8% acrylamide 8 M urea slab gel using a BioRad Sequi-Gen GT

Sequencing cell (BioRad). Gels were dried, exposed to general purpose storage phosphor screen (GE Healthcare) and scanned on a Typhoon (GE Healthcare).

3.3.5 - MICROFILTRATION

Complexes of HflX with the ribosome were formed by incubating 5 μM of wild type or variant HflX with 1 μM of 70S in the presence of 1 mM GDP or GDPNP for 15 min at 37°C. Incubation on ice for 5 min preceded dilution of samples to 500 μL of $TAKM_7$ (50 mM Tris-Cl pH 7.5 at 4°C, 70 mM NH_4Cl, 30 mM KCl, 7 mM $MgCl_2$) buffer and centrifugation for 5 min at 10 000 x*g* in Vivaspin-500 columns with a molecular weight cut off (MWCO) of 100 kDa (GE Healthcare). Once a final volume of 20 μL was reached, the samples were diluted a second time to 500 μL and refiltered. The binding of HflX to ribosomes or ribosomal subunits was analyzed using 12% SDS-PAGE gels. Experiments containing antibiotics had respective antibiotic added to a final concentration of 500 μM in both the reaction and subsequent dilution buffer.

3.3.6 – GTPASE ASSAYS

The release of [^{32}P]-labeled inorganic phosphate (P_i) from [γ-^{32}P] GTP (Perkin-Elmer) was monitored to determine the rate of GTP hydrolysis by HflX. To ensure that nucleotides were in their triphosphate form and multiple turnover experiments would not be inhibited by nucleotide diphosphates, [γ-^{32}P] GTP (~100 dpm/pmol) was incubated with 0.25 μg/μL pyruvate kinase (PK), and 3 mM phosphenolpyruvate (PEP) for 15 min at 37°C. Similarly, 15 μM HflX was also incubated with PK and PEP. Reactions were composed of 1 μM HflX, 125 μM radiolabeled nucleotide solution, 1 μM ribosomes or ribosomal subunits and carried out in $TAKM_7$ buffer. At different time points, 5 μL of reactions were removed and quenched in 50 μL of 1 M $HClO_4$ with 3 mM K_2HPO_4. Inorganic phosphate was extracted as a phosphate-molybdate complex following the addition of 300 μL of 20 mM Na_2MoO_4 and 400 μL of isopropyl acetate, mixing for 30 s and centrifugation at 17 000x*g* for 5 min. Half of the organic phase (200 μL) containing the radiolabeled inorganic phosphate was removed, added to 2 mL of scintillation cocktail (MP EcoLite) and counted in a Perkin-Elmer Tri-Carb 2800TR liquid scintillation counter. The obtained activity was converted to pmol of liberated

inorganic phosphate using the specific activity of the [γ-^{32}P] GTP solution and divided by the respective volumes to yield the concentrations. The hydrolysis of GTP independent of enzyme in solution or hydrolysis due to ribosomes alone was subtracted, for the concentration of [$^{32}P_i$] to be determined and plotted as a function of time. The rates of guanine nucleotide hydrolysis by HflX in the presence of ribosomes was obtained by fitting the multiple turnover experiments with a linear equation, where the slope is equal to the apparent rate of nucleotide hydrolysis. Experiments containing antibiotics had respective antibiotic added to a final concentration of 500 μM.

3.3.7 – STOPPED-FLOW RAYLEIGH LIGHT SCATTERING

To monitor the dissociation of 70S ribosomes into 50S and 30S ribosomal subunits, a KinTek SF-2004 Stopped-flow apparatus was utilized. Samples were kept at 20°C, excited at 436 nm and scattering was detected at 90° after passing through 400 nm long-pass cut-off filters. Reactions were performed in TAKM$_5$ buffer (50 mM Tris-Cl pH 7.5 at 4°C, 70 mM NH_4Cl, 30 mM KCl, 5 mM $MgCl_2$), by rapidly mixing 2 μM of wild type or variant HflX in the presence of 250 μM GTP and 0.30 μM of 70S ribosomes. The resulting signals were normalized with respect to the initial light scattering of the solution, setting the initial value as 100% of intact 70S ribosomes. The resulting light scattering traces were first fit with a one- or two-exponential function (Equations (1) and (2)), where k_{app} is the characteristic apparent rate constant, A is the signal amplitude, Ls is the light scattering at time t and Ls∞ is the final light scattering signal. Light scattering data were normalized with respect to the initial fit, averaged (5–10 traces typically), and refit with the appropriate equation. Kinetic constants are expressed as the final fit, ± 95% confidence interval.

$$Ls = Ls_\infty + A\exp(-k_{app}t) \quad (1)$$

$$Ls = Ls_\infty + A1\exp(-k_{app1}t) + A2\exp(-k_{app2}t) \quad (2)$$

3.4 – RESULTS

3.4.1 – HFLX BINDS NEAR THE E-SITE OF THE 70S RIBOSOME

Previous studies have shown that HflX can bind to the 70S ribosome and 50S and 30S ribosomal subunits (203). We employed covalent crosslinking of HflX to the ribosome to determine where on the ribosome HflX binds. To do so, HflX was labeled with the cysteine-specific UV-inducible cross-linker 4-Azidophenacyl bromide (Figure 3.2A). The AzP cross-linker provides an 11 Å probing radius from labeled cysteine residues. This allows for the identification of proteins and rRNA at or near the binding site of AzP labeled proteins. Three cysteine residues are present in HflX (Figure 3.1), two at positions 96 and 98 in the N-terminal HflX domain and that are likely to form a disulfide bridge, as well as one at position 415 in the unresolved C-terminal domain.

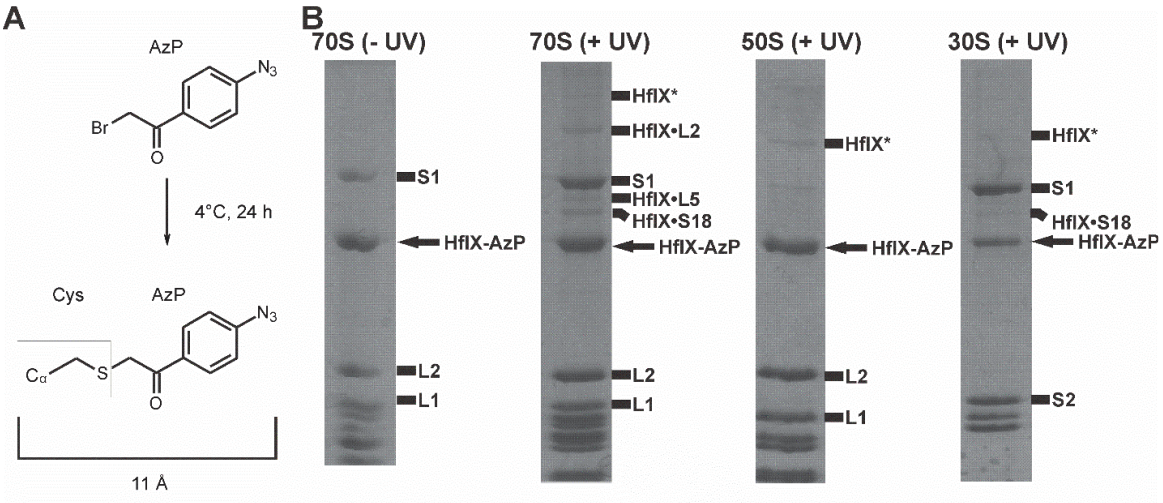

Figure 3.2 – Covalent crosslinking of HflX to the bacterial ribosome. (**A**) HflX was labeled with the cysteine specific crosslinking agent 4-azidophenacyl bromide. (**B**) Complexes of AzP-HflX and 70S ribosomes, or 50S/30S ribosomal subunits (Rb) were formed [5 μM AzP-HflX and 1 μM ribosomal particle] and separated from free AzP-HflX by microfiltration. Resuspended AzP-HflX•Rb complexes were exposed to 365 nm UV-light for 15 min before separation of ribosomal proteins by SDS-PAGE. Additional bands of higher molecular weight found in UV-treated samples were excised and sent for mass spectrometry analysis. Bands are annotated with HflX and the respective protein yielding peptides identified by mass spectrometry. Bands marked HflX* only contained peptides identified as HflX derived.

AzP labeled HflX (AzP-HflX) was incubated with 70S/50S/30S ribosomal particles before microfiltration to remove any unbound HflX before UV exposure to induce crosslinks. Upon exposing the AzP-HflX•ribosome complexes to 365 nm UV light for 15 min, samples were analyzed on SDS-PAGE gels to resolve crosslinks formed (Figure 3.2B). Additional bands of higher molecular weight than HflX were observed for HflX bound to the 70S ribosome and 50S and 30S ribosomal subunits. These bands were excised and sent for analysis by mass spectrometry. Bands at ~100, 60 and 56 kDa contained peptides corresponding to ribosomal proteins L2, L5 and S18 (Figure 3.2B, Appendix Table 3.1 and Appendix Figure 3.1). Additionally, several bands of lower mobility compared to HflX were observed after UV exposure. These bands only contained peptides derived from HflX (HflX* in Figure 3.2B), consistent with either inter-HflX or HflX-rRNA crosslinks.

These results suggest that HflX binds in or near the ribosomal E-site (Figure 3.3A). To further confirm this hypothesis, we performed primer extension analysis of rRNA isolated from UV-exposed AzP HflX•70S complexes. Prominent crosslinks to helix 23 of the 16S rRNA were identified by an increased band intensity at nucleotides A673, A681 and A687 (Figure 3.3B). These nucleotides all lie along the solvent exposed side of the helix. This is consistent with HflX localizing near ribosomal proteins L2 and S18, as helix 23 lies between both proteins in the 70S ribosome (Figure 3.3C). In addition, the crosslinking pattern observed showed nucleotide dependence, with the *apo* form of HflX yielding the highest crosslinking intensity, followed by GDP and GDPNP (Appendix Figure 3.2).

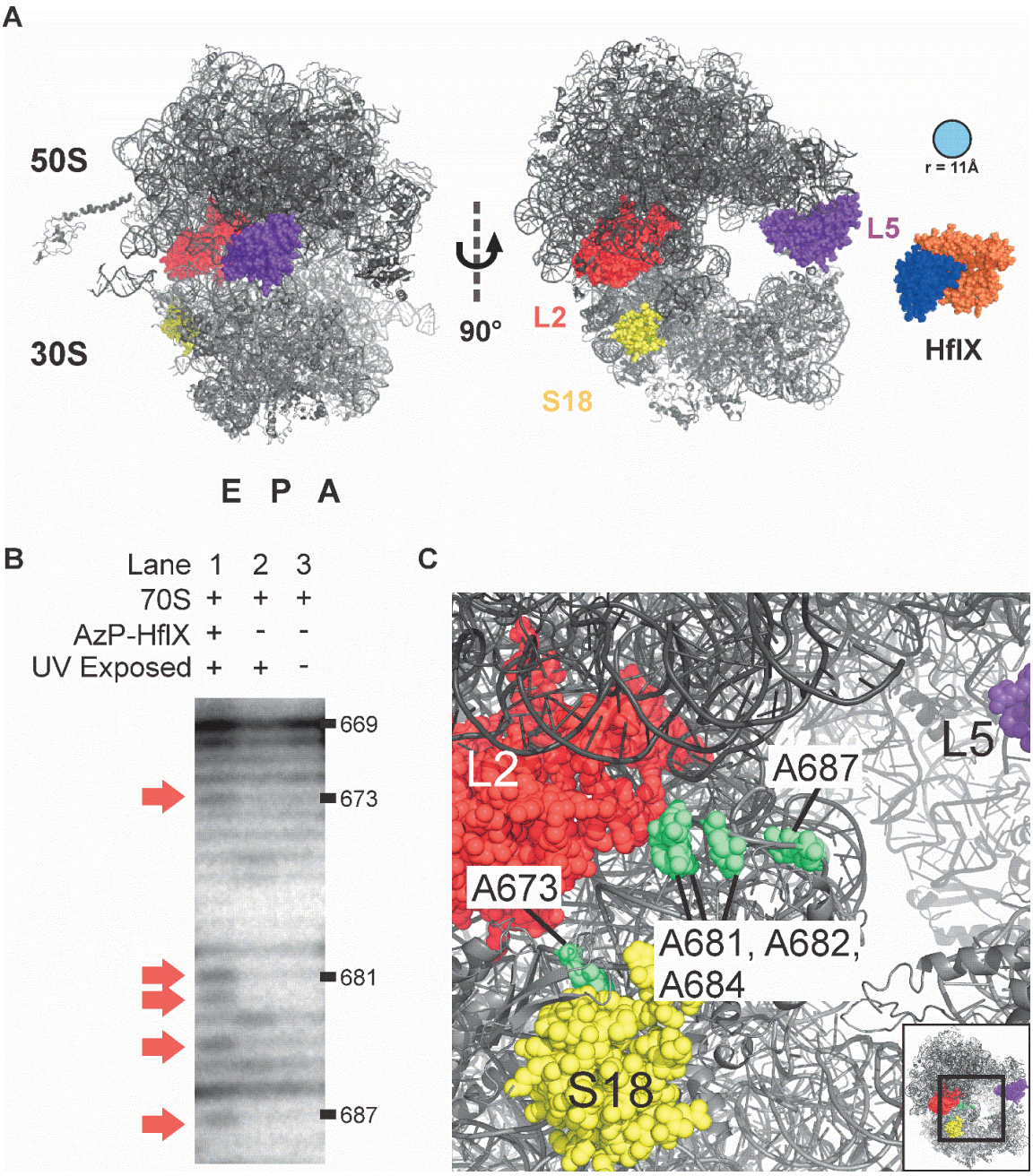

Figure 3.3 – Location of AzP-HflX crosslinks on the bacterial ribosome. (**A**) Protein crosslinks between AzP-HflX and ribosomal proteins L2, L5 and S18 (red, purple, and yellow) shown on the bacterial 70S ribosome (PDB 4V4Q). All three ribosomal proteins are on the ribosomal exit-site side of the ribosome and surround the E-site side opening. HflX is shown in blue and orange (PDB 2QTH). (**B**) To confirm the E-site side as the interaction site for HflX, rRNA from AzP-HflX crosslinked ribosome complexes was used in primer extension assays. Using a primer specific for creating cDNA products of helix 23 of the 16S rRNA that lies between ribosomal protein L2 and S18, we were able to find a distinct stopping pattern along the solvent accessible side of helix 23. (**C**) Nucleotides where reverse transcription was halted are shown by green spheres and mapped along the solvent accessible side of helix 23.

Furthermore, an HflX variant with the C-terminal cysteine residue replaced with a leucine (HflX C415L) was labeled with AzP. Crosslinking experiments were repeated and analyzed by SDS-PAGE (Appendix Figure 3.3). Samples containing AzP-HflX C415L did not contain any visible bands of higher molecular masses compared to wild type AzP-HflX. This indicates that crosslinks to ribosomal proteins L2, L5, S18 and 16S rRNA helix 23 are within 11 Å of Cys415 in HflX. These results suggest that the C-terminus of HflX is highly flexible and can move the minimal distance of 60 Å between L2 and L5.

3.4.2 – ANTIBIOTICS TARGETING THE PTC/PET INHIBIT HFLX RIBOSOME STIMULATED GTPASE ACTIVITY

To explore which functional centers of the ribosome influence GTP hydrolysis by HflX, we performed GTP hydrolysis experiments in the presence of several ribosome targeting antibiotics. Previous work by our lab revealed that chloramphenicol (CHL), a PTC binding antibiotic, prevents stimulation of the GTPase activity of HflX by the ribosome (30). This led us to test other translation inhibiting antibiotics of several classes and binding sites on the ribosome including PTC antibiotics clindamycin (CLIND), and lincomycin (LINC); PET antibiotics azithromycin (AZI) and erythromycin (ERY); decoding center binding antibiotics viomycin (VIO), tetracycline (TET), paromomycin (PARO), hygromycin B (HYGB), tobramycin (TOB) and the EF-G specific antibiotic fusidic acid (FUS). Of these antibiotics, only the macrolides (AZI/ERY), lincosamides (CLIND/LINC) and chloramphenicol had a dramatic effect on the rate of GTP hydrolysis by HflX (Figure 3.4). This effect was observed for both 70S and 50S dependent stimulation but not on intrinsic hydrolysis by HflX (Appendix Figure 3.4).

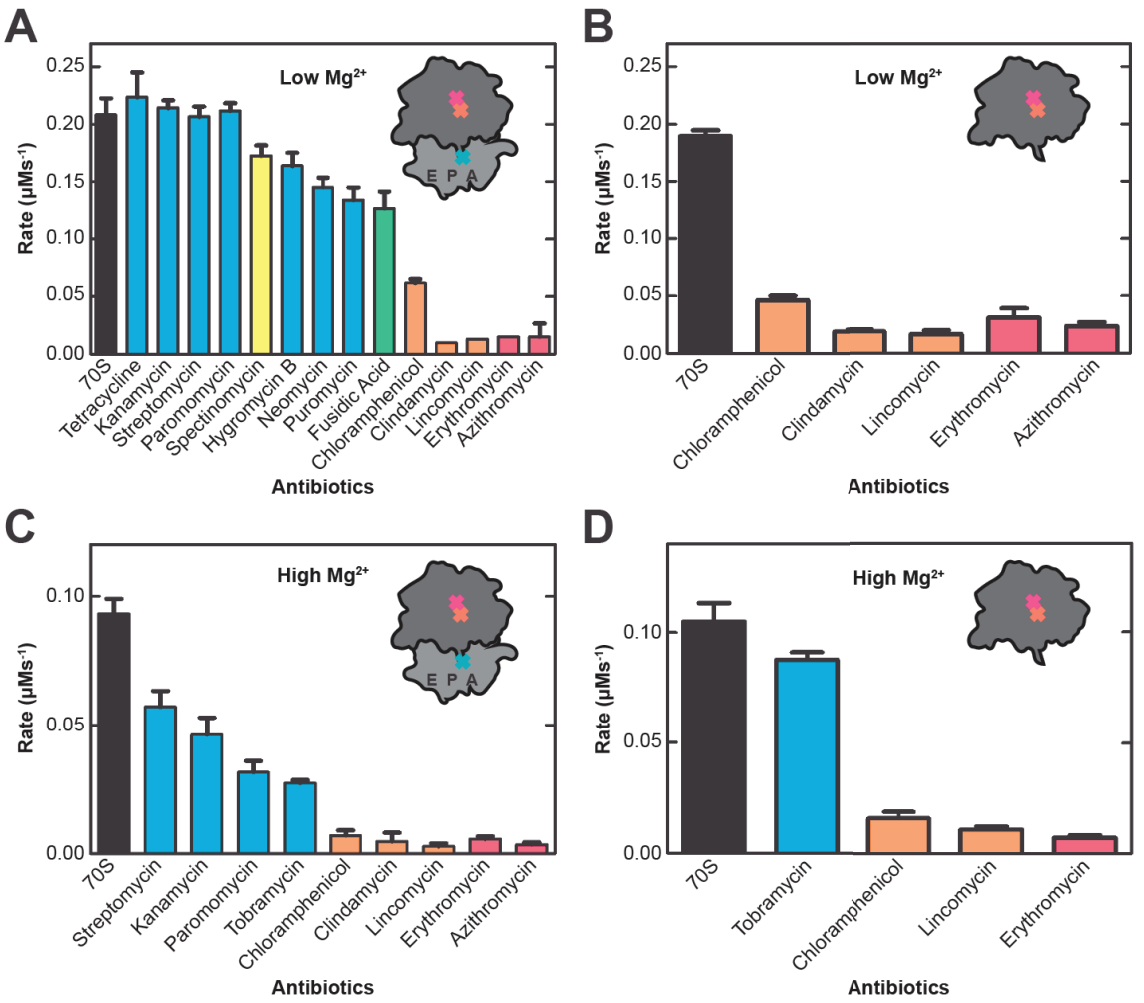

Figure 3.4 – Antibiotic Inhibition of HflX ribosome-stimulated GTP hydrolysis activity. HflX (1 μM) was incubated with (**A**) 70S ribosomes or (**B**) 50S ribosomal subunits (1 μM) in the presence of [γ-^{32}P]-GTP (125 μM) and antibiotic (500 μM) in low Mg^{2+} buffer ($TAKM_5$). Identical reactions for HflX with (**C**) 70S ribosomes and (**D**) 50S ribosomal subunits were carried out in high Mg^{2+} buffer ($TAKM_{30}$). Reactions were quenched at successive time points and the amount of released [^{32}P] inorganic phosphate was quantified to determine the rate of hydrolysis. Antibiotics that target several regions of the ribosome were tested including those that bind to the decoding centre (teal), helix 34 near the decoding centre (yellow), EF-G binding site (green), peptidyl transferase centre (orange) and peptide exit tunnel (pink).

To determine if the decreased rate of hydrolysis is due to HflX being prevented from binding to its stimulatory partner the ribosome, microfiltration assays were performed in the presence of each antibiotic (Figure 3.5). Both the GDPNP- (a non-hydrolysable analog of GTP) and GDP-bound states of HflX were examined for binding to the 50S ribosomal subunit by microfiltration and subsequent SDS-PAGE analysis. HflX incubated in the absence of ribosomes was not retained above the filter following filtration, while HflX preincubated with 50S subunits remained above the

filter as apparent by a 50.5 kDa band corresponding to the molecular weight of HflX. HflX•50S complexes were incubated with nucleotide (GDP or GDPNP) and antibiotic. No inhibition of HflX binding to the ribosome was observed with any of the antibiotics tested.

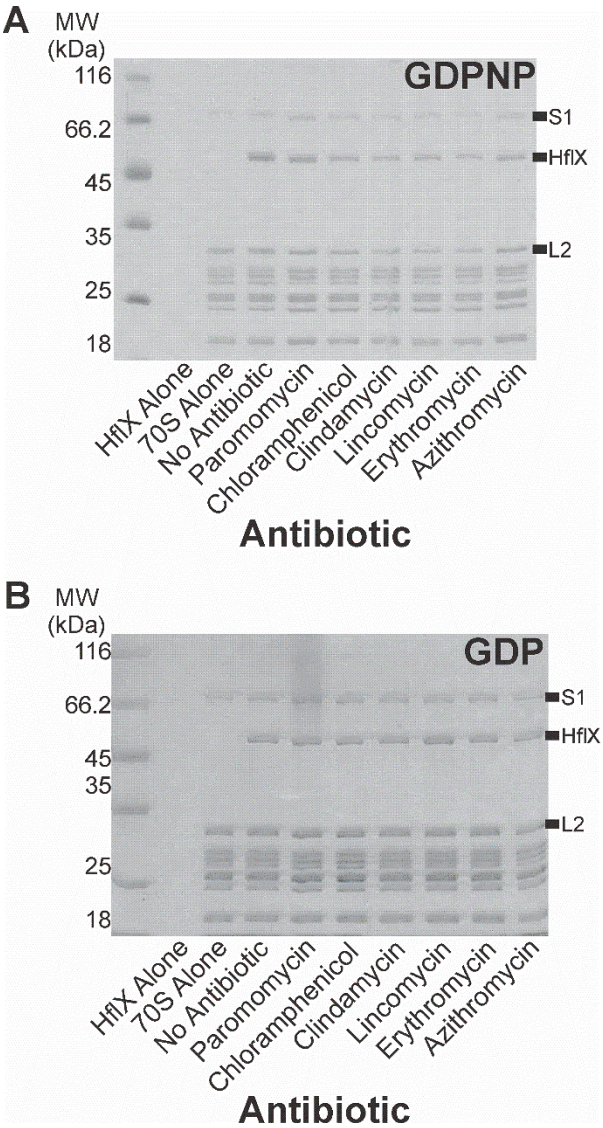

Figure 3.5 – Antibiotic effect on HflX binding to bacterial ribosome. HflX (5 μM) was incubated with 50S ribosomal subunits (1 μM) in the presence of (**A**) GDPNP or (**B**) GDP (500 μM) and the antibiotic indicated (500 μM). Complexes were separated from free HflX via filtration and subsequently washed before collecting the remaining filtrate for analysis by SDS-PAGE.

Furthermore, to verify that ribosomes were not blocking the filter, and causing the retention of HflX above the filter, we performed the same experiment with the non-ribosome associated protein, EF-Ts (Appendix Figure 3.5). EF-Ts, the nucleotide exchange factor for EF-Tu, was not retained above the filter in the presence of ribosomes (Appendix Figure 3.5B). Additionally, ultracentrifugation pelleting experiments through 10% sucrose cushions were performed to verify the specificity of HflX binding to the 70S ribosome (Appendix Figure 3.6).

3.4.3 – HFLX SPLITS THE 70S RIBOSOME INTO 50S/30S RIBOSOMAL SUBUNITS IN A NUCLEOTIDE-DEPENDENT MANNER

Initial experiments on 70S ribosome (0.15 μM final concentration) dissociation (Figure 3.6A) were performed in a buffer with a final concentration of 2.5 mM Mg^{2+}. Under these conditions, 70S ribosomes dissociate completely into 50S and 30S subunits (371). Rapid mixing of 70S ribosomes with buffer lacking Mg^{2+} (2.5 mM final Mg^{2+} concentration after mixing) resulted in a 29% decrease in light scattering intensity with an apparent rate of 0.055 ± 0.001 s^{-1}. As a control, 70S ribosomes were mixed with $TAKM_5$ buffer (5 mM Mg^{2+} final concentration) resulting in only a small (~1%) decrease in light scattering intensity. In the presence of HflX•nucleotide complexes (1 μM HflX, 125 μM nucleotide final concentrations), the rate and extent of ribosome dissociation as reflected by the overall change in light scattering varied, as a function of the nucleotide present (Figure 3.6B). Light scattering time courses were best fit with a two-exponential function. *Apo* HflX and HflX•GDP facilitated ribosome dissociation to the least extent (~1.5% LS change, $kapp^1$ = 0.0069 ± 0.0002 s^{-1} and $kapp^2$ = 0.0038 ± 0.0002 s^{-1} for HflX•GDP). HflX•GDPNP dissociated ribosomes to a greater extent than HflX•GDP, but the rate of dissociation is approximately the same (~20% LS change, $kapp^1$ = 0.017 ± 0.007 s^{-1} and $kapp^2$ = 0.0044 ± 0.0002 s^{-1}). In contrast, HflX•GTP rapidly split 70S ribosomes to the greatest extent (~30% LS change, $kapp^1$ = 0.065 ± 0.001 s^{-1} and $kapp^2$ 0.0018 ± 0.0001 s^{-1}). The rate of ribosome dissociation by HflX•GTP is approximately equal to the rate of ribosome dissociation by EF-G•GTP and RRF (369).

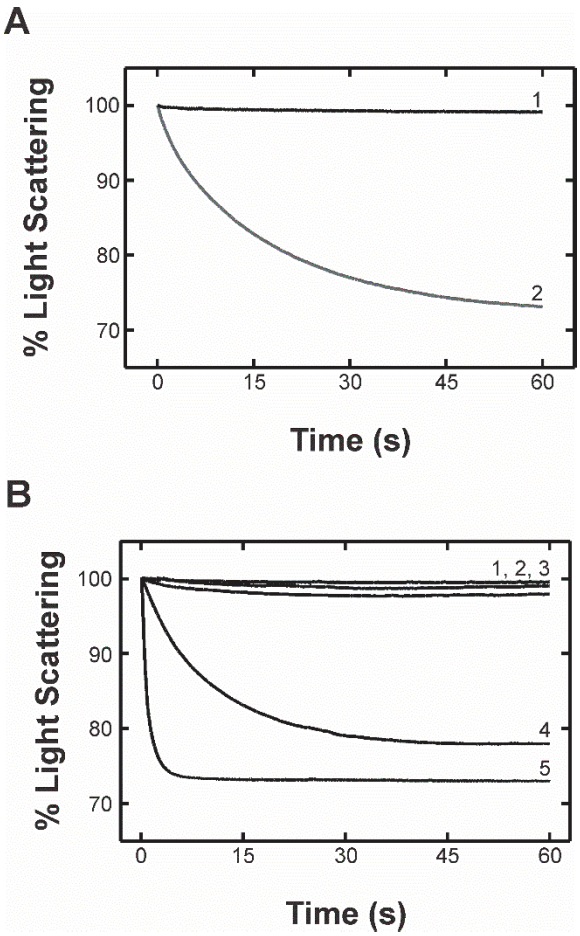

Figure 3.6 – HflX splits the 70S ribosome in a nucleotide dependant manner. Light scattering experiments monitoring the size of particles in solution carried out using a stopped-flow apparatus. Samples are exposed to 426 nm light and scattering is monitored at 90◦ to the incident light. Larger particles scatter more light than smaller particles. (**A**) 70S ribosomes in TAKM5 buffer are mixed with either TAKM5 buffer (1) or TAK buffer (2). Decreasing Mg2+ concentrations results in 70S dissociation into 50S and 30S ribosomal subunits. (**B**) 70S ribosomes mixed with TAKM5 (1), and HflX in the nucleotide free *apo* state (2), and GDP- (3), GDPNP- (4) or GTP-bound states (5).

To investigate a putative role for the C-terminal domain of HflX in 70S dissociation we created a C-terminal truncation variant at Lys372 (189). Light scattering experiments carried out using this truncation variant in the presence of GTP revealed HflXΔL372 dissociated ribosomes to a much lower extent than wild type HflX in the presence of GTP or GDPNP (~10% LS change; Appendix Figure 3.7A). As HflX dissociates the ribosome with a greater rate and extent in the presence of GTP compared to GDPNP, hydrolysis is required for optimal dissociation. Therefore, we tested the ΔL372 truncation variant for GTP hydrolysis finding that it is still active with a rate of 0.065 ± 0.006 μM s^{-1}, compared to wild type HflX, 0.103 ± 0.001 μM s^{-1} (Appendix Figure 3.7B).

To address the questions if GTP hydrolysis is coupled to splitting of the subunits, we used a higher (30 mM) Mg2+ concentration to stabilize the 70S ribosome. Under these conditions, no dissociation of the subunits could be observed after rapid mixing, either in the presence or the absence of HflX (Appendix Figure 3.8A). Also, inhibiting dissociation did not affect HflX binding (Appendix Figure 3.8B–C) or the ribosome stimulated multiple turnover GTPase activity (Figure 3.4C–D), suggesting that indeed 70S ribosome is the target of HflX and that GTP hydrolysis occurs without the dissociation of the 70S ribosome.

3.5 – DISCUSSION

Our data demonstrate that HflX covalently crosslinks with ribosomal proteins and rRNA on the E-site side of the 70S ribosome in solution (Figures 3.2 and 3.3). The localization of HflX's binding site to the tRNA exit site of the 70S ribosome makes HflX the first known trGTPase to bind at that location and whose GTPase activity is stimulated by the ribosome. Classical trGTPases (EF-G, EF-Tu, RF3, LepA and others) bind to, and are stimulated by, the SRL located at the A-site side of the ribosome, opposite to where HflX binds the 70S ribosome. While the current manuscript was under review the cryo-EM structure of a 50S ribosomal subunit HflX complex was reported, locating HflX in the A-site of the 50S ribosomal subunit (19). The cryo-EM model shows the N-terminal HflX domain reaching into the PTC, overlapping with both the A- and P-site while the G-domain is oriented away from the SRL. This suggests a different mode by which GTPases can be activated by the ribosome. The idea that the ribosome possesses additional GTPase stimulatory centres is not novel, as ObgE has previously been shown to bind to a similar region of the 50S subunit (19, 372). In addition, our data reported here demonstrate that HflX when binding to the 70S ribosome, interacts with the ribosomal E-site and that this interaction stimulates the intrinsic GTPase activity of HflX on the opposite side of the ribosome via a novel mode of activation.

Using a variant of HflX lacking the cysteine residue in the unresolved C-terminal domain (Figure 3.1B) labeled with AzP (HflX-C415L), no crosslinks were observed compared to the labeled wild type enzyme after UV exposure (Appendix Figure 3.3). Interestingly these results indicate that Cys415 can be within 11 Å of ribosomal proteins L2/S18 and L5 which are at least 60 Å apart

(Figure 3.3A). The fact that Cys415 can crosslink with ribosomal proteins on either side of the E-site opening suggests that the C-terminal domain is flexible and able to move between these positions. The flexibility of the C-terminal domain could be attributed to HflX exploring different conformations while bound to the ribosome. This is consistent with fluorescence resonance energy transfer (FRET) experiments measuring the GDPNP affinity to HflX•70S complexes that showed two-exponential behavior, an initial binding step followed by a conformational change upon GDPNP binding (203). Additionally, we observed lower efficiency of crosslink formation in the GDPNP and GDP-bound states of HflX compared to *apo,* suggesting that nucleotide binding stabilizes HflX in a certain conformation required for its activity (Appendix Figure 3.2).

Consistent with these observations is a model in which the N-terminal HflX-domain binds directly into the E-site, while the G-domain is bound to the outer surface of the ribosome resulting in the C-terminal domain being located at the periphery of the ribosome rendering it more solvent exposed. This is supported by the fact that truncations of the N-terminal domain abolish the interaction between HflX and ribosomal particles (the 70S ribosome and 50S/30S ribosomal subunits) (189) and our previous limited proteolysis experiments showing increased protection of the N-terminus in the presence of the 70S and 50S ribosome particles (203).

In addition to the previously reported effect of chloramphenicol (203), we show that other PTC/PET binding antibiotics inhibit stimulation of HflX GTPase activity (Figure 3.4). The binding site of these antibiotics, when considered with HflX bound to the E-site, suggests a communication between the P- and E-sites of the ribosome. Previously, no communication to the E-site has been shown to stimulate GTPase activity of trGTPases as all the canonical protein factors bound to the A-site are activated by the GAC and SRL. Yet several proteins have been reported to interact with the E-site during translation, such as EttA. EttA interacts with the P-site tRNA and inhibits ribosome dynamics preventing translation in energy-depleted cells (204, 205). To do this, EttA, while bound to the E-site, reaches into the P-site making direct contact with initiator $tRNA^{fMet}$. Direct contact between a factor and a location on the ribosome is one potential communication pathway, yet the signal could also be relayed through the ribosome itself to the factor. Our proposed binding site for HflX in the E-site suggests that HflX makes direct contact with the P-site, specifically the PTC/PET.

Whether or not HflX can reach into the PTC/PET, our data show that even a small molecular inhibitor bound in the PTC/PET influences the ribosome-dependent stimulation of HflX's GTP hydrolysis activity. Interestingly, HflX is not activated to hydrolyze GTP by the conformational state of antibiotic-bound PTC/PET, which indicates that inhibition of HflX may be another previously overlooked mode of action of these antibiotics. Furthermore, other conformational states of the PTC/PET induced by ribosome bound partners are likely to stimulate HflX. During elongation, a growing polypeptide chain is most common in the PTC/PET and specific sequences of the polypeptide can influence the conformation of the PET (373, 374). Work reported here on the ribosome-stimulation of HflX have all used vacant ribosomes purified from *E. coli* cells. There are two potential reasons why vacant ribosomes stimulate HflX: first, the functional role of HflX is to interact with empty 70S ribosomes, and second, vacant 70S ribosomes are able to explore several conformational states, one of which is the state that activates HflX and is also characteristic to a particular functional state of the ribosome. As GTP hydrolysis is typically tied to a GTPases functional role *in vivo*, understanding the conformational state of the ribosome that activates GTP hydrolysis is crucial to determining the function of HflX in the cell.

To address how these antibiotics, inhibit HflX stimulation, we first wanted to see if HflX binding to the ribosome was impeded by the presence of these antibiotics (Figure 3.5). The fact that the presence of antibiotics did not interfere with HflX binding to the ribosome suggests that they might instead influence the nucleotide binding properties of the HflX•ribosome complex or influence the conformation of the stimulatory region of the ribosome involved in catalysis by HflX, much like the SRL does for classical trGTPases. Additional studies are required to determine the exact cause of inhibition.

Our initial experiment attempting to obtain a cryo-EM structure of HflX bound to the 70S ribosome revealed only 50S and 30S subunits, suggesting a ribosome splitting activity of the protein. Using light scattering experiments to indirectly observe 70S dissociation into 50S and 30S ribosomal subunits (Figure 3.6A) we found that HflX is indeed able to split the 70S ribosome in a nucleotide dependent manner (Figure 3.6B). The GTP-bound state of HflX very efficiently splits the ribosome compared to the GDP-bound and *apo* states, which show no detectable levels of

ribosome dissociation. The use of the non-hydrolysable analog of GTP, GDPNP, showed that hydrolysis is not required for splitting, yet splitting occurs at a much slower rate, indicating that hydrolysis is required for efficient splitting. These results differ from those of Zhang *et al.*, who using a similar technique showed that HflX in the presence of GDPNP was more efficient at splitting compared to GTP (19). These conflicting observations could be due to differences in buffer conditions (HEPES-polymix compared to a Tris based buffer used in this report) or a contamination with GTP generated using the Pyruvate kinase/Phosphoenolpyruvate system present in their assay (19). However, more detailed mechanistic studies are required to reconcile this difference.

Furthermore, the truncation mutant of HflX lacking the C-terminal domain (HflX-ΔL372) was impaired in its ability to efficiently split the ribosome, indicating the importance of the C-terminal domain for ribosome splitting (Appendix Figure 3.7A). As HflX splits ribosomes in the GTP-bound state we confirmed that HflX-ΔL372 is still capable to bind and hydrolyze GTP (Appendix Figure 3.7B–C). Hydrolysis is unaffected by the C-terminal truncation, further supporting a functional role for the C-terminal domain in ribosome splitting. Interestingly, Zhang *et al.* show that in the 50S complex the C-terminal domain of HflX points out of the A-site and away from helix 69 (H69) of the 23S rRNA (intersubunit bridge B2a) which they propose is modulated by HflX to facilitate splitting (19). In contrast, our localization of the C-terminal domain in the E-site of 70S ribosome complex near the subunit interface between ribosomal proteins L2 and S18 (Figure 3.3 and Appendix Figure 3.3) suggests that the C-terminus is positioned to insert between the two ribosomal subunits. This could contribute to dissociation, for example, by modulating the intersubunit bridges B7a and B2awhich involves h23 of the 16S rRNA and H68 of the 23S rRNA as well as H69 and h44, respectively. Interestingly, the binding site of HflX on the 30S ribosomal subunit suggested by the crosslinking data reported here is very similar to the interaction site of IF3. As some degree of ribosome splitting is still observed in the absence of the C-terminal domain, the other domains of HflX are likely to also contribute to splitting, but the correct placement of the C-terminal domain is required for efficient splitting (Appendix Figure 3.7A). Such an effect might be caused by preventing re-association of the subunits after dissociation through occlusion of parts of the interaction surface

between the two ribosomal subunits by the bound HflX, consistent with the structure reported for the 50S•HflX complex (19).

To investigate if GTP-hydrolysis depends on the splitting activity we performed GTP-hydrolysis experiments in the presence of 30 mM Mg^{2+} which efficiently prevented ribosome dissociation by HflX•GTP (Appendix Figure 3.8A). These conditions did not affect HflX binding to or GTPase stimulation by the ribosome (Figure 3.4A–B and Appendix Figure 3.8B–C). Thus, ribosome splitting is not required for GTP hydrolysis to occur, suggesting a different mode of HflX regulation. Furthermore, this observation supports a binding site of HflX on the 70S ribosome that does not require stabilization by an altered intersubunit bridge as suggested by Zhang *et al.* (19).

The location of the *hflX* gene downstream of *hfq* under the control of a heat sensitive promoter strongly suggests that HflX is required during heat stress, as confirmed by Zhang *et al.* (19). During cellular stress, translational arrest is common (299), leaving the E-site of the ribosome empty and the PTC/PET filled with the growing polypeptide chain attached to the P-site tRNA. We propose that HflX is able to bind to the empty E-site of a stalled ribosome, sense the stalled polypeptide in the PTC/PET which triggers HflX to hydrolyze GTP, and upon hydrolysis split the ribosome, freeing up the subunits to be used in another round of translation (Figure 3.7). As the A-site of a stalled ribosome is typically filled with an aminoacyl-tRNA and the E-site is left empty after the deacylated tRNA exits, it would be possible for HflX to bind into the E-site rather than the A-site. Following splitting of the ribosome, HflX could then bind to the A-site to prevent reassociation of the 50S and 30S ribosomal subunits and block the association of other trGTPases before reassembly of a new 70S complex. Further studies are required to determine the exact role of HflX during heat stress and the mechanism by which HflX can provide a fitness advantage to cells.

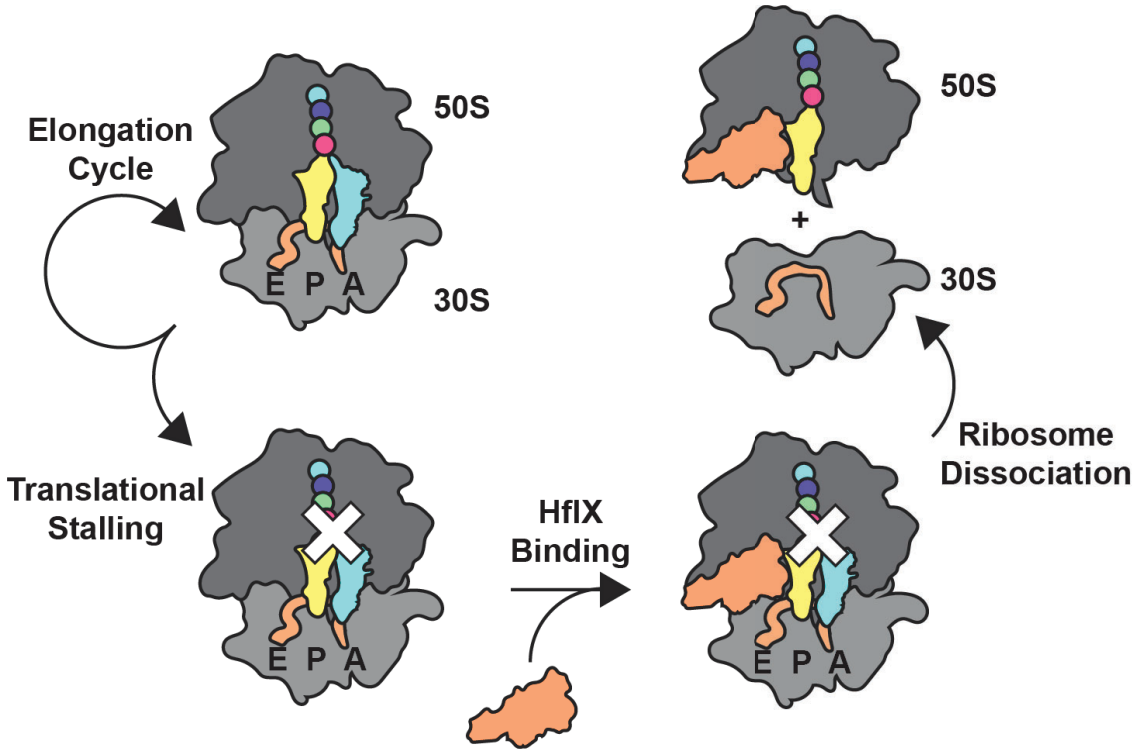

Figure 3.7 – Proposed model of HflX function. Stalling of translation occurs during cellular stress, leaving the E-site vacant. HflX can bind to the vacant E-site to assess the state of the PTC/PET. Upon recognizing the ribosome is stalled, HflX hydrolyzes GTP and splits the 70S ribosome into 50S and 30S ribosomal subunits that subsequently can be used in another round of translation.

In conclusion, this work provides for the first-time evidence that the ribosome-associated GTPase HflX can monitor the ligand induced state of the PTC, and that it catalyzes efficient splitting of the 70S ribosome in a nucleotide-dependent manner. Furthermore, our proposed location where HflX binds to the 70S ribosome, and the respective ribosome-dependent stimulation of GTP hydrolysis, indicate a previously unidentified GTPase activation site on the ribosome needed for efficient translation.

CHAPTER 4: CONFERRAL OF ANTIBIOTIC TOLERANCE THROUGH THE DISSOCIATION OF ANTIBIOTIC-BOUND RIBOSOMES BY THE CONSERVED GTPASE HFLX

4.1 – PREFACE

This chapter is the manuscript for a HflX paper detailing the involvement of *E. coli* HflX in conferring antibiotic tolerance, dissociation of antibiotic bound ribosomes, and validation of HflX being able to bind to the ribosomal E-site. The manuscript tentatively titled “Inhibition of ribosome recycling by the alternative translation factor HflX” was written for submission to Proceedings of the National Academy of Science of the United States of America (PNAS) and contains work done my Harland Brandon and Fan Mo. The project was planned by Dr. Hans-Joachim Wieden, Harland Brandon, and Fan Mo. It was written by Harland Brandon. The minimal inhibitory concentration (MIC) assays were performed by Fan Mo. All other experiments were performed and analyzed by Harland Brandon.

4.2 – INTRODUCTION

The World Health Organization (WHO) has listed antimicrobial resistance (AMR) as a global health problem that could become the leading cause of death worldwide by 2050 (WHO AMR Review). This is due to the increase in multi-drug resistant organisms (MDRO; i.e. methicillin-resistant *Staphylococcus aureus* (MRSA) and vancomycin resistant *Enterococcus faecium* (VRE)) and the low number of new antibiotics that have been developed since the golden age of antibiotics in the 1960’s and 1970’s (375-380). The resistance situation has already hit a critical point such that 12 pathogens, including *Enterobacteriaceae* such as *Escherichia coli*, are in crucial need of new therapeutics (WHO Priority Pathogen List). Understanding the AMR mechanisms present in bacteria enables the more accurate prediction of therapeutic regimens against pathogens and guides future development of new antimicrobials (381, 382). The most prevalent mechanisms of resistance include modification of the target gene, modification or destruction of the antibiotic, and alteration of the import and efflux of the antibiotic (382-384).

Recent studies have indicated that the ribosome associated GTPase HflX mediates another mechanism of resistance to lincosamide and macrolide antibiotics (201, 225, 226, 231). Lincosamides and macrolides are ribosome targeting classes of antibiotics that bind to the peptidyl transferase center (PTC) and peptide exit tunnel (PET), respectively (385). The exact mechanism by which HflX confers resistance to these antibiotics is unknown but is proposed to involve the recently discovered function of HflX to dissociate the 70S ribosome into 50S and 30S ribosomal subunits (19, 213). Structural evidence of *E. coli* HflX (EcHflX) bound to the 50S ribosomal subunit shows that the flexible loop connecting the two helices of the linker domain is positioned to interact with the PTC bound antibiotic (19), potentially dislodging the antibiotic. In *Mycobacterium smegmatis*, HflX is unable to dislodge the macrolide antibiotic erythromycin (ERY) bound to the 70S ribosome (231) arguing against a HflX-mediated antibiotic dislodging mechanism. These studies suggest that HflX may be strictly dissociating the ribosome allowing the bound antibiotic to dissociate or allowing another factor access to the PTC/PET to dislodge the bound antibiotic. HflX-mediated ribosome dissociation allows the once stalled ribosomal subunits to be used in another round of translation, and any ribosomes trailing behind the antibiotic-stalled ribosome on the mRNA to continue synthesis. Furthermore, the role of HflX in antibiotic mediated resistance would just be a result of its normal function within the cell to recycle stalled ribosomes under stress. Here we show that *E. coli* (EcHflX) does not provide antibiotic resistance to macrolide and lincosamide antibiotics in *E. coli*. Furthermore, these antibiotics do not inhibit HflX-mediated ribosome dissociation supporting the hypothesis that subunit dissociation is involved in conferring antibiotic tolerance. Surprisingly, antibiotics of the aminoglycoside class inhibit HflX-mediated ribosome dissociation. Aminoglycosides (AMGs) such as paromomycin (PAR), tobramycin (TOB), and kanamycin (KAN), bind to helix 69 (H69) of the 23S rRNA stabilizing intersubunit bridge B2a (386, 387). This provides the first biochemical evidence that HflX disrupts this intersubunit bridge to facilitate subunit dissociation. To further understand the mechanism by which HflX disrupts this intersubunit bridge it is important to know where HflX binds. Previously, we presented biochemical evidence that EcHflX binds to the 70S ribosomal E-site (213) while cryo-EM structural data suggested that EcHflX binds to the A-site of a 50S ribosomal subunit (19, 191). As two binding sites

on the ribosome exist, we asked whether HflX could bind to and dissociate the 70S ribosome from the E-site. Utilizing 70S ribosomes with EF-G•GDP locked to the ribosomal A-site with fusidic acid (FUS) (331, 332, 388) and the knowledge that AMGs prevent HflX-mediated ribosome dissociation, we were able to confirm that EcHflX can bind the ribosomal E-site. In the absence of AMGs, EcHflX could dissociate FUS locked 70S•EF-G•GDP complexes in the presence and absence of macrolide and lincosamide antibiotics. Our results suggest that while EcHflX does not confer antibiotic resistance without additional factors, it remains capable of dissociating ribosomes bound to antibiotics (aside from aminoglycosides) and that subunit dissociation can be facilitated by HflX binding to the ribosomal E-site.

4.3 – METHODS

4.3.1 – PLASMIDS AND PURIFICATION OF HFLX, EF-G, AND RIBOSOMES

The pET28a plasmid encoding HflX from *E. coli* genomic DNA was previously constructed (30) for purification of wild type HflX via an N-terminal His6-tag. HflX was purified as described in Shields *et al.* (30). EF-G was purified from pET28a via an N-terminal His6-tag. Vacant ribosomes were purified from *E. coli* MRE600 cells as described in Rodnina *et al.* (370).

4.3.2 – MINIMAL INHIBITORY CONCENTRATION (MIC) ASSAY

Antibiotic solutions were prepared to a concentration double (2x solution) that of the highest concentration desired for each. To start the serial dilution in a 96 well plate, 125 µL of 2x antibiotic solution was added to 125 µL of LB media. A series of 7 additional dilutions (8 antibiotic concentrations total) were made mixing 125 µL of the previous solution with 125 µL of LB media successively, discarding 125 µL from the lowest concentration such that all tubes begin with 125 µL of LB media and antibiotic. A ninth well for each condition contained no antibiotic, only 250 µL LB media as a control. Each strain of *E. coli* tested (wild type – BW25113; BW25113 Δ*hflX*; BW25113 Δ*hflX* Δ*kanR*) were grown to an OD_{600} of 1.0 in LB media prior to inoculating the serial dilution. A 1:1000 000 dilution of the 1.0 OD_{600} culture was prepared with LB media, and 125 µL of

the dilution added to each serial dilution tube. Cultures were grown overnight at 37°C in a shaking incubator. The MIC for each antibiotic was determined by highest antibiotic concentration with no growth as validated by spectroscopic measurement (OD_{600}) and plating on LB agar with no antibiotics. The highest concentration of each antibiotic used was: 128 μg/mL for azithromycin, 2000 μg/mL for clindamycin, 2400 μg/mL for erythromycin, 8000 μg/mL for lincomycin, 400 μg/mL for neomycin, 100 μg/mL for paromomycin, 1500 μg/mL for hygromycin B, 2000 μg/mL for spectinomycin, 400 μg/mL for streptomycin, 64 μg/mL for tobramycin, 128 μg/mL for ampicillin, and 16 μg/mL for tetracycline. For the Δ*hflX* strain containing the *kanR* gene, the highest concentration of paromomycin was 4000 μg/mL.

4.3.3 – STOPPED-FLOW RAYLEIGH LIGHT SCATTERING

To monitor the dissociation of 70S ribosomes into 50S and 30S ribosomal subunits, a KinTek SF-2004 Stopped-flow apparatus was utilized. Samples were kept at 20°C, excited at 436 nm and scattering was detected at 90° after passing through 400 nm long-pass cut-off filters. All stopped flow experiments were performed in $TAKM_5$ buffer (50 mM Tris-Cl pH 7.5 at 4°C, 70 mM NH_4Cl, 30 mM KCl, 5 mM $MgCl_2$) unless otherwise noted. Experiments containing antibiotics had respective antibiotic added to a final concentration of 500 μM. Reactions measuring HflX-mediated dissociation of empty 70S ribosomes (Figure 4.1) were carried out by rapidly mixing HflX (2 μM) in the presence GTP (250 μM) and 70S ribosomes (0.30 μM). Reactions measuring HflX-mediated dissociation of EF-G locked 70S ribosomes (Figure 4.3) were carried out by first forming 70S•EF-G•GDP•Fus complexes via microfiltration (described below). 70S•EF-G•GDP•Fus complexes (0.3 μM) were rapidly mixed with HflX (2 μM) in the presence GTP (250 μM). The resulting signals were averaged (typically 5-10 traces) and normalized with respect to the initial light scattering of the solution, setting the initial value as 100% of intact 70S ribosomes.

4.3.4 – SUCROSE GRADIENT DENSITY ULTRACENTRIFUGATION

70S ribosomes (1 μM) were incubated with HflX (1 μM) in the presence of GTP (125 μM) and antibiotic (500 μM) in $TAKM_5$ buffer for 15 minutes at 37°C before loading onto a 10-40% sucrose gradient. The 10-40% sucrose gradients made in $TAKM_5$ buffer was formed using a BioComp Gradient Master. Designated antibiotic was added to each respective gradient prior to formation to a final concentration of 500 μM. Gradients were centrifuged at 28 000 xg in a SW41 Ti rotor for 10 hours. Following centrifugation, gradients were fractionated into 1 mL fractions through an AKTA Prime Plus to measure A_{256}.

4.3.5 – MICROFILTRATION

To determine if HflX can bind to the 70S ribosome with a filled A-site 70S•EF-G•GDP•FUS complexes were formed initially. To form these complexes 70S ribosomes (1 μM) were incubated with EF-G (5 μM), GTP (125 μM), and FUS (500 μM) for 15 minutes at 37°C in a water bath. Samples were incubated on ice briefly before diluting to 500 μL with $TAKM_5$ containing nucleotide and antibiotic at the same concentration and applying to the top of a 100 kDa MWCO Vivaspin-500 column (GE Healthcare). The ultrafiltration devices were centrifuged at 10 000 g for 5 minutes or until 20 μL remained above the filter before diluting to 500 μL and centrifuging again. HflX (5 μM) was added to the resulting 70S•EF-G•GDP•Fus complexes (~1 μM) and incubated for an additional 15 minutes at 37°C in a water bath. Samples were incubated on ice briefly before diluting to 500 μL with $TAKM_5$ containing nucleotide and antibiotic at the same concentration and applying to the top of a 100 kDa MWCO Vivaspin-500 column (GE Healthcare). Ultrafiltration devices were centrifuged at 10 000 xg for 5 minutes or until 20 μL remained above the filter before diluting to 500 μL and centrifuging again. Resulting filtrate was analyzed on a 12% SDS-PAGE stained with Coomassie Blue. Experiments with antibiotics and/or nucleotides were supplemented with 125 μM nucleotide and 500 μM antibiotic in buffer used for dilution and washing.

4.4 – RESULTS

4.4.1 – *ESCHERICHIA COLI* HFLX DOES NOT CONFERS TOLERANCE TO MACROLIDE AND LINCOSAMIDE ANTIBIOTICS

In several bacterial species including *Listeria monocytogenes* and *Mycobacterium* species, HflX has been shown to provide resistance to antibiotics of the macrolides erythromycin (ERY) and azithromycin (AZI) and lincosamides clindamycin (CLIND) and lincomycin (LINC) (201, 231). We have previously shown that antibiotics of these classes inhibits the ribosome stimulated GTP hydrolysis of *E. coli* HflX (EcHflX) (213), yet it is unclear whether EcHflX is able to confer resistance to these antibiotics *in vivo*. To determine if EcHflX could confer resistance to ribosome targeting antibiotics, the minimal inhibitory concentration (MIC) of several classes of antibiotics were determined for a knockout strain of *hflX* (Δ*hflX*) from the Keio collection along with the parental strain (BW25113; referred to herein as the wild type strain) (308). The MIC for several classes of antibiotics including macrolides, lincosamides, aminoglycosides, and other ribosome targeting antibiotics were determined (Table 4.1). The Keio collection contains *E. coli* strains with individual genes replaced with a kanamycin resistance (KanR) cassette, therefore, the Δ*hflX* strain part of the Keio collection exhibited resistance to kanamycin, an aminoglycoside. To determine the MIC for aminoglycosides in the Δ*hflX* strain we removed the *kanR* gene from Δ*hflX* using λ-red recombineering and repeated the MIC assay for the aminoglycoside antibiotics (Table 4.1). Compared to the studies in *L. monocytogenes* and *Mycobacterium* species, , the macrolides (erythromycin and azithromycin) and lincosamides (lincomycin and clindamycin) showed no change in MIC in the presence or absence of *hflX* suggesting that EcHflX does not confer resistance to these antibiotics when present.

Table 4.1 – Minimal inhibitory concentrations of *E. coli* BW25113 and Δ*hflX* toward antibiotics of several ribosome targeting classes. The MIC values shown are the lowest concentration that prevented growth after 18-hour culturing. The reference strain (BW25113) was compared to the in-frame Δ*hflX* knockout replaced with the *kanR* gene, and the same Δ*hflX* knockout strain with the *kanR* gene removed. Dilutions of each antibiotic were based on published MIC values.

Antibiotic	Class	Keio wt (μg/mL)	Keio Δ*hflX* (μg/mL)	Keio Δ*hflX* Δ*kanR* (μg/mL)
Azithromycin	Macrolide	12.1 ± 4.1	11.3 ± 4.1	13.0 ± 3.9
Erythromycin	Macrolide	166.7 ± 50.0	216.7 ± 79.1	183.3 ± 66.1
Clindamycin	Lincosamide	125.0 ± 0.0	125.0 ± 0.0	125.0 ± 0.0
Lincomycin	Lincosamide	1000.0 ± 0.0	1333.3 ± 500.0	1666.7 ± 500.0
Hygromycin B	Aminoglycoside	104.2 ± 31.2	156.3 ± 46.9	135.4 ±49.4
Neomycin	Aminoglycoside	20.8 ± 6.3	200.0 ± 0.0	15.3 ± 7.7
Paromomycin	Aminoglycoside	15.3 ± 5.5	2444.4 ± 881.9	20.8 ± 6.3
Streptomycin	Aminoglycoside	27.8 ± 8.3	27.8 ± 8.3	25.0 ± 0.0
Tobramycin	Aminoglycoside	3.8 ± 1.9	6.7 ± 2.1	4.4 ± 1.3
Spectinomycin	Aminocyclitols	277.8 ± 83.3	277.8 ± 83.3	250.0 ± 0.0
Tetracycline	Tetracycline	0.5 ± 0.0	0.5 ± 0.0	0.6 ± 0.2
Ampicillin	Beta-lactam	4.0 ± 0.0	4.0 ± 0.0	4.4 ± 1.3

4.4.2 – AMINOGLYCOSIDE ANTIBIOTICS PREVENT HFLX-MEDIATED 70S RIBOSOME DISSOCIATION INTO ITS SUBUNITS

Macrolide, lincosamide, and aminoglycoside antibiotics have known effects on the ribosome stimulated GTP hydrolysis of HflX, specifically with the macrolides and lincosamides inhibiting GTP hydrolysis (213). In the GTP-bound active state, HflX can dissociate the 70S ribosome into 50S/30S ribosomal subunits, yet nucleotide hydrolysis is not required to facilitate subunit dissociation (19, 213). There are conflicting results as to whether hydrolysis increases the rate of dissociation or not, thus we decided to investigate the effect inhibition of GTP hydrolysis had on HflX-mediated ribosome dissociation. Here we used the stopped-flow technique and Rayleigh light scattering to measure the time-dependence and extent of 70S ribosome dissociation in the presence of several classes of antibiotics. HflX-mediated 70S dissociation reactions containing macrolide, lincosamide or chloramphenicol antibiotics showed dissociation of the 70S ribosome over time comparable to rection with no antibiotic present (Figure 4.1A). Surprisingly, antibiotics of the aminoglycoside family that bind to the decoding center inhibited HflX-mediated 70S ribosome dissociation (Figure 4.1AB). Of the antibiotics tested, most aminoglycosides (KAN, streptomycin (STR), hygromycin B (HYGB), and kasugamycin (KAS)) displayed no HflX-mediated 70S ribosome dissociation as indicated by no change in light scattering, however, TOB and PAR displayed an increase in light scattering in the first 20 seconds following mixing (Orange and Green time courses, respectively; Figure 4.1AB). An increase in light scattering suggests an increase in particle size, presumably in this case due to HflX being bound to the ribosome by either TOB or PAR.

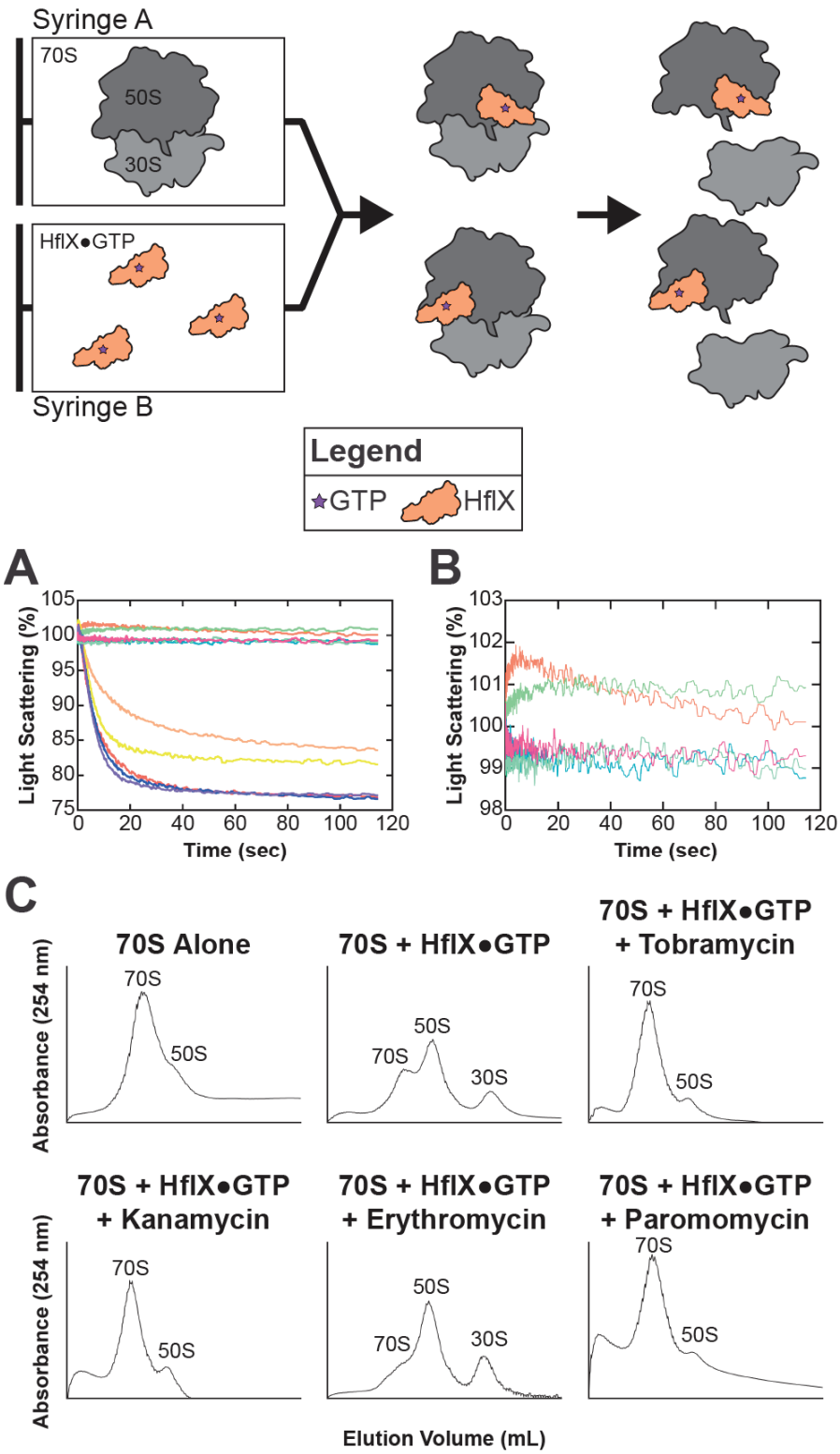

Figure 4.1 – Aminoglycoside antibiotics inhibit HflX-mediated dissociation of the 70S ribosome. Rapid mixing of HflX•GTP against 70S ribosomes results in a decrease in Rayleigh light scattering over time indicative of dissociation of the 70S ribosome into 50S and 30S ribosomal subunits. (A) Antibiotics that target the peptidyl transferase center (PTC) or peptide exit tunnel

(PET) show a decrease in light scattering characteristic of dissociation of the 70S ribosome into subunits (clindamycin – yellow; chloramphenicol – blue; erythromycin – purple; fusidic acid – light orange; tobramycin – orange; paromomycin – green; kanamycin – cyan; kasugamycin – light blue; streptomycin – pink; hygromycin B – teal; no antibiotic – red line). (B) Antibiotics that target the decoding center (DC) show no change in light scattering (kanamycin – cyan; kasugamycin – light blue; streptomycin – pink; hygromycin B – teal;) or an increasing in light scattering (tobramycin – orange; paromomycin – green). (C) 70S ribosomes incubated with HflX•GTP in the presence or absence of various antibiotics and were analyzed via sucrose density gradient ultracentrifugation on a 10-40% sucrose gradient. HflX•GTP can dissociate the 70S ribosome into 50S and 30S ribosomal subunits in the presence of erythromycin and absence of antibiotic, while aminoglycoside antibiotics (tobramycin, kanamycin, and paromomycin) inhibit 70S ribosome dissociation.

To verify the effect of aminoglycoside antibiotics on 70S dissociation, the distribution of ribosomal particles after incubating HflX•GTP with 70S ribosomes in the presence of various antibiotics was analyzed by sucrose gradient density ultracentrifugation (Figure 4.1C). In the absence of antibiotic, HflX•GTP facilitates dissociation of 70S ribosomes into 50S and 30S ribosomal subunits, as observed by the corresponding decrease in 70S ribosomes and increase in 50S/30S ribosomal subunits. In the presence of aminoglycoside antibiotics (TOB, PAR, and KAN) the 70S ribosome is not dissociated by HflX•GTP as compared to with ERY (macrolide) or in the absence of antibiotic. Analysis of 70S complexes via protein precipitation and subsequent SDS-PAGE analysis revealed that HflX remains bound to the 70S throughout the 10 h of sucrose gradient density ultracentrifugation (Appendix Figure 4.1). Furthermore, none of the antibiotics tested here interfere with ribosome binding or ribosome stimulated GTP hydrolysis (Appendix Figure 4.2 and 4.3) (213). Aminoglycosides also stabilize the 70S ribosome under magnesium depletion conditions that typically result in subunit separation (Appendix Figure 4.4) (213). Binding of aminoglycosides to Helix 69 (H69) of the large ribosomal subunit stabilizes intersubunit bridge B2a/d formed between H69 and primarily helix 44 (h44) of the small ribosomal subunit (89, 389). Overall, these results confirm that aminoglycoside antibiotics inhibit HflX-mediated 70S ribosome dissociation by further stabilization of the intersubunit bridge B2a/d and that inhibition of GTP hydrolysis does not prevent HflX-mediated 70S dissociation.

4.4.3 – HFLX BINDS TO THE RIBOSOMAL E-SITE OF STALLED 70S RIBOSOME COMPLEXES

The mechanism by which HflX dissociates the 70S ribosome is dependent on where HflX binds to the ribosome. Experimental evidence exists for both HflX binding to the A-site of a 50S ribosomal subunit by cryo-EM studies (19, 191) and for binding to the E-site of a 70S ribosome by covalent cross-linking studies (213). Previously, we had proposed that HflX binds to the E-site of a stalled 70S ribosome whose A-site is filled by an aminoacyl-tRNA and/or elongation factor as the E-site would likely be empty due to the lower affinity for tRNA (213, 390). This would be constant with the binding of other factors such as Elongation factor P (EF-P) and EttA resolving translational stalls via binding to the E site of the ribosome (204, 205, 391). To validate that HflX indeed binds to the E-site of a ribosome with an occupied A-site we performed binding studies in the presence of EF-G•GTP and the antibiotic fusidic acid (FUS; Figure 4.2). Fusidic acid locks EF-G onto the ribosome following hydrolysis of GTP to GDP thereby blocking the A-site from binding any additional factors (331, 332). The binding site of EF-G (18, 82, 392) and of HflX to the A-site (19, 191) of the ribosome overlap considerably (Appendix Figure 4.5), such that neither factor could be bound to the 70S ribosome simultaneously unless HflX is able to bind to the ribosomal E-site as well. To overcome HflX's ribosome dissociation activity in the presence of GTP, the aminoglycoside tobramycin was used throughout the experiment, and did not affect formation of 70S•EF-G•GDP•FUS complexes (Appendix Figure 4.6). 70S•EF-G•GDP•FUS•Tob complexes with increasing concentrations of EF-G were formed before incubating with HflX•GTP. Complexes were filtered through a microfiltration device to remove unbound factor as previously described (213) before analyzing the fraction bound by SDS-PAGE (Figure 4.2). At all concentrations of EF-G, the percentage of HflX bound to the 70S ribosome remained constant and did not decrease with the increase in EF-G concentration as would be expected if they shared the same binding site. These data not only indicate that HflX binds to the ribosomal E-site of the 70S ribosome with an blocked A site, but also that this is the only binding site for HflX on the 70S ribosome with physiologically relevant affinity as under the condition of the experiment in the absence of the GDP•FUS two molecules of HflX would be bound (in the E and the A site).

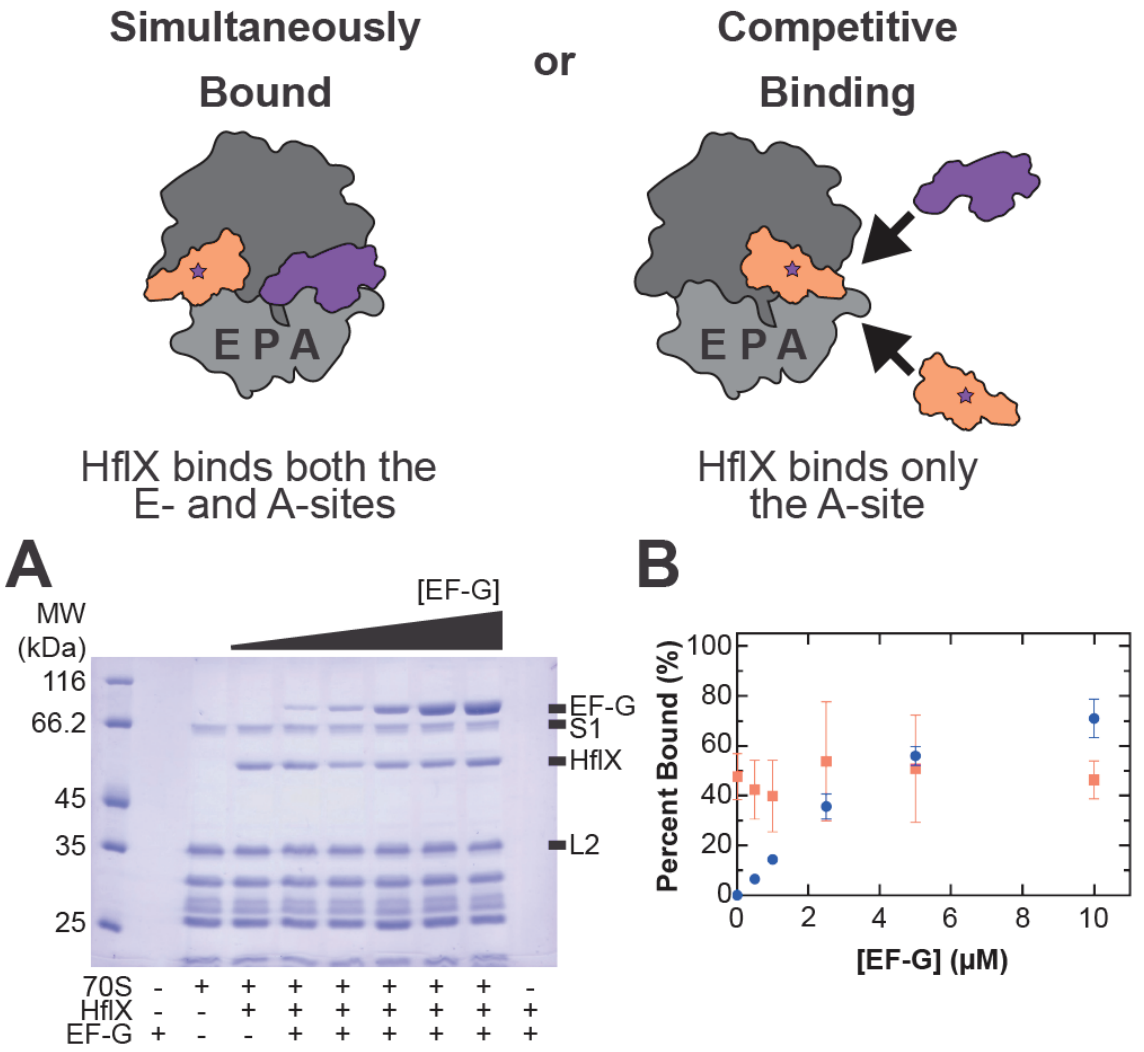

Figure 4.2 – HflX binds to the 70S ribosome with the A-site blocked by EF-G•GDP locked on by fusidic acid. (A) 70S ribosomes (1.5 μM) were incubated with EF-G (0.5-10 μM), GTP (125 μM), fusidic acid (500 μM), and tobramycin (500 μM) before filtration to remove excess EF-G. 70S•EF-G•GDP•FUS complexes (~ 1.5 μM) were then incubated with HflX (5 μM) and filtered again before analyzing complexes on a 12% SDS-PAGE stained with Coomassie brilliant blue. (B) Percent bound of HflX (Orange) and EF-G (Blue) to the 70S ribosome was determined using densitometry analysis via ImageJ and was plotted with respect to initial EF-G concentration.

4.4.4 – HFLX DISSOCIATES THE 70S RIBOSOME THROUGH BINDING TO THE RIBOSOMAL E-SITE

Ribosome dissociation by HflX plays an important role in all the proposed functional roles HflX may have *in vivo* (19, 140, 201, 213, 231). Based on the structural model of 50S•HflX•GDPNP from cryo-EM studies that shows HflX bound to the A-site, it was suggested that dissociation of the ribosomal subunits occurs from that binding site (19). As HflX can also bind to the ribosomal E-site, we sought to determine if HflX could dissociate the 70S ribosome from the E-site using Rayleigh light scattering (Figure 4.3). To do so, 70S•EF-G•GDP•FUS complexes were formed as in the previous experiment (Figure 4.2). Using the same stopped flow-based Rayleigh light scattering experiment described above (Figure 4.1), 70S complexes with EF-G•GDP•FUS locked onto the A-site were rapidly mixed with HflX•GTP and FUS (Figure 4.3). Intriguingly, HflX retains the ability to dissociate the 70S ribosome in 50S and 30S ribosomal subunits when the A-site is blocked by EF-G. Furthermore, the addition of a second antibiotic to the reaction has the expected outcome, with aminoglycosides (TOB and PAR) inhibiting HflX-mediated dissociation, while macrolide (ERY) and lincosamide (LINC) did not inhibit ribosome dissociation from the E-site. Taken together, our results show that EcHflX can bind to the ribosomal E-site and dissociate ribosomes with macrolide/lincosamide antibiotics bound and a blocked A-site *in vitro*.

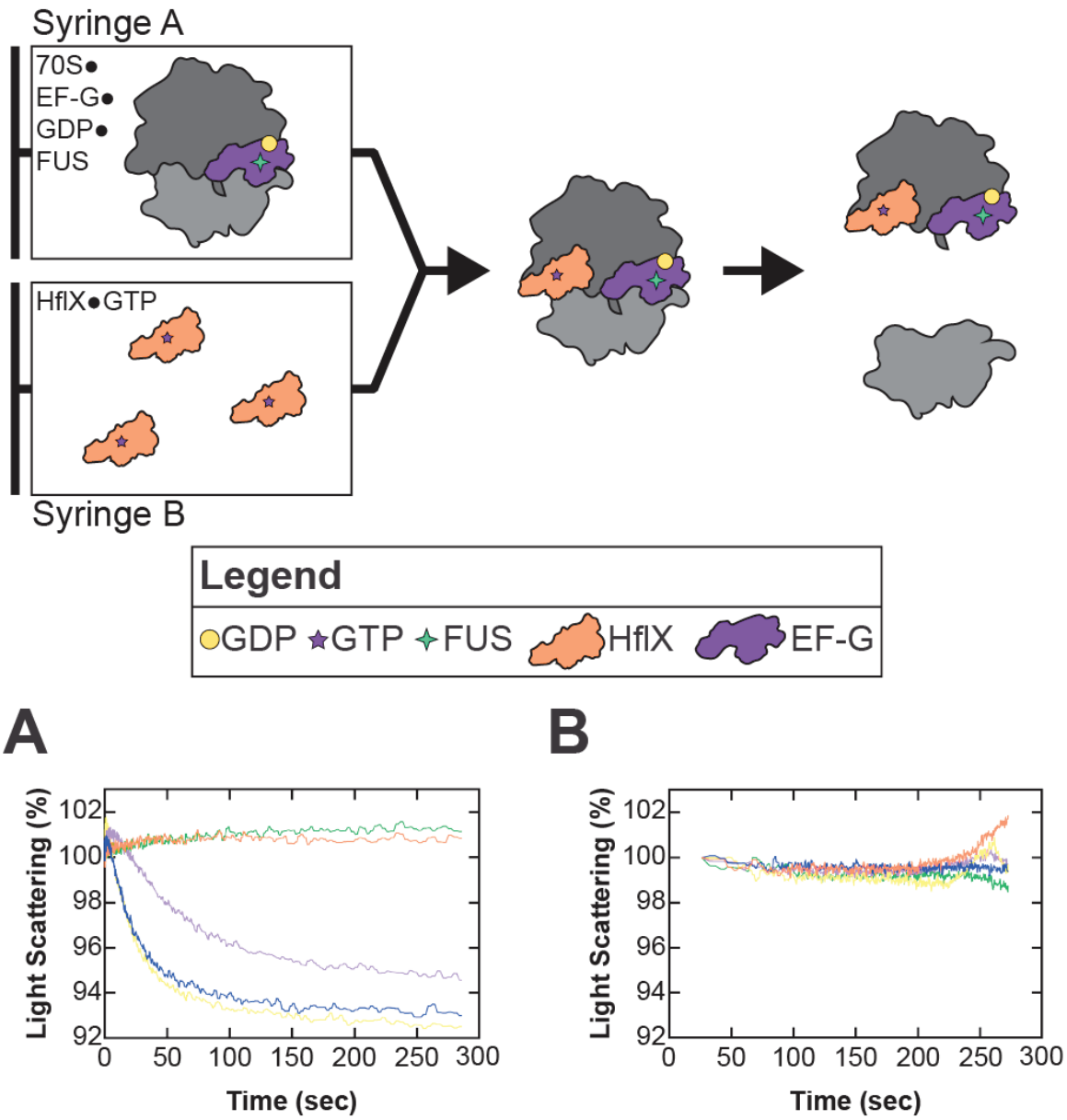

Figure 4.3 – HflX can dissociate the 70S ribosome from the ribosomal E-site. (A) 70S ribosome complexes with EF-G locked onto the ribosomal A-site were pre-formed by incubating 70S ribosomes, EF-G, FUS, and GTP together before removing free EF-G with microfiltration. 70S•EF-G•GDP•FUS complexes were then rapidly mixed with HflX•GTP and FUS resulting in a decrease in Rayleigh light scattering over time like previous stopped flow experiments (yellow). A second antibiotic was tested alongside FUS including ERY (pink), LINC (blue), TOB (orange), and PAR (green). (B) The identical experiments were carried out in the absence of HflX resulting in no ribosome dissociation over the same time course.

4.5 – DISCUSSION

HflX in several bacterial species has been shown to confer antibiotic resistance to macrolide and lincosamide classes of antibiotics (201, 225, 226, 229, 231). Dissociation of the 70S ribosome into its constituting subunits by HflX (19, 213) has been shown to be important for conferring resistance (231). In this study we show that EcHflX does not confer antibiotic resistance to *E. coli* (Table 4.1) yet EcHflX remains capable of dissociating ribosomes bound to several classes of antibiotics *in vitro*, with the notable exception of some AMGs (Figure 4.1). The AMG class of antibiotics contains many structurally unique members that bind to the decoding center and the intersubunit bridge B2a, thereby causing miscoding and inhibiting translocation (385-387, 393). Furthermore, AMGs are known to inhibit ribosome recycling by EF-G/RRF (389, 394) suggesting that HflX uses a related mode of action to facilitate subunit dissociation.

4.5.1 – MECHANISM AND RIBOSOME BINDING SITE OF HFLX-MEDIATED RIBOSOME DISSOCIATION

Aminoglycoside-mediated inhibition of ribosome dissociation by HflX provides the first mechanistic evidence of how HflX may facilitate subunit dissociation (Figure 4.1). The aminoglycoside binding site on H69 stabilizes intersubunit bridge B2a which is the primary target for EF-G/RRF-mediated ribosome recycling (82, 385, 389, 393, 394). If both HflX-mediated and EF-G/RRF-mediated subunit dissociation utilizes the disruption of intersubunit bridge B2a, then it is likely that they do so from the same position on the ribosome, the A-site (18). Structural information from cryo-EM studies show EcHflX bound to the A-site of a 50S ribosomal subunit which results in the displacement of H69 such that it would sterically clash with a bound 30S subunit (19). These results further suggest that dissociation does occur through the disruption of intersubunit bridge B2a. This 50S•EcHflX•GDPNP complex is a post-subunit dissociation complex formed *in vitro* and therefore it may not be truly indicative of HflX under *in vivo* conditions.

Our previous studies presented the first biochemical evidence of the HflX binding site on the pre-dissociation complex (213). Utilizing UV-crosslinking, we demonstrated that the C-terminal

domain (CTD) of HflX covalently cross-linked to ribosomal proteins and rRNA that are located in the periphery of the E-site. Removal of the CTD did not abolish EcHflX binding to the 70S ribosome suggesting that the N-terminal domains are positioned in the E-site of the ribosome. This raises the question of whether HflX dissociates the ribosome through the ribosomal A-site or E-site, or both. Based on the post-subunit dissociation complex and similar interactions with H69 as RRF, the A-site seems like a logical site to induce subunit dissociation, however, this does not negate the possibility that HflX may utilize the E-site for dissociation as well. We previously hypothesized that a 70S ribosome stalled mid-translation would most likely have a filled A-site containing an aminoacyl-tRNA and/or elongation factor (213) while the E-site would likely be empty due to the low affinity for tRNA to the ribosomal E-site (390). As such, HflX would be able to bind to the empty E-site and dissociate the stalled 70S ribosome. To address whether the E-site is a functional interaction site for HflX, we performed binding and subunit dissociation experiments with 70S ribosomes containing a blocked A-site (Figures 4.2 and 4.3). To block the A-site, 70S ribosomes were pre-incubated with EF-G, GTP, and fusidic acid forming a 70S•EF-G•GDP•FUS complex (Appendix Figure 4.6). Using these complexes, we confirm that EcHflX can bind to and dissociate the ribosome from the ribosomal E-site. The functional relevance of HflX binding to both the ribosomal A- and E-sites may be tied to the occupancy of the A-site of a stalled ribosome complex, or may be relevant for the dissociation of the 100S ribosome dimer (129, 140). The 100S ribosome dimer is composed of two empty 70S ribosomes joined at the 30S ribosomal subunits by the binding of hibernation promoting factor (HPF) and ribosome modulation factor (RMF) in γ-proteobacteria including *E. coli* and just an extended HPF in gram positive firmicutes including *Staphylococcus aureus*, *Bacillus subtilis*, and *L. monocytogenes* (129, 138, 145). Both the extended HPF in firmicutes and short HPF in γ-proteobacteria bind to the 30S ribosomal A- and P-sites overlapping with the site mRNA and tRNA, thereby preventing any translation by the 100S ribosome dimer. As such, HflX binding to the A-site could play a role in the disassembly of the 100S ribosome dimer by dislodging the bound HPF. Comparison of the 100S ribosomal dimer and 50S•HflX•GDPNP structures show no direct interaction between HflX and HPF (Appendix Figure 4.7) (19, 145) specifically as HflX binds the large ribosomal subunit and HPF to the rRNA of the small subunit.

This suggests that HflX may dislodge HPF through a similar structural rearrangement of the rRNA as used to disrupt the intersubunit bridge, however, this has yet to be shown.

4.5.2 – MODEL OF HFLX ACTION IN THE CELL

While EcHflX does not confer antibiotic resistance, HflX homologs in other bacterial species are able to provide resistance to macrolide and lincosamide antibiotics, yet this is likely not the functional role that HflX serves in the cell. Therefore, we sought to provide a comprehensive model for how HflX's mode of action is utilized by the cell to overcome antibiotic induced stalling of protein synthesis. Here we propose a model in which dissociation of a stalled ribosome on polysome allows for trailing ribosomes to continue translating (Figure 4.4). As mRNAs are translated by multiple ribosomes simultaneously giving rise to the classic "beads on a string", stalling of any one ribosome would indirectly stall all trailing ribosomes as well. Therefore, it is necessary to have a factor(s), like HflX or EF-G•RRF, that can dissociate the stalled ribosome and all the trailing ribosomes to continue translating the mRNA. The newly liberated ribosomal subunits are then able to be used in further rounds of translation, or in the case of an antibiotic-induced stalling, the bound antibiotic is dissociate following HflX-mediated dissociation allowing the subunit to return to the actively translating pool.

Under sub-inhibitory antibiotic conditions, only a fraction of the cellular ribosomes are inhibited by the binding of the antibiotic. Therefore, one antibiotic molecule could theoretically remove multiple ribosomes from the actively translating pool at once by binding to a leading ribosome on a polysome. If the number of inactive ribosomes grew too high, the cell would be unable to produce new proteins required for cell maintenance and growth resulting in cellular dormancy or death. HflX-mediated dissociation of the antibiotic stalled 70S ribosome would allow all non-antibiotic-bound trailing ribosomes on the same mRNA to proceed translating, effectively returning them to the actively translating pool of ribosomes. Overall, alleviating stalled ribosomes from a polysome is likely not exclusive to antibiotic-stalled ribosomes, as such, this HflX-mediated mechanism likely has a greater role in cellular fitness than conferral of antibiotic resistance.

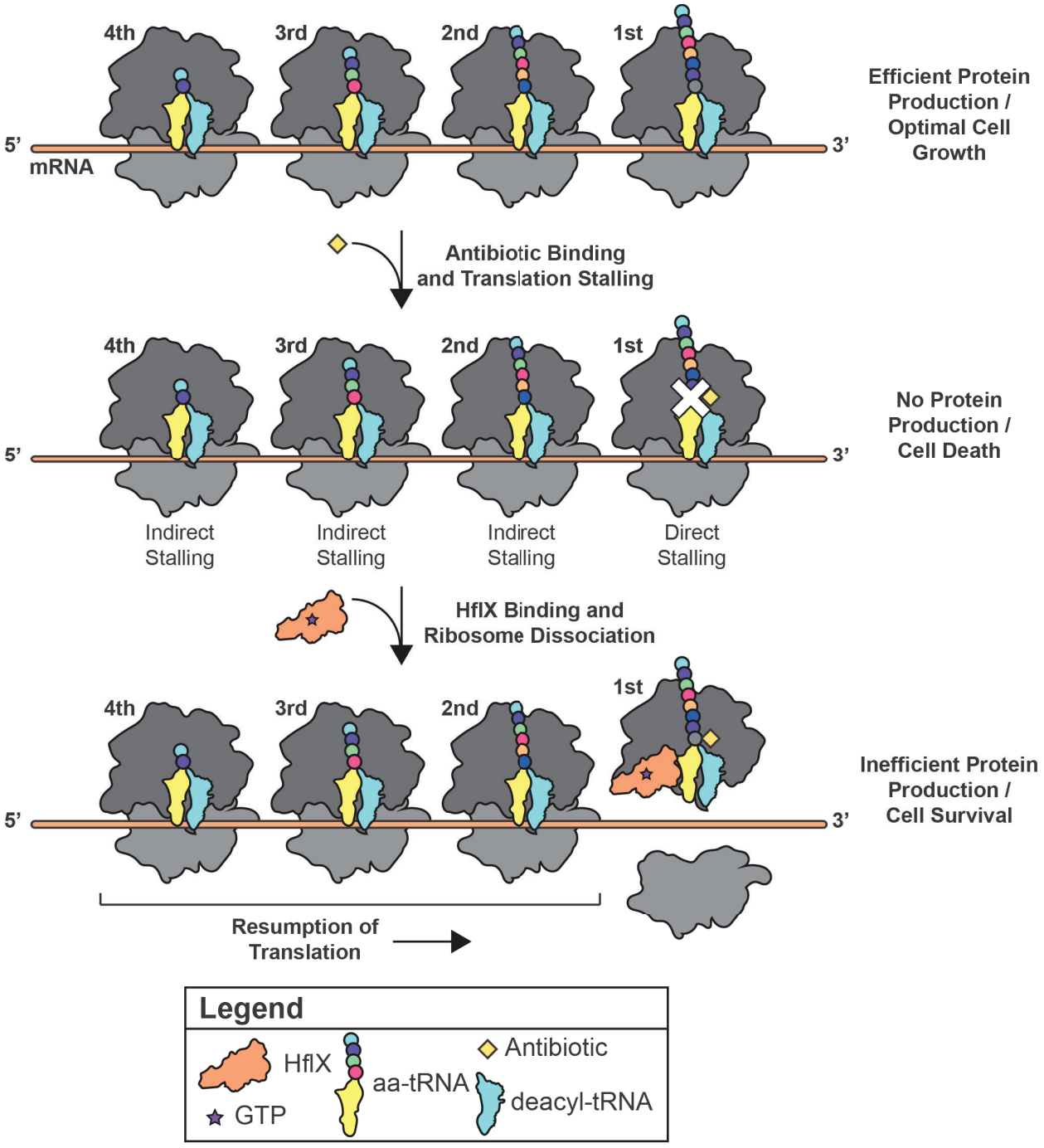

Figure 4.4 – Proposed functional role of HflX in relieving translational stalling and providing antibiotic resistance. Multiple ribosomes can be actively translating the same mRNA concurrently commonly referred to as a polysome. Antibiotic induced stalling of one ribosome in the polysome indirectly stalls all ribosomes trailing the stalled ribosome, effectively sequestering multiple ribosomes from the active translating pool. HflX-mediated dissociation of the antibiotic stalled ribosome removes it from the polysome thereby allowing the trailing ribosomes to continue translating the mRNA. Every ribosome that is removed from an mRNA due to antibiotic inhibition reduces the cellular capacity for protein synthesis unless additional factors are present that can remove the antibiotic from firstly the ribosome and secondly the cell.

Following subunit dissociation, the bound antibiotic needs to be removed before the ribosomal subunit can be used in subsequent rounds of translation. The antibiotic can be dissociated either passively through spontaneous dissociation or actively through a target protection mechanism (395). Spontaneous dissociation of the antibiotic from the ribosome is unlikely to be sufficient to facilitate antibiotic resistance at high concentrations as ERY has a half-life on the *Staphylococcus pneumoniae* ribosome of 6.9 minutes (396). Therefore, dissociation of the bound antibiotic is likely facilitated by HflX or another factor through a target protection mechanism similar to the removal of tetracycline by the GTPases TetM and TetO (364, 365, 397). Based on the structure of HflX bound to the 50S ribosomal subunit, the flexible loop between the two alpha helices of the linker domain is positioned in the PTC such that it could theoretically interact with a bound antibiotic (19, 395). However, it has been shown that HflX (specifically *Mycobacterium smegmatis* HflX (MsHflX)) is unable to remove bound macrolide antibiotics suggesting that another factor is likely involved in removal of the bound antibiotic (231). In *L. monocytogenes*, it has been proposed that the *lmo0919* gene encoding an ABC-F transporter may be involved in displacing ribosome-bound lincomycin (201). If this is the case, where HflX solely dissociates stalled ribosomes and requires an additional factor to remove the bound antibiotic, it would suggest that HflX homologs from different bacterial species could rescue knockout strains if each homolog is capable of ribosome dissociation and the additional factor is present. However, it was previously shown that EcHflX is unable to rescue *M. smegmatis* and *Mycobacterium abscessus* strains lacking their respective *hflX* genes (Δ*Ms_hflX* and Δ*Mab_hflX*) suggesting that there may be species-specific differences that prevent EcHflX interacting with and/or splitting the mycobacterial ribosome (231). If the differences between bacterial translation systems and their HflX homologs are enough to prevent complementation, it suggests that antibiotics could be developed that target these differences thereby specifically inhibiting either *E. coli* or mycobacterium. While the exact sequence differences between the *E. coli* and mycobacterial species that facilitate species-specific HflX-mediated dissociation have not been determined, the human homolog GTPBP6 and its mitochondrial ribosome target differ to an even larger extent (*E. coli* and human: 28% identity and 46% similarity; *E. coli* and *M. smegmatis*: 35% identity and 51%

similarity) making the viability of a species-specific antibiotic that do not effect the host more realistic. Further studies are required to determine to what sequence differences contribute to antibiotic resistance and what other factors are involved in providing resistance to macrolide and lincosamide antibiotics.

4.5.3 – HFLX ROLE IN RESPONSE TO NON-PTC/PET BINDING ANTIBIOTICS

Interestingly, the *hflX* gene has been implicated in the cellular response to non-PTC/PET binding antibiotics. In *Streptomyces coelicolor*, the *hflX* gene is upregulated by the WhlB transcription factor in the presence of tetracycline (229). Knockout of the *hflX* gene in *S. coelicolor* however did not render the cell more susceptible to tetracycline suggesting that upregulation of *hflX* by WhlB is a general response to ribosome targeting antibiotics which is supported by our MIC assay data for tetracycline (Table 4.1). Additionally, it has been reported that *E. coli* Δ*hflX* strains are susceptible to antibiotics that inhibit cell wall biosynthesis including ampicillin (257). Our data show that ampicillin has no effect on ribosome dissociation by HflX (Figure 4.2) nor on GTP hydrolysis (data not shown) signifying that there is no direct effect on HflX. Furthermore, ampicillin is not a ribosome binding antibiotic, so how HflX confers resistance to ampicillin remains unknown.

4.5.4 - CONCLUSION

In conclusion, EcHflX dissociates 70S ribosomes from either the ribosomal A-site or E-site through disruption of intersubunit bridge B2a which in turn induces subunit dissociation. This is the first evidence for the mechanism underlying HflX-mediated ribosome recycling. Furthermore, our data supports a model in which HflX is responsible for dissociating stalled ribosome complexes thereby preventing multiple ribosome sequestration on mRNA. This is a mechanism the cell can easily exploit to counteract the effect of ribosome stalling antibiotics suggesting that combination therapies inhibiting HflX will increase antibiotic efficacy, especially for macrolide and lincosamide

antibiotics. While EcHflX does not confer antibiotic resistance, a fundamental understanding of how HflX functions in the cell will be important for combating resistance.

CHAPTER 5: FUTURE DIRECTIONS

5.1 – YCHF

5.1.1 – FUTURE YCHF STRUCTURAL AND BIOCHEMCIAL STUDIES

There are several follow-up experiments and questions that arise from Chapter 2 about the functional role of YchF *in vivo* and the nature of the interaction between the YchF ternary complex (YchF•tRNA•ATP) and the ribosomal A-site. Through a collaboration with Drs Alexey Amunts and Yuruzu Itoh, we have knowledge of the *Plasmodium falciparum* YchF homolog (PfYchF) bound to the 80S ribosome and a tRNA (personal communication). Comparison of this 80S•PfYchF•tRNA structure to that modelled for EcYchF bound to the 70S ribosome and tRNA (Chapter 2) shows a similar binding location and interaction with the A-site of the ribosome. It will be important to verify this interaction site for the *E. coli* complex and as such, the conditions to form stable 70S•EcYchF•tRNA•ATP complexes will need to be determined prior to cryo-EM and structural model building. We hypothesize that YchF acts upon 70S ribosomes with improperly folded rRNA such that they are incapable of carrying out translation. 70S ribosomes typically form following translation initiation (see *Section 1.5 – Translation initiation in bacteria*) and as such contain an initiator tRNA in the P-site and an mRNA (a 70S IC), however, recent evidence suggests that following ribosome biogenesis of each subunit individually, these subunits are brought together to test intersubunit connections and communications (52, 53). This late-stage biogenesis 70S complex may or may not contain additional factors such as mRNA or tRNA. The exact functional 70S ribosome target of YchF remains to be confirmed and will be an important experimental question to answer moving forward. Here I will outline the next major experimental questions with respect to unravelling the cellular function and mechanistic details of YchF. The interaction between YchF and tRNA observed *in vivo* and *in vitro* led to several new hypotheses as to what determinants are required for binding and what the functional role of this interaction is. Structural modeling (Figure 2.4D) suggests that YchF binds to deacylated tRNA. To confirm this,

nitrocellulose filter binding assays will be performed using $tRNA^{Phe}$ aminoacylated with ^{3}H or ^{14}C-labeled phenylalanine. If YchF is able to bind aminoacylated tRNA, the radiolabeled aminoacyl-tRNA should remain on the nitrocellulose filter while bound to YchF. This experiment will be performed in different nucleotide bound states of YchF and with EF-Tu as a control. In addition to preferring deacyl-tRNA over aminoacyl-tRNA, YchF may prefer specific tRNAs or isoacceptors. This was partially addressed by the deep sequencing of RNA that co-purifies with YchF (Figure 2.3B). The one issue with how this experiment was performed is that prior to using the NEBNext Multiplex Small RNA Sample Prep Kit, there was no hydrolysis step carried out to remove the amino acid from any aminoacylated tRNA that could have co-purified with YchF. Not removing the amino acid from aminoacylated tRNA prevents them from being processed with the Sample Prep kit, thereby biasing the deep sequencing results. The relative cellular levels of aminoacylation of each isoacceptor differ among isoacceptors, however, on average about 60% of all tRNAs are aminoacylated under ideal growth conditions (344). While the results presented in Figure 2.3B suggest that there is no strong bias towards any specific tRNA isoacceptor, the experiment will need to be repeated, ensuring that the aminoacyl-tRNA bond is hydrolyzed before proceeding.

The hypothesis that YchF acts as an RNA chaperone has yet to be confidently confirmed. Primarily the experiment (Chapter 2 Figure 2.2) needs to be repeated using excess RNA duplex with respect to YchF (and control proteins). The experiment performed (Figure 2.2) had an excess of YchF (500 nM) relative to the fluorescently labeled oligo (10 nM) and competitor oligo (200 nM). Under such conditions, YchF could bind non-specifically to single stranded RNA and act as a dead end complex thereby preventing competitor oligo from binding after RNA duplex unwinding, and/or binding to either labeled RNA after spontaneous dissociation of the duplex. As such, there maybe no RNA unwinding activity at all observed in the previous experiment but merely a sequestration of dissociated RNA strands. To correct this, as mentioned above, using excess RNA duplex (and competitor oligo) to YchF (and the respective control proteins) should be performed in a similar manner as described in Section 2.3.12 – RNA Unwinding Assay. Furthermore, this assay could also be adapted for measurement using the stopped-flow approach, thereby allowing for a real-time measurement of RNA unwinding.

Once RNA chaperone activity can be confirmed, the next question is what the target RNA for YchFs activity is in the cell. Does YchF act as an RNA chaperone to the rRNA of the 50S ribosomal subunit, or to the tRNA which YchF binds? I hypothesize that it is the rRNA that YchF unfolds and provides it with a second chance to refold properly. Studies examining the unwinding activity of YchF toward specific RNA molecules, including tRNA and fragments of the rRNA such as the SRL, can be carried out to determine whether YchF has specificity toward a particular RNA species. Computational simulation work done previously in the Wieden lab shows that there is a structural motif within the G domain comprised of histidine 102 and tyrosine 204 that can pivot allowing this alpha helical domain to act as a lever (Ian Andrews honours thesis, 2014). From this new structural and biochemical information, it seems like tRNA bound to YchF acts as an extension to the alpha-helical domain, extending toward the decoding center of the small ribosomal subunit. It is hypothesized that this levering motion about the His102/Tyr204 pivot can position the flexible catalytic loop where the catalytic histidine (H114) resides in the “closed” conformation such that catalysis can occur. Therefore, it is hypothesized that the correct positioning of the tRNA into the decoding center results in a conformational change in YchF favourable for nucleotide hydrolysis. This pivot/lever hypothesis still remains to be confirmed biochemically with information from the structural model of PfYchF bound to the 80S, or a cryo-EM structural model of the EcYchF ternary complex bound to the 70S ribosome, perhaps serving to guide future studies. Of particular interest will be what contacts within the ribosome are responsible for triggering this hinging motion about the pivot. Furthermore, several biochemical studies characterizing the interaction between the YchF ternary complex and the ribosome are required to update the kinetic model that previously did not include tRNA. These include measuring the affinity of the YchF ternary complex to the 70S ribosome and the rate of nucleotide hydrolysis in the presence and absence of correct codon-anticodon interactions.

5.2 – HFLX

5.2.1 – KINETICS OF HFLX-MEDIATED RIBOSOME DISSOCIATION

The kinetic constants that govern the interactions between biomolecules can provide insight into exactly how each biomolecule progresses through its molecular mechanism within the cell. Specifically, we hope to determine the kinetic constants that govern the interaction of HflX with the ribosome and guanine nucleotides. Several studies have investigated the kinetic parameters that govern the interactions HflX makes with guanine nucleotides and the ribosome, including the dissociation of the 70S ribosome into its subunits (19, 30, 203, 213). Specifically, kinetic constants that remain to be determined include 1) the rate of association and dissociation of HflX to the 70S ribosome and 50S ribosomal subunit, 2) the rate of guanine nucleotide exchange on the 70S ribosome (GDP to GTP), and 3) the rate of ribosome dissociation relative to that of GTP hydrolysis and phosphate release (Figure 5.1).

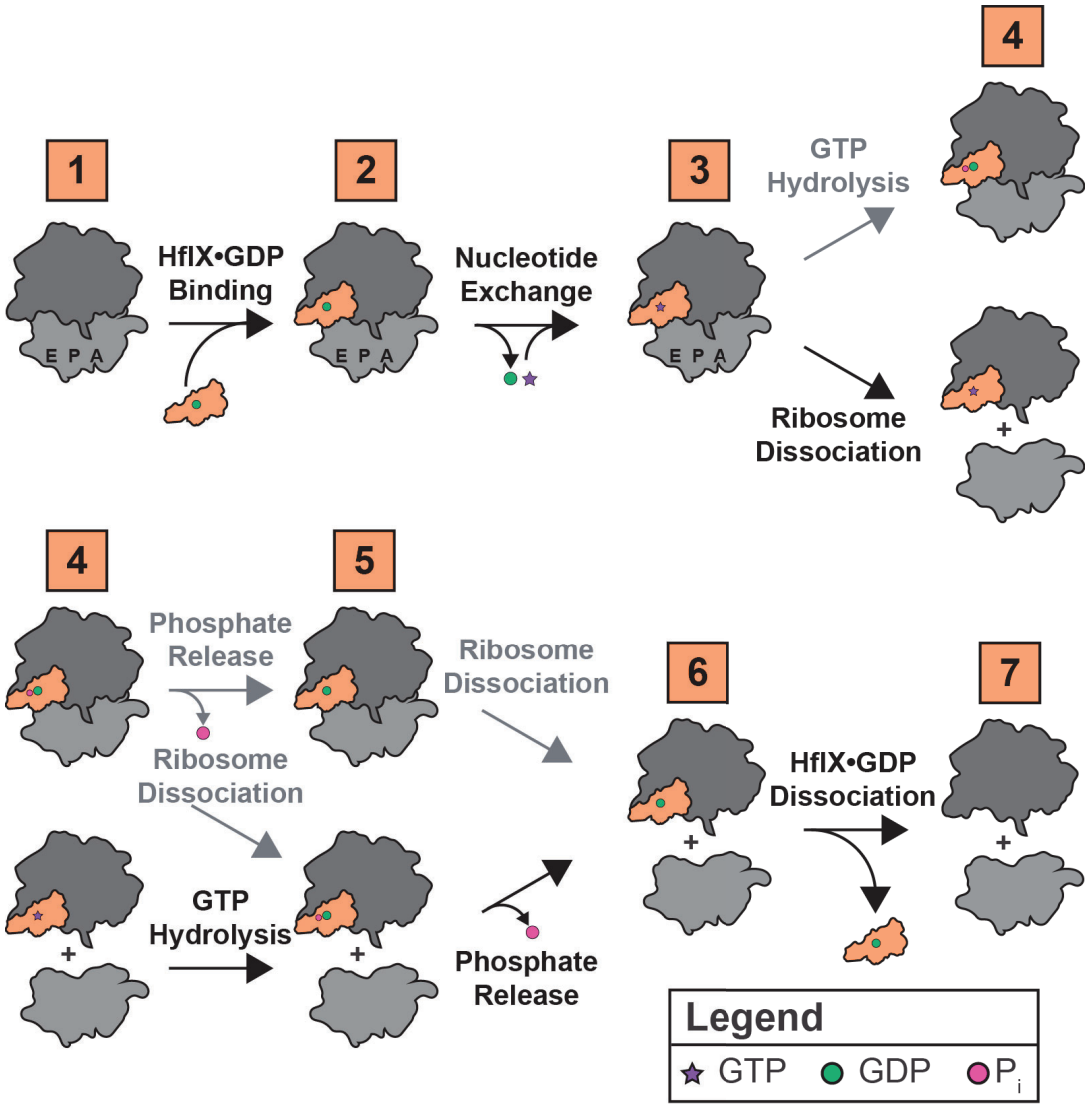

Figure 5.1 – Kinetic model of HflX-mediated ribosome dissociation and missing kinetic rate constants. HflX is primarily bound to GDP prior to binding the 70S ribosome [1]. Following ribosome binding [2], nucleotide exchange occurs putting HflX into the GTP-bound active state [3]. In the GTP-bound active state, HflX either hydrolyzes GTP to GDP and phosphate (Pi) or dissociates the 70S ribosome in 50S and 30S ribosomal subunits [4]. If GTP hydrolysis occurs before ribosome dissociation, then either phosphate release occurs prior to ribosome dissociation or following ribosome dissociation [6]. If ribosome dissociation occurs before GTP hydrolysis, then GTP hydrolysis [5] must follow proceeded by phosphate release [6]. Following ribosome dissociation, GTP hydrolysis, and phosphate release (not necessarily in that order as indicated above), HflX•GDP remains bound to the 50S ribosomal subunit [6] prior to dissociation from the 50S subunit [7]. The black arrows indicate the current hypothesis for HflX-mediated ribosome dissociation, however, the pathways indicated with grey arrows can not be ruled out without a thorough kinetic analysis. For simplicity, the target 70S ribosome complex HflX targets in the cell is referred to just at the 70S ribosome in this figure.

Initial measurement of HflX association and dissociation from different ribosomal particles has been performed utilizing a fluorescein dye labeled HflX variant (Fl-HflX) and performing rapid mixing stopped flow experiments. Wild-type HflX was labeled with fluorescein similar as to the 4AzP labeling of HflX in Chapter 3. There was a labeling ratio of 1.5:1 suggesting that the half of the labeled HflX molecules had a fluorophore attached to one of the cysteine residues (C96 or C98 *E. coli* numbering) buried in the N-terminal HflX domain (Mackenzie Coatham M.Sc. thesis). Association studies utilizing Fl-HflX have been performed at varying concentrations in preparation for global fitting of the kinetic data. Currently, other kinetic data sets need to be collected before global fitting can be performed.

Of the other data sets to be measured, the single turnover rate of GTP hydrolysis and rate of 70S ribosome dissociation have been measured while the rate of phosphate release (P_i) from 70S•HflX•GDP•Pi complexes is in early stages. These phosphate release measurements are performed utilizing a fluorescently labeled phosphate binding protein (PhoS) produced in-house to quantify the amount of free inorganic phosphate (P_i) in solution (398). Finally, to measure nucleotide exchange, a simple chase experiment utilizing [^{3}H]-GDP and excess unlabeled GDP would need to be performed as in Zavialov *et al*. (80). These nucleotide exchange experiments have not been initiated. Overall, these studies of the kinetic mechanism of HflX-mediated ribosome dissociation constituted one of the other major projects I was working on during the later stages of my PhD.

5.2.2 – KINETICS OF 100S RIBOSOME DIMER FORMATION AND DISSOCIATION

HflX has been implicated in the disassembly of 100S ribosome dimers following cellular dormancy to allow translation to resume rapidly (see *Section 1.12.6 – Role in ribosome hibernation*) (140). Formation of 100S ribosomes is not exclusive to cellular dormancy but helps cells to survive various environmental stresses and even has implications in virulence of some bacterial species (see *Section 1.10 – Ribosome hibernation in bacteria*) (129). Interestingly, there exists differences in the 100S structure between gram-positive and gram-negative bacteria species raising the question whether HflX-mediated 100S dissociation differs in subunit dissociation order or binding site, or if the differences are irrelevant to HflX-mediated ribosome dissociation. Using

purified components from both gram-negative *E. coli* and gram-positive *S. aureus* to form their respective 100S ribosome dimer complexes, stopped-flow light scattering experiments can be performed to monitor the disassembly of 100S dimers. Furthermore, it remains to be determined when HflX is involved in 100S ribosome *disassembly in vivo* as it has recently been shown that EF-G/RRF-mediated ribosome dissociation can also trigger 100S disassembly (139).

Performing *in vitro* kinetic analysis of the dissociation of the 100S ribosome dimer complex by HflX will require the purification of both EcRMF and EcHPF for *E. coli* 100S complexes and SaHPF for *S. aureus* 100S complexes. The abovementioned components can also be utilized to study the assembly of 100S ribosome dimers as well. It is unclear in the literature whether the hibernation factors bind to two 30S subunits causing them to dimerize initially followed by 50S subunit binding, or whether hibernation factors binding starts with the formation of an inactive 70S followed by 100S dimerization (Figure 1.13). Using stopped-flow light scattering experiments under will allow to dissect the pathway for 100S formation in both gram-positive and gram-negative bacteria.

5.2.3 – CHARACTERIZATION OF HFLX HOMOLOGS THAT CONFER ANTIBIOTIC RESISTANCE

As described in *Section 1.12.7 – Role in antibiotic resistance* and Chapter 4, it is evident that HflX can confer a fitness advantage to cells inhibited with protein synthesis targeting antibiotics. One of the most intriguing questions that arose from HflX-mediated antibiotic resistance is why some organisms contain a duplication of the *hflX* gene in which one copy confers resistance and the other does not. Specifically, what are the differences between the duplicated *hflX* genes in *Listeria monocytogenes* that allow one copy (*lmo0762* – LmHflXr) to provide resistance to lincomycin while the other *hflX* gene (*lmo1296* – LmHflX) cannot? (201) Are both hflX gene products capable of dissociating ribosomes, and if so, why does only LmHflXr confer antibiotic resistance? Sequence alignment of both *L. monocytogenes hflX* genes (201), both mycobacterium *hflX* genes involved in resistance (231), and *E. coli hflX* (see *Chapter 4*) doesn't provide any obvious differences that would indicate why LmHflX does not confer resistance. There are regions between

the HflX homologs that may be responsible for species specific resistance explaining how EcHflX cannot rescue the mycobacterial *hflX* knockout strain (231).

Furthermore, all studies so far suggest that ribosome dissociation is important for antibiotic resistance, yet this has still to be confirmed. Rudra *et al*. show that truncation variants of MsHflX cannot dissociate the 70S ribosome but fail to show whether these truncations are able retain binding to the 70S ribosome (231). An EcHflX variant (K62A) has been created that has previously been shown (19) to prevent HflX-mediated ribosome dissociation. Testing whether EcHflX K62A can bind to the ribosome binding, and if it can compensate for the knockout of the wild type *hflX* gene in *E. coli* MIC assays will address the question of whether ribosome dissociation is required for antibiotic tolerance in *E. coli*. Ribosome dissociation is likely how HflX confers antibiotic resistance as we hypothesized in Chapter 4 through alleviating ribosome sequestration in non-active polysomes (Figure 4.4). If ribosome dissociation is not important for the antibiotic resistance conferred by HflX, then potentially HflX binding to the antibiotic bound ribosome recruits additional factors that work together to alleviate stalling and/or remove the bound antibiotic. Overall, it will be important to determine whether all organisms contain a homolog of HflX that is able to confer antibiotic resistance, what makes some homologs more effective at conferring resistance and whether organisms have additional factors that increase resistance with the help of HflX.

5.2.4 – HFLX ROLE IN RIBOSOME REPAIR

Another role described for HflX in the literature is in repairing damaged ribosomes, whether due to high heat or other conditions that lead to folding of the rRNA into non-productive structures incapable of supporting efficient translation (Figure 5.2) (191). HflX was shown previously to have helicase activity that unwinds RNA duplexes and the 23S rRNA in the presence of ATP, but not GTP. *In vitro* translation assays carried out with ribosomes either untreated, heated to 50°C, or heated to 50°C and then treated with HflX•ATP showed that HflX•ATP was able to restore activity to ribosomes after heat treatment (191). This is consistent with the requirement of HflX to confer protection from 50°C heat stress in *E. coli* (19). It is hypothesized that the helicase activity unwinds the PTC that under high heat may take on non-productive conformations and that do not allow for

efficient peptide bond formation (191). This is supported by the structural information of HflX bound to the 50S ribosomal subunit with and without the ATP analog ADPNP (see *Chapters 3 and 4 for Ribosomal binding site and Section 1.12.4 – Second Nucleotide Binding site* sections). Furthermore, 50S ribosomal subunits washed with high salt, leading to a loss of some ribosomal proteins and more rRNA dynamics, stimulated HflX ATPase activity to a greater extent than 50S subunits washed with buffer, suggesting that damaged ribosomes may be the functional target for HflX (191). Whether HflX repairs the PTC, or other regions of the ribosome has yet to be determined. Interestingly, the helicase activity for repairing the PTC may have implications in the antibiotic resistance activity other groups have found HflX to possess (see *Section 1.12.7 – Role in Antibiotic Resistance* section). There are many unresolved questions regarding HflX's role in ribosome repair including: Can HflX repair both the 70S ribosome and/or just the 50S ribosomal subunit? What role does GTP-binding and hydrolysis play in ribosome repair? Is the PTC the target of HflX's helicase activity?

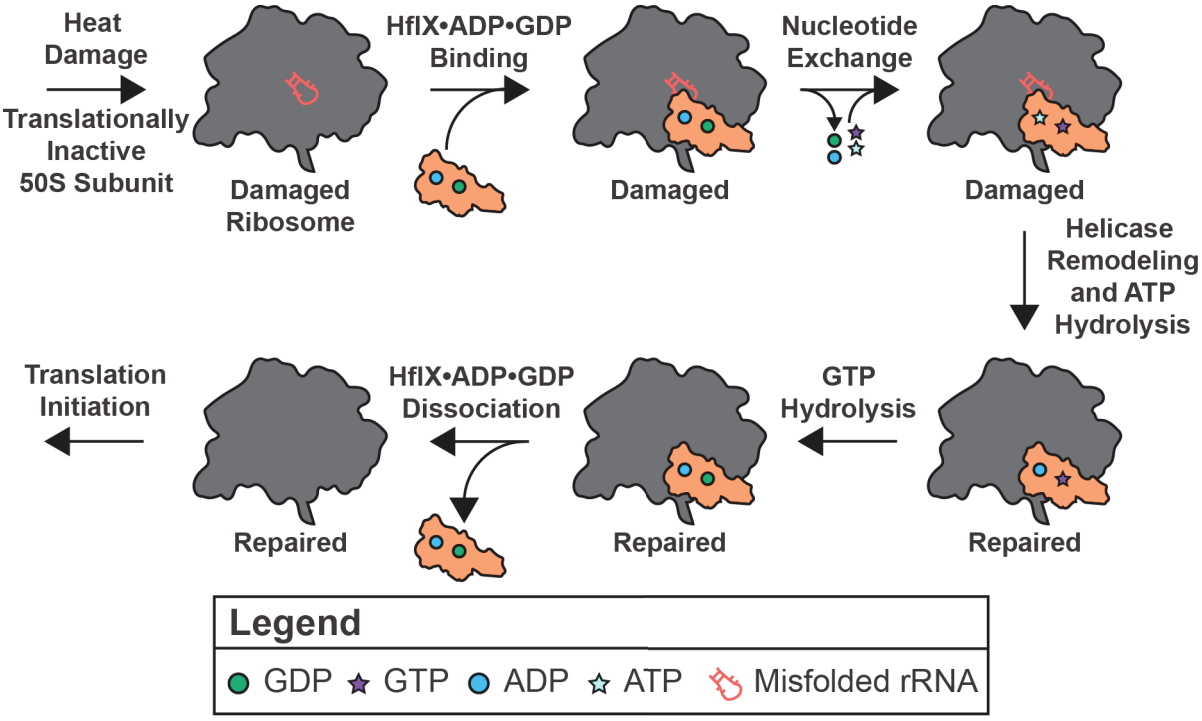

Figure 5.2 – Role of HflX in Ribosome Repair. Heat stress can cause local unwinding and refolding of the rRNA into non-productive structures that can affect translational fidelity or prevent synthesis by the improperly folded ribosome. HflX can act as an ATP-dependent helicase repairing heat damaged ribosomes. HflX•ATP•GDP binds to the A-site of a heat damaged 70S ribosome, or 50S ribosomal subunit (shown here) where it would be in proximity of several important functional centers of the ribosome including the peptidyl transferase center, decoding center (if repairing the 70S ribosome), and Sarcin-Ricin loop. Hydrolysis of ATP results in helicase unwinding of the rRNA allowing it to refold into its proper structure. At which point, GTP hydrolysis is proposed to occur and HflX•ADP•GDP dissociates from the repaired ribosomal particle. Based on model presented in Dey *et al*. (191).

Another role of HflX's helicase activity could be the disruption of the intersubunit bridges between the 50S and 30S ribosomal subunit during ribosome dissociation of either the 70S ribosome or 100S ribosome dimer, however this seems less likely as the 70S dissociation experiments (19, 140, 213) were carried out in the absence of ATP which is required for helicase activity. While the exact role RNA helicase activity plays in HflX's function is still unknown, it seems likely that it is important for HflX's function on the ribosome. Further studies will have to address what region(s) of the ribosomal RNA HflX is able to unwind and what functional implications this has on the ribosome. It is possible that HflX plays several functional roles on the ribosome depending on the cellular environment.

CHAPTER 6: SUMMARY

Protein synthesis is a complex process that has evolved numerous factors and pathways to mediate issues that can arise from a range of environmental stresses. Errors in protein synthesis can lead to damaged or incorrectly translated proteins that need to be degraded constituting a waste of energy, which if occurs too frequently can be detrimental to the cell. Aside from the canonical translation factors that are involved in the core stages of the ribosome cycle (Figure 1.2) there is a growing pool of alternative translation factors involved in different ribosome-related processes. These processes include, but are not limited to, ribosome biogenesis (e.g. RbbA, RsgA, etc.), translation of difficult proteins (e.g. EF-P), detecting cellular stress such as nutrient starvation (e.g. RelA), throttling of translation (e.g. EttA), protection of ribosomes during cellular dormancy (e.g. HPF and RMF), and alleviating stalled translation on damaged mRNAs (e.g. tmRNA, ArfA, and ArfB). The aim of this thesis was to further our understanding of two ribosome-associated factors, HflX and YchF. Both HflX and YchF are members of the GTPase superfamily and are present in all domains of life suggesting that their functional roles provide an advantage to the cell compared to their absence.

YchF is unique within the GTPase superfamily having an altered nucleotide binding motif that allows YchF to bind to and utilize ATP over GTP. Here we show for the first time that YchF forms a ternary complex with tRNA and nucleotide (YchF•tRNA•ATP) like that formed by EF-Tu during the delivery of aminoacylated tRNAs to ribosome (see *Section 1.6 – Translation elongation in bacteria*). The functional implications of YchF ternary complexes remains to be determined, but we propose it is tied to positioning YchF on the 70S ribosome. Through docking studies based on a structurally similar ribosome binding protein RelA, and chemical modification assays analyzed by primer extension, we were able to show for the first time that YchF binds to the ribosomal A-site. More recently, cryo-EM structural models of the YchF homolog in Plasmodium bound to the eukaryotic 80S ribosome confirmed YchF binds the A-site in eukaryotes as well (personal communication with Drs Alexey Amunts and Yuruzu Itoh). Finally, data presented here show that YchF provides a fitness advantage to *E. coli* cells grown at reduced temperatures and that YchF

acts as a nucleotide-independent RNA chaperone. Taken together our work has led to the proposal of a mechanism by which the YchF ternary complex binds to a “damaged” or “improperly produced” 70S ribosome that has a key segment of the rRNA folded improperly. The YchF ternary complex positions YchF onto the ribosome near the Sarcin-Ricin loop (SRL) which is crucial for protein synthesis, suggesting that this might be the functional region of the rRNA that YchF unwinds with its RNA chaperone activity, repairing the ribosome such that it can continue to be used in protein synthesis instead of being degraded.

HflX on the other hand is a GTPase that our lab and the Gao lab independently have shown to be able to dissociate the 70S ribosome into 50S and 30S ribosomal subunits (Chapter 3 (213) and (19)). This ribosome dissociation activity is like that of the EF-G/RRF-mediated ribosome recycling (see *Section 1.8 – Ribosome recycling in bacteria*) including that aminoglycoside antibiotics that prevent EF-G/RRF disruption of intersubunit bridge B2a also prevent HflX-mediated ribosome dissociation. This is the first mechanistic evidence that HflX disrupts intersubunit bridge B2a to facilitate dissociation of the ribosome. Furthermore, covalent crosslinking and binding site competition assays have shown that HflX binds to the E-site of the bacterial ribosome in addition to the A-site. Binding to the E-site allows HflX to act upon stalled 70S translation complexes even if the A-site is blocked by other translation factors or tRNAs. We propose that HflX dissociates stalled translation complexes to prevent the sequestration of multiple ribosomes translating the same mRNA downstream of the stalled ribosome. The dissociated ribosomal subunits are then free to be used in subsequent rounds of translation allowing the cell to overcome cellular stresses that inhibit translation. Intriguingly, studies have shown HflX as a novel antibiotic resistance mechanism in several bacterial species through dissociation of antibiotic stalled translation complexes (201, 231). *In vivo* studies done in our lab have shown that *E. coli* HflX also confers antibiotic tolerance to a range of ribosome targeting antibiotics aside from the aminoglycosides. Furthermore, work in this thesis has shown that HflX is able to dissociate antibiotic bound 70S ribosomes and can do so from the ribosomal E-site. We propose that HflX-mediate antibiotic resistance comes from its ability to dissociate stalled ribosomes and prevent sequestration of non-stalled ribosomes translating the same mRNA. Furthermore, dissociation of the subunits allows other enzymes to access the

antibiotic binding sites and remove the antibiotic, however, if these enzymes aren't present alongside HflX, HflX is still able to provide a base level fitness advantage under low antibiotic stress.

In conclusion, the work presented here in this thesis provides the first proposed functional role for YchF on the ribosome repairing an important improperly folded region of the rRNA. While work on HflX has brought to light the ability for HflX to bind to the ribosomal E-site and how mechanistically HflX is able to dissociate the 70S ribosome. Both facts help support a functional role in which HflX can relieve stalled translation, such as antibiotic stress on the cell. Overall, these results and proposed models provide the basis for future studies into the function both HflX and YchF.

REFERENCES

1. Balasingam N, Brandon HE, Ross JA, Wieden HJ, & Thakor N (2020) Cellular roles of the human Obg-like ATPase 1 (hOLA1) and its YchF homologs. *Biochemistry and Cell Biology* 98(1):1-11.

2. Kubitschek HE (1969) Growth during the bacterial cell cycle: analysis of cell size distribution. *Biophys J* 9(6):792-809.

3. Bakshi S, Siryaporn A, Goulian M, & Weisshaar JC (2012) Superresolution imaging of ribosomes and RNA polymerase in live Escherichia coli cells. *Molecular Microbiology* 85(1):21-38.

4. Mills EW & Green R (2017) Ribosomopathies: There's strength in numbers. *Science (New York, N.Y.)* 358(6363).

5. Farley-Barnes KI, Ogawa LM, & Baserga SJ (2019) Ribosomopathies: Old Concepts, New Controversies. *Trends in Genetics* 35(10):754-767.

6. Sulima SO, Kampen KR, & De Keersmaecker K (2019) Cancer Biogenesis in Ribosomopathies. *Cells* 8(3).

7. Teng T, Thomas G, & Mercer CA (2013) Growth control and ribosomopathies. *Current Opinion in Genetics & Development* 23(1):63-71.

8. Arenz S & Wilson DN (2016) Bacterial Protein Synthesis as a Target for Antibiotic Inhibition. *Cold Spring Harbor Perspectives in Medicine* 6(9).

9. Noller HF, Hoffarth V, & Zimniak L (1992) Unusual resistance of peptidyl transferase to protein extraction procedures. *Science (New York, N.Y.)* 256(5062):1416-1419.

10. Wower J*, et al.* (1995) Peptidyl transferase and beyond. *Biochemistry and Cell Biology* 73(11-12):1041-1047.

11. Leipe DD, Wolf YI, Koonin EV, & Aravind L (2002) Classification and evolution of P-loop GTPases and related ATPases. *Journal of molecular biology* 317(1):41-72.

12. Caldon CE & March PE (2003) Function of the universally conserved bacterial GTPases. *Current opinion in microbiology* 6(2):135-139.

13. Rodnina MV, Savelsbergh A, Katunin VI, & Wintermeyer W (1997) Hydrolysis of GTP by elongation factor G drives tRNA movement on the ribosome. *Nature* 385(6611):37-41.

14. Rodnina MV, Peske F, Peng BZ, Belardinelli R, & Wintermeyer W (2020) Converting GTP hydrolysis into motion: versatile translational elongation factor G. *Biological Chemistry* 401(1):131-142.

15. Rodnina MV (2018) Translation in Prokaryotes. *Cold Spring Harbor Perspectives in Biology* 10(9).

16. Bourne HR (1995) GTPases - A family of molecular switches and clocks. *Philosophical Transactions of the Royal Society B-Biological Sciences* 349(1329):283-289.

17. Vetter IR & Wittinghofer A (2001) Signal transduction - The guanine nucleotide-binding switch in three dimensions. *Science (New York, N.Y.)* 294(5545):1299-1304.

18. Zhou J, Lancaster L, Donohue JP, & Noller HF (2013) Crystal structures of EF-G-ribosome complexes trapped in intermediate states of translocation. *Science (New York, N.Y.)* 340(6140):1236086.

19. Zhang Y*, et al.* (2015) HflX is a ribosome-splitting factor rescuing stalled ribosomes under stress conditions. *Nat Struct Mol Biol* 22(11):906-913.

20. Teplyakov A*, et al.* (2003) Crystal structure of the YchF protein reveals binding sites for GTP and nucleic acid. *Journal of Bacteriology* 185(14):4031-4037.

21. Sprink T*, et al.* (2016) Structures of ribosome-bound initiation factor 2 reveal the mechanism of subunit association. *Science Advances* 2(3).

22. Fislage M*, et al.* (2018) Cryo-EM shows stages of initial codon selection on the ribosome by aa-tRNA in ternary complex with GTP and the GTPase-deficient EF-Tu(H84A). *Nucleic Acids Research* 46(11):5861-5874.

23. Graf M*, et al.* (2018) Visualization of translation termination intermediates trapped by the Apidaecin 137 peptide during RF3-mediated recycling of RF1. *Nature Communications* 9.

24. Zhang D*, et al.* (2016) EF4 disengages the peptidyl-tRNA CCA end and facilitates back-translocation on the 70S ribosome. *Nat Struct Mol Biol* 23(2):125-131.

25. Sprang SR (1997) G protein mechanisms: Insights from structural analysis. *Annual Review of Biochemistry* 66:639-678.

26. Anand B, Majumdar S, & Prakash B (2013) Structural Basis Unifying Diverse GTP Hydrolysis Mechanisms. *Biochemistry* 52(6):1122-1130.

27. Mishra R, Gara SK, Mishra S, & Prakash B (2005) Analysis of GTPases carrying hydrophobic amino acid substitutions in lieu of the catalytic glutamine: Implications for GTP hydrolysis. *Proteins-Structure Function and Bioinformatics* 59(2):332-338.

28. Paduch M, Jeleń F, & Otlewski J (2001) Structure of small G proteins and their regulators. *Acta biochimica Polonica* 48(4):829-850.

29. Bourne HR, Sanders DA, & McCormick F (1991) The GTPase superfamily: conserved structure and molecular mechanism. *Nature* 349(6305):117-127.

30. Shields MJ, Fischer JJ, & Wieden H-J (2009) Toward Understanding the Function of the Universally Conserved GTPase HflX from *Escherichia coli*: A Kinetic Approach. *Biochemistry* 48(45):10793-10802.

31. Becker M*, et al.* (2012) The 70S ribosome modulates the ATPase activity of Escherichia coli YchF. *RNA biology* 9(10):1288-1301.

32. Clementi N & Polacek N (2010) Ribosome-associated GTPases The role of RNA for GTPase activation. *Rna Biology* 7(5):521-527.

33. Peluso P, Shan SO, Nock S, Herschlag D, & Walter P (2001) Role of SRP RNA in the GTPase cycles of ffh and FtsY. *Biochemistry* 40(50):15224-15233.

34. Endo Y, Mitsui K, Motizuki M, & Tsurugi K (1987) The mechanism of action of ricin and related toxic lectins on eukaryotic ribosomes. The site and the characteristics of the modification in 28 S ribosomal RNA caused by the toxins. *J Biol Chem* 262(12):5908-5912.

35. Endo Y & Wool IG (1982) The site of action of alpha-sarcin on eukaryotic ribosomes - The sequence at the alpha-sarcin cleavage site in 28S-ribosomal ribonucleic acid. *Journal of Biological Chemistry* 257(15):9054-9060.

36. Hausner T-P, Atmadja J, & Nierhaus KH (1987) Evidence that the G2661 region of 23S rRNA is located at the ribosomal binding sites of both elongation factors. *Biochimie* 69(9):911-923.

37. Forchhammer K, Rucknagel KP, & Boeck A (1990) Purification and Biochemical Characterization of SelB, a Translation factor involved in Selenoprotein synthesis. *Journal of Biological Chemistry* 265(16):9346-9350.

38. Fischer N*, et al.* (2016) The pathway to GTPase activation of elongation factor SelB on the ribosome. *Nature* 540(7631):80-85.

39. Mercier E, Holtkamp W, Rodnina MV, & Wintermeyer W (2017) Signal recognition particle binds to translating ribosomes before emergence of a signal anchor sequence. *Nucleic Acids Research* 45(20):11858-11866.

40. Doudna JA & Batey RT (2004) Structural insights into the signal recognition particle. *Annual Review of Biochemistry* 73:539-557.

41. Heller JLE, Kamalampeta R, & Wieden H-J (2017) Taking a Step Back from Back-Translocation: an Integrative View of LepA/EF4's Cellular Function. *Molecular and Cellular Biology* 37(12).

42. Verstraeten N, Fauvart M, Versees W, & Michiels J (2011) The universally conserved prokaryotic GTPases. *Microbiol Mol Biol Rev* 75(3):507-542, second and third pages of table of contents.

43. Britton RA (2009) Role of GTPases in Bacterial Ribosome Assembly. *Annual Review of Microbiology* 63:155-176.

44. Choi E, Jeon H, Oh JI, & Hwang J (2019) Overexpressed L20 Rescues 50S Ribosomal Subunit Assembly Defects of bipA-Deletion in Escherichia coli. *Frontiers in microbiology* 10:2982.

45. Ni XD*, et al.* (2016) YphC and YsxC GTPases assist the maturation of the central protuberance, GTPase associated region and functional core of the 50S ribosomal subunit. *Nucleic Acids Research* 44(17):8442-8455.

46. Fislage M, Wauters L, & Versees W (2016) MnmE, a GTPase That Drives a Complex tRNA Modification Reaction. *Biopolymers* 105(8):568-579.

47. Prado S, Villarroya M, Medina M, & Armengod ME (2013) The tRNA-modifying function of MnmE is controlled by post-hydrolysis steps of its GTPase cycle. *Nucleic Acids Research* 41(12):6190-6208.

48. Davis JH & Williamson JR (2017) Structure and dynamics of bacterial ribosome biogenesis. *Philos Trans R Soc Lond B Biol Sci* 372(1716).

49. Shajani Z, Sykes MT, & Williamson JR (2011) Assembly of Bacterial Ribosomes. *Annual Review of Biochemistry, Vol 80,* Annual Review of Biochemistry, eds Kornberg RD, Raetz CRH, Rothman JE, & Thorner JW), Vol 80, pp 501-526.

50. Gibbs MR & Fredrick K (2018) Roles of elusive translational GTPases come to light and inform on the process of ribosome biogenesis in bacteria. *Molecular Microbiology* 107(4):445-454.

51. Connolly K, Rife JP, & Culver G (2008) Mechanistic insight into the ribosome biogenesis functions of the ancient protein KsgA. *Molecular Microbiology* 70(5):1062-1075.

52. Shetty S & Varshney U (2016) An evolutionarily conserved element in initiator tRNAs prompts ultimate steps in ribosome maturation. *Proceedings of the National Academy of Sciences of the United States of America* 113(41):E6126-E6134.

53. Gibbs MR*, et al.* (2017) Conserved GTPase LepA (Elongation Factor 4) functions in biogenesis of the 30S subunit of the 70S ribosome. *Proceedings of the National Academy of Sciences of the United States of America* 114(5):980-985.

54. Karbstein K (2013) Quality control mechanisms during ribosome maturation. *Trends in Cell Biology* 23(5):242-250.

55. Strunk BS, Novak MN, Young CL, & Karbstein K (2012) A Translation-Like Cycle Is a Quality Control Checkpoint for Maturing 40S Ribosome Subunits. *Cell* 150(1):111-121.

56. Milon P, Maracci C, Filonava L, Gualerzi CO, & Rodnina MV (2012) Real-time assembly landscape of bacterial 30S translation initiation complex. *Nat Struct Mol Biol* 19(6):609-615.

57. Laursen BS, Sorensen HP, Mortensen KK, & Sperling-Petersen HU (2005) Initiation of protein synthesis in bacteria. *Microbiol Mol Biol Rev* 69(1):101-123.

58. Kudla G, Murray AW, Tollervey D, & Plotkin JB (2009) Coding-Sequence Determinants of Gene Expression in Escherichia coli. *Science (New York, N.Y.)* 324(5924):255-258.

59. Lopez-Alonso JP*, et al.* (2017) Structure of a 30S pre-initiation complex stalled by GE81112 reveals structural parallels in bacterial and eukaryotic protein synthesis initiation pathways. *Nucleic Acids Research* 45(4):2179-2187.

60. Beck HJ & Janssen GR (2017) Novel Translation Initiation Regulation Mechanism in Escherichia coli ptrB Mediated by a 5 '-Terminal AUG. *Journal of Bacteriology* 199(14).

61. Mitchell SF & Parker R (2015) Modifications on Translation Initiation. *Cell* 163(4):796-798.

62. Vigar JRJ & Wieden HJ (2017) Engineering bacterial translation initiation - Do we have all the tools we need? *Biochimica Et Biophysica Acta-General Subjects* 1861(11):3060-3069.

63. Reeve B, Hargest T, Gilbert C, & Ellis T (2014) Predicting translation initiation rates for designing synthetic biology. *Frontiers in bioengineering and biotechnology* 2:1.

64. Nilsson J & Nissen P (2005) Elongation factors on the ribosome. *Current Opinion in Structural Biology* 15(3):349-354.

65. Pang YLJ, Poruri K, & Martinis SA (2014) tRNA synthetase: tRNA aminoacylation and beyond. *Wiley Interdisciplinary Reviews-Rna* 5(4):461-480.

66. Schmeing TM*, et al.* (2009) The Crystal Structure of the Ribosome Bound to EF-Tu and Aminoacyl-tRNA. *Science (New York, N.Y.)* 326(5953):688-694.

67. Gromadski KB, Wieden HJ, & Rodnina MV (2002) Kinetic mechanism of elongation factor Ts-catalyzed nucleotide exchange in elongation factor Tu. *Biochemistry* 41(1):162-169.

68. Cai YC, Bullard JM, Thompson NL, & Spremulli LL (2000) Interaction of mitochondrial elongation factor Tu with aminoacyl-tRNA and elongation factor Ts. *Journal of Biological Chemistry* 275(27):20308-20314.

69. Kothe U, Wieden HJ, Mohr D, & Rodnina MV (2004) Interaction of helix D of elongation factor Tu with helices 4 and 5 of protein L7/12 on the ribosome. *Journal of Molecular Biology* 336(5):1011-1021.

70. Diaconu M*, et al.* (2005) Structural basis for the function of the ribosomal L7/12 stalk in factor binding and GTPase activation. *Cell* 121(7):991-1004.

71. Ogle JM*, et al.* (2001) Recognition of cognate transfer RNA by the 30S ribosomal subunit. *Science (New York, N.Y.)* 292(5518):897-902.

72. Fischer N*, et al.* (2015) Structure of the E. coli ribosome-EF-Tu complex at <3 A resolution by Cs-corrected cryo-EM. *Nature* 520(7548):567-570.

73. Geggier P*, et al.* (2010) Conformational Sampling of Aminoacyl-tRNA during Selection on the Bacterial Ribosome. *Journal of Molecular Biology* 399(4):576-595.

74. Adio S*, et al.* (2015) Fluctuations between multiple EF-G-induced chimeric tRNA states during translocation on the ribosome. *Nat Commun* 6:7442.

75. Belardinelli R*, et al.* (2016) Choreography of molecular movements during ribosome progression along mRNA. *Nature Structural & Molecular Biology* 23(4):342-348.

76. Adio S*, et al.* (2018) Dynamics of ribosomes and release factors during translation termination in E. coli. *Elife* 7.

77. Korostelev AA (2011) Structural aspects of translation termination on the ribosome. *Rna* 17(8):1409-1421.

78. Svidritskiy E, Demo G, Loveland AB, Xu C, & Korostelev AA (2019) Extensive ribosome and RF2 rearrangements during translation termination. *Elife* 8.

79. Grentzmann G, Brechemier-Baey D, Heurgue V, Mora L, & Buckingham RH (1994) Localization and characterization of the gene encoding release factor RF3 in Escherichia coli. *Proc Natl Acad Sci U S A* 91(13):5848-5852.

80. Zavialov AV, Buckingham RH, & Ehrenberg M (2001) A posttermination ribosomal complex is the guanine nucleotide exchange factor for peptide release factor RF3. *Cell* 107(1):115-124.

81. Peske F, Kuhlenkoetter S, Rodnina MV, & Wintermeyer W (2014) Timing of GTP binding and hydrolysis by translation termination factor RF3. *Nucleic Acids Research* 42(3):1812-1820.

82. Gao N, Zavialov AV, Ehrenberg M, & Frank J (2007) Specific interaction between EF-G and RRF and its implication for GTP-dependent ribosome splitting into subunits. *Journal of Molecular Biology* 374(5):1345-1358.

83. Gao N*, et al.* (2005) Mechanism for the disassembly of the posttermination complex inferred from cryo-EM studies. *Molecular Cell* 18(6):663-674.

84. Borg A, Pavlov M, & Ehrenberg M (2016) Complete kinetic mechanism for recycling of the bacterial ribosome. *Rna* 22(1):10-21.

85. Peske F, Rodnina MV, & Wintermeyer W (2005) Sequence of steps in ribosome recycling as defined by kinetic analysis. *Molecular Cell* 18(4):403-412.

86. Zavialov AV, Hauryliuk VV, & Ehrenberg M (2005) Splitting of the posttermination ribosome into subunits by the concerted action of RRF and EF-G. *Molecular Cell* 18(6):675-686.

87. Fu Z*, et al.* (2016) Key Intermediates in Ribosome Recycling Visualized by Time-Resolved Cryoelectron Microscopy. *Structure* 24(12):2092-2101.

88. Yokoyama T*, et al.* (2012) Structural insights into initial and intermediate steps of the ribosome-recycling process. *Embo Journal* 31(7):1836-1846.

89. Liu Q & Fredrick K (2016) Intersubunit Bridges of the Bacterial Ribosome. *Journal of Molecular Biology* 428(10):2146-2164.

90. Savelsbergh A, Rodnina MV, & Wintermeyer W (2009) Distinct functions of elongation factor G in ribosome recycling and translocation. *Rna* 15(5):772-780.

91. Chen Y, Kaji A, Kaji H, & Cooperman BS (2017) The kinetic mechanism of bacterial ribosome recycling. *Nucleic Acids Research* 45(17):10168-10177.

92. Seshadri A & Varshney U (2006) Mechanism of recycling of post-termination ribosomal complexes in eubacteria: a new role of initiation factor 3. *Journal of Biosciences* 31(2):281-289.

93. Hirokawa G*, et al.* (2005) The role of ribosome recycling factor in dissociation of 70S ribosomes into subunits. *Rna* 11(8):1317-1328.

94. Prabhakar A, Capece MC, Petrov A, Choi J, & Puglisi JD (2017) Post-termination Ribosome Intermediate Acts as the Gateway to Ribosome Recycling. *Cell Reports* 20(1):161-172.

95. Giudice E & Gillet R (2013) The task force that rescues stalled ribosomes in bacteria. *Trends in Biochemical Sciences* 38(8):403-411.

96. Himeno H, Nameki N, Kurita D, Muto A, & Abo T (2015) Ribosome rescue systems in bacteria. *Biochimie* 114:102-112.

97. Neubauer C, Gillet R, Kelley AC, & Ramakrishnan V (2012) Decoding in the Absence of a Codon by tmRNA and SmpB in the Ribosome. *Science (New York, N.Y.)* 335(6074):1366-1369.

98. Rae CD, Gordiyenko Y, & Ramakrishnan V (2019) How a circularized tmRNA moves through the ribosome. *Science (New York, N.Y.)* 363(6428):740-744.

99. Weis F*, et al.* (2010) tmRNA-SmpB: a journey to the centre of the bacterial ribosome. *Embo Journal* 29(22):3810-3818.

100. Moore SD & Sauer RT (2007) The tmRNA system for translational surveillance and ribosome rescue. *Annual Review of Biochemistry* 76:101-124.

101. Sundermeier TR, Dulebohn DP, Cho HJ, & Karzai AW (2005) A previously uncharacterized role for small protein B (SmpB) in transfer messenger RNA-mediated trans-translation. *Proceedings of the National Academy of Sciences of the United States of America* 102(7):2316-2321.

102. Fu J*, et al.* (2010) Visualizing the transfer-messenger RNA as the ribosome resumes translation. *Embo Journal* 29(22):3819-3825.

103. Ramrath DJF*, et al.* (2012) The complex of tmRNA-SmpB and EF-G on translocating ribosomes. *Nature* 485(7399):526-U140.

104. Chadani Y, Ito K, Kutsukake K, & Abo T (2012) ArfA recruits release factor 2 to rescue stalled ribosomes by peptidyl-tRNA hydrolysis in Escherichia coli. *Molecular Microbiology* 86(1):37-50.

105. Chadani Y, Ono K, Kutsukake K, & Abo T (2011) Escherichia coli YaeJ protein mediates a novel ribosome-rescue pathway distinct from SsrA- and ArfA-mediated pathways. *Molecular Microbiology* 80(3):772-785.

106. Chadani Y*, et al.* (2010) Ribosome rescue by Escherichia coli ArfA (YhdL) in the absence of trans-translation system. *Molecular Microbiology* 78(4):796-808.

107. Goralski TDP, Kirimanjeswara GS, & Keiler KC (2018) A New Mechanism for Ribosome Rescue Can Recruit RF1 or RF2 to Nonstop Ribosomes. *Mbio* 9(6).

108. Shimokawa-Chiba N*, et al.* (2019) ResQ, a release factor-dependent ribosome rescue factor in the Gram-positive bacterium *Bacillus subtilis*. *bioRxiv*:732420.

109. Handa Y, Inaho N, & Nameki N (2011) YaeJ is a novel ribosome-associated protein in Escherichia coli that can hydrolyze peptidyl-tRNA on stalled ribosomes. *Nucleic Acids Research* 39(5):1739-1748.

110. Lytvynenko I*, et al.* (2019) Alanine Tails Signal Proteolysis in Bacterial Ribosome-Associated Quality Control. *Cell* 178(1):76-90 e22.

111. Huter P*, et al.* (2017) Structural basis for ArfA-RF2-mediated translation termination on mRNAs lacking stop codons. *Nature* 541(7638):546-549.

112. Demo G*, et al.* (2017) Mechanism of ribosome rescue by ArfA and RF2. *Elife* 6.

113. Ma C*, et al.* (2017) Mechanistic insights into the alternative translation termination by ArfA and RF2. *Nature* 541(7638):550-553.

114. Kurita D, Chadani Y, Muto A, Abo T, & Himeno H (2014) ArfA recognizes the lack of mRNA in the mRNA channel after RF2 binding for ribosome rescue. *Nucleic Acids Research* 42(21):13339-13352.

115. Goldman E & Jakubowski H (1990) Uncharged tRNA, protein synthesis, and the bacterial stringent response. *Mol Microbiol* 4(12):2035-2040.

116. Arenz S*, et al.* (2016) The stringent factor RelA adopts an open conformation on the ribosome to stimulate ppGpp synthesis. *Nucleic Acids Research* 44(13):6471-6481.

117. Winther KS, Roghanian M, & Gerdes K (2018) Activation of the Stringent Response by Loading of RelA-tRNA Complexes at the Ribosomal A-Site. *Mol Cell* 70(1):95-105 e104.

118. Loveland AB*, et al.* (2016) Ribosome center dot RelA structures reveal the mechanism of stringent response activation. *Elife* 5.

119. Haseltine WA & Block R (1973) Synthesis of guanosine tetra- and pentaphosphate requires the presence of a codon-specific, uncharged transfer ribonucleic acid in the acceptor site of ribosomes. *Proc Natl Acad Sci U S A* 70(5):1564-1568.

120. Haseltine WA, Block R, Gilbert W, & Weber K (1972) MSI and MSII made on ribosome in idling step of protein synthesis. *Nature* 238(5364):381-384.

121. Maisonneuve E & Gerdes K (2014) Molecular Mechanisms Underlying Bacterial Persisters. *Cell* 157(3):539-548.

122. Poole K (2012) Bacterial stress responses as determinants of antimicrobial resistance. *Journal of Antimicrobial Chemotherapy* 67(9):2069-2089.

123. Dalebroux ZD, Svensson SL, Gaynor EC, & Swanson MS (2010) ppGpp conjures bacterial virulence. *Microbiol Mol Biol Rev* 74(2):171-199.

124. Akiyama T*, et al.* (2017) Resuscitation of Pseudomonas aeruginosa from dormancy requires hibernation promoting factor (PA4463) for ribosome preservation. *Proceedings of the National Academy of Sciences of the United States of America* 114(12):3204-3209.

125. Kussell E, Kishony R, Balaban NQ, & Leibler S (2005) Bacterial persistence: A model of survival in changing environments. *Genetics* 169(4):1807-1814.

126. Kolter R, Siegele DA, & Tormo A (1993) The stationary phase of the bacterial life cycle. *Annual Review of Microbiology,* Annual Review of Microbiology, ed Ornston LN), Vol 47, pp 855-874.

127. Shimada T, Yoshida H, & Ishihama A (2013) Involvement of Cyclic AMP Receptor Protein in Regulation of the rmf Gene Encoding the Ribosome Modulation Factor in Escherichia coli. *Journal of Bacteriology* 195(10):2212-2219.

128. Song S & Wood TK (2020) ppGpp ribosome dimerization model for bacterial persister formation and resuscitation. *Biochem. Biophys. Res. Commun.* 523(2):281-286.

129. Gohara DW & Yap MF (2018) Survival of the drowsiest: the hibernating 100S ribosome in bacterial stress management. *Current genetics* 64(4):753-760.

130. Wada A, Igarashi K, Yoshimura S, Aimoto S, & Ishihama A (1995) Ribosome modulation factor: Stationary growth phase-specific inhibitor of ribosome functions from Escherichia coli. *Biochem. Biophys. Res. Commun.* 214(2):410-417.

131. Yamagishi M*, et al.* (1993) Regulation of the Escherichia coli rmf gene encoding the ribosome modulation factor: Growth phase- and growth rate-dependent control. *EMBO (European Molecular Biology Organization) Journal* 12(2):625-630.

132. Wei X & Zhang J (2018) On the Origin of Compositional Features of Ribosomes. *Genome Biology and Evolution* 10(8):2010-2016.

133. Strunk BS & Karbstein K (2009) Powering through ribosome assembly. *Rna* 15(12):2083-2104.

134. Maitra A & Dill KA (2015) Bacterial growth laws reflect the evolutionary importance of energy efficiency. *Proceedings of the National Academy of Sciences of the United States of America* 112(2):406-411.

135. Niess A, Siemann-Herzberg M, & Takors R (2019) Protein production in Escherichia coli is guided by the trade-off between intracellular substrate availability and energy cost. *Microbial Cell Factories* 18:8.

136. Wilson DN & Nierhaus KH (2007) The weird and wonderful world of bacterial ribosome regulation. *Critical Reviews in Biochemistry and Molecular Biology* 42(3):187-219.

137. Wada A, Yamazaki Y, Fujita N, & Ishihama A (1990) Structure and probable genetic location of a "ribosome modulation factor" associated with 100S ribosomes in stationary-phase Escherichia coli cells. *Proc Natl Acad Sci U S A* 87(7):2657-2661.

138. Polikanov YS, Blaha GM, & Steitz TA (2012) How Hibernation Factors RMF, HPF, and YfiA Turn Off Protein Synthesis. *Science (Washington D C)* 336(6083):915-918.

139. Basu A, Shields KE, & Yap M-NF (2020) The hibernating 100S complex is a target of ribosome-recycling factor and elongation factor G in Staphylococcus aureus. *Journal of Biological Chemistry* 295(18):6053-6063.

140. Basu A & Yap MN (2017) Disassembly of the Staphylococcus aureus hibernating 100S ribosome by an evolutionarily conserved GTPase. *Proc Natl Acad Sci U S A* 114(39):E8165-e8173.

141. Ueta M*, et al.* (2013) Conservation of two distinct types of 100S ribosome in bacteria. *Genes to Cells* 18(7):554-574.

142. Ueta M, Wada C, & Wada A (2010) Formation of 100S ribosomes in Staphylococcus aureus by the hibernation promoting factor homolog SaHPF. *Genes to Cells* 15(1):43-58.

143. Basu A & Yap M-NF (2016) Ribosome hibernation factor promotes Staphylococcal survival and differentially represses translation. *Nucleic Acids Research* 44(10):4881-4893.

144. Troesch R & Willmund F (2019) The conserved theme of ribosome hibernation: from bacteria to chloroplasts of plants. *Biological Chemistry* 400(7):879-893.

145. Beckert B*, et al.* (2018) Structure of a hibernating 100S ribosome reveals an inactive conformation of the ribosomal protein S1. *Nature Microbiology* 3(10):1115-1121.

146. Matzov D*, et al.* (2017) The cryo-EM structure of hibernating 100S ribosome dimer from pathogenic Staphylococcus aureus. *Nature Communications* 8:723.

147. Franken LE*, et al.* (2017) A general mechanism of ribosome dimerization revealed by single-particle cryo-electron microscopy. *Nature Communications* 8.

148. Beckert B*, et al.* (2017) Structure of the Bacillus subtilis hibernating 100S ribosome reveals the basis for 70S dimerization. *Embo Journal* 36(14):2061-2072.

149. Feaga HA, Kopylov M, Kim JK, Jovanovic M, & Dworkin J (2020) Ribosome Dimerization Protects the Small Subunit. *Journal of Bacteriology* 202(10):e0000-0020.

150. Kohler R, Mooney RA, Mills DJ, Landick R, & Cramer P (2017) Architecture of a transcribing-translating expressome. *Science (Washington D C)* 356(6334).

151. Maki Y, Yoshida H, & Wada A (2000) Two proteins, YfiA and YhbH, associated with resting ribosomes in stationary phase Escherichia coli. *Genes to Cells* 5(12):965-974.

152. Agafonov DE, Kolb VA, Nazimov IV, & Spirin AS (1999) A protein residing at the subunit interface of the bacterial ribosome. *Proceedings of the National Academy of Sciences of the United States of America* 96(22):12345-12349.

153. Puri P*, et al.* (2014) Lactococcus lactis YfiA is necessary and sufficient for ribosome dimerization. *Molecular Microbiology* 91(2):394-407.

154. Vila-Sanjurjo A, Schuwirth B-S, Hau CW, & Cate JHD (2004) Structural basis for the control of translation initiation during stress. *Nature Structural & Molecular Biology* 11(11):1054-1059.

155. Izutsu K, Wada A, & Wada C (2001) Expression of ribosome modulation factor (RMF) in Escherichia coli requires ppGpp. *Genes to Cells* 6(8):665-676.

156. Terui Y*, et al.* (2010) Ribosome Modulation Factor, an Important Protein for Cell Viability Encoded by the Polyamine Modulon. *Journal of Biological Chemistry* 285(37):28698-28707.

157. Tagami K*, et al.* (2012) Expression of a small (p)ppGpp synthetase, YwaC, in the (p)ppGpp(0) mutant of Bacillus subtilis triggers YvyD-dependent dimerization of ribosome. *MicrobiologyOpen* 1(2):115-134.

158. Krokowski D*, et al.* (2011) Characterization of hibernating ribosomes in mammalian cells. *Cell Cycle* 10(16):2691-2702.

159. Koller-Eichhorn R*, et al.* (2007) Human OLA1 defines an ATPase subfamily in the Obg family of GTP-binding proteins. *The Journal of biological chemistry* 282(27):19928-19937.

160. Gradia DF*, et al.* (2009) Characterization of a novel Obg-like ATPase in the protozoan Trypanosoma cruzi. *International journal for parasitology* 39(1):49-58.

161. Cheung MY*, et al.* (2016) ATP binding by the P-loop NTPase OsYchF1 (an unconventional G protein) contributes to biotic but not abiotic stress responses. *Proc Natl Acad Sci U S A* 113(10):2648-2653.

162. Teplyakov A*, et al.* (2003) Crystal structure of the YchF protein reveals binding sites for GTP and nucleic acid. *J Bacteriol* 185(14):4031-4037.

163. Rosler KS, Mercier E, Andrews IC, & Wieden HJ (2015) Histidine 114 Is Critical for ATP Hydrolysis by the Universally Conserved ATPase YchF. *J Biol Chem* 290(30):18650-18661.

164. Leipe DD, Wolf YI, Koonin EV, & Aravind L (2002) Classification and evolution of P-loop GTPases and related ATPases. *Journal of Molecular Biology* 317(1):41-72.

165. Cheung MY, Li MW, Yung YL, Wen CQ, & Lam HM (2013) The unconventional P-loop NTPase OsYchF1 and its regulator OsGAP1 play opposite roles in salinity stress tolerance. *Plant Cell Environ* 36(11):2008-2020.

166. Tomar SK, Kumar P, & Prakash B (2011) Deciphering the catalytic machinery in a universally conserved ribosome binding ATPase YchF. *Biochem Biophys Res Commun* 408(3):459-464.

167. Danese I*, et al.* (2004) The Ton system, an ABC transporter, and a universally conserved GTPase are involved in iron utilization by Brucella melitensis 16M. *Infect Immun* 72(10):5783-5790.

168. Hannemann L*, et al.* (2016) Redox Activation of the Universally Conserved ATPase YchF by Thioredoxin 1. *Antioxid Redox Signal* 24(3):141-156.

169. Zhang JW, Rubio V, Zheng S, & Shi ZZ (2009) Knockdown of OLA1, a regulator of oxidative stress response, inhibits motility and invasion of breast cancer cells. *J Zhejiang Univ Sci B* 10(11):796-804.

170. Chen H*, et al.* (2015) OLA1 regulates protein synthesis and integrated stress response by inhibiting eIF2 ternary complex formation. *Scientific reports* 5:13241.

171. Wenk M*, et al.* (2012) A universally conserved ATPase regulates the oxidative stress response in Escherichia coli. *J Biol Chem* 287(52):43585-43598.

172. Zhang J, Rubio V, Lieberman MW, & Shi Z-Z (2009) OLA1, an Obg-like ATPase, suppresses antioxidant response via nontranscriptional mechanisms. *Proceedings of the National Academy of Sciences of the United States of America* 106(36):15356-15361.

173. Akhova AV & Tkachenko AG (2014) ATP/ADP alteration as a sign of the oxidative stress development in Escherichia coli cells under antibiotic treatment. *Fems Microbiology Letters* 353(1):69-76.

174. Becker M*, et al.* (2012) The 70S ribosome modulates the ATPase activity of Escherichia coli YchF. *RNA Biology* 9(10):1288-1301.

175. Olinares PDB, Ponnala L, & van Wijk KJ (2010) Megadalton Complexes in the Chloroplast Stroma of Arabidopsis thaliana Characterized by Size Exclusion Chromatography, Mass Spectrometry, and Hierarchical Clustering. *Molecular & Cellular Proteomics* 9(7):1594-1615.

176. Tomar SK, Kumar P, & Prakash B (2011) Deciphering the catalytic machinery in a universally conserved ribosome binding ATPase YchF. *Biochem. Biophys. Res. Commun.* 408(3):459-464.

177. Guerrero C, Tagwerker C, Kaiser P, & Huang L (2006) An integrated mass spectrometry-based proteomic approach: quantitative analysis of tandem affinity-purified in vivo cross-

linked protein complexes (QTAX) to decipher the 26 S proteasome-interacting network. *Molecular & cellular proteomics : MCP* 5(2):366-378.

178. Hirano Y, Ohniwa RL, Wada C, Yoshimura SH, & Takeyasu K (2006) Human small G proteins, ObgH1, and ObgH2, participate in the maintenance of mitochondria and nucleolar architectures. *Genes to Cells* 11(11):1295-1304.

179. Adekambi T*, et al.* (2011) Core gene set as the basis of multilocus sequence analysis of the subclass Actinobacteridae. *PLoS One* 6(3):e14792.

180. Xu D*, et al.* (2016) Obg-like ATPase 1 regulates global protein serine/threonine phosphorylation in cancer cells by suppressing the GSK3beta-inhibitor 2-PP1 positive feedback loop. *Oncotarget* 7(3):3427-3439.

181. Zhang J, Rubio V, Lieberman MW, & Shi ZZ (2009) OLA1, an Obg-like ATPase, suppresses antioxidant response via nontranscriptional mechanisms. *Proc Natl Acad Sci U S A* 106(36):15356-15361.

182. Ding Z*, et al.* (2016) OLA1, a Translational Regulator of p21, Maintains Optimal Cell Proliferation Necessary for Developmental Progression. *Mol Cell Biol* 36(20):2568-2582.

183. Mao RF*, et al.* (2013) OLA1 protects cells in heat shock by stabilizing HSP70. *Cell Death Dis* 4:e491.

184. Sun H*, et al.* (2010) DOC45, a novel DNA damage-regulated nucleocytoplasmic ATPase that is overexpressed in multiple human malignancies. *Molecular cancer research : MCR* 8(1):57-66.

185. Jeyabal PV, Rubio V, Chen H, Zhang J, & Shi ZZ (2014) Regulation of cell-matrix adhesion by OLA1, the Obg-like ATPase 1. *Biochem Biophys Res Commun* 444(4):568-574.

186. Bai L*, et al.* (2016) OLA1 contributes to epithelial-mesenchymal transition in lung cancer by modulating the GSK3beta/snail/E-cadherin signaling. *Oncotarget* 7(9):10402-10413.

187. Chiba N (2015) [BRCA1-interacting protein OLA1 functions in the maintenance of genome integrity by centrosome regulation]. *Seikagaku* 87(6):741-743.

188. Wu H*, et al.* (2010) Structure of the ribosome associating GTPase HflX. *Proteins-Structure Function and Bioinformatics* 78(3):705-713.

189. Jain N, Vithani N, Rafay A, & Prakash B (2013) Identification and characterization of a hitherto unknown nucleotide-binding domain and an intricate interdomain regulation in HflX-a ribosome binding GTPase. *Nucleic Acids Research* 41(20):9557-9569.

190. Ghosh A, Dutta D, Bandyopadhyay K, & Parrack P (2016) Characterization of the autophosphorylation property of HflX, a ribosome-binding GTPase from Escherichia coli. *FEBS open bio* 6(7):651-659.

191. Dey S, Biswas C, & Sengupta J (2018) The universally conserved GTPase HflX is an RNA helicase that restores heat-damaged Escherichia coli ribosomes. *Journal of Cell Biology* 217(7):2519-2529.

192. Srinivasan K, Dey S, & Sengupta J (2019) Structural modules of the stress-induced protein HflX: an outlook on its evolution and biological role. *Current genetics* 65(2):363-370.

193. Huang B*, et al.* (2010) Functional study on GTP hydrolysis by the GTP-binding protein from Sulfolobus solfataricus, a member of the HflX family. *Journal of Biochemistry* 148(1):103-113.

194. Noble JA*, et al.* (1993) The *Escherichia coli hflA* locus encodes a putative GTP-binding protein and 2 membrane-proteins, one of which contains a protease-like domain. *Proceedings of the National Academy of Sciences of the United States of America* 90(22):10866-10870.

195. Dutta D, Bandyopadhyay K, Datta AB, Sardesai AA, & Parrack P (2009) Properties of HflX, an Enigmatic Protein from *Escherichia coli*. *Journal of Bacteriology* 191(7):2307-2314.

196. Torres-Quesada O*, et al.* (2010) The Sinorhizobium meliloti RNA chaperone Hfq influences central carbon metabolism and the symbiotic interaction with alfalfa. *Bmc Microbiology* 10.

197. Chuang SE & Blattner FR (1993) Characterization of twenty-six new heat shock genes of Escherichia coli. *J Bacteriol* 175(16):5242-5252.

198. Tsui HC & Winkler ME (1994) Transcriptional patterns of the mutL-miaA superoperon of Escherichia coli K-12 suggest a model for posttranscriptional regulation. *Biochimie* 76(12):1168-1177.

199. Tsui HCT, Feng G, & Winkler ME (1996) Transcription of the *mutL* repair, *miaA* tRNA modification, *hfq* pleiotropic regulator, and *hflA* region protease genes of *Escherichia coli* K-12 from clustered E sigma(32)-specific promoters during heat shock. *Journal of Bacteriology* 178(19):5719-5731.

200. McQuillan JS & Shaw AM (2014) Differential gene regulation in the Ag nanoparticle and Ag+-induced silver stress response in Escherichia coli: A full transcriptomic profile. *Nanotoxicology* 8(Suppl. 1):177-184.

201. Duval M*, et al.* (2018) HflXr, a homolog of a ribosome-splitting factor, mediates antibiotic resistance. *Proceedings of the National Academy of Sciences of the United States of America* 115(52):13359-13364.

202. Jain N*, et al.* (2009) *E. coli* HflX interacts with 50S ribosomal subunits in presence of nucleotides. *Biochem. Biophys. Res. Commun.* 379(2):201-205.

203. Fischer JJ*, et al.* (2012) The ribosome modulates the structural dynamics of the conserved GTPase HflX and triggers tight nucleotide binding. *Biochimie* 94(8):1647-1659.

204. Boel G*, et al.* (2014) The ABC-F protein EttA gates ribosome entry into the translation elongation cycle. *Nature Structural & Molecular Biology* 21(2):143.

205. Chen B*, et al.* (2014) EttA regulates translation by binding the ribosomal E site and restricting ribosome-tRNA dynamics. *Nature Structural & Molecular Biology* 21(2):152.

206. Tomar SK, Dhimole N, Chatterjee M, & Prakash B (2009) Distinct GDP/GTP bound states of the tandem G-domains of EngA regulate ribosome binding. *Nucleic Acids Research* 37(7):2359-2370.

207. Karcher A, Büttner K, Märtens B, Jansen RP, & Hopfner KP (2005) X-ray structure of RLI, an essential twin cassette ABC ATPase involved in ribosome biogenesis and HIV capsid assembly. *Structure* 13(4):649-659.

208. Crowe-McAuliffe C*, et al.* (2018) Structural basis for antibiotic resistance mediated by the Bacillus subtilis ABCF ATPase VmlR. *Proc Natl Acad Sci U S A* 115(36):8978-8983.

209. Corrigan RM, Bellows LE, Wood A, & Grundling A (2016) ppGpp negatively impacts ribosome assembly affecting growth and antimicrobial tolerance in Gram-positive bacteria. *Proc Natl Acad Sci U S A* 113(12):E1710-1719.

210. Zhang Y, Zbornikova E, Rejman D, & Gerdes K (2018) Novel (p)ppGpp Binding and Metabolizing Proteins of Escherichia coli. *mBio* 9(2):e02188-02117.

211. Dalebroux ZD & Swanson MS (2012) ppGpp: magic beyond RNA polymerase. *Nature reviews. Microbiology* 10(3):203-212.

212. Hauryliuk V, Atkinson GC, Murakami KS, Tenson T, & Gerdes K (2015) Recent functional insights into the role of (p)ppGpp in bacterial physiology. *Nature reviews. Microbiology* 13(5):298-309.

213. Coatham ML, Brandon HE, Fischer JJ, Schummer T, & Wieden HJ (2016) The conserved GTPase HflX is a ribosome splitting factor that binds to the E-site of the bacterial ribosome. *Nucleic Acids Res* 44(4):1952-1961.

214. Banuett F & Herskowitz I (1987) Identification of Polypeptides encoded by an Escherichia coli Locus (hflA) that governs the Lysis-Lysogeny decision of Bacteriophage lambda. *Journal of Bacteriology* 169(9):4076-4085.

215. Tomoyasu T*, et al.* (1995) Escherichia coli FtsH is a membrane-bound, ATP-dependent protease which degrades the heat-shock transcription factor sigma 32. *The EMBO Journal* 14(11):2551-2560.

216. Akiyama Y, Kihara A, Tokuda H, & Ito K (1996) FtsH (HflB) is an ATP-dependent protease selectively acting on SecY and some other membrane proteins. *Journal of Biological Chemistry* 271(49):31196-31201.

217. Kihara A, Akiyama Y, & Ito K (1997) Host regulation of lysogenic decision in bacteriophage lambda: Transmembrane modulation of FtsH (HflB), the cII degrading protease, by HflKC (HflA). *Proceedings of the National Academy of Sciences of the United States of America* 94(11):5544-5549.

218. Kihara A, Akiyama Y, & Ito K (2001) Revisiting the lysogenization control of bacteriophage lambda - Identification and characterization of a new host component, HflD. *Journal of Biological Chemistry* 276(17):13695-13700.

219. Parua PK, Mondal A, & Parrack P (2010) HflD, an Escherichia coli protein involved in the lambda lysis-lysogeny switch, impairs transcription activation by lambda CII. *Archives of Biochemistry and Biophysics* 493(2):175-183.

220. Kaur G*, et al.* (2014) Novel MntR-Independent Mechanism of Manganese Homeostasis in *Escherichia coli* by the Ribosome-Associated Protein HflX. *Journal of Bacteriology* 196(14):2587-2597.

221. Yoshida H & Wada A (2014) The 100S ribosome: ribosomal hibernation induced by stress. *Wiley Interdisciplinary Reviews-Rna* 5(5):723-732.

222. Kato T*, et al.* (2010) Structure of the 100S Ribosome in the Hibernation Stage Revealed by Electron Cryomicroscopy. *Structure* 18(6):719-724.

223. Ortiz JO*, et al.* (2010) Structure of hibernating ribosomes studied by cryoelectron tomography in vitro and in situ. *Journal of Cell Biology* 190(4):613-621.

224. Ueta M*, et al.* (2008) Role of HPF (hibernation promoting factor) in translational activity in Escherichia coli. *Journal of Biochemistry* 143(3):425-433.

225. Gonzalez-Plaza JJ, *et al.* (2018) Functional Repertoire of Antibiotic Resistance Genes in Antibiotic Manufacturing Effluents and Receiving Freshwater Sediments. *Frontiers in microbiology* 8:2678.

226. Lau CH-F, van Engelen K, Gordon S, Renaud J, & Topp E (2017) Novel Antibiotic Resistance Determinants from Agricultural Soil Exposed to Antibiotics Widely Used in Human Medicine and Animal Farming. *Applied and Environmental Microbiology* 83(16).

227. Dar D, *et al.* (2016) Term-seq reveals abundant ribo-regulation of antibiotics resistance in bacteria. *Science (New York, N.Y.)* 352(6282).

228. Ishizuka M, *et al.* (2018) A possible mechanism for lincomycin induction of secondary metabolism in Streptomyces coelicolor A3(2). *Antonie van Leeuwenhoek* 111(5):705-716.

229. Lee J-H, *et al.* (2020) The WblC/WhiB7 Transcription Factor Controls Intrinsic Resistance to Translation-Targeting Antibiotics by Altering Ribosome Composition. *mBio* 11(2):e00625-00620.

230. Hurst-Hess K, Rudra P, & Ghosh P (2017) Mycobacterium abscessus WhiB7 Regulates a Species-Specific Repertoire of Genes To Confer Extreme Antibiotic Resistance. *Antimicrobial Agents and Chemotherapy* 61(11).

231. Rudra P, Hurst-Hess KR, Cotten KL, Partida-Miranda A, & Ghosh P (2020) Mycobacterial HflX is a ribosome splitting factor that mediates antibiotic resistance. *Proceedings of the National Academy of Sciences of the United States of America* 117(1):629-634.

232. Polkinghorne A, *et al.* (2008) Chlamydophila pneumoniae HflX belongs to an uncharacterized family of conserved GTPases and associates with the Escherichia coli 50S large ribosomal subunit. *Microbiology (Reading)* 154(Part 11):3537-3546.

233. Blombach F, *et al.* (2011) An HflX-Type GTPase from *Sulfolobus solfataricus* Binds to the 50S Ribosomal Subunit in All Nucleotide-Bound States. *Journal of Bacteriology* 193(11):2861-2867.

234. Polkinghorne A, Hogan RJ, Vaughan L, Summersgill JT, & Timms P (2006) Differential expression of chlamydial signal transduction genes in normal and interferon gamma-induced persistent Chlamydophila pneumoniae infections. *Microbes and Infection* 8(1):61-72.

235. John M, *et al.* (2005) Use of in vivo-induced antigen technology for identification of Escherichia coli O157 : H7 proteins expressed during human infection. *Infection and Immunity* 73(5):2665-2679.

236. Zhang F*, et al.* (2016) Immunoprotective Efficacy of Six In vivo-Induced Antigens against Actinobacillus pleuropneumoniae as Potential Vaccine Candidates in Murine Model. *Frontiers in microbiology* 7:1623.

237. Zhang F*, et al.* (2015) Identification of Actinobacillus pleuropneumoniae Genes Preferentially Expressed During Infection Using In Vivo-Induced Antigen Technology (IVIAT). *Journal of Microbiology and Biotechnology* 25(10):1606-1613.

238. Wang Y*, et al.* (2009) Genetic diversity between two Vibrio anguillarum strains exhibiting different virulence by suppression subtractive hybridization. *Weishengwu Xuebao* 49(3):363-370.

239. Ellis TC*, et al.* (2014) Correction: In Vivo Expression Technology Identifies a Novel Virulence Factor Critical for Borrelia burgdorferi Persistence in Mice. *PLoS Pathog* 10(6):e1004260.

240. Ma Z*, et al.* (2015) Identification of novel genes expressed during host infection in Streptococcus equi ssp zooepidemicus ATCC35246. *Microbial Pathogenesis* 79:31-40.

241. Fernandez CM*, et al.* (2019) Genetic differences in Chlamydia pecorum between neighbouring sub-populations of koalas (Phascolarctos cinereus). *Veterinary Microbiology* 231:264-270.

242. Zocevic A*, et al.* (2012) Molecular characterization of atypical *Chlamydia* and evidence of their dissemination in different European and Asian chicken flocks by specific real-time PCR. *Environmental Microbiology* 14(8):2212-2222.

243. Ikryannikova LN, Shkarupeta MM, Shitikov EA, Il'ina EN, & Govorun VM (2010) Comparative evaluation of new typing schemes for urogenital Chlamydia trachomatis isolates. *Fems Immunology and Medical Microbiology* 59(2):188-196.

244. Pannekoek Y*, et al.* (2008) Multi locus sequence typing of Chlamydiales: clonal groupings within the obligate intracellular bacteria Chlamydia trachomatis. *BMC Microbiol* 8:42.

245. Feodorova VA*, et al.* (2018) Urogenital Chlamydia trachomatis multilocus sequence types and genovar distribution in chlamydia infected patients in a multi-ethnic region of Saratov, Russia. *PLoS One* 13(4):e0195386.

246. Brzuszkiewicz E*, et al.* (2006) How to become a uropathogen: Comparative genomic analysis of extraintestinal pathogenic Escherichia coli strains. *Proceedings of the National Academy of Sciences of the United States of America* 103(34):12879-12884.

247. Lisher JP & Giedroc DP (2013) Manganese acquisition and homeostasis at the host-pathogen interface. *Front Cell Infect Microbiol* 3:91.

248. Grunenwald CM*, et al.* (2019) Manganese Detoxification by MntE Is Critical for Resistance to Oxidative Stress and Virulence of Staphylococcus aureus. *mBio* 10(1).

249. Juttukonda LJ & Skaar EP (2015) Manganese homeostasis and utilization in pathogenic bacteria. *Molecular Microbiology* 97(2):216-228.

250. Helmann JD (2014) Specificity of Metal Sensing: Iron and Manganese Homeostasis in Bacillus subtilis. *Journal of Biological Chemistry* 289(41):28112-28120.

251. Anjem A & Imlay JA (2012) Mononuclear Iron Enzymes Are Primary Targets of Hydrogen Peroxide Stress. *Journal of Biological Chemistry* 287(19):15544-15556.

252. Anjem A, Varghese S, & Imlay JA (2009) Manganese import is a key element of the OxyR response to hydrogen peroxide in Escherichia coli. *Molecular Microbiology* 72(4):844-858.

253. Kehres DG, Zaharik ML, Finlay BB, & Maguire ME (2000) The NRAMP proteins of Salmonella typhimurium and Escherichia coli are selective manganese transporters involved in the response to reactive oxygen. *Molecular Microbiology* 36(5):1085-1100.

254. Cotruvo JA, Jr. & Stubbe J (2012) Metallation and mismetallation of iron and manganese proteins in vitro and in vivo: the class I ribonucleotide reductases as a case study. *Metallomics* 4(10):1020-1036.

255. Jakubovics NS & Jenkinson HF (2001) Out of the iron age: new insights into the critical role of manganese homeostasis in bacteria. *Microbiology-Sgm* 147:1709-1718.

256. Waters LS, Sandoval M, & Storz G (2011) The Escherichia coli MntR Miniregulon Includes Genes Encoding a Small Protein and an Efflux Pump Required for Manganese Homeostasis. *Journal of Bacteriology* 193(21):5887-5897.

257. Sengupta S, Mondal A, Dutta D, & Parrack P (2018) HflX protein protects Escherichia coli from manganese stress. *Journal of Biosciences (Bangalore)* 43(5):1001-1013.

258. Du S & Lutkenhaus J (2017) Assembly and activation of the Escherichia coli divisome. *Molecular Microbiology* 105(2):177-187.

259. Errington J, Daniel RA, & Scheffers DJ (2003) Cytokinesis in bacteria. *Microbiol Mol Biol Rev* 67(1):52-65, table of contents.

260. Sun T*, et al.* (2019) Inhibitory Effect of Two Traditional Chinese Medicine Monomers, Berberine and Matrine, on the Quorum Sensing System of Antimicrobial-Resistant Escherichia coli. *Frontiers in microbiology* 10:2584.

261. Gianfrancesco F*, et al.* (1998) A novel pseudoautosomal gene encoding a putative GTP-binding protein resides in the vicinity of the Xp/Yp telomere. *Human Molecular Genetics* 7(3):407-414.

262. Mangs AH & Morris BJ (2007) The human pseudoautosomal region (PAR): Origin, function and future. *Current Genomics* 8(2):129-136.

263. Ciccodicola A*, et al.* (2000) Differentially regulated and evolved genes in the fully sequenced Xq/Yq pseudoautosomal region. *Human Molecular Genetics* 9(3):395-401.

264. Vawter MP, HarVey PD, & DeLisi LE (2007) Dysregulation of X-linked gene expression in Klinefelter's syndrome and association with verbal cognition. *American Journal of Medical Genetics Part B-Neuropsychiatric Genetics* 144B(6):728-734.

265. Belling K*, et al.* (2017) Klinefelter syndrome comorbidities linked to increased X chromosome gene dosage and altered protein interactome activity. *Human Molecular Genetics* 26(7):1219-1229.

266. Zitzmann M*, et al.* (2015) Gene Expression Patterns in Relation to the Clinical Phenotype in Klinefelter Syndrome. *Journal of Clinical Endocrinology & Metabolism* 100(3):E518-E523.

267. Crespi B (2013) Diametric gene-dosage effects as windows into neurogenetic architecture. *Current Opinion in Neurobiology* 23(1):143-151.

268. Tarpey PS*, et al.* (2009) A systematic, large-scale resequencing screen of X-chromosome coding exons in mental retardation. *Nature Genetics* 41(5):535-543.

269. Mohandas TK*, et al.* (1992) Role of the pseudoautosomal region in sex-chromosome pairing during male meiosis: meiotic studies in a man with a deletion of distal Xp. *Am J Hum Genet* 51(3):526-533.

270. Jorgez CJ*, et al.* (2011) Aberrations in Pseudoautosomal Regions (PARs) Found in Infertile Men with Y-Chromosome Microdeletions. *Journal of Clinical Endocrinology & Metabolism* 96(4):E674-E679.

271. Chianese C*, et al.* (2014) X chromosome-linked CNVs in male infertility: discovery of overall duplication load and recurrent, patient-specific gains with potential clinical relevance. *PLoS One* 9(6):e97746.

272. Krausz C*, et al.* (2012) High resolution X chromosome-specific array-CGH detects new CNVs in infertile males. *PLoS One* 7(10):e44887.

273. Bastian VA, Burns NR, & Nettelbeck T (2005) Emotional intelligence predicts life skills, but not as well as personality and cognitive abilities. *Personality and Individual Differences* 39(6):1135-1145.

274. Thul PJ*, et al.* (2017) A subcellular map of the human proteome. *Science (New York, N.Y.)* 356(6340).

275. Uhlen M*, et al.* (2017) A pathology atlas of the human cancer transcriptome. *Science (New York, N.Y.)* 357(6352):660-+.

276. Lau YFC & Zhang JQ (2000) Expression analysis of thirty one Y chromosome genes in human prostate cancer. *Molecular Carcinogenesis* 27(4):308-321.

277. Autsavapromporn N*, et al.* (2019) Identification of novel biomarkers for lung cancer risk in high levels of radon by proteomics: A pilot study. *Radiation Protection Dosimetry* 184(3-4):496-499.

278. Lavdovskaia E*, et al.* (2020) Dual function of GTPBP6 in biogenesis and recycling of human mitochondrial ribosomes. *Nucleic Acids Research* 48(22):12929-12942.

279. Almagro Armenteros JJ*, et al.* (2019) Detecting sequence signals in targeting peptides using deep learning. *Life Sci Alliance* 2(5):e201900429.

280. Taanman J-W (1999) The mitochondrial genome: structure, transcription, translation and replication. *Biochimica et Biophysica Acta (BBA) - Bioenergetics* 1410(2):103-123.

281. Greber BJ & Ban N (2016) Structure and Function of the Mitochondrial Ribosome. *Annual Review of Biochemistry* 85(1):103-132.

282. Oughtred R*, et al.* (2018) The BioGRID interaction database: 2019 update. *Nucleic Acids Research* 47(D1):D529-D541.

283. Orchard S*, et al.* (2014) The MIntAct project--IntAct as a common curation platform for 11 molecular interaction databases. *Nucleic Acids Res* 42(Database issue):D358-363.

284. Hein MY*, et al.* (2015) A human interactome in three quantitative dimensions organized by stoichiometries and abundances. *Cell* 163(3):712-723.

285. Huttlin EL*, et al.* (2017) Architecture of the human interactome defines protein communities and disease networks. *Nature* 545(7655):505-509.

286. Huttlin EL*, et al.* (2015) The BioPlex Network: A Systematic Exploration of the Human Interactome. *Cell* 162(2):425-440.

287. Giurato G*, et al.* (2018) Quantitative mapping of RNA-mediated nuclear estrogen receptor β interactome in human breast cancer cells. *Scientific Data* 5(1):180031.

288. Nassa G*, et al.* (2019) The RNA-mediated estrogen receptor α interactome of hormone-dependent human breast cancer cell nuclei. *Scientific Data* 6(1):173.

289. Valera-Alberni M & Canto C (2018) Mitochondrial stress management: a dynamic journey. *Cell Stress* 2(10):253-274.

290. Topf U, Uszczynska-Ratajczak B, & Chacinska A (2019) Mitochondrial stress-dependent regulation of cellular protein synthesis. *Journal of Cell Science* 132(8).

291. Akabane S, Ueda T, Nierhaus KH, & Takeuchi N (2014) Ribosome Rescue and Translation Termination at Non-Standard Stop Codons by ICT1 in Mammalian Mitochondria. *PLoS Genetics* 10(9):e1004616.

292. Ayyub SA, Gao F, Lightowlers RN, & Chrzanowska-Lightowlers ZM (2020) Rescuing stalled mammalian mitoribosomes - what can we learn from bacteria? *Journal of Cell Science* 133(1):jcs231811.

293. Richter R*, et al.* (2010) A functional peptidyl-tRNA hydrolase, ICT1, has been recruited into the human mitochondrial ribosome. *EMBO (European Molecular Biology Organization) Journal* 29(6):1116-1125.

294. Wesolowska MT, Richter-Dennerlein R, Lightowlers RN, & Chrzanowska-Lightowlers ZMA (2014) Overcoming stalled translation in human mitochondria. *Frontiers in microbiology* 5:374.

295. Ren Y-p, Huang R-w, & Lü Z-r (2006) Ouabain at pathological concentrations might induce damage vascular endothelial cells. *Acta Pharmacologica Sinica* 27(2):165-172.

296. Hamlyn JM*, et al.* (1991) Identification and characterization of a ouabain-like compound from human plasma. *Proc Natl Acad Sci U S A* 88(14):6259-6263.

297. Zorova LD*, et al.* (2018) Mitochondrial membrane potential. *Analytical biochemistry* 552:50-59.

298. Sahin E*, et al.* (2011) Telomere dysfunction induces metabolic and mitochondrial compromise. *Nature (London)* 470(7334):356-362.

299. Starosta AL, Lassak J, Jung K, & Wilson DN (2014) The bacterial translation stress response. *FEMS Microbiology Reviews* 38(6, Sp. Iss. SI):1172-1201.

300. Cole SE, LaRiviere FJ, Merrikh CN, & Moore MJ (2009) A Convergence of rRNA and mRNA Quality Control Pathways Revealed by Mechanistic Analysis of Nonfunctional rRNA Decay. *Molecular Cell* 34(4):440-450.

301. Bayfield MA, Dahlberg AE, Schulmeister U, Dorner S, & Barta A (2001) A conformational change in the ribosomal peptidyl transferase center upon active/inactive transition. *Proceedings of the National Academy of Sciences of the United States of America* 98(18):10096-10101.

302. Willi J*, et al.* (2018) Oxidative stress damages rRNA inside the ribosome and differentially affects the catalytic center. *Nucleic Acids Research* 46(4):1945-1957.

303. Fujii K, Kitabatake M, Sakata T, Miyata A, & Ohno M (2009) A role for ubiquitin in the clearance of nonfunctional rRNAs. *Genes & Development* 23(8):963-974.

304. Pulk A*, et al.* (2010) Ribosome reactivation by replacement of damaged proteins. *Molecular Microbiology* 75(4):801-814.

305. Mathis AD*, et al.* (2017) Mechanisms of In Vivo Ribosome Maintenance Change in Response to Nutrient Signals. *Molecular & Cellular Proteomics* 16(2):243-254.

306. Sampson JR, Direnzo AB, Behlen LS, & Uhlenbeck OC (1989) Nucleotides in yeast tRNAPhe required for the specific recognition by its cognate synthetase. *Science (New York, N.Y.)* 243(4896):1363-1366.

307. Brosius J*, et al.* (1981) Construction and fine mapping of recombinant plasmids containing the rrnB ribosomal RNA operon of E. coli. *Plasmid* 6(1):112-118.

308. Baba T*, et al.* (2006) Construction of Escherichia coli K-12 in-frame, single-gene knockout mutants: the Keio collection. *Mol Syst Biol* 2:2006 0008.

309. Rosler KS, Mercier E, Andrews IC, & Wieden H-J (2015) Histidine 114 Is Critical for ATP Hydrolysis by the Universally Conserved ATPase YchF. *Journal of Biological Chemistry* 290(30):18650-18661.

310. Dolinsky TJ*, et al.* (2007) PDB2PQR: expanding and upgrading automated preparation of biomolecular structures for molecular simulations. *Nucleic Acids Research* 35:W522-W525.

311. Baker NA, Sept D, Joseph S, Holst MJ, & McCammon JA (2001) Electrostatics of nanosystems: Application to microtubules and the ribosome. *Proceedings of the National Academy of Sciences of the United States of America* 98(18):10037-10041.

312. Celniker G*, et al.* (2013) ConSurf: Using Evolutionary Data to Raise Testable Hypotheses about Protein Function. *Israel Journal of Chemistry* 53(3-4):199-206.

313. Ramon Lopez-Blanco J, Aliaga JI, Quintana-Orti ES, & Chacon P (2014) iMODS: internal coordinates normal mode analysis server. *Nucleic Acids Research* 42(W1):W271-W276.

314. Duval M*, et al.* (2013) Escherichia coli ribosomal protein S1 unfolds structured mRNAs onto the ribosome for active translation initiation. *PLoS Biol* 11(12):e1001731.

315. Wright JR, Keffer-Wilkes LC, Dobing SR, & Kothe U (2011) Pre-steady-state kinetic analysis of the three Escherichia coli pseudouridine synthases TruB, TruA, and RluA reveals uniformly slow catalysis. *Rna* 17(12):2074-2084.

316. Schneider CA, Rasband WS, & Eliceiri KW (2012) NIH Image to ImageJ: 25 years of image analysis. *Nature Methods* 9(7):671-675.

317. Rajkowitsch L & Schroeder R (2007) Dissecting RNA chaperone activity. *RNA* 13(12):2053-2060.

318. Foerstner KU, Vogel J, & Sharma CM (2014) READemption-a tool for the computational analysis of deep-sequencing-based transcriptome data. *Bioinformatics* 30(23):3421-3423.

319. Monk JM*, et al.* (2016) Multi-omics Quantification of Species Variation of Escherichia coli Links Molecular Features with Strain Phenotypes. *Cell Syst* 3(3):238-251 e212.

320. Pfennig PL & Flower AM (2001) BipA is required for growth of Escherichia coli K12 at low temperature. *Molecular Genetics and Genomics* 266(2):313-317.

321. Horn G, Hofweber R, Kremer W, & Kalbitzer HR (2007) Structure and function of bacterial cold shock proteins. *Cellular and Molecular Life Sciences* 64(12):1457-1470.

322. Jagessar KL & Jain C (2010) Functional and molecular analysis of Escherichia coli strains lacking multiple DEAD-box helicases. *Rna* 16(7):1386-1392.

323. Awano N*, et al.* (2007) Complementation analysis of the cold-sensitive phenotype of the Escherichia coli csdA deletion strain. *Journal of Bacteriology* 189(16):5808-5815.

324. Kaczanowska M & Ryden-Aulin M (2007) Ribosome biogenesis and the translation process in Escherichia coli. *Microbiol Mol Biol Rev* 71(3):477-494.

325. Qu X, Lancaster L, Noller HF, Bustamante C, & Tinoco I, Jr. (2012) Ribosomal protein S1 unwinds double-stranded RNA in multiple steps. *Proceedings of the National Academy of Sciences of the United States of America* 109(36):14458-14463.

326. Doetsch M, Gstrein T, Schroeder R, & Fuertig B (2010) Mechanisms of StpA-mediated RNA remodeling. *Rna Biology* 7(6):735-743.

327. Lamech LT, Mallam AL, & Lambowitz AM (2014) Evolution of RNA-protein interactions: non-specific binding led to RNA splicing activity of fungal mitochondrial tyrosyl-tRNA synthetases. *PLoS Biol* 12(12):e1002028.

328. Jarmoskaite I & Russell R (2014) RNA Helicase Proteins as Chaperones and Remodelers. *Annual Review of Biochemistry, Vol 83,* Annual Review of Biochemistry, ed Kornberg RD), Vol 83, pp 697-725.

329. Brown A, Fernandez IS, Gordiyenko Y, & Ramakrishnan V (2016) Ribosome-dependent activation of stringent control. *Nature* 534(7606):277-280.

330. Keffer-Wilkes LC, Veerareddygari GR, & Kothe U (2016) RNA modification enzyme TruB is a tRNA chaperone. *Proceedings of the National Academy of Sciences of the United States of America* 113(50):14306-14311.

331. Moazed D, Robertson JM, & Noller HF (1988) Interaction of Elongation-factors EF-G and EF-Tu with a conserved loop in 23S RNA. *Nature* 334(6180):362-364.

332. Chen Y, Koripella RK, Sanyal S, & Selmer M (2010) *Staphylococcus aureus* elongation factor G - structure and analysis of a target for fusidic acid. *FEBS Journal* 277(18):3789-3803.

333. Maracci C & Rodnina MV (2016) Translational GTPases. *Biopolymers* 105(8):463-475.

334. Arigoni F*, et al.* (1998) A genome-based approach for the identification of essential bacterial genes. *Nature Biotechnology* 16(9):851-856.

335. Schaefer L*, et al.* (2006) Multiple GTPases participate in the assembly of the large ribosomal subunit in Bacillus subtilis. *Journal of Bacteriology* 188(23):8252-8258.

336. Soper SFC, Dator RP, Limbach PA, & Woodson SA (2013) In Vivo X-Ray Footprinting of Pre-30S Ribosomes Reveals Chaperone-Dependent Remodeling of Late Assembly Intermediates. *Molecular Cell* 52(4):506-516.

337. Voorhees RM, Schmeing TM, Kelley AC, & Ramakrishnan V (2010) The Mechanism for Activation of GTP Hydrolysis on the Ribosome. *Science (Washington D C)* 330(6005):835-838.

338. Taylor DE & Chau A (1996) Tetracycline resistance mediated by ribosomal protection. *Antimicrobial Agents and Chemotherapy* 40(1):1-5.

339. Connell SR, Tracz DM, Nierhaus KH, & Taylor DE (2003) Ribosomal protection proteins and their mechanism of tetracycline resistance. *Antimicrobial Agents and Chemotherapy* 47(12):3675-3681.

340. Chopra I & Roberts M (2001) Tetracycline antibiotics: mode of action, applications, molecular biology, and epidemiology of bacterial resistance. *Microbiol Mol Biol Rev* 65(2):232-260 ; second page, table of contents.

341. Blanchard SC, Gonzalez RL, Kim HD, Chu S, & Puglisi JD (2004) tRNA selection and kinetic proofreading in translation. *Nature Structural & Molecular Biology* 11(10):1008-1014.

342. Anonymous (!!! INVALID CITATION !!! {}).

343. Li GW, Burkhardt D, Gross C, & Weissman JS (2014) Quantifying absolute protein synthesis rates reveals principles underlying allocation of cellular resources. *Cell* 157(3):624-635.

344. Avcilar-Kucukgoze I*, et al.* (2016) Discharging tRNAs: a tug of war between translation and detoxification in Escherichia coli. *Nucleic Acids Res* 44(17):8324-8334.

345. Dong HJ, Nilsson L, & Kurland CG (1996) Co-variation of tRNA abundance and codon usage in Escherichia coli at different growth rates. *Journal of Molecular Biology* 260(5):649-663.

346. Villa E*, et al.* (2009) Ribosome-induced changes in elongation factor Tu conformation control GTP hydrolysis. *Proceedings of the National Academy of Sciences of the United States of America* 106(4):1063-1068.

347. Ban N, Nissen P, Hansen J, Moore PB, & Steitz TA (2000) The complete atomic structure of the large ribosomal subunit at 2.4 angstrom resolution. *Science (New York, N.Y.)* 289(5481):905-920.

348. Wimberly BT*, et al.* (2000) Structure of the 30S ribosomal subunit. *Nature* 407(6802):327-339.

349. Schluenzen F*, et al.* (2000) Structure of functionally activated small ribosomal subunit at 3.3 angstrom resolution. *Cell* 102(5):615-623.

350. Yusupov MM*, et al.* (2001) Crystal structure of the ribosome at 5.5 angstrom resolution. *Science (New York, N.Y.)* 292(5518):883-896.

351. Yusupova G & Yusupov M (2014) High-Resolution Structure of the Eukaryotic 80S Ribosome. *Annual Review of Biochemistry, Vol 83,* Annual Review of Biochemistry, ed Kornberg RD), Vol 83, pp 467-486.

352. Wilson DN & Doudna Cate JH (2012) The structure and function of the eukaryotic ribosome. *Cold Spring Harb Perspect Biol* 4(5).

353. Nissen P, Kjeldgaard M, & Nyborg J (2000) Macromolecular mimicry. *EMBO (European Molecular Biology Organization) Journal* 19(4):489-495.

354. Kristensen O, Laurberg M, Liljas A, & Selmer M (2002) Is tRNA binding or tRNA mimicry mandatory for translation factors? *Current protein & peptide science* 3(1):133-141.

355. Nakamura Y (2001) Molecular mimicry between protein and tRNA. *Journal of Molecular Evolution* 53(4-5):282-289.

356. Czworkowski J, Wang J, Steitz TA, & Moore PB (1994) The crystal structure of elongation factor G complexed with GDP, at 2.7 A resolution. *EMBO (European Molecular Biology Organization) Journal* 13(16):3661-3668.

357. Nissen P*, et al.* (1995) Crystal structure of the ternary complex of Phe-tRNAPhe, EF-Tu, and a GTP analog. *Science (New York, N.Y.)* 270(5241):1464-1472.

358. Valle M*, et al.* (2002) Cryo-EM reveals an active role for aminoacyl-tRNA in the accommodation process. *EMBO (European Molecular Biology Organization) Journal* 21(13):3557-3567.

359. Gao H, Valle M, Ehrenberg M, & Frank J (2004) Dynamics of EF-G interaction with the ribosome explored by classification of a heterogeneous cryo-EM dataset. *Journal of Structural Biology* 147(3):283-290.

360. Datta PP, Sharma MR, Qi L, Frank J, & Agrawal RK (2005) Interaction of the G ' domain of elongation factor G and the C-terminal domain of ribosomal protein L7/L12 during translocation as revealed by cryo-EM. *Molecular Cell* 20(5):723-731.

361. Evans RN, Blaha G, Bailey S, & Steitz TA (2008) The structure of LepA, the ribosomal back translocase. *Proceedings of the National Academy of Sciences of the United States of America* 105(12):4673-4678.

362. De laurentiis EI & Wieden H-J (2015) Identification of Two Structural Elements Important for Ribosome-Dependent GTPase Activity of Elongation Factor 4 (EF4/LepA). *Scientific Reports* 5:8573.

363. Kumar V*, et al.* (2015) Structure of BipA in GTP form bound to the ratcheted ribosome. *Proceedings of the National Academy of Sciences of the United States of America* 112(35):10944-10949.

364. Arenz S, Nguyen F, Beckmann R, & Wilson DN (2015) Cryo-EM structure of the tetracycline resistance protein TetM in complex with a translating ribosome at 3.9-angstrom resolution. *Proceedings of the National Academy of Sciences of the United States of America* 112(17):5401-5406.

365. Spahn CMT*, et al.* (2001) Localization of the ribosomal protection protein Tet(O) on the ribosome and the mechanism of tetracycline resistance. *Molecular Cell* 7(5):1037-1045.

366. Nechifor R, Murataliev M, & Wilson KS (2007) Functional interactions between the G ' subdomain of bacterial translation factor EF-G and ribosomal protein L7/L12. *Journal of Biological Chemistry* 282(51):36998-37005.

367. Heffron SE*, et al.* (2006) Molecular complementarity between tetracycline and the GTPase active site of elongation factor Tu. *Acta Crystallographica Section D Biological Crystallography* 62(Part 11):1392-1400.

368. Ruusala T & Kurland CG (1984) Streptomycin preferentially perturbs ribosomal proofreading. *Molecular and General Genetics* 198(1):100-104.

369. Hirokawa G, Iwakura N, Kaji A, & Kaji H (2008) The role of GTP in transient splitting of 70S ribosomes by RRF (ribosome recycling factor) and EF-G (elongation factor G). *Nucleic Acids Research* 36(21):6676-6687.

370. Rodnina MV, Fricke R, & Wintermeyer W (1994) Transient conformational states of aminoacyl-tRNA during ribosome binding catalyzed by elongation factor Tu. *Biochemistry* 33(40):12267-12275.

371. Goerisch H, Goss DJ, & Parkhurst LJ (1976) Kinetics of ribosome dissociation and subunit association studied in a light scattering stopped flow apparatus. *Biochemistry* 15(26):5743-5753.

372. Feng B*, et al.* (2014) Structural and Functional Insights into the Mode of Action of a Universally Conserved Obg GTPase. *PLoS Biology* 12(5):e1001866.

373. Arenz S*, et al.* (2014) Drug Sensing by the Ribosome Induces Translational Arrest via Active Site Perturbation. *Molecular Cell* 56(3):446-452.

374. Arenz S*, et al.* (2014) Molecular basis for erythromycin-dependent ribosome stalling during translation of the ErmBL leader peptide. *Nature Communications* 5:3501.

375. Dzidic S & Bedekovic V (2003) Horizontal gene transfer-emerging multidrug resistance in hospital bacteria. *Acta Pharmacologica Sinica* 24(6):519-526.

376. Zhen X, Lundborg CS, Sun X, Hu X, & Dong H (2019) Economic burden of antibiotic resistance in ESKAPE organisms: a systematic review. *Antimicrob Resist Infect Control* 8(1):137.

377. Mulani MS, Kamble EE, Kumkar SN, Tawre MS, & Pardesi KR (2019) Emerging Strategies to Combat ESKAPE Pathogens in the Era of Antimicrobial Resistance: A Review. *Frontiers in microbiology* 10:539.

378. Christaki E, Marcou M, & Tofarides A (2020) Antimicrobial Resistance in Bacteria: Mechanisms, Evolution, and Persistence. *Journal of Molecular Evolution* 88(1):26-40.

379. Ventola CL (2015) The antibiotic resistance crisis: part 1: causes and threats. *P & T : a peer-reviewed journal for formulary management* 40(4):277-283.

380. Bartlett JG, Gilbert DN, & Spellberg B (2013) Seven Ways to Preserve the Miracle of Antibiotics. *Clinical Infectious Diseases* 56(10):1445-1450.

381. Ventola CL (2015) The antibiotic resistance crisis: part 2: management strategies and new agents. *P & T : a peer-reviewed journal for formulary management* 40(5):344-352.

382. Munita JM & Arias CA (2016) Mechanisms of Antibiotic Resistance. *Microbiol Spectr* 4(2).

383. Peterson E & Kaur P (2018) Antibiotic Resistance Mechanisms in Bacteria: Relationships Between Resistance Determinants of Antibiotic Producers, Environmental Bacteria, and Clinical Pathogens. *Frontiers in microbiology* 9:2928.

384. Blair JMA, Webber MA, Baylay AJ, Ogbolu DO, & Piddock LJV (2015) Molecular mechanisms of antibiotic resistance. *Nature Reviews Microbiology* 13(1):42-51.

385. Wilson DN (2014) Ribosome-targeting antibiotics and mechanisms of bacterial resistance. *Nature Reviews Microbiology* 12(1):35-48.

386. Wasserman MR*, et al.* (2015) Chemically related 4,5-linked aminoglycoside antibiotics drive subunit rotation in opposite directions. *Nat Commun* 6:7896.

387. Scheunemann AE, Graham WD, Vendeix FAP, & Agris PF (2010) Binding of aminoglycoside antibiotics to helix 69 of 23S rRNA. *Nucleic Acids Research* 38(9):3094-3105.

388. Hansson S, Singh R, Gudkov AT, Liljas A, & Logan DT (2005) Structural insights into fusidic acid resistance and sensitivity in EF-G. *Journal of Molecular Biology* 348(4):939-949.

389. Borovinskaya MA*, et al.* (2007) Structural basis for aminoglycoside inhibition of bacterial ribosome recycling. *Nature Structural & Molecular Biology* 14(8):727-732.

390. Lill R, Robertson JM, & Wintermeyer W (1986) Affinities of tRNA binding sites of ribosomes from Escherichia coli. *Biochemistry* 25(11):3245-3255.

391. Blaha G, Stanley RE, & Steitz TA (2009) Formation of the first peptide bond: the structure of EF-P bound to the 70S ribosome. *Science (New York, N.Y.)* 325(5943):966-970.

392. Gao YG*, et al.* (2009) The Structure of the Ribosome with Elongation Factor G Trapped in the Posttranslocational State. *Science (New York, N.Y.)* 326(5953):694-699.

393. Tsai A*, et al.* (2013) The Impact of Aminoglycosides on the Dynamics of Translation Elongation. *Cell Reports* 3(2):497-508.

394. Hirokawa G*, et al.* (2002) Post-termination complex disassembly by ribosome recycling factor, a functional tRNA mimic. *EMBO (European Molecular Biology Organization) Journal* 21(9):2272-2281.

395. Wilson DN, Hauryliuk V, Atkinson GC, & O'Neill AJ (2020) Target protection as a key antibiotic resistance mechanism. *Nature reviews. Microbiology* 18(11):637-648.

396. Svetlov MS, Vázquez-Laslop N, & Mankin AS (2017) Kinetics of drug-ribosome interactions defines the cidality of macrolide antibiotics. *Proceedings of the National Academy of Sciences of the United States of America* 114(52):13673-13678.

397. Connell SR*, et al.* (2002) The tetracycline resistance protein Tet(O) perturbs the conformation of the ribosomal decoding centre. *Molecular Microbiology* 45(6):1463-1472.

398. Smith DD, Girodat D, Wieden H-J, & Selinger LB (2017) Streamlined purification of fluorescently labeled Escherichia coli phosphate-binding protein (PhoS) suitable for rapid-kinetics applications. *Analytical Biochemistry* 537:106-113.

APPENDIX TO

BIOPHYSICAL STUDIES OF THE UNIVERSALLY CONSERVED NTPASES HFLX AND YCHF

BY HARLAND EDWARD BRANDON

Includes Appendix Figures, Tables, and Methods separated into sections corresponding to each thesis chapter.

TABLE OF CONTENTS

SECTION 1 – INTRODUCTION APPENDIX

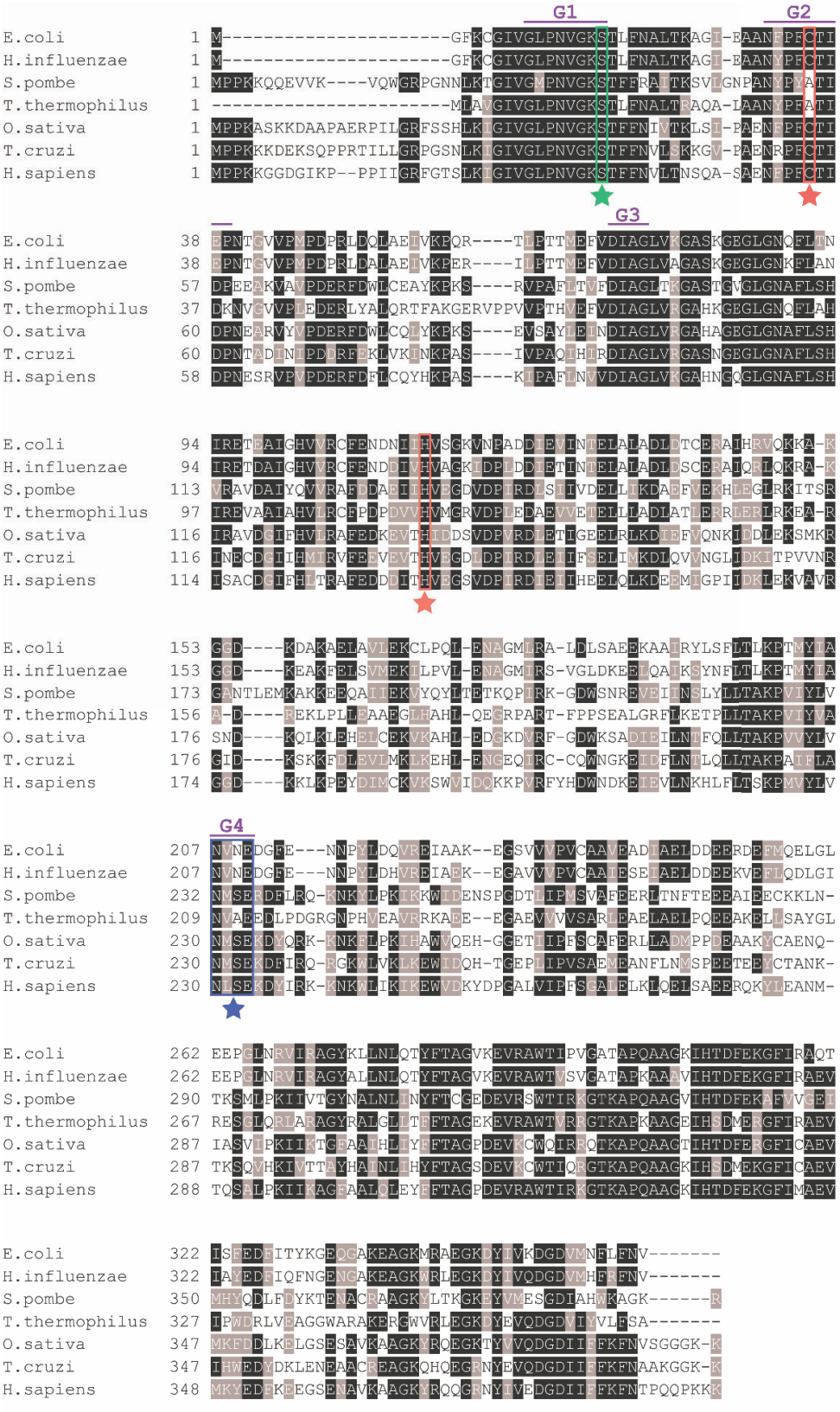

[Figure on previous page]

Appendix Figure 1.1 – Sequence alignment of hOLA1/YchF homologs. Each homolog with a solved crystal structure (*H. influenzae*, *S. pombe*, *T. thermophilus*, *O. sativa*, and *H. sapiens*) was aligned against other well-studied YchF homologs (*E. coli* and *T. cruzi*). Identical amino acid residues are shaded black; similar residues are shaded grey. The conserved serine residue that is phosphorylated, the conserved cysteine residue implicated in dimerization, the conserved catalytic histidine, and the altered G4 motif are highlighted in green, red, orange, and blue, respectively. The sequence alignment was generated using T-coffee and Boxshade.

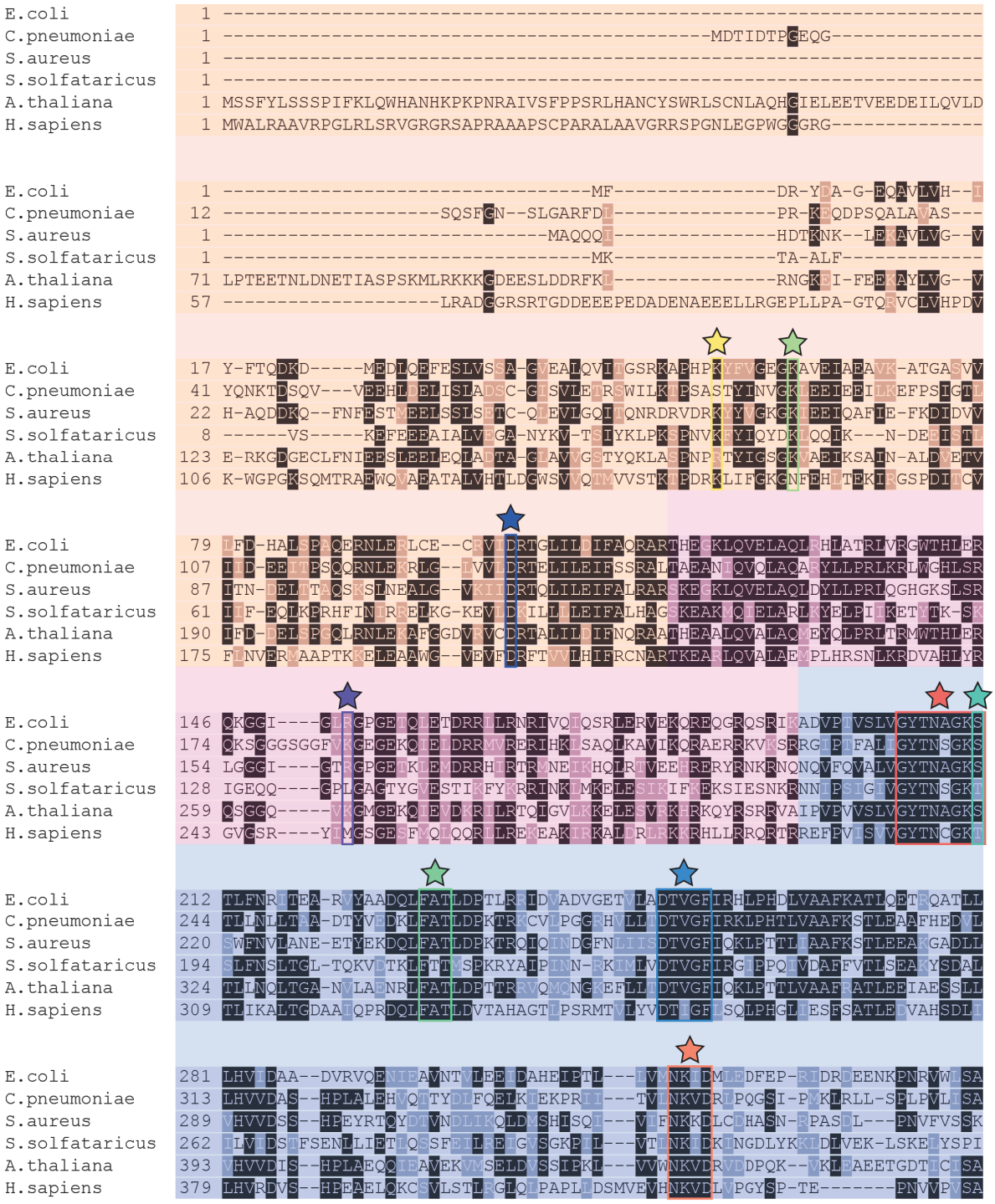

Continued next page.

Appendix Figure 1.2 – Sequence alignment of HflX orthologs. Orthologs that have structural and biochemical information in the literature were aligned against one another. Identical amino acid residues are shaded black; similar residues are shaded grey. Background colour indicates domain consistent with Figure 2. The starred residue(s) in order are as listed: K55 in yellow, K62 in light green, D102 in dark blue, R153 in purple, G1 motif in red, S211 in teal, G2 motif in green, G3 motif in blue, and G4 in orange. The sequence alignment was generated using T-coffee and Boxshade.

Appendix Table 1.1 – Confirmed protein or RNA interacting partners of YchF in different organisms.

Interacting Partner	Organism(s) in which interaction confirmed	Functional role of the interacting partner	Proposed functional interaction with YchF/hOLA1	Reference(s)
Ribosomal Protein L26	*T. cruzi*	Ribosomal protein in the large subunit	Potential YchF binding site on the ribosome	(1)
Ribosomal Protein S7	*T. cruzi*	Ribosomal protein in the small subunit	Potential YchF binding site on the ribosome	(1)
RPN10	*T. cruzi*	Non-ATPase subunit of the proteasome	Potential binding site on the proteasome	(1)
80S (70S) ribosome	*T. cruzi*, *E. coli, H. sapiens* (A549 cells)	Monomer of the full ribosomal complex	Undetermined functional role during protein synthesis, ribosome biogenesis, stress response	(1-3)
Polysomes	*T. cruzi*, *E. coli, H. sapiens* (A549 cells)	Multiple ribosomes actively translating along one mRNA	Undetermined functional role during protein synthesis, ribosome biogenesis, stress response	(1, 2)
60S (50S) large ribosomal subuntis	*T. cruzi*, *E. coli, H. sapiens* (A549 cells)	Large subunit of the ribosome	Undetermined functional role during protein synthesis, ribosome biogenesis, stress response	(1-3)
40S (30S) small ribosomal subunit	*T. cruzi*, *E. coli, H. sapiens* (A549 cells)	Small subunit of the ribosome	Undetermined functional role during protein synthesis, ribosome biogenesis, stress response	(1, 3)
26 S proteosome	*S. cerevisiae*	26 S proteasome involved in protein degradation	Unclear; confirmed Proteasome interacting protein	(4)
KatG	*E. coli*	Catalase	YchF negatively regulates antioxidant activity through inhibition of KatG	(5, 6)
KatE	*E. coli*	Catalase	YchF negatively regulates antioxidant activity potentially through inhibition of KatE	(5, 6)
AhpCF	*E. coli*	Alkyl hydroperoxide reductase	YchF negatively regulates antioxidant activity potentially through inhibition of AhpCF	(5, 6)
Dps	*E. coli*	Iron scavenging protein	Unclear	(5)

Gag polyprotein	*H. sapiens* (Jurkat and HEK293) + HIV-1	Virion assembly, Plasma membrane interaction, Packaging of viral RNA	Unclear	(7)
HSP70	*H. sapiens* (HEK-293T cells)	Heat-shock protein 70	hOLA1 stabilizes and protects HSP70 degradation	(8)
OsGAP1	*O. satvia*	GTPase activating protein for OsYchF1 in plants	OsGAP1 regulates OsYchF1 GTPase activity	(9)
BARD1	*H. sapiens* (HEK-293T cells)	BRCA1-associated RING domain protein; ubiquitin ligase inconjuction with BRCA1	hOLA1 interacts with the BARD1:BRCA1:γ-Tubulin complex to regulate centromeres	(10)
BRCA1	*H. sapiens* (HEK-293T cells)	Breast cancer-associated gene 1; ubiquitin ligase inconjuction with BARD1	hOLA1 interacts with the BARD1:BRCA1:γ-Tubulin complex to regulate centromeres	(10)
γ-Tubulin	*H. sapiens* (HEK-293T cells)	Microtubule protein found in centromeres and spindle pole bodies	hOLA1 interacts with the BARD1:BRCA1:γ-Tubulin complex to regulate centromeres	(10)
eIF2α	*H. sapiens* (HEK-293T cells)	Protein synthesis initiation factor	hOLA1 binds eIF2α and hydrolyzes all local GTP preventing eIF2α•GTP•Met-tRNAi ternary complex formation thus blocking initiation of translation	(11)
GSK3β	*H. sapiens* (HEK-293T cells)	Serine/threonine kinase	Unclear	(12)
TrxA	*E. coli*	Thioredoxin 1; redox homeostasis controlling protein	Binds to YchF homodimers and dissociates them by reducing the disulfide bridge	(6)
TrxC	*E. coli*	Thioredoxin 2; redox homeostasis controlling protein	Presumably reduces the disulfide bridge of YchF homodimers like TrxA; unconfirmed role	(6)
Bcp	*E. coli*	Peroxiredoxin; redox homeostasis controlling protein	Presumably reduces the disulfide bridge of YchF homodimers like TrxA; unconfirmed role	(6)
Glutaredoxin 4	*E. coli*	redox homeostasis controlling protein	Presumably reduces the disulfide bridge of YchF homodimers like	(6)

			TrxA; unconfirmed role	

SECTION 2 – CHAPTER 2 SUPPLEMENTAL MATERIAL

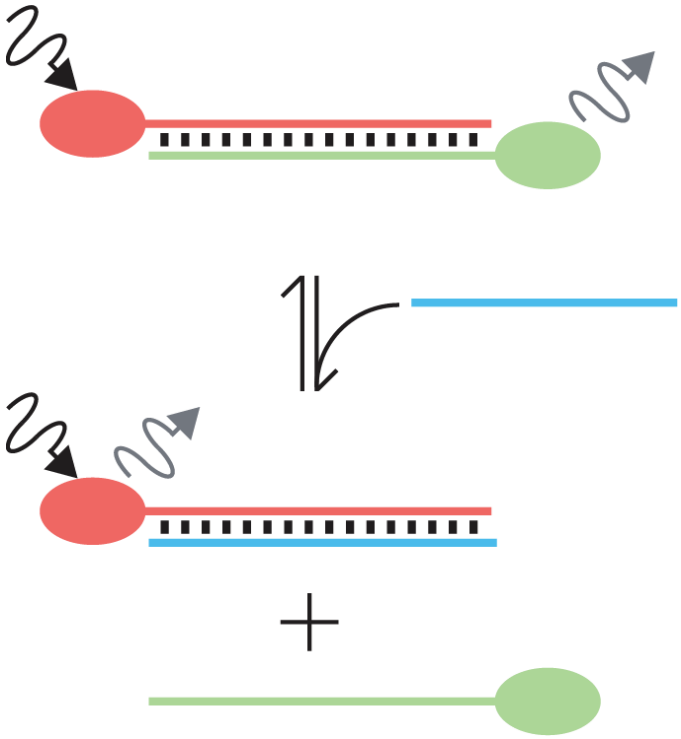

Appendix Figure 2.1 – YchF is an RNA chaperone. Experimental set-up for strand displacement assay to test for RNA unwinding activity of YchF. Dye-tagged 21-mer RNAs were annealed. 20-fold excess unlabelled 21-mer RNA & indicated protein were added to the reaction. Reactions were excited at 535 nm and FRET was measured. If the protein unwinds the duplex, unlabelled RNA competes for binding to labelled RNA and the FRET signal is reduced.

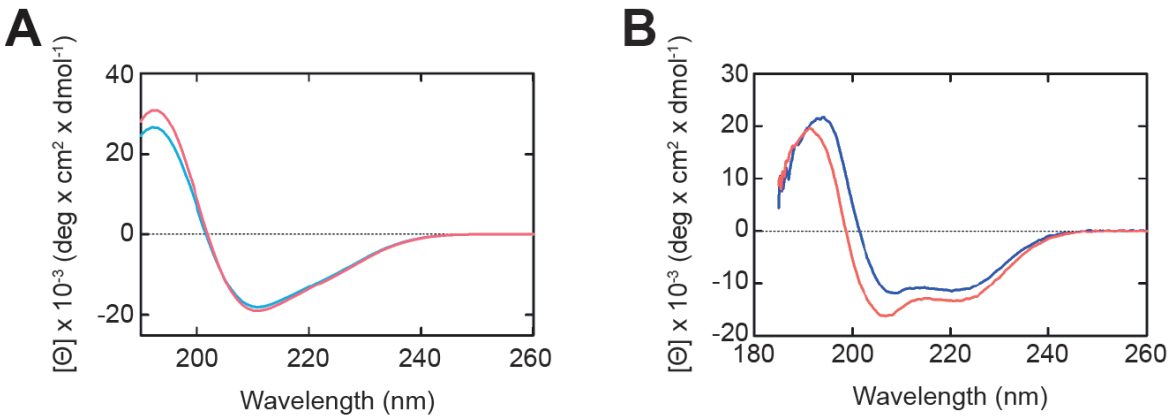

Appendix Figure 2.2 – The overall fold of YchF and ΔTGS-YchF is similar based on CD spectroscopy results. (A) CD spectra showing similar folds for wild type YchF (blue) and ΔTGS YchF (red). The secondary structure composition analysis of the CD spectroscopy data in panel (A) is depicted in pie charts for (B) Wild type YchF and (C) ΔTGS YchF. The category designated others includes random coils and 3-10 helices.

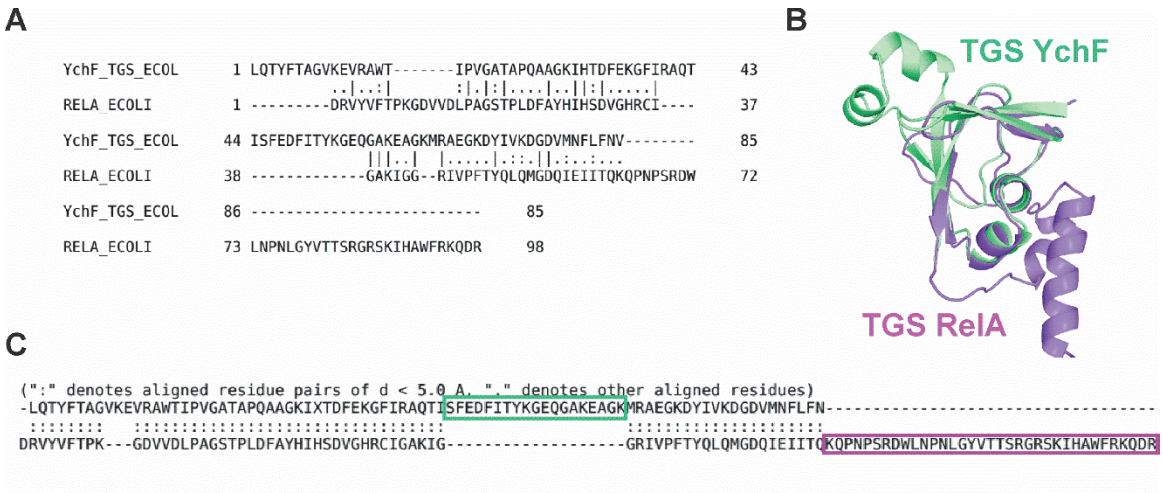

Appendix Figure 2.3 – YchF and RelA share a structurally similar TGS domain but the overall sequence similarity is low. (A) Full sequence alignment of the amino acid sequence for the TGS domains of YchF (green) and RelA (pink). A line between aligned amino acids indicates identical residues, whereas two dots indicate that the side chains have similar properties and one dot signifies that the side chains are different. (B) Structural alignment of the TGS domains of *E. coli* YchF (green) and *E. coli* RelA (pink) prepared in PyMol. (C) Regions of the amino acid sequence alignment where the boxed regions represent sequences that are unique to each enzyme.

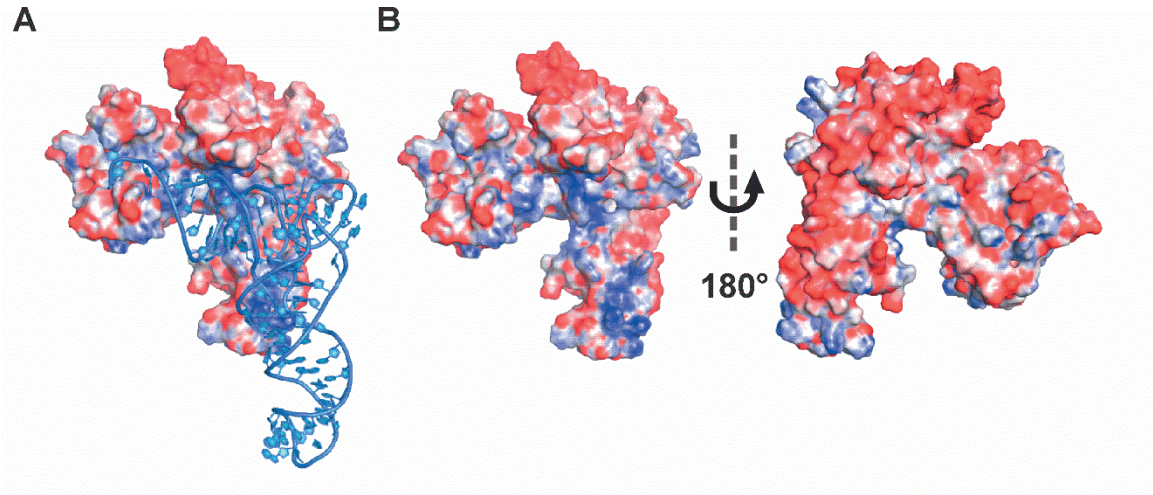

Appendix Figure 2.4 – The docked structure of tRNA aligns with the cleft on YchF containing positively charged residues. The predicted electrostatic surface potential for (A) the docked *E. coli*-YchF tRNA complex, showing positively charged regions in blue and negatively charged regions in red. The tRNA backbone can be seen to interact with the clusters of positive charges on the surface of YchF. (B) Front and back views of the electrostatic surface potential of YchF without tRNA.

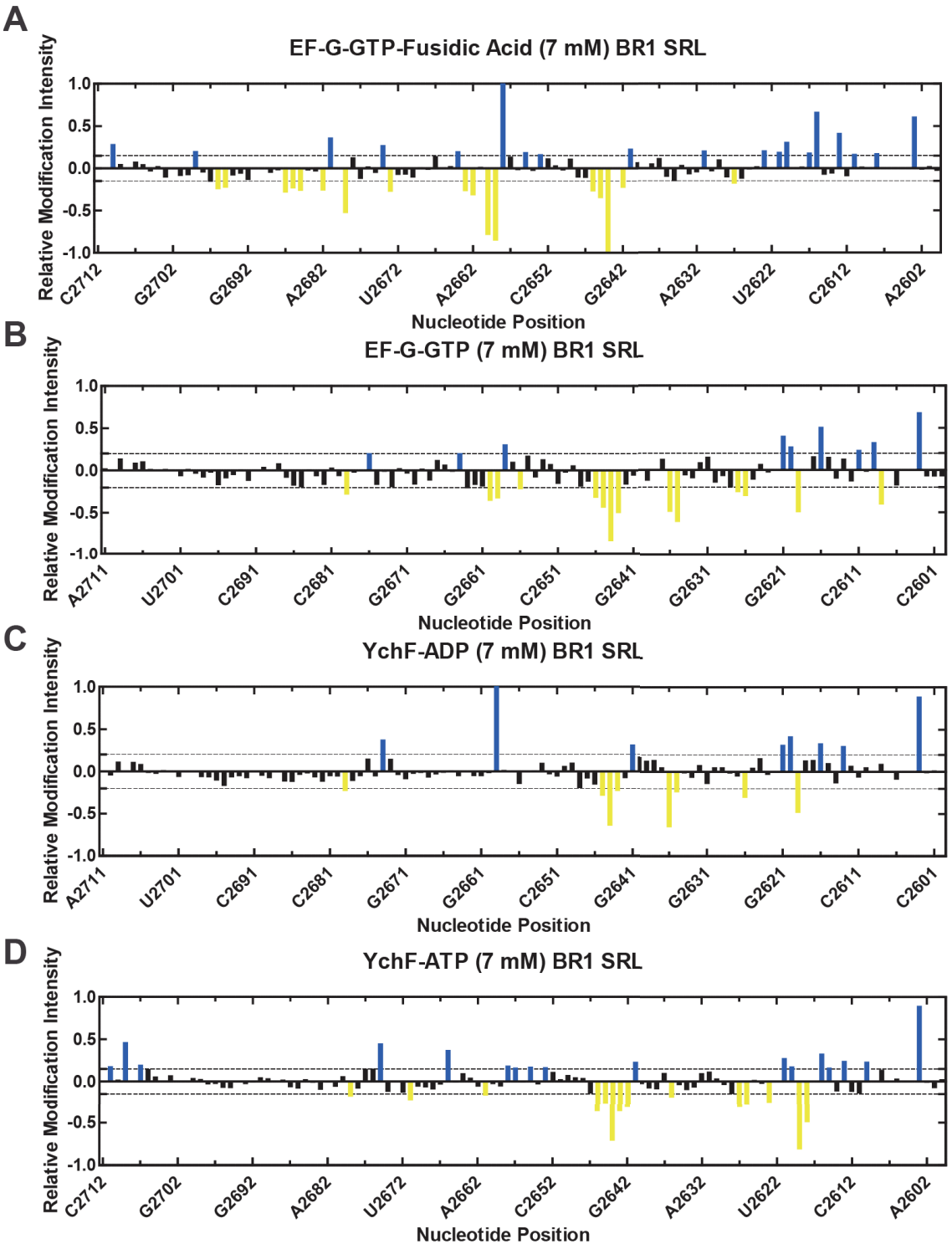

Appendix Figure 2.5 – Binding of both YchF and EF-G to the SRL affects the conformation of rRNA sites distant from the binding site at a physiological concentration of $MgCl_2$. Histograms showing regions of 23S rRNA whose DMS modification pattern is altered upon YchF binding in buffer containing 7 mM $MgCl_2$. Blue indicates a deprotection from modification and yellow indicates a protection from modification.

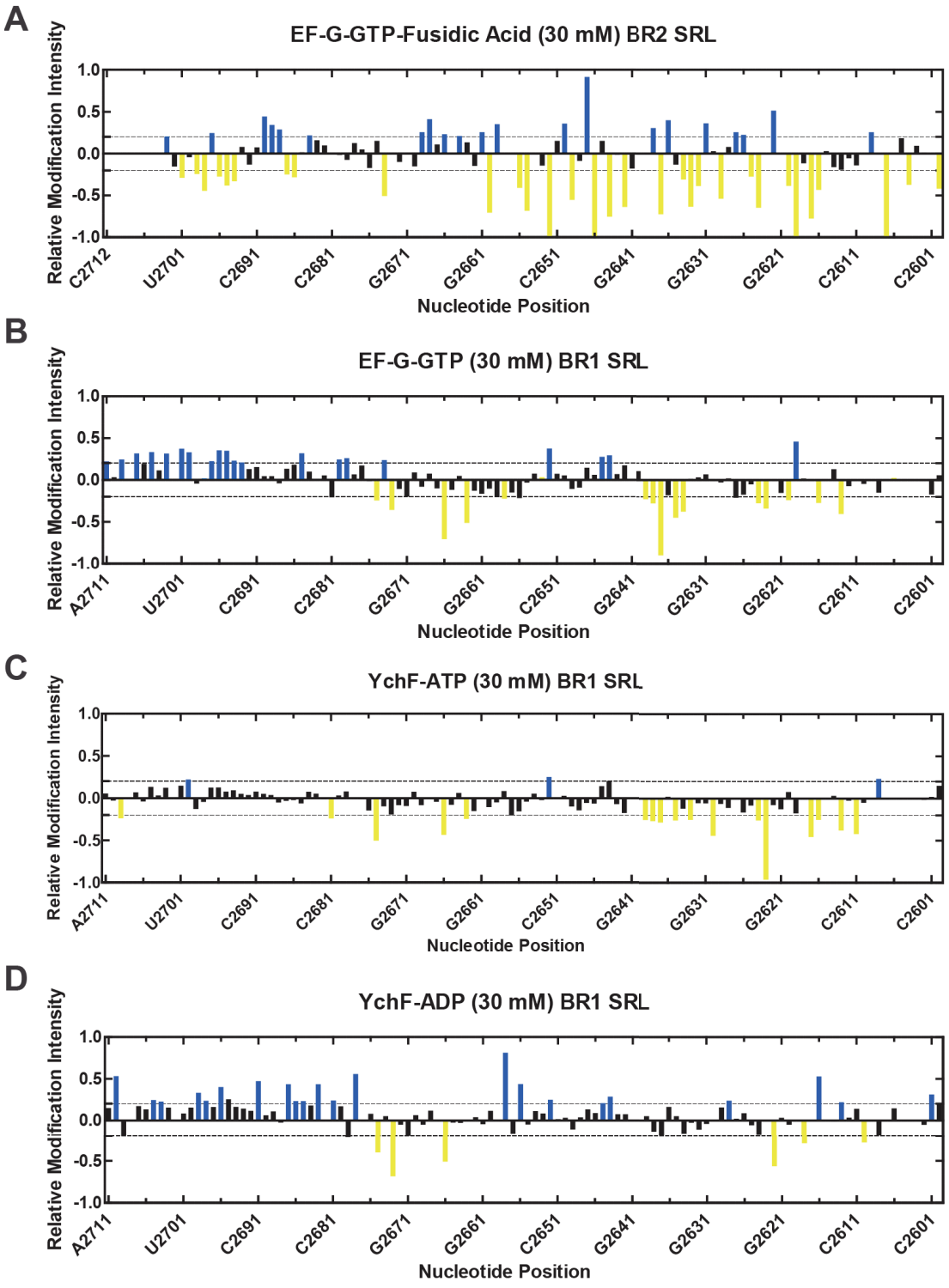

Appendix Figure 2.6 – Binding of both YchF and EF-G to the SRL affects the conformation of sites distant from the binding site at a high concentration of $MgCl_2$. Histograms showing regions of 23S rRNA whose DMS modification pattern is altered upon YchF binding. Blue indicates a deprotection from modification and yellow indicates a protection from modification.

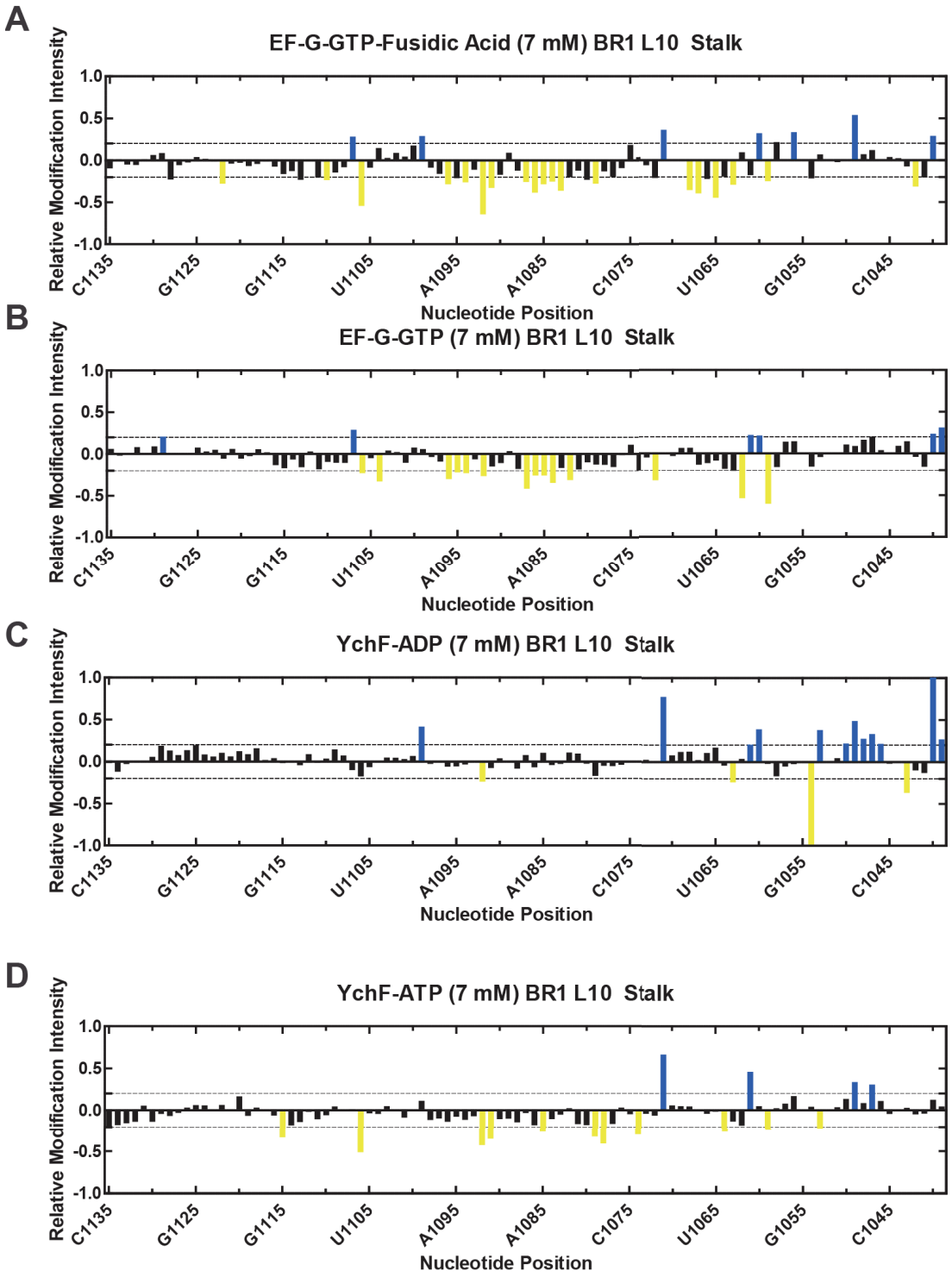

Appendix Figure 2.7 – Binding of both YchF and EF-G to the ribosomal L10 stalk affects the conformation of sites distant from the binding site with physiological concentrations of $MgCl_2$. Histograms showing regions of 23S rRNA whose DMS modification pattern is altered upon YchF binding. Blue indicates a deprotection from modification and yellow indicates a protection from modification.

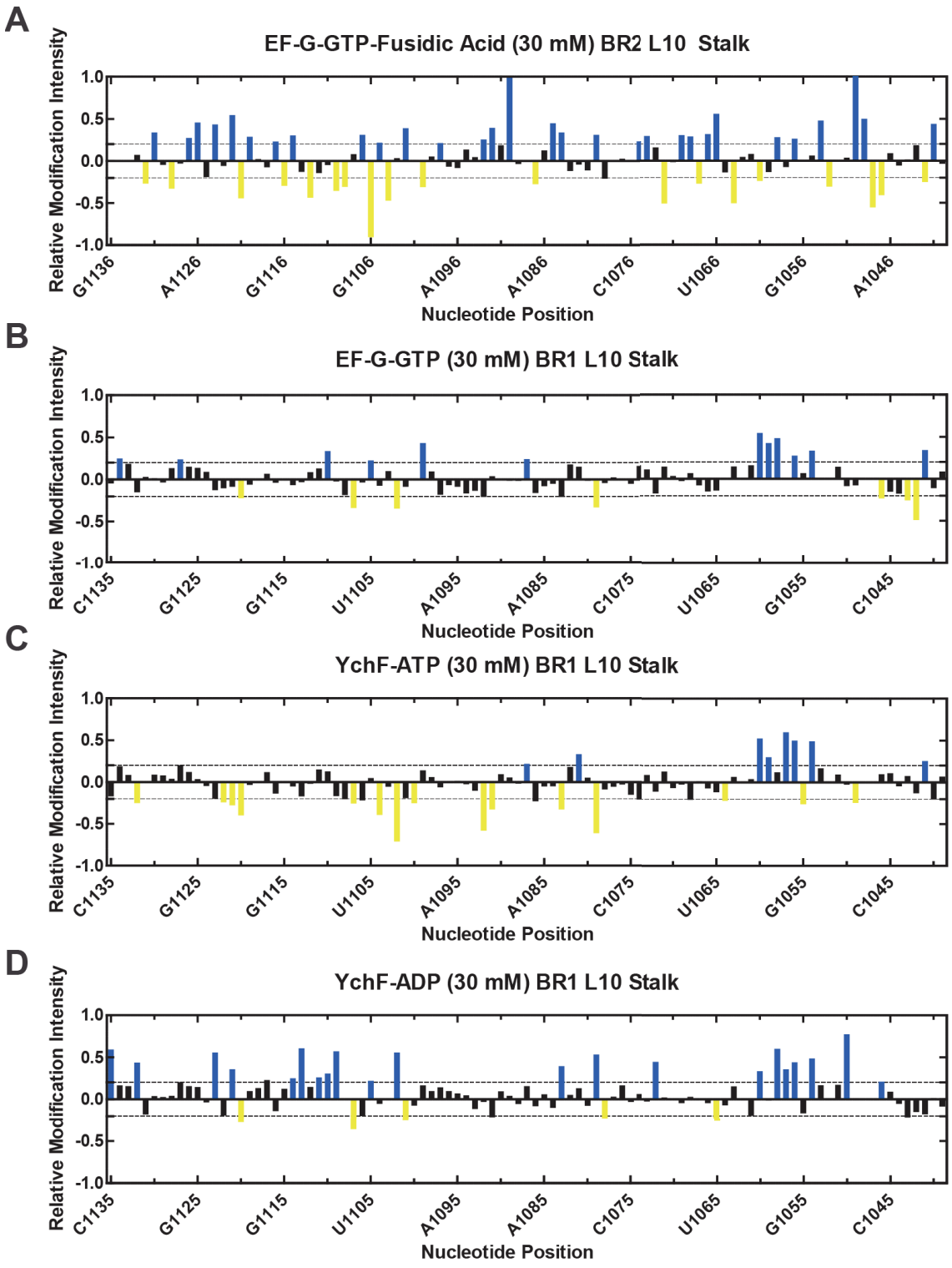

Appendix Figure 2.8 – Binding of both YchF and EF-G to the L10 stalk affects the conformation of sites distant from the binding site with a high concentration of $MgCl_2$. Histograms showing regions of 23S rRNA whose DMS modification pattern is altered upon YchF binding. Blue indicates a deprotection from modification and yellow indicates a protection from modification.

Appendix Table 2.1 – Comparison of nucleotide binding affinities of YchF and ΔTGS YchF. Affinities marked with an asterisk are from Becker *et al.* (3).

Nucleotide	K_D for Wild-type YchF	K_D for ΔTGS YchF
ATP	n.d.	31 ± 4
ADP	14 ± 5*	22 ± 5
ADPNP	9 ± 8*	7 ± 1
GTP	206 ± 5*	n.d.
GDP	151 ± 38*	n.d.
GDPNP	n.d.	n.d.

Appendix Table 2.2. Secondary structure composition analysis of CD spectroscopy data.

Secondary Structure Element	Estimated Content (%)	
	Wild-type YchF	ΔTGS YchF
Helix	**23.3**	**31.7**
Helix 1 (regular)	12.8	17.9
Helix 2 (distorted)	10.5	13.7
Anti-parallel beta sheet	**21.8**	**5.5**
Anti 1 (left-twisted)	4.9	0.0
Anti 2 (relaxed)	9.0	0.0
Anti 3 (right-twisted)	7.9	5.5
Parallel beta sheet	**0.0**	**2.9**
Turn	**14.0**	**14.8**
Others	**40.8**	**45.1**

Appendix Table 2.3. Sequences of RNA oligomers used in the strand displacement assay.

Oligomer Name	Oligomer Sequence
Cy5-5'	**Cy5-5'-AUGUGGAAAAUCUCUAGCAGU-3'**
Cy3-5'	**Cy3-5'-ACUGCUAGAGAUUUUCCACAU-3'**
Unlabeled Competitor	**5'-ACUGCUAGAGAUUUUCCACAU-3'**

Appendix Methods

Circular Dichroism Spectroscopy

Circular dichroism (CD) spectroscopy was performed as described in earlier work (13) unless otherwise specified. The final concentration of wild type YchF or ΔTGS-YchF was 3.31 μM in 50 mM potassium phosphate (pH 8.0). The measured range was 260 nm to 185 nm. The CD spectroscopy data was analyzed using the BeStSel (Beta Structure Selection) web server (14).

Equilibrium fluorescence titration of ΔTGS-YchF with nucleotides

The binding affinity of ΔTGS-YchF for ATP, ADP and ADPNP was measured using intrinsic equilibrium fluorescence measurements as described previously (13).

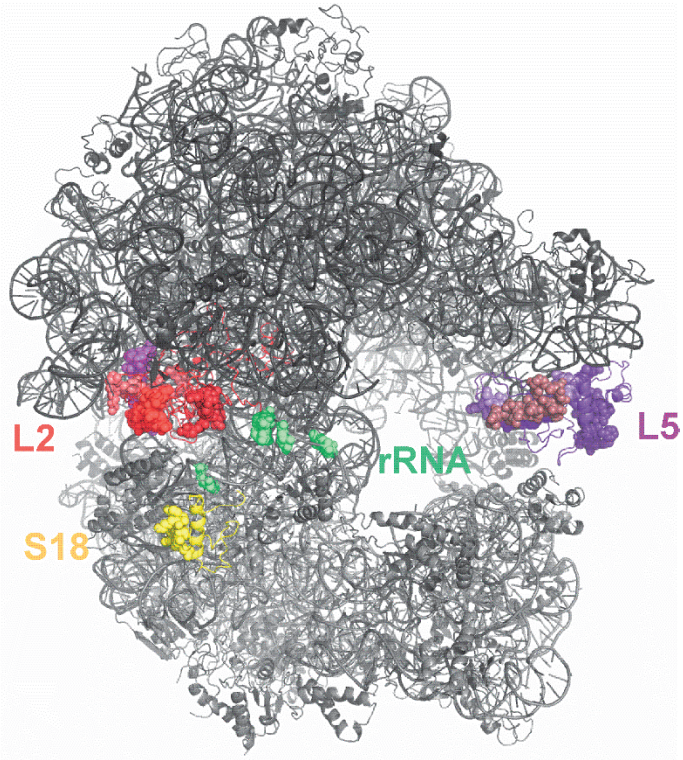

Appendix Figure 3.1 - Peptides identified by mass-spectrometry following crosslinking of the 70S ribosome with AzP-HflX. The respective ribosomal proteins identified by mass spectrometry (listed in Appendix Table 3.1) are shown on the 70S ribosome structure (PDB 4V4Q) as shades of red, purple, and yellow. Spheres indicate peptides identified matching L2, L5, and S18 respectively. The respective rRNA crosslinks are shown as green spheres.

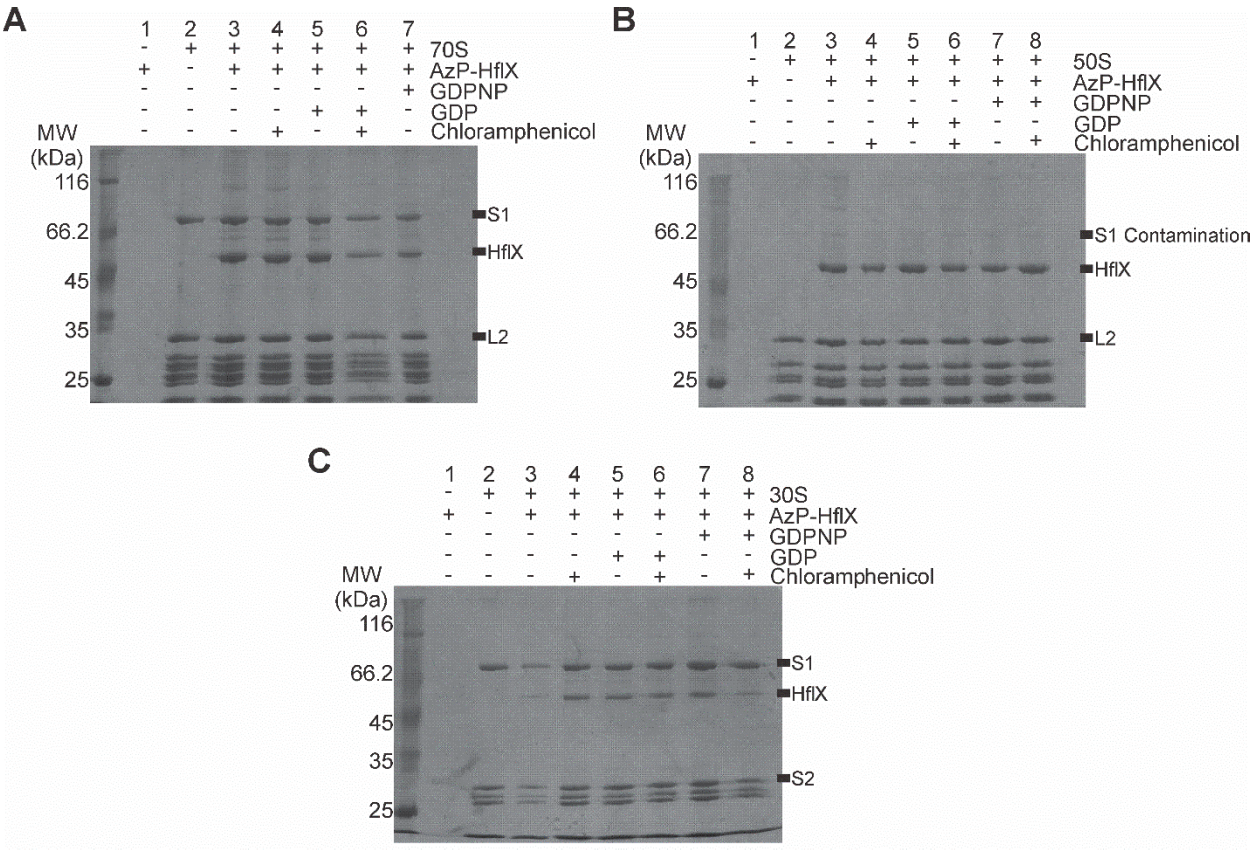

Appendix Figure 3.2 - Crosslinking of AzP-HflX to 70S ribosomes, and 50S/30S ribosomal subunits in different nucleotide bound states. AzP-HflX was incubated with (a) 70S ribosomes, (b) 50S and (c) 30S ribosomal subunits in the presence of no nucleotide (*apo)*, GDP, or GDPNP to test the effect of the nucleotide bound state on the crosslinking efficiency and pattern. Furthermore, no effect of a bound PTC binding antibiotic (chloramphenicol) was observed.

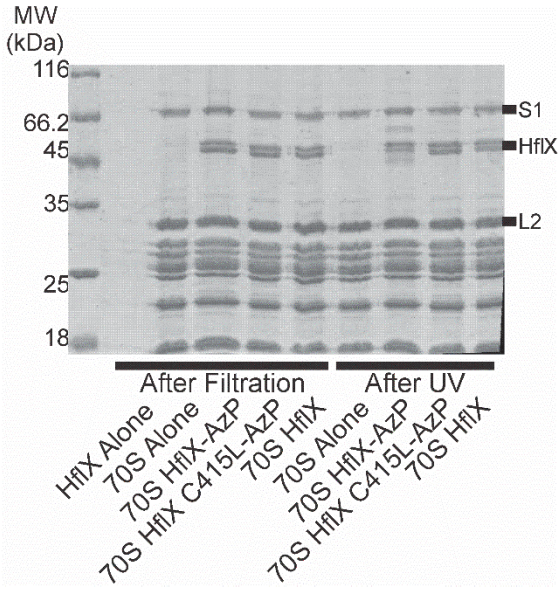

Appendix Figure 3.3 - Removal of the C-terminal cysteine in HflX (Cys415) abolishes crosslinks formed with AzP labeled protein. HflX C415L labeled with AzP bound to the 70S ribosome were subjected to microfiltration to remove unbound HflX C415L-AzP and subsequently analyzed by SDS-PAGE (before and after UV-exposure). No additional higher molecular weight bands are observed for HflX C415L-AzP or unlabeled wild-type HflX compared to those observed for wild-type AzP labeled HflX.

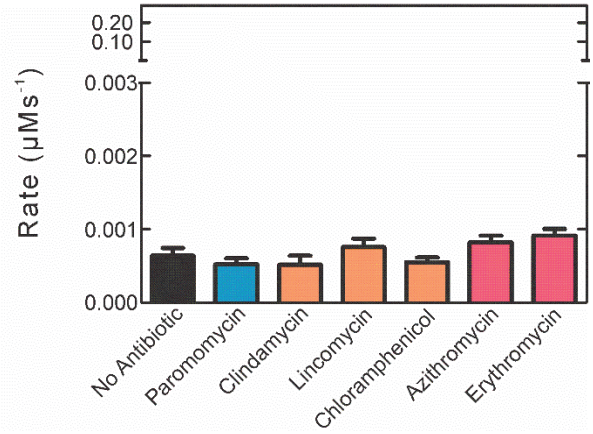

Appendix Figure 3.4 - Antibiotics do not inhibit intrinsic hydrolysis by HflX. HflX (1 μM) was incubated with [γ^{32}P]-GTP (125 μM) and antibiotic (500 μM). Reactions were quenched at successive time points and the amount of released [^{32}P] inorganic phosphate was quantified to determine the rate of hydrolysis. Antibiotics that target several regions of the ribosome were tested including those that bind to the decoding centre (teal), peptidyl transferase centre (orange), and peptide exit tunnel (pink).

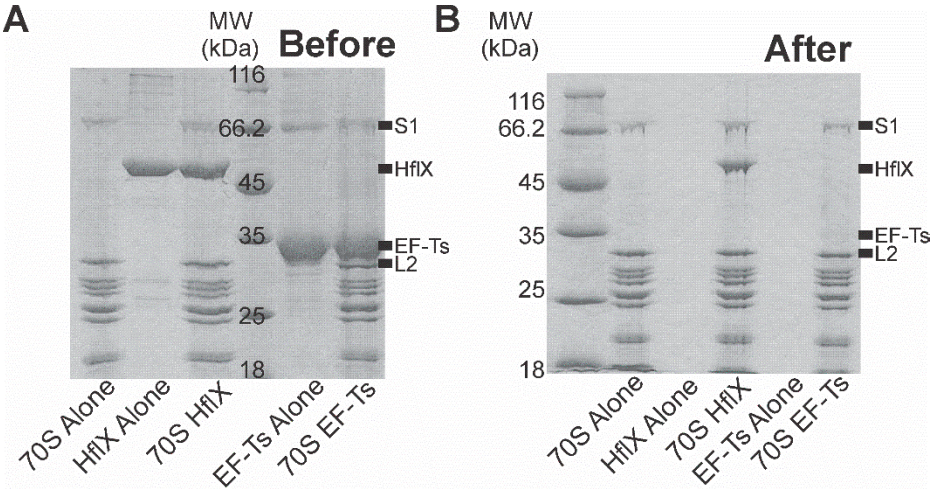

Appendix Figure 3.5 - Microfiltration experiments to confirm that ribosomes do not interfere with proteins passing through the filter. EF-Ts, the nucleotide exchange factor for EF-Tu, was used as it does not interact with the ribosome. EF-Ts or HflX (5 μM) was incubated with 70S ribosome (1 μM) before filtration. Samples of the (a) before and (b) after filtration solutions were analyzed by SDS-PAGE to verify correct stoichiometry and that HflX remained above the filter due to an interaction with ribosomes. EF-Ts was observed to not remain above the filter even in the presence of ribosomes.

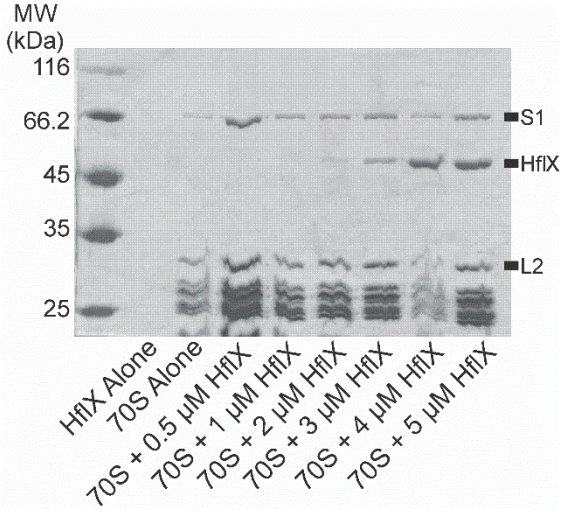

Appendix Figure 3.6 - Sucrose cushion ultracentrifugation experiments confirm HflX binding to the 70S ribosomes. Increasing amounts of HflX (0.5 – 5 μM) were incubated with 70S ribosomes (0.5 μM) prior to loading onto a 10% sucrose cushion. Following centrifugation in a MX 150 Sorvall micro-ultracentrifuge (Thermo Scientific) using an S140 AT rotor for 4 hours at 89 000 rpm, the supernatant was carefully removed before the pellets were resuspended in buffer and subsequently analyzed by SDS-PAGE and silver staining.

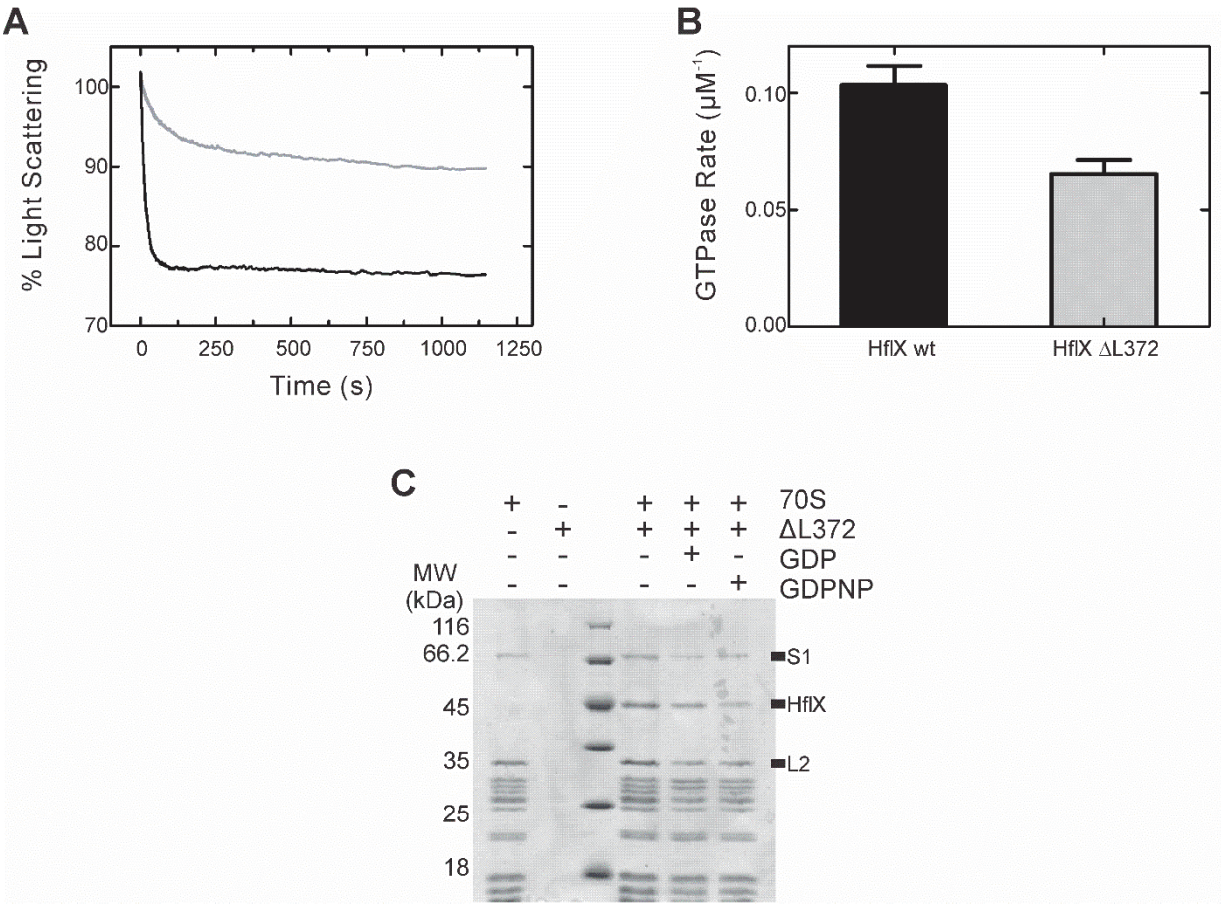

Appendix Figure 3.7 - The C-terminal domain of HflX is required for efficient ribosome splitting. (a) 70S dissociation experiments using HflX ΔL372•GTP (light grey) show a decrease in light scattering and a slower rate of dissociation compared to wild-type HflX (dark grey). (b) Rate of GTP hydrolysis by HflX ΔL372 is not affected by the removal of 55 amino acids at the C-terminus. (c) HflX ΔL372 can bind the 70S ribosome in all nucleotide bound states.

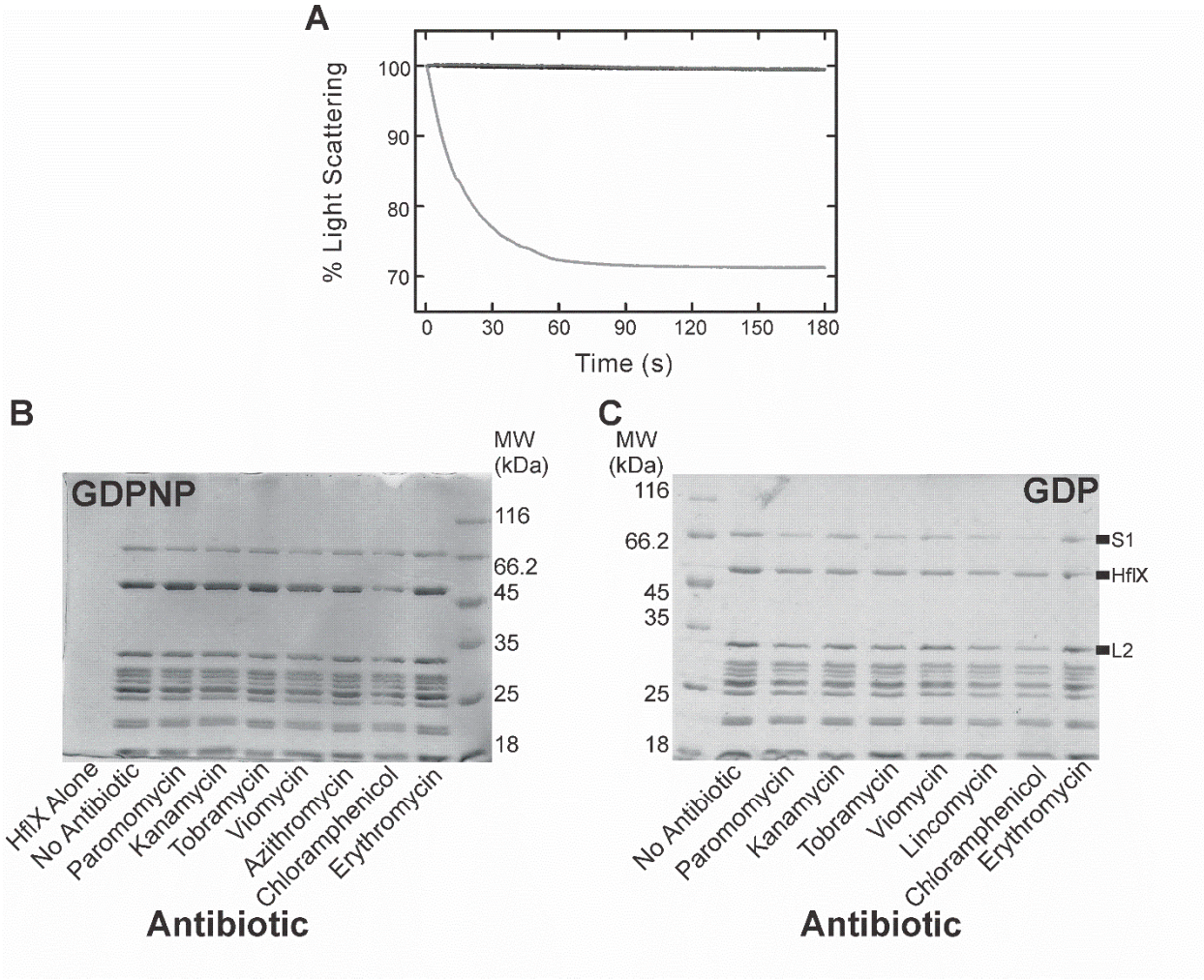

Appendix Figure 3.8 - Effect of 30 mM Mg^{2+} on ribosome splitting, binding, and GTPase stimulation of HflX. (A) 70S splitting in the presence of HflX•GTP was inhibited by the presence of 30 mM Mg^{2+} ($TAKM_{30}$, dark grey). Controls of 70S ribosomes in $TAKM_5$ buffer are mixed with either TAKM5 buffer (black) or TAK buffer (light grey). GTPase inhibiting antibiotics do not interfere with binding of HflX to the 70S ribosome, either in the presence of 500 µM GDPNP (B) or 500 µM GDP (C). All experiments in (B) and (C) are carried out in the presence of $TAKM_{30}$ (50 mM Tris-Cl pH 7.5 at 4°C, 70 mM NH_4Cl, 30 mM KCl, 30 mM $MgCl_2$), preventing the dissociation of the 70S ribosomes into 50S and 30S subunits.

Appendix Table 3.1 - List of peptides found by mass-spectrometry analysis.

Band Label	Peptide #	Sequence	Amino Acids	Color
HflX*	HflX-1	KAVEIAEAVKA	62-72	
	HflX-2	RTGLILDIFAQRA	103-115	
	HflX-3	KLQVELAQLRH	121-131	
	HflX-4	RGPGETQLETDRRL	153-166	
	HflX-5	KADVPTVSLVGYTNAGKS	194-211	
	HflX-6	RVYAADQLFATLDPTLRR	221-238	
	HflX-7	RHLPHDLVAAFKA	257-269	
	HflX-8	RQATLLLHVIDAADVRV	274-291	
	HflX-9	KIDMLEDFEPRI	318-329	
	HflX-10	RLSGEVAGHTLRL	360-372	
	HflX-11	RFYQLQAIEKE	382-392	
		Percent Coverage HflX:	35.68%	

Band Label	Peptide #	Sequence	Amino Acids	Color
HflX-L2				
	L2-1	KGKPFAPLLEKN	26-37	pink
	L2-2	RSANIALVLYKD	87-98	light red
	L2-3	KAGDQIQSGVDAAIKPGNT	111-129	red
	L2-4	RDGAYVTLRL	167-176	dark red
		Percent Coverage L2:	19.41%	
	HflX-1	KAVEIAEAVKA	62-72	
	HflX-2	RTGLILDIFAQRA	103-115	
	HflX-3	KLQVELAQLRH	121-131	
	HflX-4	KADVPTVSLVGYTNAGKS	194-211	
	HflX-5	RVYAADQLFATLDPTLRR	221-238	
	HflX-6	RHLPHDLVAAFKA	257-269	
	HflX-7	RQATLLLHVIDAADVRV	274-291	
	HflX-8	KIDMLEDFEPRI	318-329	
	HflX-9	RLSGEVAGHTLRL	360-372	
	HflX-10	RFYQLQAIEKE	382-392	
		Percent Coverage HflX:	32.39%	

Band Label	Peptide #	Sequence	Amino Acids	Color
HflX-L5				
	L5-1	KITLNMGVGEAIADKKL	33-49	lightest purple
	L5-2	KLLDNAAADLAAISGQKP	48-65	light purple
	L5-3	RGLDITITTTAKS	150-162	purple
	L5-4	RALLAAFDFPFRK	167-179	dark purple
		Percent Coverage L5:	34.08%	
	HflX-1	RTGLILDIFAQRA	103-115	
	HflX-2	RQATLLLHVIDAADVRV	274-291	
		Percent Coverage HflX:	7.28%	

Band Label	Peptide #	Sequence	Amino Acids	Color
HflX-S18				
	S18-1	RFTAEGVQEIDYKD	12-25	yellow
		Percent Coverage S18:	18.67%	
	HflX-1	RYDAGEQAVLVHI	4-16	
	HflX-2	KAVEIAEAVKA	62-72	
	HflX-3	KATGASVVLFDHALSPAQERN	71-91	
	HflX-4	RTGLILDIFAQRA	103-115	
	HflX-5	KLQVELAQLRH	121-131	
	HflX-6	KADVPTVSLVGYTNAGKS	194-211	
	HflX-7	RVYAADQLFATLDPTLRR	221-238	
	HflX-8	RHLPHDLVAAFKA	257-269	
	HflX-9	RQATLLLHVIDAADVRV	274-291	
	HflX-10	KIDMLEDFEPRI	318-329	
	HflX-11	RLSGEVAGHTLRL	360-372	
	HflX-12	RFYQLQAIEKE	382-392	
		Percent Coverage HflX:	40.38%	

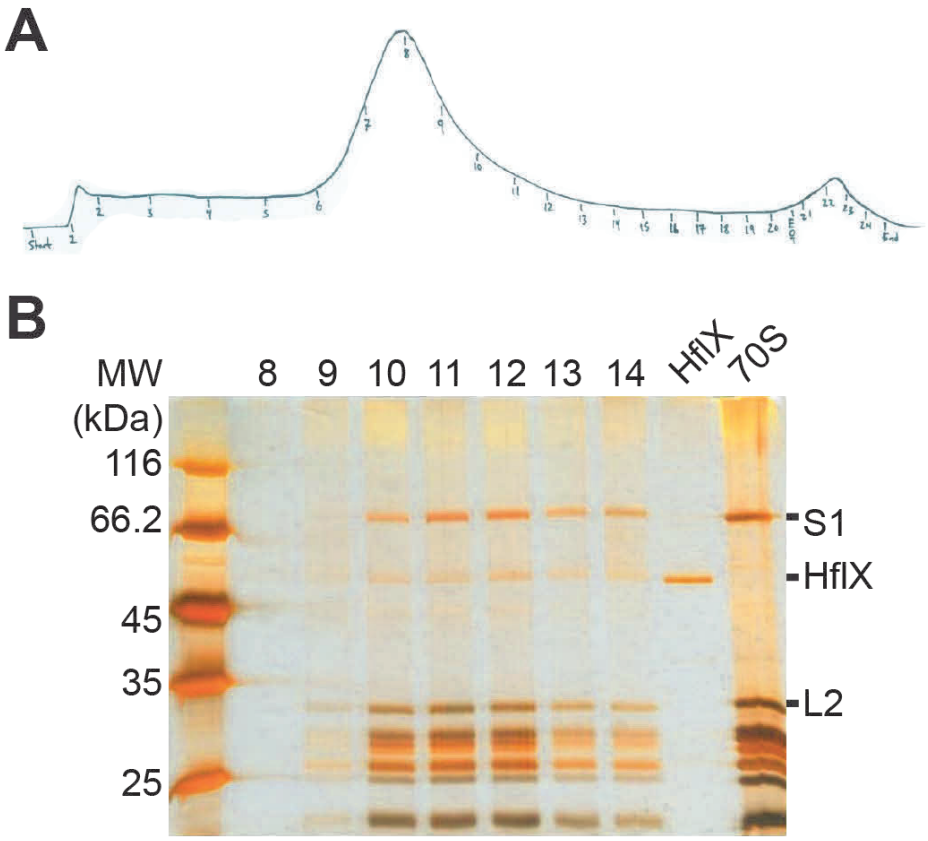

Appendix Figure 4.1 – HflX•GDPNP remains partially bound to the 70S ribosome in the presence of tobramycin. (A) 70S•HflX•GDPNP•Tob complexes were spun through a 10-40% sucrose gradient containing Tobramycin. Chromatogram was recorded using a chart recorder and UV detector, with a slight delay between the UV detector and fraction collector of about 1.5 mL (3 fractions). (B) Fractions were TCA precipitated and run on a 12% SDS-PAGE stained with silver.

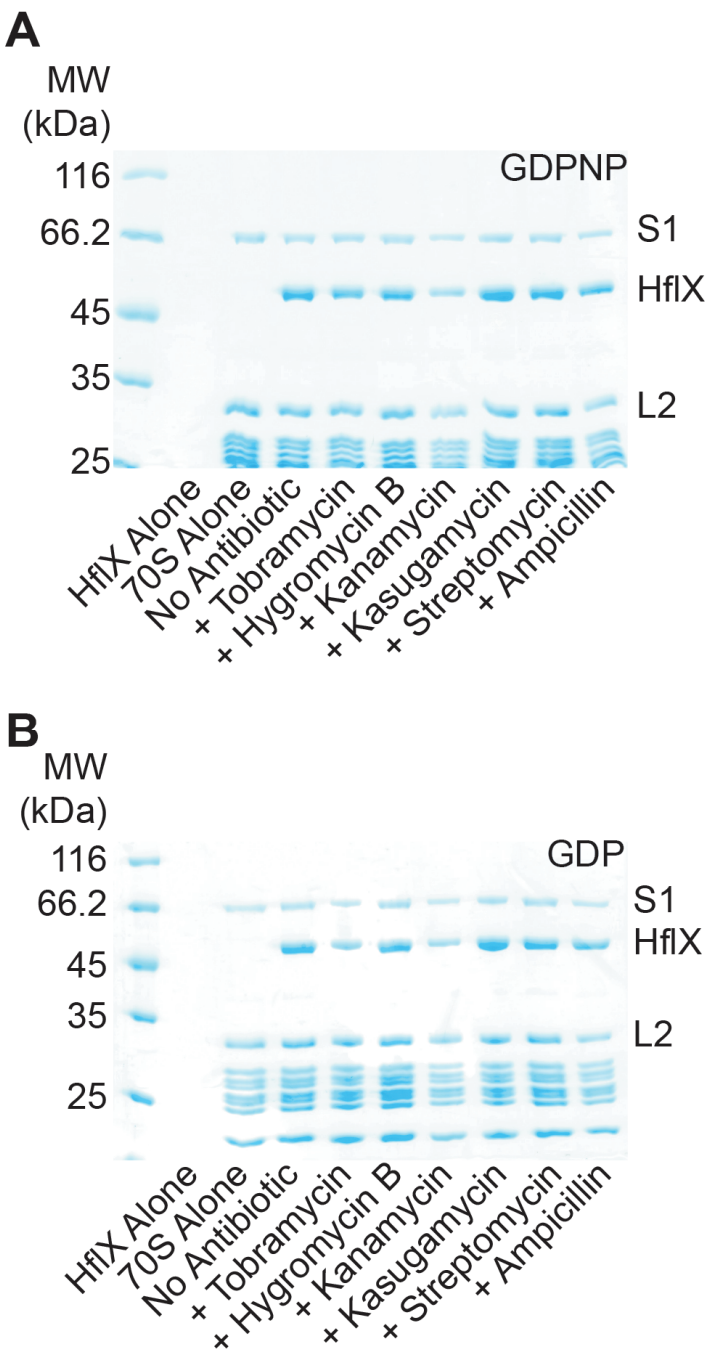

Appendix Figure 4.2 – Antibiotic effect on HflX binding to bacterial ribosome. HflX (5 μM) was incubated with 70S ribosomes (1 μM) in the presence of (**A**) GDPNP or (**B**) GDP (500 μM) and the antibiotic indicated (500 μM). Complexes were separated from free HflX via filtration and subsequently washed before collecting the remaining filtrate for analysis by SDS-PAGE.

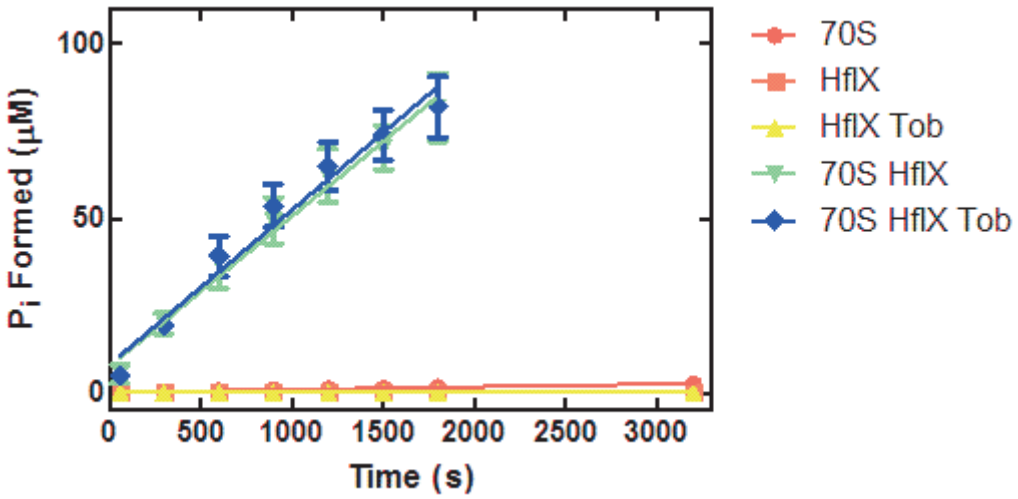

Appendix Figure 4.3 – Antibiotic Inhibition of HflX ribosome-stimulated GTP hydrolysis activity. HflX (1 μM) was incubated with 70S ribosomes (1 μM) in the presence of [γ-^{32}P]-GTP (125 μM) and tobramycin (500 μM) in TAKM$_5$ buffer. Reactions were quenched at successive time points and the amount of released [^{32}P] inorganic phosphate was quantified to determine the rate of hydrolysis.

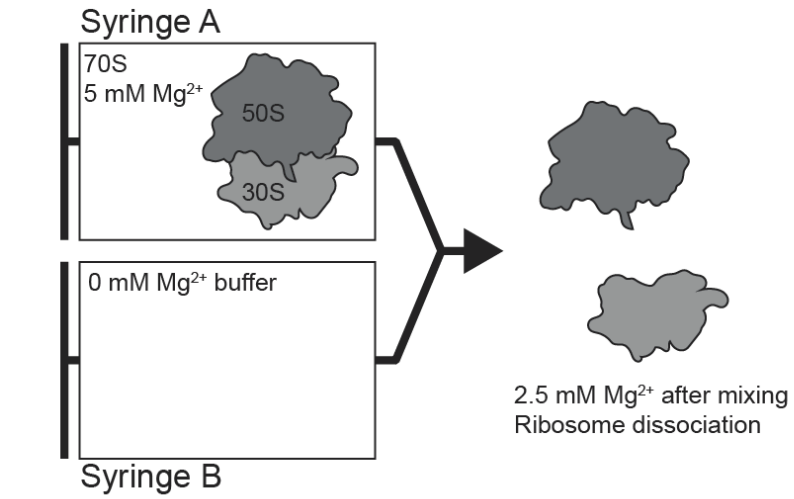

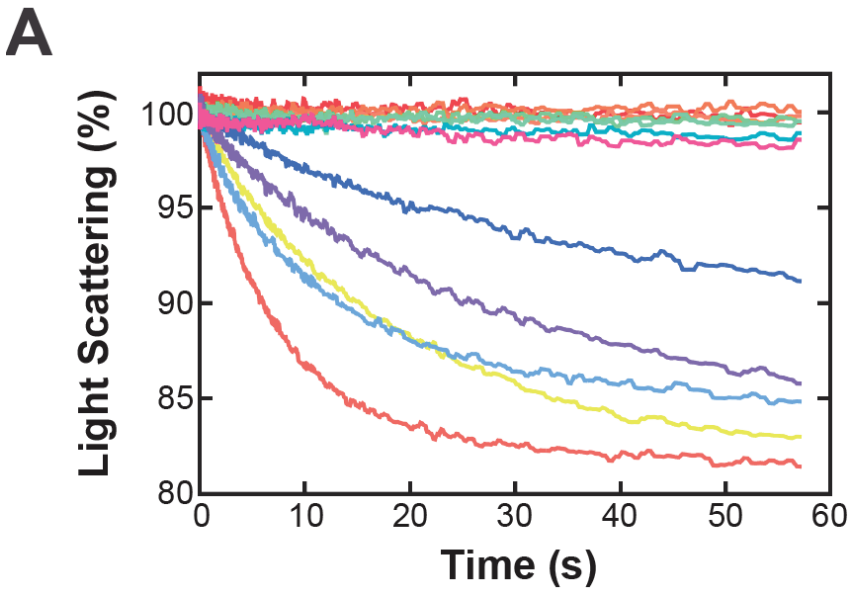

Appendix Figure 4.4 – Stabilization of the 70S ribosome by aminoglycosides under magnesium depletion conditions. Rapid mixing of 70S ribosomes in TAKM$_5$ buffer against TAK buffer results in a final magnesium concentration of 2.5 mM and a decrease in Rayleigh light scattering over time indicative of dissociation of the 70S ribosome into 50S and 30S ribosomal subunits. (A) Antibiotics that target the peptidyl transferase center (PTC) or peptide exit tunnel (PET) show a decrease in light scattering characteristic of dissociation of the 70S ribosome into subunits (clindamycin – yellow; chloramphenicol – blue; erythromycin – purple; tobramycin – orange; paromomycin – green; kanamycin – cyan; kasugamycin – light blue; streptomycin – pink; hygromycin B – teal; no antibiotic – red line).

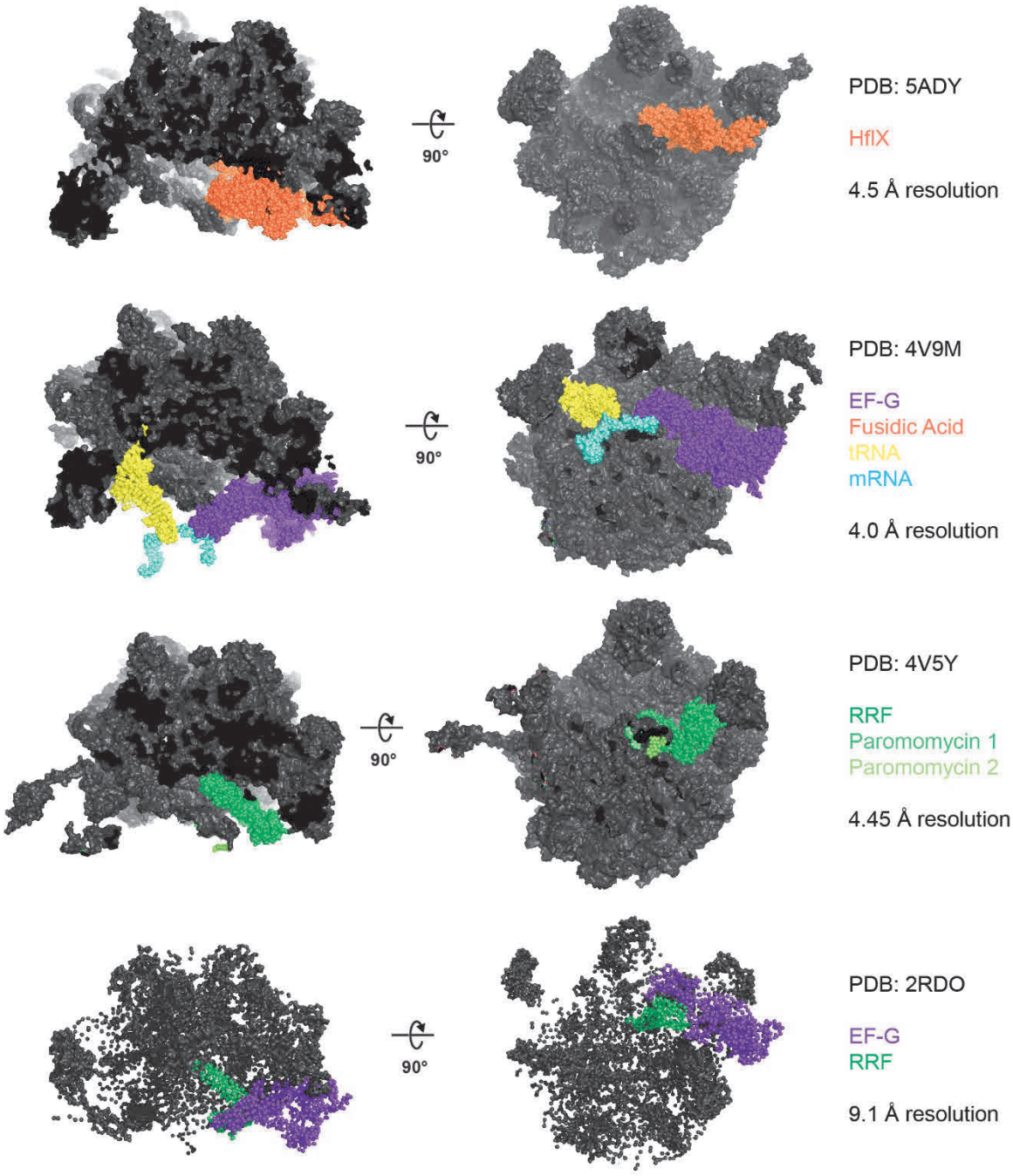

Appendix Figure 4.5 – Structural comparison of the HflX, EF-G, and RRF binding sites on the ribosome. Only the 50S ribosomal subunit is shown from the structures that contain the full 70S ribosome for easy comparison.

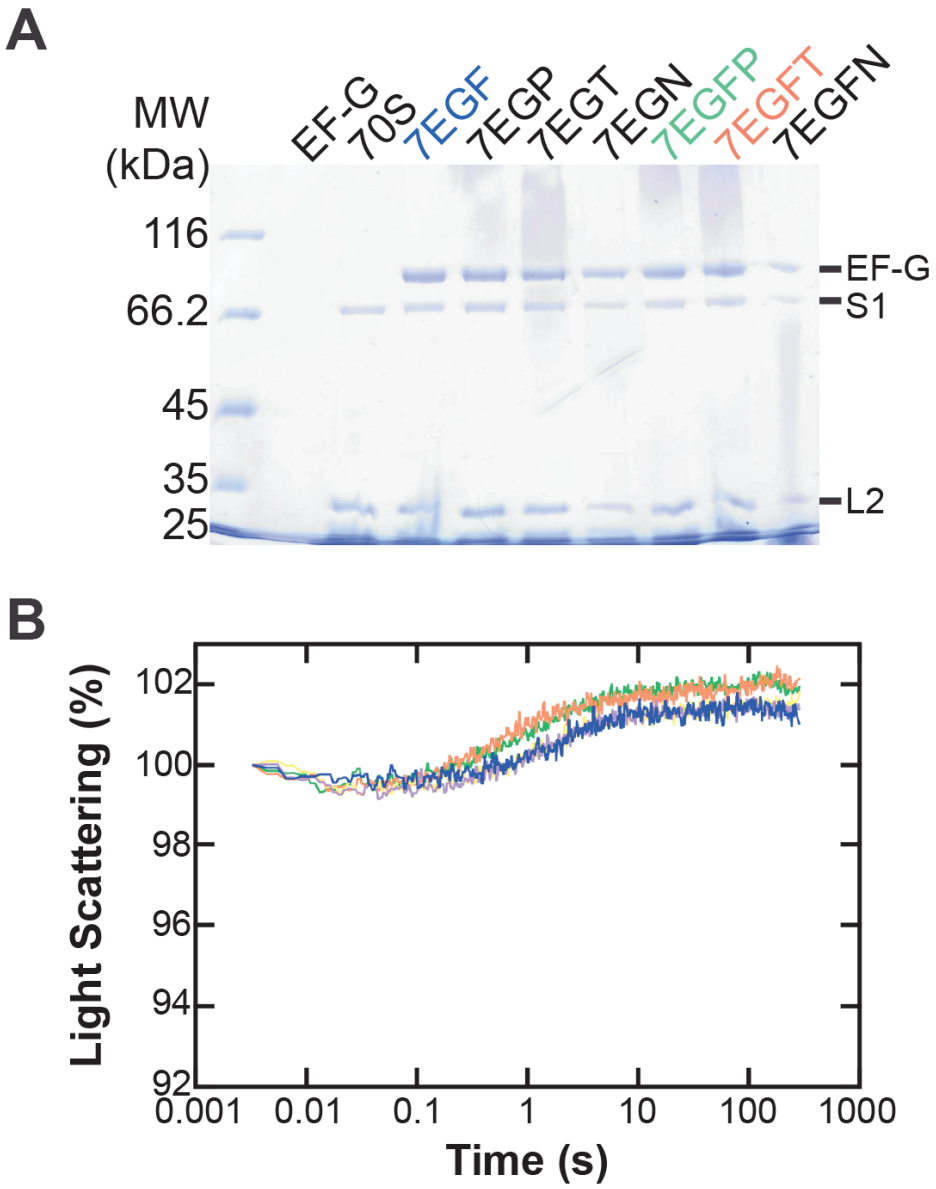

Appendix Figure 4.6 – Effect of aminoglycosides on the formation of 70S•EF-G•GDP•FUS complexes. (A) 70S•EF-G•GTP•FUS was pre-incubated at 37°C before microfiltration to allow one round of GTP hydrolysis to occur, locking EF-G onto the ribosomal A-site by Fusidic acid (FUS). Microfiltration allowed the removal of unbound EF-G leaving 70S•EF-G•GDP•FUS complexes above the membrane. Aminoglycoside antibiotics prevent ribosome dissociation through the stabilization of the 70S ribosome. To determine if EF-G could be locked onto the A-site of aminoglycosides stabilized 70S ribosomes, complexes were prepared in the presence of one or two antibiotics before and during microfiltration. Aminoglycosides tested include paromomycin (P), tobramycin (T), and neomycin (N). (B) Formation of 70S•EF-G•GDP•FUS complexes in the presence of a second antibiotic was also tested using Rayleigh light scattering. Rapid mixing of 70S ribosomes in $TAKM_5$ buffer against EF-G•GTP buffer both in the presence of fusidic acid (500 μM) and a second antibiotic (500 μM) where noted resulted in an increase in Rayleigh light scattering over time indicative of EF-G binding to the 70S ribosome. Only fusidic acid – blue; lincomycin – yellow; erythromycin – pink; tobramycin – orange; paromomycin – green.

APPENDIX REFERENCES

1. Gradia DF*, et al.* (2009) Characterization of a novel Obg-like ATPase in the protozoan Trypanosoma cruzi. *International journal for parasitology* 39(1):49-58.

2. Tomar SK, Kumar P, & Prakash B (2011) Deciphering the catalytic machinery in a universally conserved ribosome binding ATPase YchF. *Biochem. Biophys. Res. Commun.* 408(3):459-464.

3. Becker M*, et al.* (2012) The 70S ribosome modulates the ATPase activity of Escherichia coli YchF. *RNA Biology* 9(10):1288-1301.

4. Guerrero C, Tagwerker C, Kaiser P, & Huang L (2006) An integrated mass spectrometry-based proteomic approach: quantitative analysis of tandem affinity-purified in vivo cross-linked protein complexes (QTAX) to decipher the 26 S proteasome-interacting network. *Molecular & cellular proteomics : MCP* 5(2):366-378.

5. Wenk M*, et al.* (2012) A universally conserved ATPase regulates the oxidative stress response in Escherichia coli. *J Biol Chem* 287(52):43585-43598.

6. Hannemann L*, et al.* (2016) Redox Activation of the Universally Conserved ATPase YchF by Thioredoxin 1. *Antioxid Redox Signal* 24(3):141-156.

7. Jager S*, et al.* (2011) Global landscape of HIV-human protein complexes. *Nature* 481(7381):365-370.

8. Mao RF*, et al.* (2013) OLA1 protects cells in heat shock by stabilizing HSP70. *Cell Death & Disease* 4:e491.

9. Cheung M-Y*, et al.* (2008) Constitutive expression of a rice GTPase-activating protein induces defense responses. *New Phytologist* 179(2):530-545.

10. Matsuzawa A*, et al.* (2014) The BRCA1/BARD1-interacting protein OLA1 functions in centrosome regulation. *Mol Cell* 53(1):101-114.

11. Chen H*, et al.* (2015) OLA1 regulates protein synthesis and integrated stress response by inhibiting eIF2 ternary complex formation. *Scientific reports* 5:13241.

12. Xu D*, et al.* (2016) Obg-like ATPase 1 regulates global protein serine/threonine phosphorylation in cancer cells by suppressing the GSK3beta-inhibitor 2-PP1 positive feedback loop. *Oncotarget* 7(3):3427-3439.

13. Rosler KS, Mercier E, Andrews IC, & Wieden H-J (2015) Histidine 114 Is Critical for ATP Hydrolysis by the Universally Conserved ATPase YchF. *Journal of Biological Chemistry* 290(30):18650-18661.

14. Micsonai A*, et al.* (2015) Accurate secondary structure prediction and fold recognition for circular dichroism spectroscopy. *Proceedings of the National Academy of Sciences*:201500851.